ELECTROCHROMIC AND PHOTOELECTROCHROMIC SWITCHING DEVICES BASED ON ARYL AMINE REDOX CHEMISTRY

by

MELODY DIANE KELLEY

SILAS C. BLACKSTOCK, COMMITTEE CHAIR

MARTIN G. BAKKER
JAMES W. HARRELL
SHANLIN PAN
KEVIN H. SHAUGHNESSY
THOMAS P. VAID

A DISSERTATION

Submitted in partial fulfillment of the requirements
for the degree of Doctor of Philosophy
in the Department of Chemistry
in the Graduate School of
The University of Alabama

TUSCALOOSA, ALABAMA

2014

Copyright Melody Diane Kelley 2014
ALL RIGHTS RESERVED

ABSTRACT

Electrochromic Materials are of interest as fundamental components in smart windows, displays, and fabrics. A new class of organic arylamine molecular electrochromes (both ionic and neutral) has been developed to afford optimal optical and electrochemical switching properties in the absorptive/transmissive electrochromic device state. By controlling the number of redox active units, structuring their internal electronic coupling and alternating the charge state of the electrochrome, a range of optical states are afforded. N, N, N´, N´-Tetraanisyl-1,4-phenylenediame (TAPD) is optimized for use as multi-colored electrochromic molecular dye in the type I (solution) device state.

Anionic polyarylamines are prepared and tested in transmissive singular type I electrochromic devices. The application of a small bias ($\leq 2\ V$) leads to highly colored stable radical zwitterions. Lack of formal net charge in the oxidized form of the molecule influences its mass transport in the device to yield faster switching times. Devices with these anionic electrochromes also exhibit faster open circuit bleaching kinetics in contrast to neutral devices.

In addition to their device studies, stable radical zwitterions have been synthesized (via chemical oxidation), and characterized using cyclic voltammetry, electron paramagnetic resonance (EPR) spectroscopy and optical spectroscopy. Information gained from these studies has led to an improved understanding of the rational design of isolable radical zwitterions.

The phenomenon of electrochromism is further demonstrated in a novel redox auxiliary (RA) photoelectrochromic switch. An amino substituted norbornadiene (AA-N-Ts) undergoes photochemical rearrangement to its colorless quadricyclane isomer (AA-Q-Ts), which can be reversibly transformed back to the yellow AA-N-Ts upon oxidative catalysis at an electrode in solution. Similarly, amino substituted azobenzene derivatives isomerize between the contracted (Z) form and the expanded (E) form as a result of photochemical and electrochemical stimuli, respectively. Using the technology of type I electrochromic devices, the photoelectrochromic switching of these systems is demonstrated with large duty cycles (~1000 cycles). The photoelectrochromic device (PECD) also provides an analytical platform for the study of redox auxiliary catalysis. A new photoelectrochromic switching media has been developed for cycling aromatic photoelectrochromic systems. The general utility of this media in the photoelectrochromic cycling redox auxiliary systems is established.

LIST OF ABBREVIATIONS AND SYMBOLS

A	Amperes
AA	arylamino
anhyd	anhydrous
br	broad (spectral)
°C	degree Celsius
calc	calculated
CAN	ceric ammonium nitrate
C_6D_6	deuterated benzene
$CDCl_3$	deuterated chloroform
cm	centimeter(s)
conc	concentrated
CV	cyclic voltammetry
Δ	heat
δ	chemical shift
d	doublet (spectral)
dd	doublet of doublets (spectral)

DMSO-*d*6	deuterated dimethylsulfoxide
ECD	electrochromic device
E°′	formal oxidation potential
g	gram(s)
h	hour(s)
hν	light energy
HOMO	highest occupied molecular orbital
HRMS	high resolution mass spectroscopy
Hz	Hertz
I	electrical current
irr	irradiation
ITO	indium tin oxide
J	coupling constant (NMR)
LED	light emitting diode
LUMO	lowest unoccupied molecular orbital
m	multiplet (spectral)
M	molar
mg	milligram(s)
MHz	megahertz
min	minute(s)
mL	milliliter(s)
mM	millimolar
mmol	millimole(s)

mol	mole(s)
mp	melting point
mV	millivolt(s)
μA	microamperes
N	norbornadiene
OTE	optically transparent electrode
nm	nanometer(s)
NMR	nuclear magnetic resonance
PD	*p*-phenylenediamino
PECD	photoelectrochromic device
$Pd(dba)_2$	bis-(dibenzylideneacetone)palladium
Ph	phenyl
ppm	part(s) per million
Pt	platinum
$P(t\text{-}Bu)_3$	tri-*tert*-butylphosphine
Q	quadricyclane
RT	room temperature
s	second(s); singlet (spectral)
SCE	saturated calomel electrode
$TBABF_4$	*n*-tetrabutylammonium tetrafluoroborate
TLC	thin-layer chromatography
Tol	toluene
TMS	tetramethylsilane

Ts	tosyl
V	volt(s)

ACKNOWLEDGMENTS

This page is perhaps the most difficult to write. However, as Gladys B. Stern once said, “Silent gratitude isn’t much use to anyone.” My success as a graduate student has had everything to do with my advisor, Dr. Silas C. Blackstock. I am thankful for his guidance, patience, and exceptional ability to motivate me (even when my morale is at its lowest). I couldn’t have chosen a more knowledgeable and supportive dissertation committee. To Dr.’s Bakker, Harrell, Vaid, Shaughnessy, and Pan, thank you for your technical input and encouragement. I have also learned a great deal from my coworkers in the Blackstock Research Group. Their polite and meaningful discourse over the years is greatly appreciated.

The contribution of my family and friends can be conveniently summed up in one word: BALANCE. Thank you for emphasizing the importance of being a well-rounded person.

Lastly, none of this would be possible without the peace and strength of Jesus Christ, my Lord and Savior.

“But those who hope in the Lord will renew their strength.
They will soar on wings like eagles;
They will run and not grow weary,
They will walk and not be faint.” – Isaiah 40:31

CONTENTS

ABSTRACT ii

LIST OF ABBREVIATIONS AND SYMBOLS iv

ACKNOWLEDGMENTS viii

LIST OF TABLES xiii

LIST OF FIGURES xiv

LIST OF SCHEMES xx

COMPOUND STRUCTURE LEGEND xxii

CHAPTER 1

TYPE I MULTI-ELECTROCHROMIC SWITCHING DEVICES BASED ON *P*-PHENYLENEDIAMINE (PD) REDOX CHEMISTRY

1.1 Electrochromism: Applications from Environmental Sustainability to Wearable Display Technology 1

1.2 Metrics of Electrochromic Materials and Their Devices 4

1.3 The Application of Phenylenediamine Redox Chemistry to Electrochromic Materials 6

1.4.1 Synthesis of **TAPD** 12

1.4.2 Optical and Electrochemical Properties of **TAPD** in Solution State 14

1.4.3 Chemical Stability **TAPD** in Solution State 17

1.4.4 Application of **TAPD** to Singular Type I Absorptive/Transmissive Electrochromic Device 20

1.4.4.1 ITO as a Counter Electrode Material for Singular Electrochromic Devices 24

1.4.4.2 Electrochromic Profile of **TAPD** in Singular Device State 29

1.4.4.3 Multi-Electrochromism: Control of Color by Varying Potential 31

1.4.4.4 Open Circuit Stability: Self Bleaching Feature 33

1.4.4.5 Electrochromic Device Switching in Singular Device State 37

1.4.5 Electrochromic Device Switching in Complementary Dual Device State 39

1.5 Experimental 47

CHAPTER 2

THE SYNTHESIS AND STUDY OF ANIONIC ARYLAMINES AS NEW RADICAL ZWITTERIONS AND ELECTROCHROMIC MOLECULAR SWITCHES

2.1 Introduction 51

2.1.1 Motivation #1: Investigating the Effect of Formal Molecular Charge on Electrochromic Switching Kinetics 51

2.1.2 Motivation #2: Electrochromic Switching Studies as a Platform for the Isolation of New Stable Radicals 54

2.2 Synthesis Characterization of Anionic Aryl Amines: A New Class of Radical Based Internal Salts 55

2.2.1 Synthesis of **AA-SO$_3^-$ Na$^+$** via Indole Sulfonamide Protecting Group 55

2.2.2 Characterization of New Triarylamine Radical Zwitterion: Electrochemistry, Optical Spectroscopy, and Electron Paramagnetic Resonance (EPR) Studies 57

2.2.3 Synthesis of **PD-SO$_3^-$ Na$^+$** via Indole Sulfonamide Protecting Group 62

2.2.4 Characterization of New Phenylenediamine Radical Zwitterion: Electrochemistry, Optical Spectroscopy, and Electron Paramagnetic Resonance (EPR) Studies 64

2.3 Electrochromic Switching of **PD-SO$_3^-$ Na$^+$** vs **TAPD**: The Effect of Molecular Charge on Switching Kinetics in Type I Electrochromic Device State 72

2.3.1 Spectroelectrochemical Response of **PD-Sulfonate** in ECD State: Turn-on and Operating Voltages 72

2.3.2 Multielectrochromic Switching of **PD-Sulfonate** 80

2.4 Perspectives on Future Work: Additional Synthetic Adjustments to Electrochrome Charge State 82

2.5 Experimental 83

CHAPTER 3

DEVELOPMENT OF PHOTOELECTROCHROMIC SWITCHING DEVICES BASED ON REDOX AUXILIARY CATALYSIS

3.1 Introduction 93

3.2 Results and Discussion: Photoelectrochromic Cycling of Redox-Auxiliary Appended Photosystems....97

3.2.1 $(Tol)_3TBABF_4$ as a Gel Electrolyte for Photoelectrochromic Cycling....98

3.2.2 Irradiation of **AA-N-Ts** and Chemical Stability of **AA-Q-Ts** 101

3.2.3 Electrochemistry of **AA-N-Ts** in $(Tol)_3TBABF_4$ Bulk Solution State 102

3.2.4 Oxidative Catalysis of **AA-Q-Ts** to **AA-N-Ts** via Chemical Oxidation in $(Tol)_3TBABF_4$104

3.2.5 Photoelectrochromic Switching of **AA-N-Ts** in Device State....105

3.2.5.1 Turn-On Voltage of **AA-N-Ts** PECD....110

3.2.5.2 Photoelectrochromic Cycling of **AA-N-Ts** in PECD 111

3.2.6. Photoelectrochromic Cycling of **AA-N-Ts** in PECD: Evidence of Redox Auxilliary Catalysis 116

3.2.7 Expanding the Scope: Photoelectrochromic Cycling of RA-Appended Azobenzene Derivatives 121

3.2.8. Towards Totally Automated Photoelectrochemical Switching : 1000 Cycles and Counting....125

3.2.9 Shelf-Life of $(Tol)_3TBABF_4$ – based PECD 128

3.3 Experimental 130

APPENDIX A – NMR Spectra.....139

LIST OF TABLES

1.2.1. Classification of Electrochromic Materials 5

1.3.1. Summary of selected switching data taken from literature.....12

1.4.1. Summary of redox couple data for the **TAPD/HV(BF_4)$_2$** ECD 41

1.4.2. Comparison of results obtained in this work with selected data taken from literature.....43

2.2.1. Summary of electrochemical data for **AA-Sulfonate** and **AA-Sulfonamide** 58

2.2.2 Electrochemical data for **PD-Sulfonate**, **PD-Indole**, and **TAPD** 66

2.2.3. Summary of optical and electrochemical data of **TAPD** and **PD-Sulfonate** 75

3.2.1. Physical properties of (tol)$_3$TBABF_4 100

LIST OF FIGURES

1.1.1. Electrochromic windows in use at Chabot College in Hayward, CA. 2

1.1.2. Cooling energy vs. Electric Lighting energy per unit of floor area for different types of chromogenic and non-chromogenic windows 3

1.3.1. Wurster dye redox chemistry. 8

1.3.2. Representative structures of PD polyamides. 9

1.3.3. Spectroelectrochemical profile of PD polyamides. 10

1.3.4. TMPD/**HV** electrochromic device. 11

1.3.1. Structures of **TMPD** and **TAPD**.....12

1.4.1. Cyclic voltammogram of 1.0 mM **TAPD** at Pt disc electrode in CH_2Cl_2 (0.1 M Bu_4NBF_4) at 100 mVs^{-1} scan rate. 15

1.4.2 UV-vis optical absorption spectra for **TAPD** (1.03 x 10^{-5} M in acetonitrile).....16

1.4.3 UV-vis optical absorption spectra for $\mathbf{TAPD^{\cdot+}\ NO_3^-}$ (1.03 x 10^{-5} M in acetonitrile).....16

1.4.4 UV-vis optical absorption spectra for $\mathbf{TAPD^{2+}\ (NO_3)_2^{2-}}$ (1.03 x 10^{-5} M in acetonitrile) 17

1.4.5. Time-resolved UV-vis optical absorption spectra for $\mathbf{TAPD^{\cdot+}\ (PF_6)}$ (1.29 x 10^{-5} M) in HPLC-grade acetonitrile). 18

1.4.6. Time-resolved UV-vis optical absorption spectra for $\mathbf{TAPD^{++}\ (PF_6)_2}$ (1.29 x 10^{-5} M in HPLC-grade acetonitrile).....19

1.4.7. Time-resolved UV-vis optical absorption spectra for $\mathbf{TAPD^{++}\ (PF_6)_2}$ (1.29 x 10^{-5} M in HPLC-grade acetonitrile with 2.5 v/v% TFAA) 19

1.4.8. Generic operation of Type I Absorptive/Transmissive Electrochromic Device.....21

1.4.9. Photograph of prepared electrochromic device with labeled components 23

1.4.10. ECD Spectroelectrochemistry Apparatus 23

1.4.11. General schematic of an electrochromic device with two-electrode set-up 24

1.4.12. ITO electrochromism 28

1.4.13. Cyclic Voltammetry at 50 mV/s of ITO electrode in 1M $LiClO_4$ in propylene carbonate 28

1.4.14. 3D optical profile of **TAPD** in the device state after the application of 3 V for 30 s.....29

1.4.15. Time-resolved UV-vis optical absorption spectra of the first color transition, corresponding to the formation **TAPD**$^{\cdot+}$(brownish-red) from **TAPD** (colorless) 30

1.4.16. Time-resolved UV-vis optical absorption spectra of the second color transition, corresponding to the formation **TAPD**$^{++}$ (blue) from **TAPD**$^{\cdot+}$ (brownish-red).....31

1.4.17. Spectroelectrochemical response of **TAPD** in ECD. Each voltage is held for 30 s, until steady state current is reached.....32

1.4.18. Pictures of **TAPD** ECD at chosen operating voltages 33

1.4.19. Time-resolved UV-vis optical absorption spectra of **TAPD** in the "On" device state.....34

1.4.20. Time-resolved UV-vis optical absorption spectra of **TAPD** in the "Off" device state 35

1.4.21 Bleaching time comparison of the "blue" absorbance band (766 nm) and the reddish brown absorbance band (414 nm).....36

1.4.22. Generic representation of recombination process in **TAPD** based singular ECD.....37

1.4.23. Electrochromic switching of **TAPD** at 766 nm 38

1.4.24. Cyclic voltammogram of 1.0 mM **$HV(BF_4)_2$** at Pt disc electrode in propylene carbonate (0.1 M Bu_4NBF_4) at 200 mVs^{-1} scan rate 40

1.4.25. Cyclic voltammogram of **TAPD/$HV(BF_4)_2$** ECD at 100 mVs^{-1} 41

1.4.26. Spectroelectrochemical response of **TAPD/$HV(BF_4)_2$** dual-type ECD at low potentials (0.0-0.6 V).....41

1.4.27. **TAPD/$HV(BF_4)_2$** dual-type ECD at various applied potentials, 0.0 V-2.5 V. Each potential was held 30 s, until steady state current reached 42

1.4.28. TAPD/HV(BF_4)$_2$ dual-type ECD at various applied voltages.....42

1.4.29. Electrochromic switching of **TAPD/HV(BF_4)$_2$** dual-type ECD (On= 0.8 V for 4 s, Off= 0.0 V for 4 s) at 766 nm (a), 414 nm (b), and 600 nm (b) 44

1.4.30. Electrochromic cycling of **TAPD/HV(BF_4)$_2$** dual-type ECD using operating voltages of 2.5 V (a) and 0.8 V (b).....45

2.1.1. Pictorial demonstration of rationale behind the design of the anionic PD electrochrome 54

2.2.1. Cyclic voltammogram of 1.0 mM **AA-Sulfonate** (**4**) (blue line) and 1.0 mM (**3**) (red dashed line) at Pt disc electrode in MeCN (0.1 M Bu_4NBF_4) at 50 mVs^{-1} scan rate.....58

2.2.2. Structure and oxidation potential of Orange CRET (CRET).....59

2.2.3. Chemical stability of 7.84x10^{-5} M **AA-Sulfonamide** radical cation (**3**$^{\cdot+}$). in CH_2Cl_2.....60

2.2.4 Chemical stability of 6.87 x10^{-5} M **AA-Zwitterion** (**5**) in CH_2Cl_2 61

2.2.5 EPR spectra of **AA-Zwitterion** (**5**) in CH_2Cl_2 (0.05 mM) at 22° C.....62

2.2.7 Cyclic voltammogram of 1.0 mM **PD-Indole** at Pt disc electrode in MeCN (0.1 M Bu_4NBF_4) at 50 mVs^{-1} scan rate 65

2.2.8 Cyclic voltammogram of 1.0 mM **PD-Sulfonate** (purple solid) and **TAPD** at Pt disc electrode in MeCN (0.1 M Bu_4NBF_4) at 50 mVs^{-1} scan rate.....66

2.2.9. Structure and oxidation potential of $Th^{\cdot+}ClO_4^-$ 67

2.2.10. UV-vis scale redox titration of **PD-Sulfonate (**5.46x10^{-5} M in CH_2Cl_2) with $Th^{\cdot+}ClO_4^-$ 67

2.2.11. Time-resolved Optical Spectra of **PD-Zwitterion** after oxidation of **PD-Sulfonate** (1.12x10^{-4} M in CH_2Cl_2) with 1 eq. CRET.....68

2.2.12. UV-vis scale titration of **PD-Zwitterion** (5.46x10^{-5} M in CH_2Cl_2) with $Th^{\cdot+}$ ClO_4^- 69

2.2.13. UV-vis scale titration of **PD-Zwitterion** (5.46x10^{-5} M in CH_2Cl_2) with $Th^{\cdot+}$ ClO_4^- 70

2.2.14. EPR spectra of **PD-Zwitterion** in CH_2Cl_2 (0.05 mM) at 22° C.....71

2.2.15. Electron spin resonance (ESR) spectra on 0.05 mM **TAPD$^{\cdot+}$ ClO_4^-** at 22° C 71

2.3.1. General Schematic of Type I ECD 72

2.3.2. Spectroelectrochemical response of **PD-Sulfonate** in ECD singular device state 73

2.3.4. Absorbance at 422 nm as a result of applied voltages between 0-2 V 74

2.3.5. Absorbance at 780 nm as a result of applied voltages between 0-2 V 75

2.3.6 Electrochemical coloration of **TAPD** (.00754 M gel in electrolyte) in ECD state.....76

2.3.7 Open circuit bleaching of **TAPD** (.00754 M in gel electrolyte) in ECD state 77

2.3.8 Electrochemical coloration of **PD-Sulfonate** (.00934 M in gel electrolyte) in ECD state...78

2.3.9 Open circuit bleaching of **PD-Sulfonate** (.00934 M in gel electrolyte) in ECD state. 78

2.3.10. Electrochromic switching of **PD-Sulfonate** (.0116 M in gel electrolyte) in singular ECD from reddish brown to colorless 80

2.3.11. Electrochromic switching of **PD-Sulfonate** (.0116 M in gel electrolyte) in singular ECD to blue colored state 81

2.4.1. Generic illustration of potential PD-based cationic/anionic electrochromes.....82

3.1.1. Cartoon of redox auxiliary effect.....95

3.2.1. Photograph of $(tol)_3TBABF_4$ /toluene heterogeneous mixture 100

3.2.2. Cyclic voltammogram of $(tol)_3TBABF_4$ with scan rate of 100 mV/s at Pt disc electrode 100

3.2.3. Irradiation of 0.97 mM AA-N-Ts in $(tol)_3TBABF_4$ using an arc lamp equipped with 385 nm filter.....102

3.2.4. Photograph showing the negative photochromism of **AA-N-Ts**/**AA-Q-Ts** system 102

3.2.5. Cyclic Voltammetry (CV)of 0.97 mM **AA-N-Ts** (**N**) in $(tol)_3TBABF_4$ Bulk Solution State 103

3.2.6. Cyclic Voltammograms of 1.0 mM **AA-N-Ts (N)** (red dash) and 1.0 mM **AA-Q-Ts (Q)** (green dot) 104

3.2.7. Electrochemical response of **AA-Q-Ts** (0.97 mM in $(Tol)_3TBABF_4$) at Pt disc electrode 104

3.2.8. Catalytic conversion of **AA-Q-Ts** (1.0 mM) to **AA-N-Ts** after addition of 1 mol% CRET

.....105

3.2.9. Generic representation of photoelectrochromic device with labeled components 106

3.2.10. Picture of **AA-N-Ts**/**AA-Q-Ts** negative photochromism in the device state.....106

3.2.11. Photograph of PECD apparatus equipped with 380 nm LED flashlight 107

3.2.12. Irradiation of .00765 M **AA-N-Ts** to **AA-Q-Ts** with arc lamp in PECD state.....108

3.2.13. Irradiation of .01 M **AA-N-Ts** to **AA-Q-Ts** with 380 nm LED in PECD state.....109

3.2.14. Electrochemical back conversion of **AA-Q-Ts** to **AA-N-Ts** in PECD state.....110

3.2.15. Absorbance vs applied voltage data for .00934 M **AA-N-Ts** in PECD.....111

3.2.16. Photoelectrochromic cycling of 0.00798 M **AA-N-Ts** in PECD. (a) A single cycle with labeled segments 112

3.2.17. Overlay (a) and blow-up (b) of optical spectra from cycles 2, 5, 8, 11, 14, and 17 of figure 3.2.16 113

3.2.18. Photoelectrochromic cycling of **AA-N-Ts** PECD's with various cell gaps 115

3.2.19. Photoelectrochromic cycling of 0.00750 M **AA-N-Ts** PECD with an extended **AA-N-Ts** hold time 116

3.2.20. Time resolved optical spectra of **AA-N-Ts** PECD irradiation. Spectra taken every 5 s 117

3.2.21. Time resolved optical spectra of **AA-Q-Ts** PECD as 1.5 V is applied for 5 s. 117

3.2.22. Absorbance vs time profile of **AA-Q-Ts** PECD as 1.5 V is applied for 5 s.....118

3.2.23. Calculation process for % of $\mathbf{N}^{\cdot+}$ generated at electrode 119

3.2.24. Background current of **AA-N-Ts** (00728 M) PECD at 1.4 V.....120

3.2.25. Actual values used to calculate $\%N^{\cdot+}$ 120

3.2.26. Photograph of ***trans*** **AA-NN-Ph** PECD 122

3.2.27. Irradiation of 0.00733 M *trans* **AA-NN-Ph** PECD to yield *cis* **AA-NN-Ph** in photostationary state (PSS) 122

3.2.28. Electrochemical back conversion of *cis* **AA-NN-Ph** to *trans* **AA-NN-Ph**.....123

3.2.29. 100 photoelectrochromic switching cycles in .0083 M **AA-NN-Ph** in PECD 124

3.2.30. Optical absorbance spectra of *cis* and *trans* **AA-NN-Ph** every 20 cycles during the 100 cycles shown in figure 3.2.29 125

3.2.31. Photograph of automated photoelectrochromic cycling set-up. 126

3.2.32. Automated photoelectrochromic cycling (> 250) of **AA-NN-An** 127

3.2.33. Automated photoelectrochromic cycling (> 1300) of **AA-NN-An** 127

3.2.34 Shelf life study of 0.00728 M **AA-N-Ts** / $(Tol)_3$ $((Bu_4N)BF_4)$ based PECD 129

LIST OF SCHEMES

1.4.1 Synthesis of **TAPD** 14

1.4.2. TAPD redox chemistry 15

1.4.3. Redox scheme for heptyl viologen (**HV**) 39

2.1.1. Bipyridil redox chemistry 54

2.2.1. Synthesis of **AA-Sulfonate** (**4**) and **AA-Zwitterion** (**5**) 56

2.2.2. Electrochemistry of **AA-Sulfonamide** 57

2.2.3. Electrochemistry of **AA-Sulfonate** 57

2.2.4. Electrochemistry of dianisylphenylamine 58

2.2.5. Synthesis of **PD-Sulfonate** 63

2.2.6. Electrochemistry of **PD-Indole** 64

2.2.7. Electrochemistry of **PD-Sulfonate** 65

2.2.8. Disproportionation reaction of **PD-Sulfonate** and **PD-Cation** 79

3.1.1. Photo/thermal cycling between **AA-N.-Ts** and **AA-Q-Ts** 95

3.1.2. Photo/electrochemical cycling between **AA-N-Ts** and **AA-Q-Ts** 96

3.1.3. Photoelectrochromic cycling mechanism 96

3.1.4. Photoelectrochromic cycling between **AA-N-Ts** and **AA-Q-Ts** 97

3.2.1. Photochemical conversion of **AA-N-Ts** to **AA-Q-Ts** 101

3.2.2. Oxidative back conversion of **AA-Q-Ts** to **AA-N-Ts** with CRET 105

3.2.3. Photochemical conversion of **AA-N-Ts** to **AA-Q-Ts** 108

3.2.4. Electrochemical back conversion of **AA-Q-Ts** to **AA-N-Ts** with 1.5 V.....110

3.2.5. Photoelectrochemical cis/trans isomerism of **AA-NN-Ph**.....121

COMPOUND STRUCTURE LEGEND

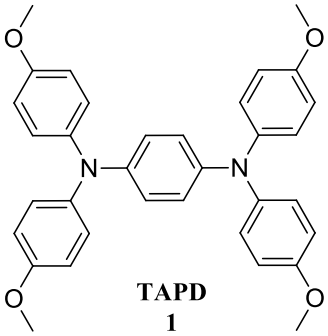

TAPD
1

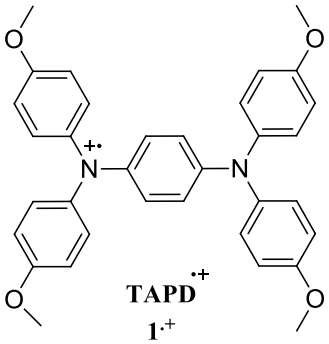

TAPD$^{\cdot+}$
1$^{\cdot+}$

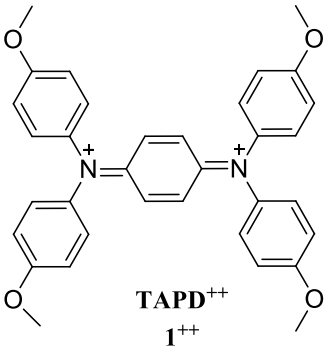

TAPD^{++}
1^{++}

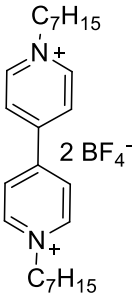

HVBF$_4$
3

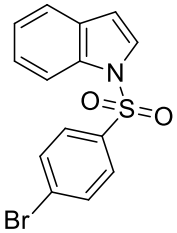

4

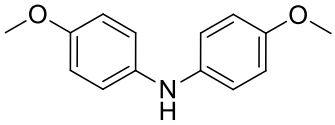

5

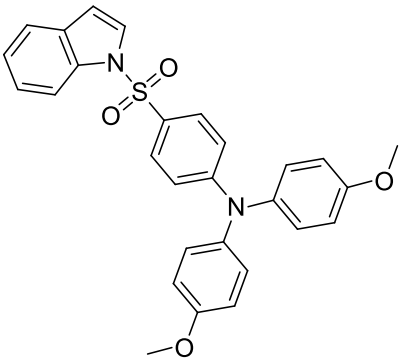

AA-Sulfonamide
6

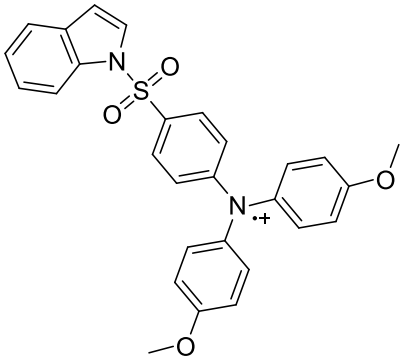

AA-Sulfonamide$^{\cdot+}$
6$^{\cdot+}$

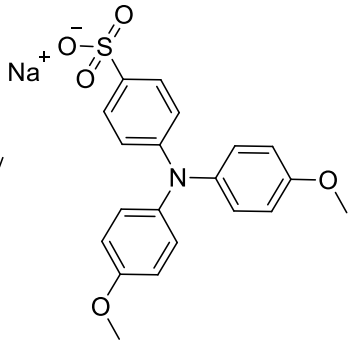

AA-Sulfonate
7

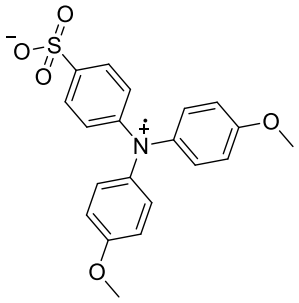

AA-Zwitterion
8

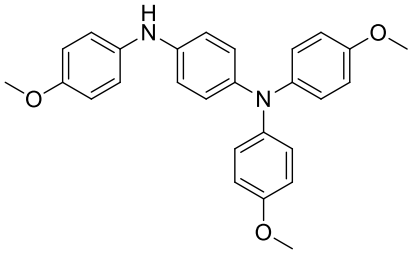

9

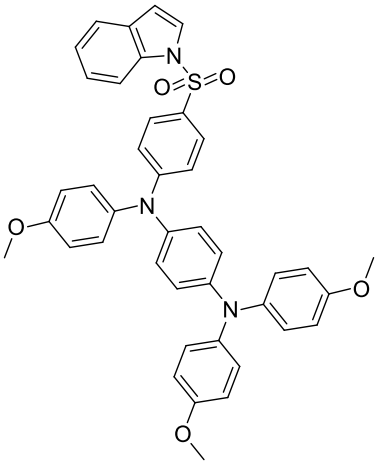

PD-Sulfonamide
10

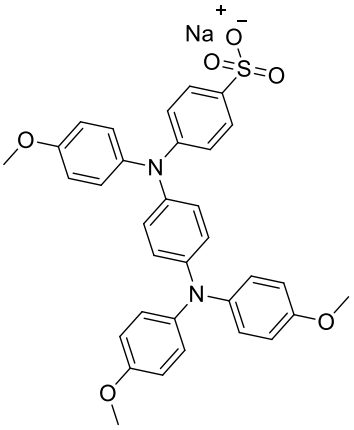

PD-Sulfonate
11

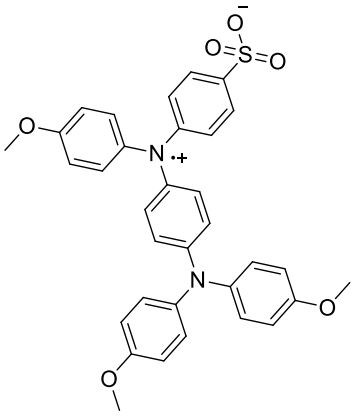

PD-Zwitterion
12

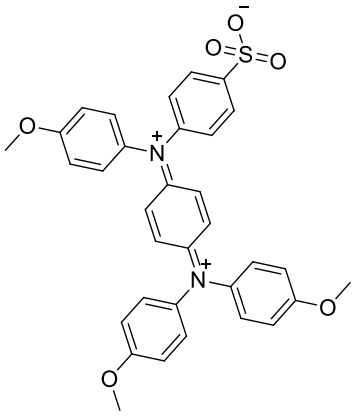

PD-Cation
13

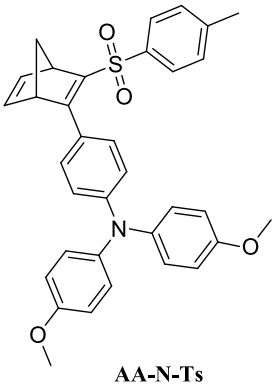

AA-N-Ts
14

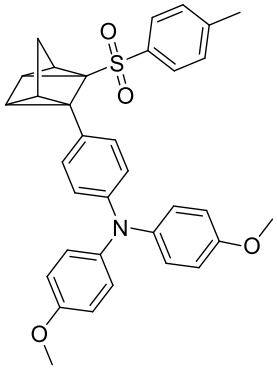

AA-Q-Ts
15

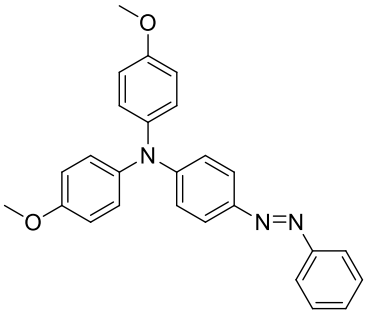

***trans* - AA-NN-Ph**
16

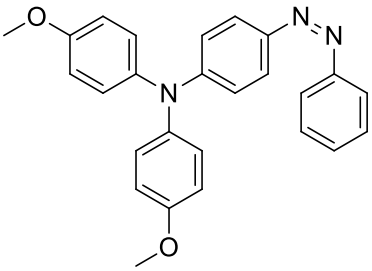

***cis* - AA-NN-Ph**
17

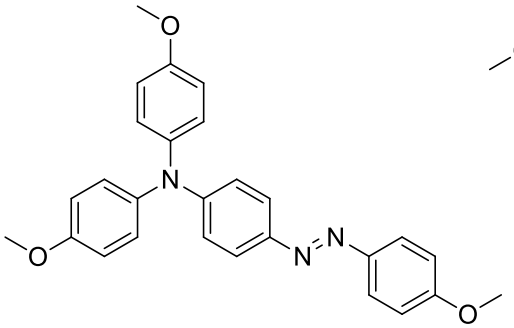

***trans* - AA-NN-An**
18

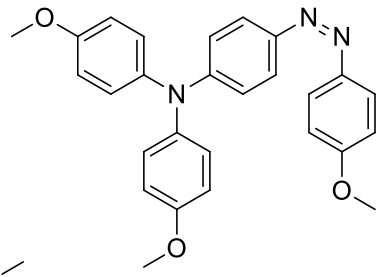

***cis* - AA-NN-An**
19

Chapter 1

Type I Multi-Electrochromic Switching Devices based on *p*-Phenylenediamine (PD) Redox Chemistry

"….the ability to survive depends on the ability to adapt to climate change and to the reduction of the sustenance resources, caused by an increase in population, and the impoverishment of natural resources, which naturally occurs." –Charles Darwin in *The Origin of Species, by means of Natural Selection*[1]

1.1 Electrochromism: Applications from Environmental Sustainability to Wearable Display Technology

Electrochromic (EC) technology aims to exploit functional materials that modulate electromagnetic radiation in response to an applied electrical bias.[2,3,4] Electrochromic (Smart)

[1] Darwin, C. *The Origin of Species, by Means of Natural Selection*; John Murray: London, 1859.
[2] Monk, P.M.S.; Mortimer, R. J.; Rosseinsky, D. R. *Electrochromism and Electrochromic Devices;* Cambridge: UK, 2007.
[3] Monk, P.M.S.; Mortimer, R. J.; Rosseinsky, D. R. *Electrochromism: Fundamental and Applications;* VCH: Weihein, 1995.
[4] Mortimer, R. J. Electrochromic Materials. *Annual Review of Materials Research* **2011,** *41,* 241-268.

windows for buildings (Figure 1.1.1) are currently a fairly lucrative commodity, lowering architectural energy cost in comparison to the standard low-emittance coatings.[5]

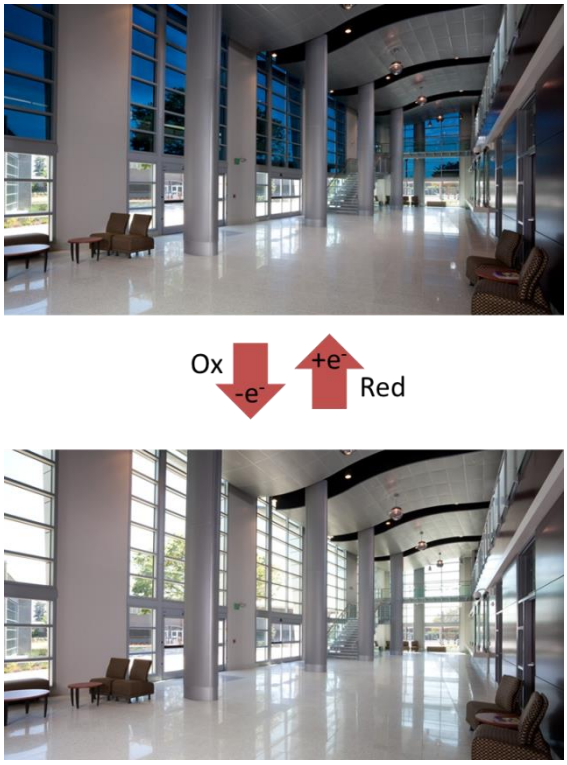

Figure 1.1.1. Electrochromic windows in use at Chabot College in Hayward, CA. Taken from www.sageglass.com

Figure 1.1.2 has been reproduced from a study carried out by Madison Gas and Electric Company of Madison, WI.[6] While thermochromic materials reduced the company's need for cooling by transmitting and absorbing heat, photochromic materials reduced the company's lighting energy by responding to sunlight. Modulation of electrochromic windows occur

[5] Roberts, D. R. *Preliminary Assessment of the Energy-Saving Potential of Electrochromic Windows in Residential Buildings*; NREL/TP-550-46916; National Renewable Energy Labs: December 2009, 2009; pp 1-12.

[6] http://www.mge.com/saving-energy/business/bea/_escrc_0013000000DP22YAAT-2_BEA1_PA_PA_BuildingEnvelope_PA-06.html

independently of temperature or exposure to light, placing electrochromic technology with the operational advantage of being able to modulate both heat and light at the user's pleasure. As a result, electrochromic smart windows performed superiorly to both photochromic and thermochromic windows by lowering *both* cooling and electric lighting energy.

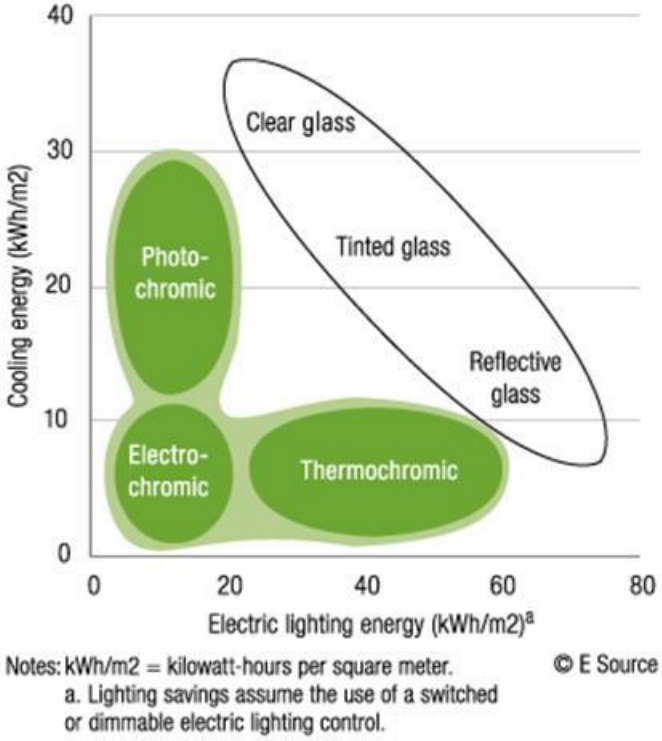

Figure 1.1.2. Cooling energy vs. Electric Lighting energy per unit of floor area for different types of chromogenic and non-chromogenic windows. Taken from ref. 6

There is also opportunity for commercialization in the areas of electrochromic displays and textiles. Recent accounts have demonstrated that electrochromic fabrics can be obtained by simply coating a conducting fabric substrate with an electrochromic material. Semiconducting fabric substrates have been prepared by soaking commercial Lycra spandex, cotton, or stainless steel mesh in a conducting polymer, namely PEDOT:PSS. Conductivities range from ca. 0.1

S/cm to 9800 S/cm for the Lycra and stainless steel, respectively.[7,8] Metal-plated conducting fabrics have also been used in literature accounts as substrates for electrochromic fabric studies.[9] Nickel, copper, or silver plated materials are available commercially (LessEMF, Inc.). It is in these areas that new electrochromic materials as developed by our research could find relevance. The ability of an electrochromic system to exhibit multiple colors with respect to applied voltage is particularly desired for aesthetic electrochromic applications such as electrochromic fabrics.

In parallel to more mature disciplines like photovoltaics, light-emitting diodes, or semiconductors, electrochromic device (ECD) materials have a range of chemical compositions (metal oxides, organometallic complexes, conjugated polymers, etc.) with the organic based materials gaining attention more recently. Organic EC materials have the benefits of compatibility with flexible substrates, preparation from relatively cheap materials, and synthetic tunability.

1.2 Metrics of Electrochromic Materials and Their Devices

Materials that exhibit electrochromic behavior are classified based on the solubility and phase state of their various redox states.[10,11,12] A type I electrochrome is characterized as being

---

[7] Iverndale, M.A.; Ding, Y.; Sotzing, G. A. All Organic Electrochromic Spandex. *ACS Appl. Mater. Inter.* **2010,** *2*, 296-300.
[8] Ding, Y.; Inverndale, M.A.; Sotzing, G. A. Conductivity Trends of PEDOT-PSS Impregnated Fabric and the Effect of Conductivity on Electrochromic Textile. *ACS Appl. Mater. Inter.* **2010,** *2*, 1588-1593.
[9] Beaupre´, S.; Dumas, J.; Leclerc, M. Toward the Development of New Textile/Plastic Electrochromic Cells Using Triphenylamine-Based Copolymers. *Chem. Mater.* **2006**, *18*, 4011-4018.
[10] Monk, P.M.S.; Mortimer, R. J.; Rosseinsky, D. R. *Electrochromism and Electrochromic Devices;* Cambridge: UK, 2007.

soluble in each optical state, forming electrochromic liquid states. A type II electrochrome has mixed solubility, existing as both an electrochromic solution and as an electrochromic film deposited onto the electrode. In type III electrochromism, the color switching material exists solely as an insoluble thin film on an electrode surface. Table 1.2.1 gives examples of electrochromes of each type with their respective patented applications.[13,14,15]

Type of Electrochrome	Example(s)	Application(s)
I	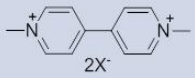 Methyl Viologen (MV) Tetramethylphenylenediamine (TMPD)	Gentex Night Vision System (NVS©) Mirror
II	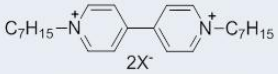 Heptyl Viologen (HV)	Electrochromic Paper
III	WO_3 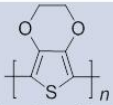 poly(3,4-ethylenedioxythiophene) (PEDOT)	Electrochromic Aircraft Windows (Boeing 757)

Table 1.2.1. Classification of electrochromic materials with example systems and applications.

While parameters for electrochromic materials and devices are application dependent, they are generally characterized by several criteria: [10,11,12]

Description of Color - The color of an electrochromic system is described by its optical spectra of associated redox states in terms of absorption, transmission, or reflectance at various

---

[11] Monk, P.M.S.; Mortimer, R. J.; Rosseinsky, D. R. *Electrochromism: Fundamental and Applications;* VCH: Weihein, 1995.
[12] Mortimer, R. J. Electrochromic Materials. *Annual Review of Materials Research* **2011,** *41*, 241-268.

[13] Byker, H. J. Single-Compartment, Self-erasing, Solution-Phase Electrochromic Devices, solutions for use therein and uses thereof. U.S. Patent 5751467, 1987.
[14] Mortimer, R.J.; Warren, C. P. Cyclic Voltammetric Studies of Prussian Blue and Viologens within a Paper Matrix for Electrochromic Printing Applications. *J. Electroanal. Chem.* **1999,** *460*, 263-266.
[15] www.gentex.com/aerospace/aircraft-windows

wavelengths. In addition, systems are qualitatively described by their appearance to the human eye. *In-situ* colorimetric analysis has recently been developed to numerically describe the color of electrochromic materials in terms of hue, saturation, and brightness.[16,17,18,19]

Optical Contrast - The optical contrast (or contrast ratio) of an electrochromic system describes the changes in color intensity between optical states. It is expressed as a change in percent transmission (Δ%T) at a particular λ_{max}. The contrast ratio (CR) of an electrochromic system is the ratio of the transmittance or reflectance in the bleached state to the transmittance or reflectance in the colored state(s).

Electrochromic Switching Time - With respect to an applied voltage, the electrochromic switching time is defined as the amount of time required to generate 90% of an optical state after which time, the color change is no longer detectable by the eye.

Device Cycle Life (Duty Cycle) - The cycle life of an electrochromic system is reported as a number of electrochromic switching cycles under a set of specific conditions with a specified retention of optical contrast. Additionally, any degradation of the optical contrast is reported. For display applications, about 10^5 cycles with a deterioration of $\Delta T\% \leq 50\%$ is acceptable.

1.3 The Application of Phenylenediamine Redox Chemistry to Electrochromic Materials

[16] Thompson, B. C.; Schottland, P.; Zong, K.; Reynolds, J.R. In Situ Colorimetric Analysis of Electrochromic Polymers and Devices. *Chem. Mater.* **2000,** *12,* 1563-1571.
[17] Thompson, B. C.; Schottland, P., Sonmez, G.; Reynolds, J. R. In Situ Colorimetric Analysis of Electrochromic Polymers and Devices. *Synthetic Metals* **2001,** *119,* 333-334.
[18] Sonmez, G.; Meng, H.; Wudl, F. Organic Polymeric Electrochromic Devices: Polychromism with Very High Coloration Efficiency. *Chem. Mater.* **2004,** *16,* 574-580.
[19] Mortimer, R. J.; Reynolds, J. R. In- situ Colorimetric and Composite Coloration Efficiency Measurements for Electrochromic Prussian Blue. *J. Mater. Chem.* **2005,** *15,* 2226-2233.

Arylamine redox chemistry has gained considerable notoriety for its application in the development of organic electronic devices (light-emitting diodes, field effect transistors, bulk heterojunction solar cells, etc).[20] Phenylenediamine (PD) derivatives have drawn interest due to their robust anodic electrochemistry leading to stable, often isolable, amminium cation salts.[21,22,23,24,25,26] To understand charge dynamics and distribution in the positively charged oxidation states, optical spectroscopy is employed,with an emphasis on evaluation of any near-IR bands resulting from low energy intervalence electronic transitions.[27,2829,30] A notable feature of

---

[20] (a) Grimsdale, A. C.; Chan, K. L.; Martin, R. E.; Jokisz, P. G.; Holmes, A. B. Synthesis of Light-Emitting Conjugated Polymers for Applications in Electroluminescent Devices. *Chem. Rev.* **2009,** 109, 897−1091. (b) Brabec, C.; Scherf, U.; Dyakonov, V. Organic Photovoltaics: Materials, Device Physics, and Manufacturing Technologies; Wiley-VCH: Weinheim, Germany, 2008. (c) Allard, S.; Forster, M.; Souharce, B.; Thiem, H.; Scherf, U. Organic Semiconductors for Solution-Processable Field-Effect Transistors. *Angew. Chem., Int. Ed.* **2008,** *47*, 4070−4098. (d) Borsenberger, P. M.; Weiss, D. S. Organic Photoreceptors for Xerography; Marcel Dekker Inc.: New York, 1998.

[21] Selby, T. D.; Blackstock, S. C. Preparation of a Redox Gradient Dendrimer. Polyamines Designed for One-Way Electron Transfer and Charge Capture. *J. Am. Chem. Soc.* **1998,** *120*, 12155.

[22] Kim, K.-Y. Polyarylamino Redox Arrays for Control of Charge Transport and Charge Storage. Ph.D. Dissertation, The University of Alabama, Tuscaloosa, AL, 2003.

[23] Selby, T. D.; Kim, K.-Y.; Blackstock, S. C. Patterned Redox Arrays of Polyarylamines I. Synthesis and Electrochemistry of a *p*-Phenylenediamine and Arylamino-Appended *p*-Phenylenediamine Arrays. *Chem. Mater.* **2002,** *14*, 1685.

[24] Kim, K.-Y.; Hassenzahl, J. D.; Selby, T. D.; Szulczewski, G. J.; Blackstock, S. C. Patterned Redox Arrays of Polyarylamines II. Growth of Thin Films and Their Electrochemical Behavior. *Chem. Mater.* **2004,** *14*, 1691.

[25] Li, J. C.; Kim, K.-Y.; Blackstock, S. C.; Szulczewski, G. J. Patterned Redox Arrays of Polyarylamines III. Effect of Molecular Structure and Oxidation Potential on Film Morphology and Hole-Injection in Single-Layer Organic Diodes. *Chem. Mater*. **2004,** *16*, 4711.

[26] Gray, L.T. The Application of Arylamines as Redox Auxiliaries, Polar Crystals and Organic Semiconductors. Ph.D Dissertation, The University of Alabama, Tuscaloosa, AL, 2012.

[27] Nelsen, S. F.; Tran, H. Q.; Nagy, M. A. Comparison of V Values for Some Nitrogen- and Metal-Centered π-Bridged Mixed-Valence Compounds. *J. Am. Chem. Soc.* **1998,** *120*, 298-304.

[28] Lambert, C.; Nöll, G. The Class II/III Transition in Triarylamine Redox Systems. *J. Am. Chem. Soc.* **1999,** *121*, 8434-8442.

[29] Ito, A.; Sakamaki, D.; Ichikawa, Y.; Tanaka, K. Spin-Delocalization in Charge State of *para*-Phenylene-Linked Dendritic Oligoarlamines. *Chem. Mater.* **2011,** *23*, 841-850.

these systems is that while the neutral arylamine is often colorless (absorbing mainly in the UV region), each oxidation state is characterized by an intense color (figure 1.3.1). It is this reversible modulation of optical absorption in the visible region of the electromagnetic spectrum as a result of changes in electron content along with the robust stability of the redox states of these systems that makes phenylenediamines especially attractive components of multi-colored electrochromic materials.

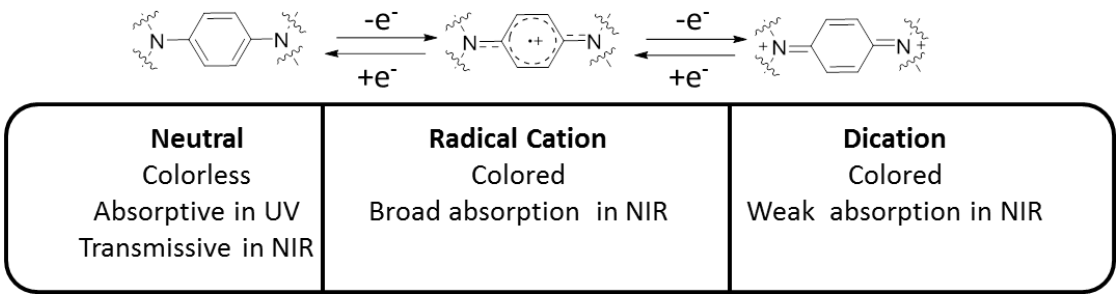

Figure 1.3.1. Redox chemistry of phenylenediamines (Wurster dyes) with general description of optical behavior in each redox state.

Multielectrochromic thin films have been prepared based on polyamides with phenylenediamino (PD) pendant groups.[31,32,33] As figure 1.3.2 shows, linkages vary, with the *p*-phenoxy linkage producing polymeric electrochromes able to switch up to 10,000 cycles.[30] The colorless-green-blue multielectrochromism in the films is directly attributable to phenylenediamine redox chemistry, which is described by three distinct redox/optical states

---

[30] Hankache, J.; Wenger, O. Organic Mixed Valence. *Chem. Rev.* **2011,** *111,* 5138-5178.
[31] Hsiao, S-H.; Liou, G-S.; Kung, Y-C.; Yen, H-J. High Contrast Ratio and Rapid Switching Electrochromic Polymeric Films Based on 4-(Dimethylamino)triphenylamine-Functionalized Aromatic Polyamides. *Macromolecules,* **2008,** *41,* 2800-2808.
[32] Liou, G-S.; Chang, C-W. Highly Stable Anodic Electrochromic Aromatic Polyamides Containing *N,N,N´,N´* - Tetraphenyl- *p*- Phenylenediamine Moieties: Synthesis, Electrochemical, and Electrochromic Properties. *Macromolecules,* **2008,** *41,* 1667-1674.
[33] Yen, H-J.; Liou, G-S. Solution-Processable Novel Near-Infared Electrochromic Aromatic Polyamides Based on Electroactive Tetraphenyl-*p*- Phenylenediamine Moieties. *Chem. Mater.* **2009,** *21,* 4062-4070.

(figure 1.3.3). We seek to expoit this multielectrochromic feature of molecular phenylenediamines as liquids in electrochromic devices.

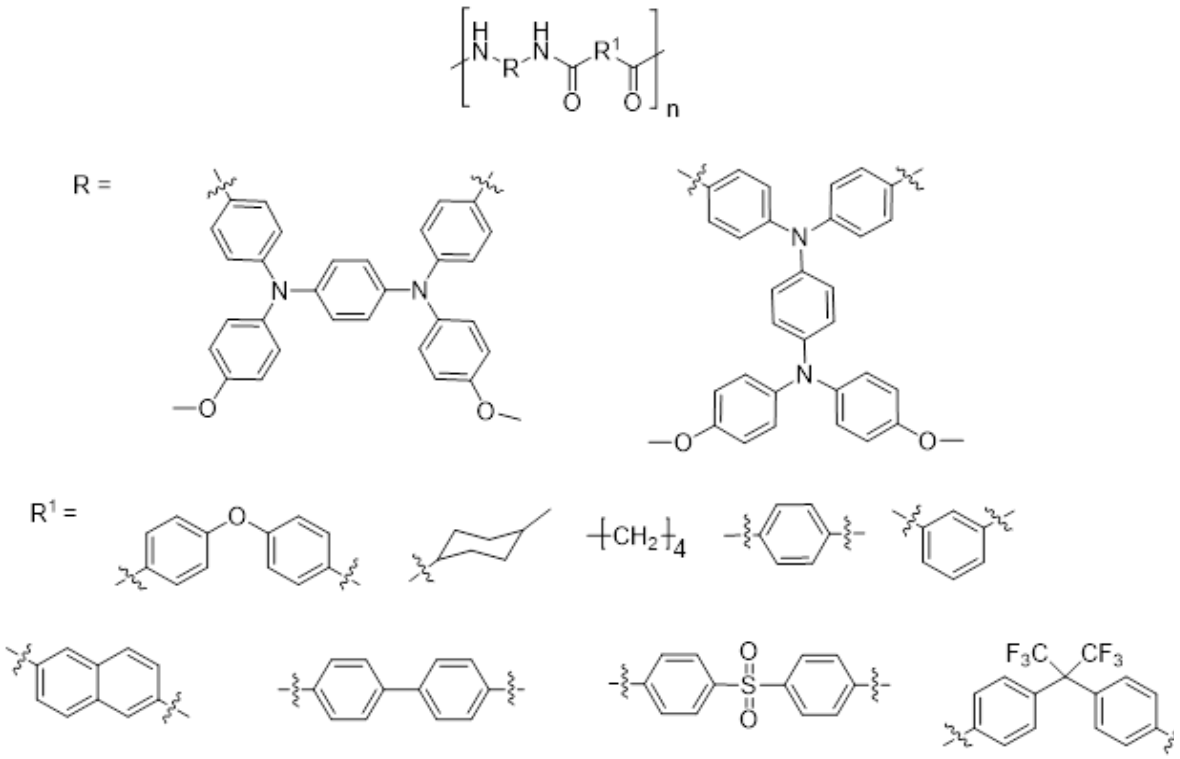

Figure 1.3.2. Representative structures of electrochromic PD polyamides (references 29, 30, 31).

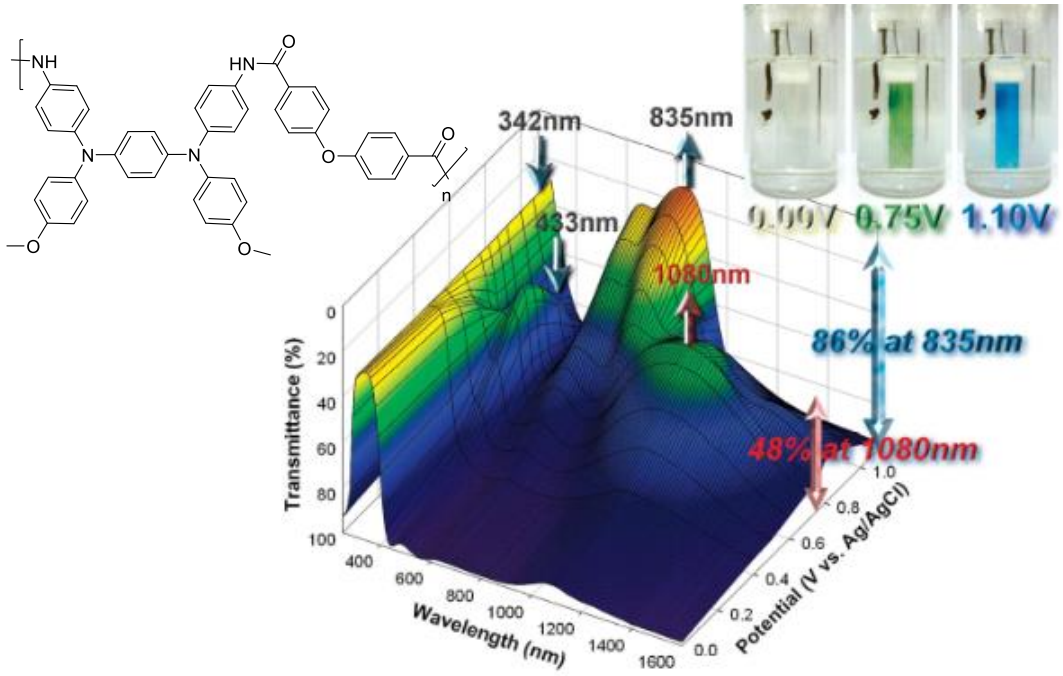

Figure 1.3.3. Multielectrochromic spectroelectrochemical profile of PD polyamide. Optical contrast values at 835 nm and 1080 nm are shown as well as the photographs of the polymer films at 0.0 V, 0.75 V, and 1.10 V (vs Ag/AgCl). Figure taken from reference 30.

To our knowledge, there are only two published examples of aryl amines being used as electrochromic molecular dyes in solution based Type I electrochromic devices, one cell by K. C. Ho and another by N. Leventis.[34,35,36] In both examples, N,N, N´, N´-tetramethyl-1,4-phenylenedamine (TMPD) was used as a charge balancing, solution-phase counter electrochrome. As the primary electrochrome, both studies used 1,1´-diheptly-4,4´-bipyridium (heptyl viologen; HV). The electrochromic cell (shown in figure 1.3.4) is only capable of undergoing one color change reversibly, the one electron reduction of the HV^{2+} and subsequent one electron oxidation of TMPD (colorless)- yielding $HV^{\cdot+}$ and $TMPD^{\cdot+}$ (blue), respectively.

[34] Ho, K. C.; Fang, Y-W.; Hsu, Y-C; Chen, L-C. The Influences of Operating Voltage and Cell Gap on the Performance of a Solution-Phase Electrochromic Device Containing HV and TMPD. *Solid State Ionics* **2003,** *165,* 279-287.
[35] Ho, K. C.; Fang, Y-W.; Hsu, Y-C; Yu, F.-C. A Study on the Electro-Optical Properties of HV and TMPD with Their Application in Electrochromic Devices. *Proc. Electrochem. Soc.***2003,** *2003-17,* 266-278.
[36] Leventis, N.; Chem, M.; Liapis, A. I.; Johnson, J. W.; Jain, A. Characterization of 3 x 3 Matrix Arrays of Solution-Phase Electrochromic Cells. *J. Electrochem. Soc.* **1998,** *145,* L55-L58.

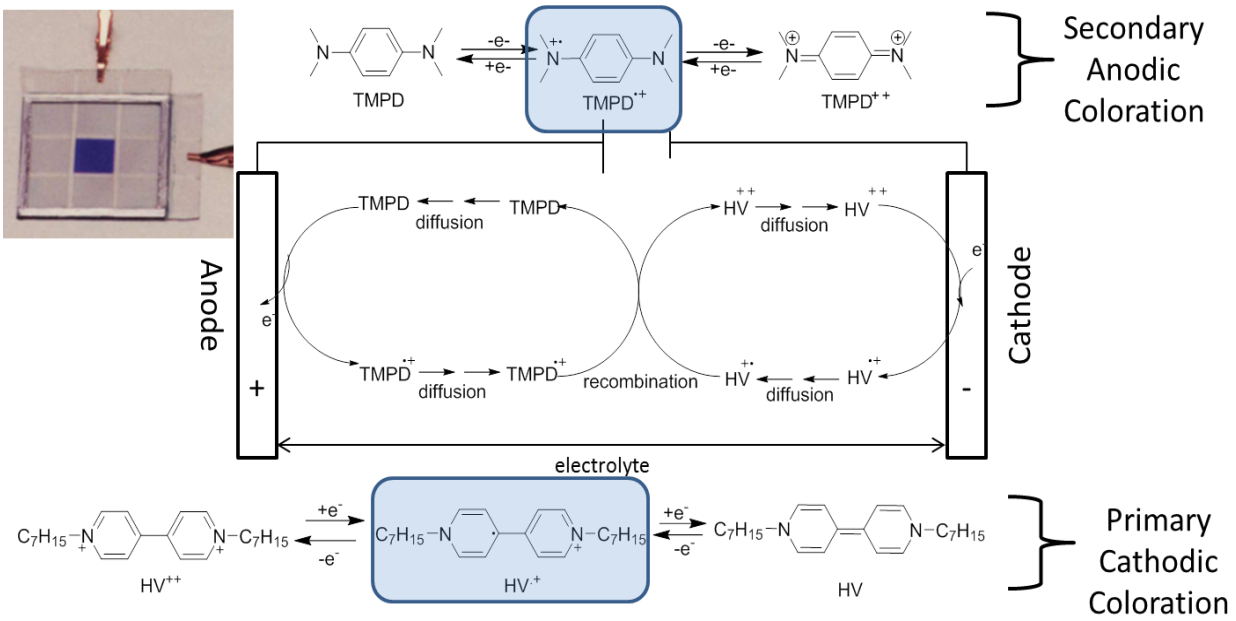

Figure 1.3.4. TMPD/HV electrochromic device (reference 34).

A second redox process produces HV^0 and $TMPD^{++}$, both materials exhibit no absorbance in the visible region of the electromagnetic spectrum and lead to a colorless state. While these processes are electrochemically reversible, Ho et al. note the appearance of an insoluble yellow-brown film on the electrode of the electrochromic device.[32] This is the result of dimerization between the neutral HV^0 and the dication HV^{++}, yielding the radical cation dimer, $(HV^{\cdot+})_2$.[37] Using the HV/TMPD based electrochromic device, Ho et al. addressed issues such as cycle life, cell operating voltage, optical contrast and cell spacer thickness. In Leventis' work, patterned ITO electrodes were used to fabricate 3 X 3 matrix arrays of pixels based on HV/TMPD dual electrochromism.[34] Table 1.3.1 summarizes the results of these studies. In our work, we aim to add to this rather limited pool of information by using an *N*- arylated phenylene

[37] Compton, R.G.; Monk, P.M.S.; Rosseinsky, D.R.; Waller, A.M. Electron Paramagnetic Resonance Spectroscopy of Electrodeposited Species from Solutions of 1,1′-bis-(*p*-cyanophenyl)-4,4′-bipyridilium (cyanophenyl paraquat, CPQ). *J. Chem. Soc. Faraday Trans.* **1990,** *86*, 2583.

diamine (PD) based electrochrome as the primary color changing species in a device setting. We seek to explore **TAPD** as a functional electrochromic molecular dye for application in EC device technology. Shown in figure 1.3.5, we expect **TAPD** to be a particularly interesting electrochrome compared to **TMPD** because of the extra stability of its redox states and the richer colors afforded (as a result of more extended pi conjugation). Using **TAPD**, we are able to exploit multi-electrochromism, a quality that has yet to be demonstrated in this class of materials.

Anodic Material	Cathodic Material	Electrochrome Concentration (M)	Cell Gap (μm)	Solution Phase	Operating Voltage	Δ%T (%)	τ_c (s)	τ_b (s)	Cycle Life	ref.
TMPD	$HV(ClO_4)_2$	0.05 M	190.0	MeCN	0.6 V	84	N/A	N/A	N/A	34
TMPD	$HV(BF_4)_2$	0.05 M	140.0	$TBABF_4$/PMMA/PC	0.8 V	75.5	2.5	8	10^2	32, 33

Table 1.3.1. Summary of selected data taken from literature. Δ%T represents percent transmission, τ_c and τ_b represent coloration and bleaching times, respectively.

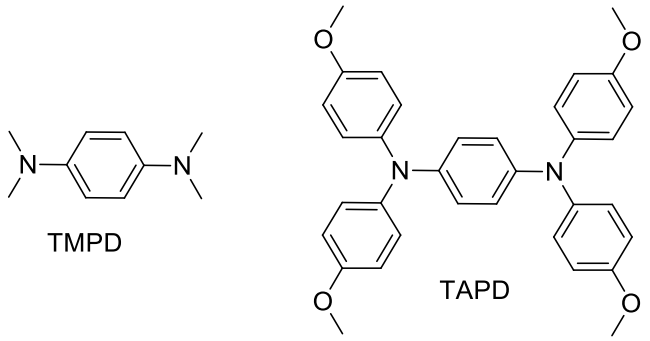

Figure 1.3.5. Structures of **TMPD** and **TAPD**.

1.4 Results and Discussion: TAPD as Anodically Coloring Dichromic Electrochromic Molecular Dye

1.4.1 Synthesis of TAPD

Tetraanisylphenylenediamine (**TAPD**) was first reported by our group in 1998 as a product of the coupling of *p*-diiodobenzene with di-*p*-anisylamine under Ullman conditions.[11,13,38,39] The synthesis has since been reported on numerous occasions, including

[38] Ullmann, F. Ueber eine neue Bildungsweise von Diphenylamine-derivaten. *Ber. Dtsch. Chem.. Ges.* **1903,** *5*, 559.

replacing the Ullman reaction with Pd catalysis (i.e. Hartwig Buchwald N-arylation)[40,41,42] conditions. [43,44] Recently, Bender et al. reported a yield of 86% using 1,4-phenylenediamine and 4-bromoanisole as the reacting substrates.[45] The conditions included using sodium *tert*-butoxide (1.5 molar equivalent with respect to reactive N-H), *bis*(dibenzylideneacetone)palladium (0.50 mol% with respect to reactive N-H), and tri-*tert*-butylphosphine (0.83 molar equivalent with respect to palladium) to catalytically facilitate the coupling of the two substrates. In our lab, **TAPD** was prepared by Dr. Lester T. Gray using the same conditions with the exception of significantly less bis(dibenzylideneacetone) palladium (0.20 mol% with respect to reactive N-H).[46] Shown in scheme 1.4.1, the optimized method netted a purified yield of 80%. It is important to note that even after the most vigorous work-ups, coupled products can still contain some residual Pd. Reducing the amount of Pd used in the coupling reaction helps ensure the compositional integrity of the product analyte in subsequent experiments (UV-vis spectroscopy,

---

[39] Selby, T. D. Polyamino Redox Arrays for Control of Spin Alignment and Charge Transport. Ph.D. Dissertation, The University of Alabama, Tuscaloosa, AL, 2001.
[40] Hartwig, John F.; Kawatsura, Motoi; Hauck, Sheila I.; Shaughnessy, Kevin H.; Alcazar-Roman, Luis M. Room-Temperature Palladium-Catalyzed Amination of Aryl Bromides and Chlorides and Extended Scope of Aromatic C-N Bond Formation with a Commercial Ligand. *J. Org. Chem.* **1999**, *64*, 5575-5580.
[41] Hartwig, John F. Transition Metal Catalyzed Synthesis of Arylamines and Aryl Ethers from Aryl Halides and Triflates: Scope and Mechanism. *Angewandte Chemie, International Edition* **1998**, *37*, 2046-2067.
[42] Wolfe, John P.; Wagaw, Seble; Marcoux, Jean-Francois; Buchwald, Stephen L. Rational Development of Practical Catalysts for Aromatic Carbon-Nitrogen Bond Formation. *Acc. Chem. Res.* **1998**, *31*, 805-818.
[43] Kim, K.-Y. Polyarylamino Redox Arrays for Control of Charge Transport and Charge Storage. Ph.D. Dissertation, The University of Alabama, Tuscaloosa, AL, 2003.
[44] Gray, L.T. The Application of Arylamines as Redox Auxiliaries, Polar Crystals and Organic Semiconductors. Ph.D Dissertation, The University of Alabama, Tuscaloosa, AL, 2012.
[45] Kamino, B. A.; Mills, B.; Reali, C.; Gretton M. J.; Brook, M. A.; Bender, T. P. Liquid Triarylamines: The Scope and Limitations of Piers− Rubinsztajn Conditions for Obtaining Triarylamine−Siloxane Hybrid Materials. *J. Org. Chem.* **2012**,*77*, 1663-1674.

[46] Gray, L.T. The Application of Arylamines as Redox Auxiliaries, Polar Crystals and Organic Semiconductors. Ph.D Dissertation, The University of Alabama, Tuscaloosa, AL, 2012.

etc). In our lab, minimal amounts of Pd catalyst (≤1%) are preferred in target compound synthesis and products are characterized by ^{1}H- and ^{13}C- NMR and subjected to CHN combustion analysis for confirmation of analytical purity.

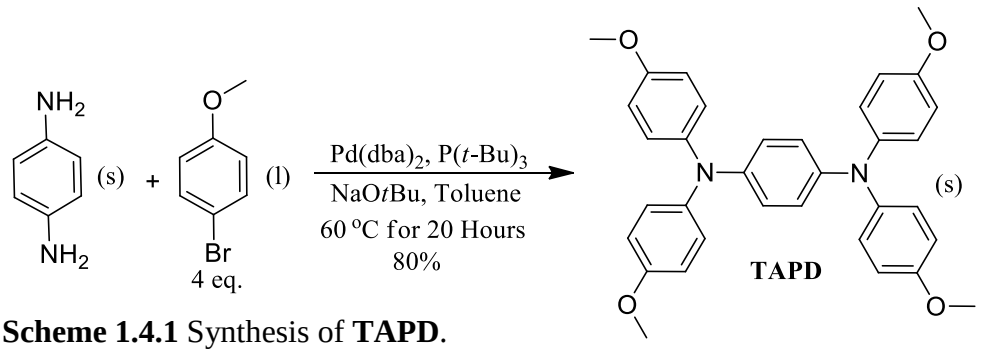

Scheme 1.4.1 Synthesis of **TAPD**.

1.4.2 Optical and Electrochemical Properties of TAPD in Solution State

When exposed to an anodic potential scan, **TAPD** undergoes two one-electron oxidation processes (scheme 1.4.2). Due to TAPD's type II/III delocalized mixed valence character, the two oxidation occur at significantly different potentials ($\Delta E° = 0.46$ V). The redox chemistry is both chemically and electrochemically reversible, characteristics that are depicted in the symmetrical peaks of the cyclic voltammogram in Figure 1.4.1.

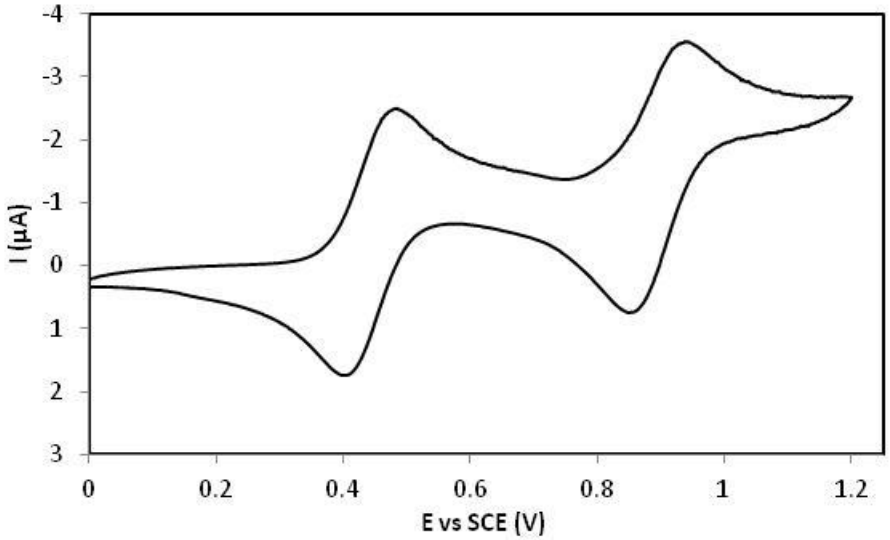

E°´(1)= 0.46 V vs. SCE

$E_{pp}(1)$= 0.082 V

E°´(2)= 0.92 V vs. SCE

$E_{pp}(2)$= 0.084 V

Figure 1.4.1. Cyclic voltammogram of 1.0 mM **TAPD** at Pt disc electrode in CH_2Cl_2 (0.1 M Bu_4NBF_4) at 100 mVs^{-1} scan rate.

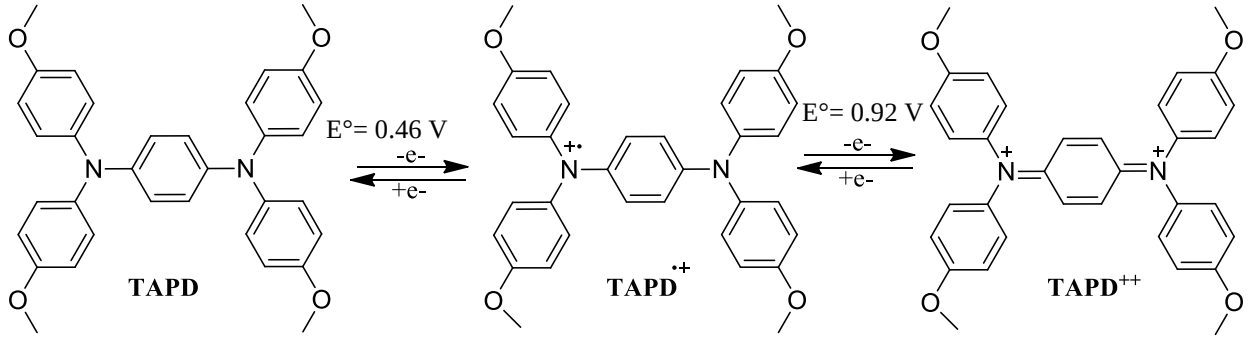

Scheme 1.4.2. TAPD redox chemistry

Interestingly, each cationic redox state is characterized by an intense color. The UV-vis optical absorbance profiles for **TAPD**, **TAPD**$^{\cdot+}$ **NO**$_3^-$, and **TAPD**$^{++}$ **(NO**$_3$**)**$_2^{2-}$ are shown in Figures 1.4.2, 1.4.3, 1.4.4, respectively. The nitrate salts were prepared in solution by chemical oxidation with the inorganic oxidant, ceric ammonium nitrate (CAN) – $(NH_4)_2\,Ce(NO_3)_6$. As an oxidant, CAN is desirable due to its high oxidation potential (E° ≈ 1.06 V vs. SCE), inert counter-ion, and long shelf-life.

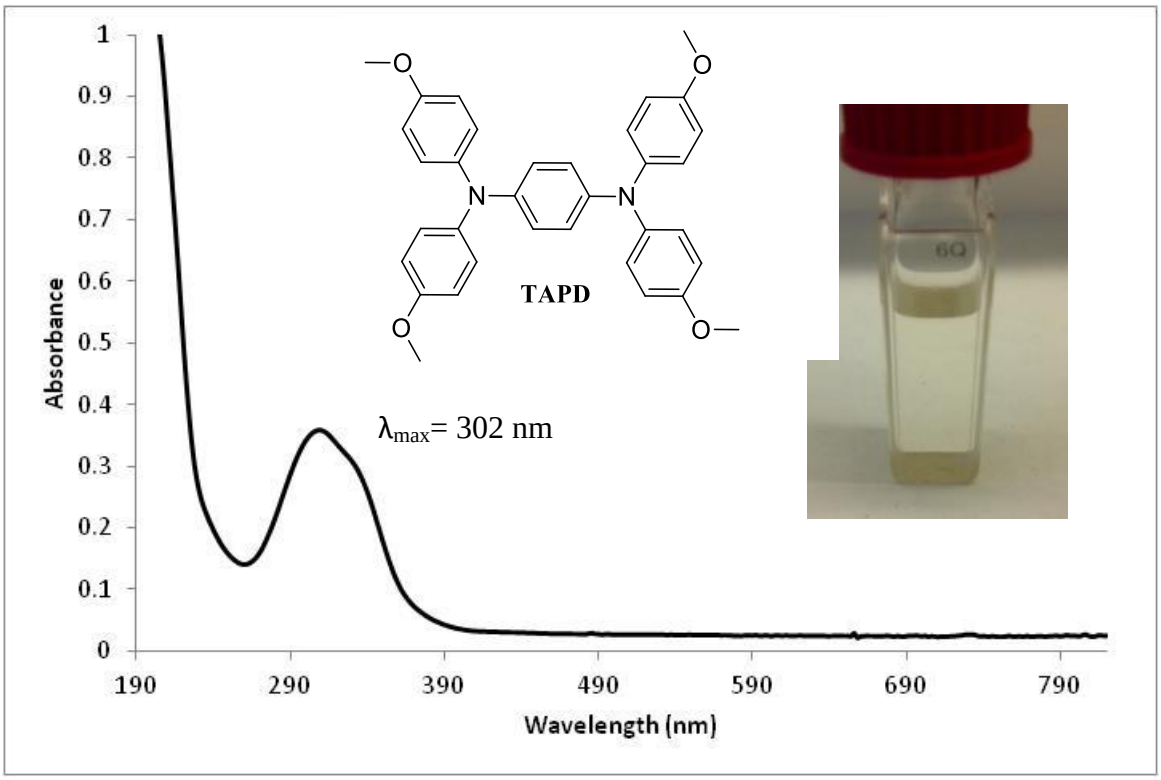

Figure 1.4.2 UV-vis optical absorption spectra for TAPD (1.03 x 10^{-5} M in acetonitrile).

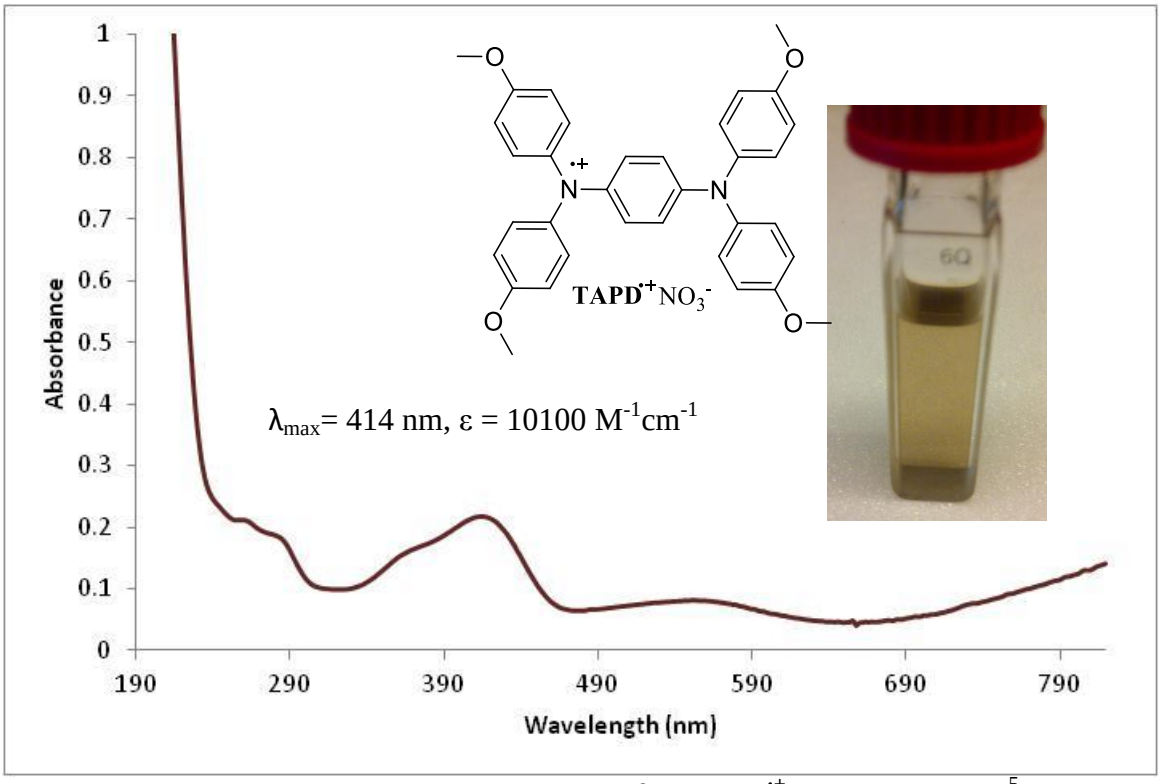

Figure 1.4.3 UV-vis optical absorption spectrum for **TAPD$^{\cdot+}$ NO$_3^-$** (1.03 x 10^{-5} M in acetonitrile).

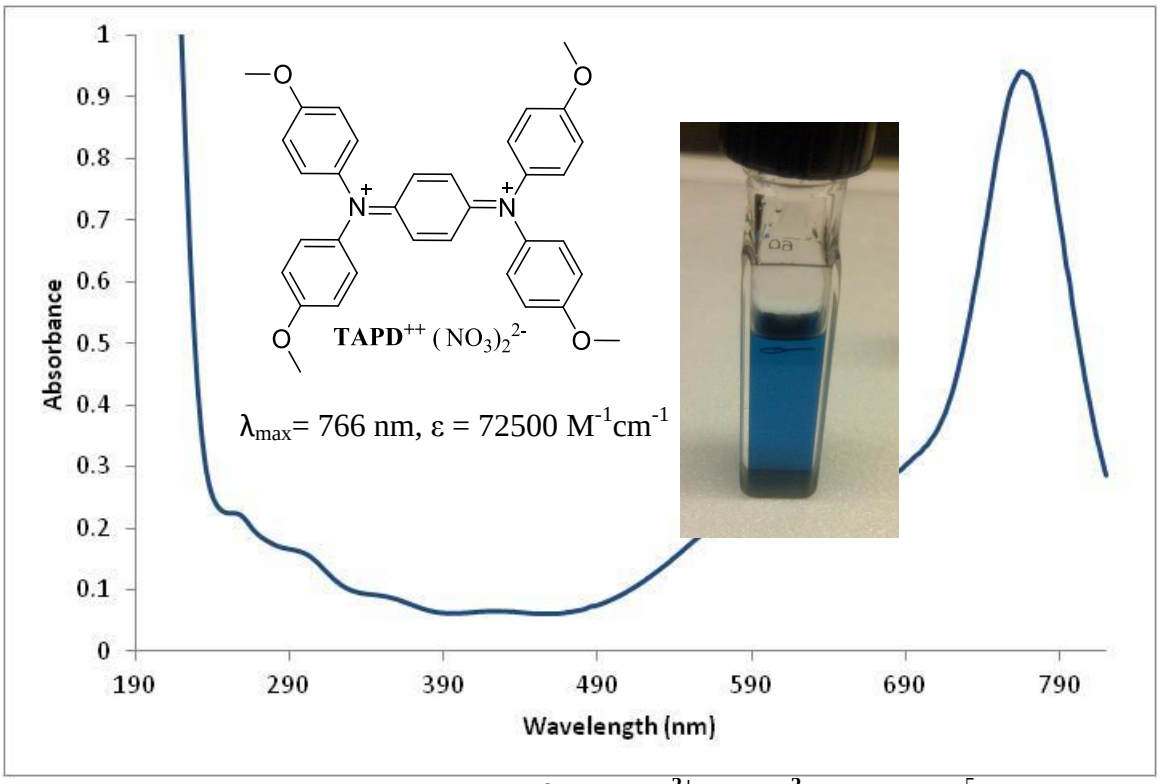

Figure 1.4.4 UV-vis absorption spectrum for **$TAPD^{2+}$ $(NO_3)_2^{2-}$** (1.03 x 10^{-5} M in acetonitrile).

1.4.3 Chemical Stability of TAPD in Solution State

An important feature of an electrochromic molecular dye is solution-state chemical stability. Dr. Les Gray studied the stability of **$TAPD^{\cdot+}$ (PF_6), and $TAPD^{++}$ $(PF_6)_2$** in commercial HPLC-grade acetonitrile (purchased from *Aldrich Chemical Company*).[47] The results are shown in Figures 1.4.5, 1.4.6, and 1.4.7. **$TAPD^{\cdot+}(PF_6)$** exhibited only a negligible amount of decomposition over the course of an hour in acetonitrile. Within 20 minutes, **$TAPD^{++}$ $(PF_6)_2$** began to reduce to **$TAPD^{\cdot+}$ (PF_6)** and required the addition of trifluoroacetic anhydride, TFAA (2.5 v/v%) to optimize its solution stability.

[47] Gray, L.T. The Application of Arylamines as Redox Auxiliaries, Polar Crystals and Organic Semiconductors. Ph.D Dissertation, The University of Alabama, Tuscaloosa, AL, 2012.

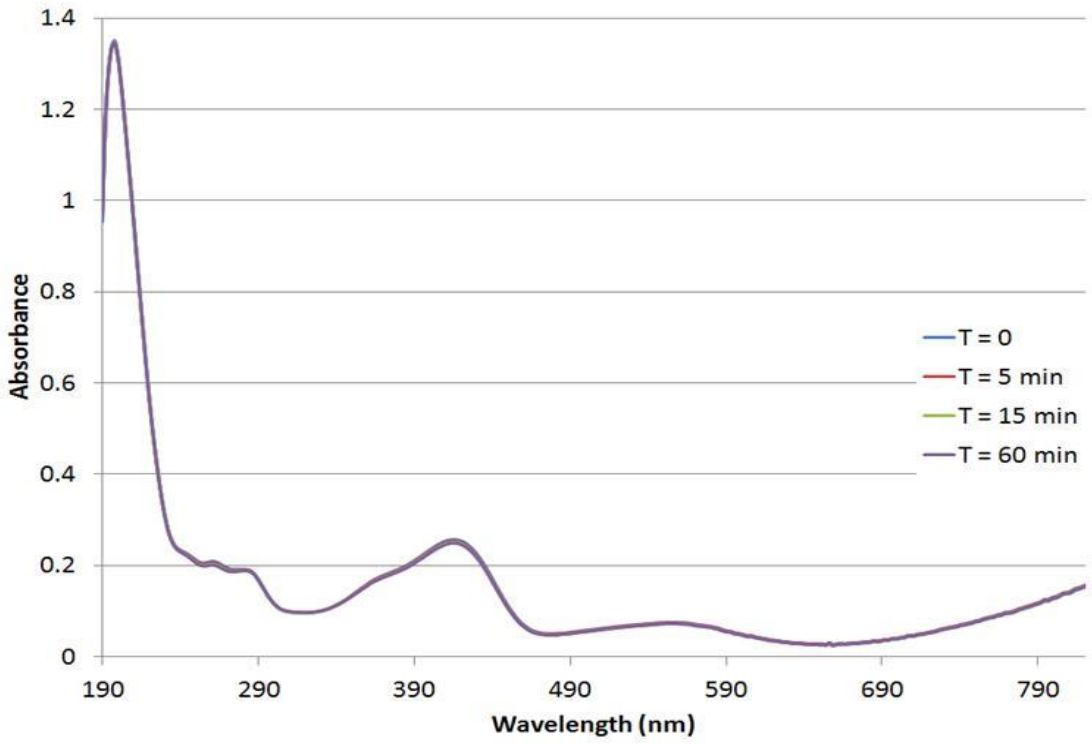

Figure 1.4.5. Time-resolved UV-vis absorption spectra for **TAPD$^{\cdot+}$ (PF_6)** (1.29 x 10^{-5} M) in HPLC-grade acetonitrile) over 60 minutes.

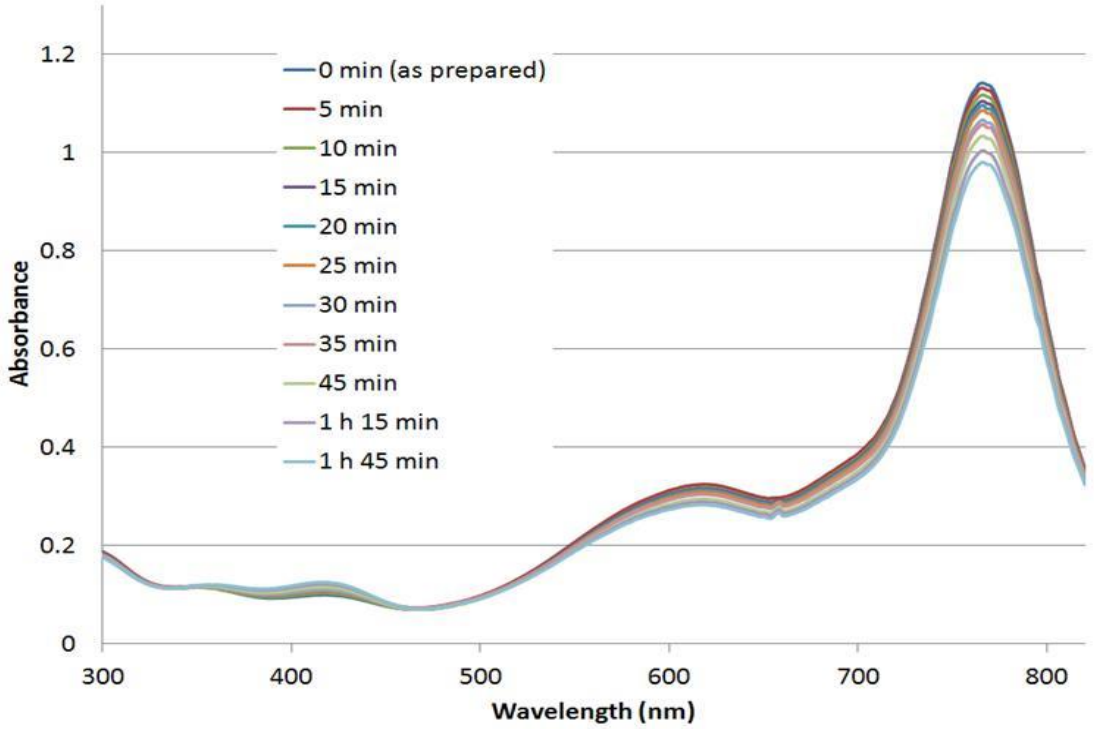

Figure 1.4.6. Time-resolved UV-vis absorption spectra for **TAPD^{++} (PF$_6$)$_2$** (1.29 x 10^{-5} M in HPLC-grade acetonitrile) over 105 minutes.

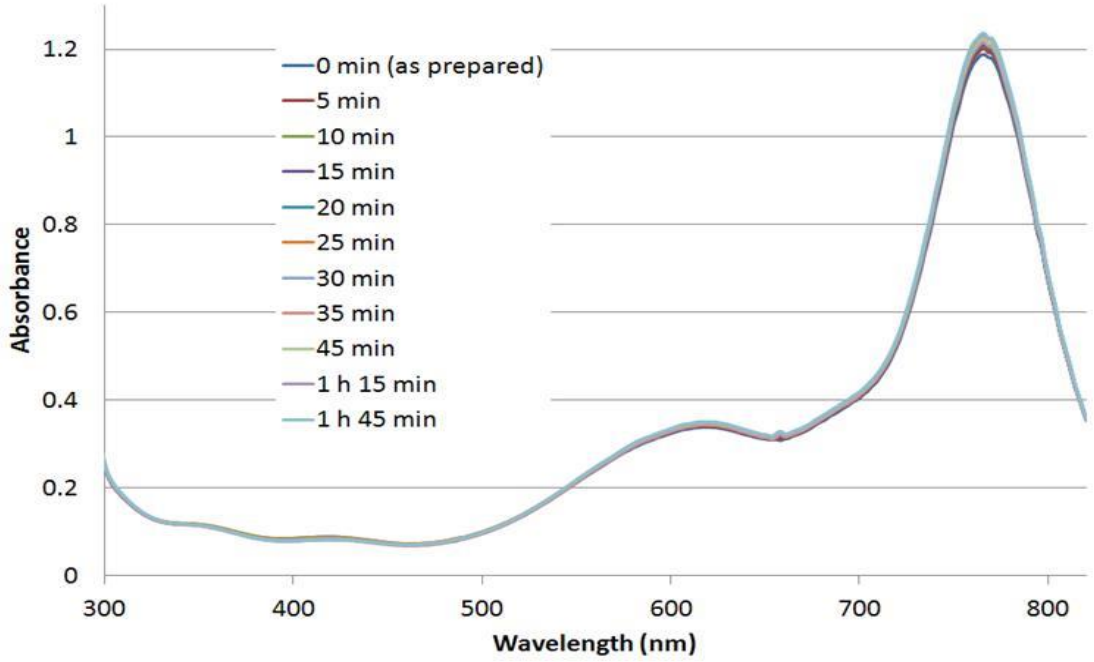

Figure 1.4.7. Time-resolved UV-vis spectra for **TAPD^{++} (PF$_6$)$_2$** (1.29 x 10^{-5} M in HPLC-grade acetonitrile with 2.5 v/v% TFAA) over 105 minutes.

1.4.4 Application of TAPD to Singular Type I Absorptive/Transmissive Electrochromic Device

TAPD is a viable candidate as a primary electrochrome based on several criteria:

1. **TAPD** undergoes two (chemically and electrochemically) reversible 1 e^- processes at a Pt disc electrode.
2. **TAPD**$^{\cdot+}$ and **TAPD**$^{++}$ salts absorb strongly in the visible region of the electromagnetic spectrum leading to intense coloring.
3. **TAPD**$^{\cdot+}$ and **TAPD**$^{++}$ salts are chemically stable in HPLC-grade acetonitrile which is advantageous since many solution-state gel electrolytes employed in ECD's are acetonitrile based.

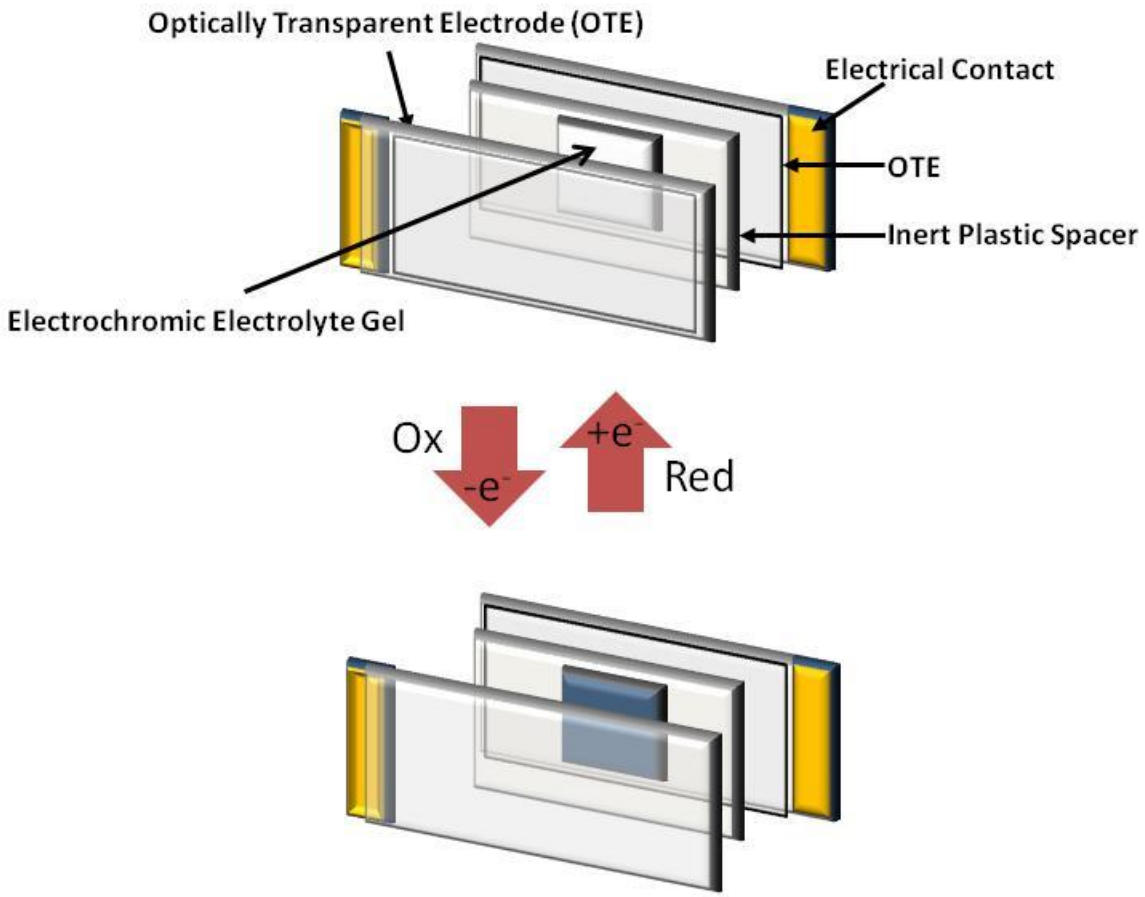

Figure 1.4.8. Generic operation of Type I Absorptive/Transmissive Electrochromic Device.

In a window-type electrochromic device, there are generally two modes: absorptive and transmissive. If the objective is to modulate visible light, then the absorptive mode will be colored while the transmissive phase is colorless. Switching between the two occurs as a result of an applied potential. Figure 1.2.8 depicts such a device. It is a sandwich type configuration with commercially purchased indium tin oxide (ITO) as the optically transparent semiconducting electrode (OTE). Generally, ITO is purchased on a borosilicate glass substrate. For efficient contact between the ITO electrode and the spring clip of the potentiostat, aluminum tape is used. Commercially available painter's plastic is employed as a spacer for the device. Because it can be purchased in multiple thicknesses, the cell gap can be easily varied. A small square (~1 cm^2) is manually cut from the plastic to form the active area of the device. Attention is paid to making

sure the active area of the device is larger than the size of the beam from the lamp of the spectrophotometer. Syringed into the active area is the electrochromic media, which is composed of the electrochrome of interest dissolved in a gel electrolyte. The electrolyte is made by dissolving a polymer (polymethylmethacrylate), a plasticizer (propylene carbonate), and a lithium salt ($LiClO_4$) into a volatile organic solvent (acetonitrile). Leclerc et al. give a detailed account of the preparation of this electrolytic medium.[48]

Instead of a sealant, which is commonly employed in literature accounts, the device components are held together by two metal Hoffman clamps. The clamps provide a platform for the window to sit up independently in front of the spectrophotometer for measurement (Figure 1.4.9). More importantly, clamping the device instead of chemically sealing it allows for the components to be taken apart and reused- a useful quality in a research setting. The set-up for the spectroelectrochemical analysis of the switching device is shown in Figure 1.4.10. The UV-vis spectrophotometer and potentiostat are used in tandem to generate the electrochemical and optical data necessary to effectively characterize electrochromic switching.

[48] Beaupre´, S.; Dumas, J.; Leclerc, M. Toward the Development of New Textile/Plastic Electrochromic Cells Using Triphenylamine-Based Copolymers. *Chem. Mater.* **2006**, *18*, 4011-4018

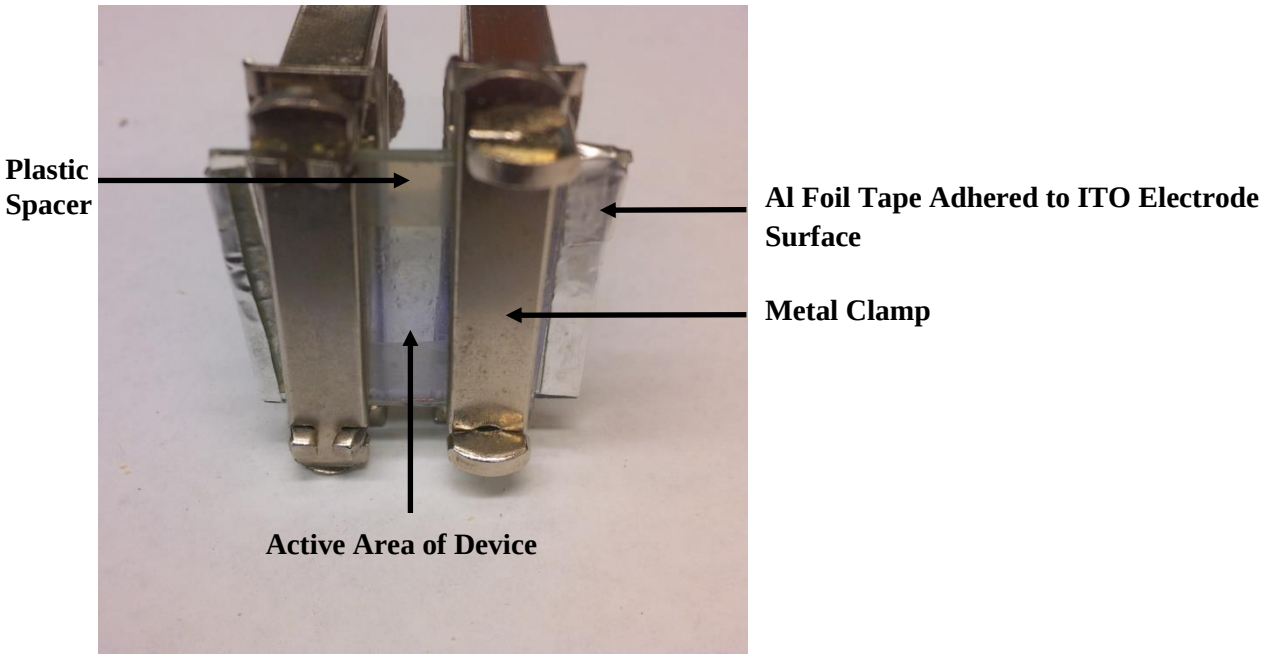

Figure 1.4.9. Photograph of prepared electrochromic device with labeled components.

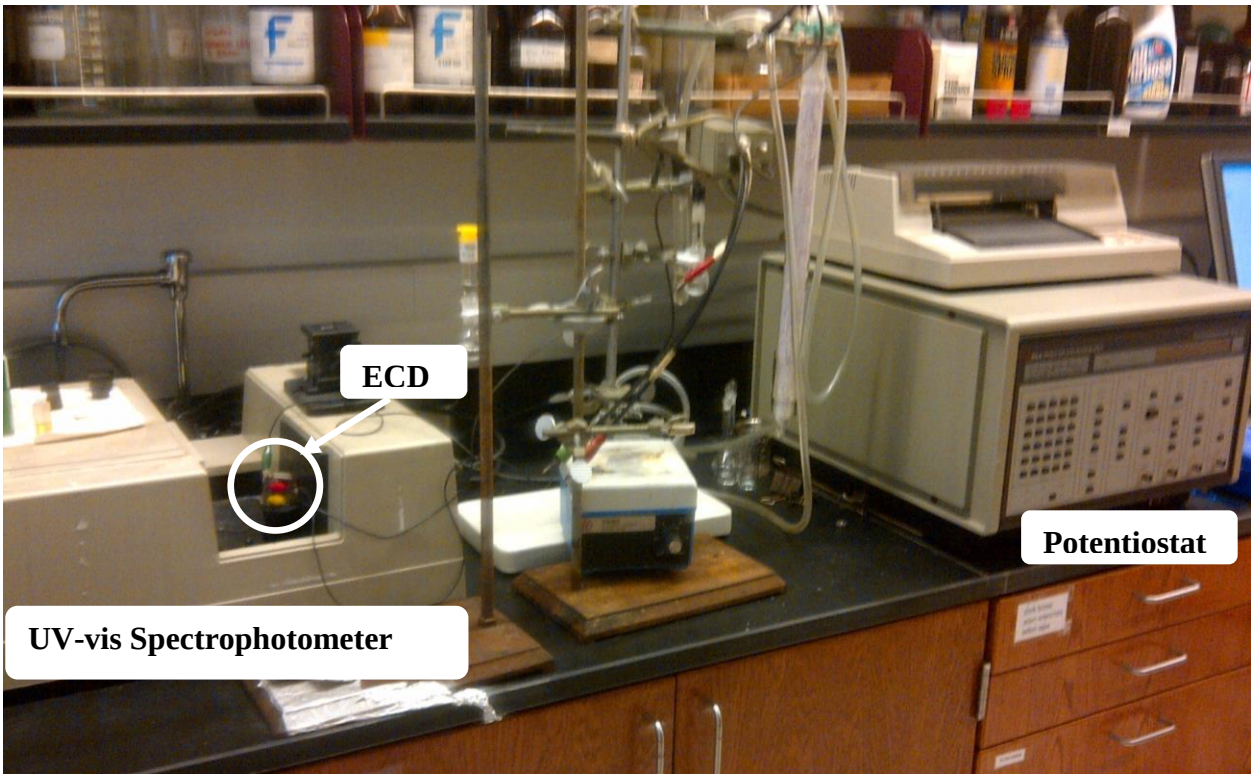

Figure 1.4.10. ECD Spectroelectrochemistry Apparatus.

1.4.4.1 ITO as a Counter Electrode Material for Singular Electrochromic Devices

In order to efficiently incorporate anodically coloring EC molecular dyes into a device, a suitable cathodic process must be considered. This process is expected to occur at the counter electrode of the device. A precise understanding of this cathodic electrochemical process is not only essential to the overall performance of the device but also to the referencing of potentials. It should be noted that in a two-electrode set up, like in Figure 1.4.11, the counter electrode and reference electrode are coupled.

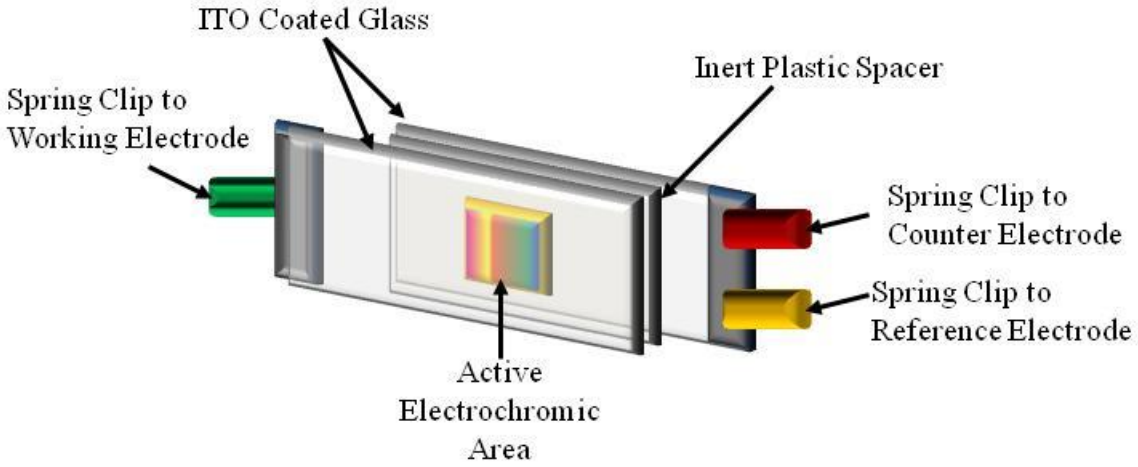

Figure 1.4.11. General schematic of an electrochromic device with two-electrode set-up.

Incorporating a counter electrode material that modulates electromagnetic radiation in the visible region of the spectrum would hinder our ability to adequately exploit the type of multi-electrochromism that TAPD and PTe uniquely exhibit. Thus, in the case of multi-colored electrochromes, an optically passive cathodic process at the counter electrode is ideal.

A counter electrode for an ECD must meet the following criterion:[49]

[49] Golden, S. J.; Steele, B. C.H. Thin Film Tin-Doped Indium oxide Counter-Electrode For Electrochromic Applications. *Solid State Ionics* **1987,** *28-30,* 1733-1737.

1. Reversible electrochemical insertion of electroactive species.
2. Appreciable optical transmission while acting as source of the electroactive species.
3. Low cost and ease of fabrication into thin films.

Metal oxides are the predominating form of optically passive EC materials. Recently developed examples include V_2O_5:2CeO_2, CeO_2:ZrO_2, and In_2O_3:V_2O_5.[50,51,52] However, a practical option is ITO. Besides meeting the criterion listed above for counter electrode materials, it is accessible as a commercially available product.[53] A drawback to ITO is its lack of long-term electrochemical stability which has prevented it from being incorporated into commercial EC applications as a counter electrode material.[54,55,56]Since the primary purpose of this project is to demonstrate multi-electrochromism and not to engineer a commercially applicable cell, ITO does suffice.

In the presence of Li cations (or H^+, Na^+) and a cathodic potential, lithium ion insertion occurs- accompanied by a reduction of ITO. It is still a debate whether Sn or In is being reduced.

---

[50] Malini, D. R.; Sanjeeviraja, C. H^+-intercalation Electrochemical/Electrochromic Properties of V-Ce Mixed Oxide Thin Films. *Int. J. Electrochem. Sci.* **2013,** *8,* 1349-1365.
[51] Bhosale, A.K.; Shinde, P. S.; Tarwal, N.L.; Pawar, R.C.; Kadam, P.M.; Patil, P.S. Synthesis and Characterization of Highly Stable Optically Passive CeO_2-ZrO_2 Counter Electrode. *Electrochimica Acta* **2010,** *55,* 1900-1906.
[52] Artuso, F.; Decker, F.; Krasilnikova, A.; Liberatore, M.; Loureco, A.; Masetti, E.; Pennisi, A.; Simone, F. Indium-Vanadium Ovides Deposited by Radio Grequency Sputtering: New Thin Film Transparent Materials for Li-Insertion Electrochemical Devices. *Chem. Mater.* **2002,** *14,* 636-642.
[53] ITO for dissertation research was purchased from Delta Technologies (CB-50IN-1111).
[54] Radhakrisnan, S.; Unde, S.; Madale, A.B. Spurce of Instability in Solid State Polymeric Electrochromic Cells: the Deterioration if Indium Tin Oxides Electrodes. *Mat. Chem. Phys.* **1997,** *48,* 268-271.
[55] Meulenkamp, E. A.; Bressers, P. M. M. C. The Electrochromic Behavior of Indium Tin Oxide in Propylene Carbonate Solutions. *J. Electrochem. Soc.* **1998,** *145,* 2225-2230.
[56] Brotherson, I.D.; Cao, Z.; Thomas, G.; Weglicki, P.; Owen, J. R. Counterelectrode Films for Electrochromic Windows. *Sol.Ener. Mater.* **1995,** *39,* 257-270.

An occasionally observed brown color has been attributed to the reduction of Sn.[57] Eq. 1.4.1 shows the equation for the process, assuming Sn is being reduced.

$$\mathrm{ITO\ (s)} + x(\mathrm{M^+} + \mathrm{e^-}) \rightleftharpoons \mathrm{M_x Sn^{IV,II} O_2 (In_2O_3)\ (s)}$$

$$\mathrm{M = Li^+,\ H^+,\ Na^+}$$

$$\mathrm{E^\circ = \sim 1.5\ V\ vs.\ Li^+/Li}$$

Eq. 1.4.1 Reduction of ITO.

Another area of controversy is the existence and nature of ITO electrochromism. A 1985 paper by Svensson and Granqvist suggested that electrochromism in ITO was not an intrinsic property, but one that depends on the structure of the ITO surface.[58] Figure 1.4.12 (a), published almost simultaneously shows a reversible change in transmission in an ITO glass upon what was described as "Li^+ ion injection."[59] The optical contrast is minimal, with darkening occurring only as a result of high levels of lithiation. Figure 1.4.12 (b), a study published in 1987 by Golden and Steele, demonstrated this loss of transparency. They concluded that above a charge density of 15 mC/cm^2 ($x \approx 0.15$ in Eq. 1.4.1) the ITO film was no longer highly transmissive in the visible region.[60] This feature was later demonstrated in lithiated SnO_2 films, providing further evidence that Sn not In undergoes reduction at the counter electrode.[61]

---

[57] Monk, P. M. S.; Mortimer, R. J.; Rosseinsky, D. R. *Electrochromism ans Electrochromic Devices;* Cambridge University Press: New York, 2007.

[58] Svensson, J. S. E. M.; Granqvist, C. G. No Visible Electrochromism in High-Quality e-beam Evaporated In_2O_3:Sn Films. *Applied Optics* **1985,** *24,* 2284-2285.

[59] Goldner, R. B.; Foley, G.; Golder, E.L.; Norton, P.; Wong, K.; Haas, T.; Seward, G.; Chapman, R. Electrochromic behavior in ITO and Related Oxides. *Applied Optics* **1985,** *24,* 2283-2284.

[60] Golden, S. J.; Steele, B. C.H. Thin Film Tin-Doped Indium oxide Counter-Electrode For Electrochromic Applications. *Solid State Ionics* **1987,** *28-30,* 1733-1737.

[61] Isidorsson, J.; Granqvist, C. G.; Häggström, L.; Nordström, E. Electrochromism in Lithiated Sn Oxide: Mössbauer Spectroscopy data on Valence State Changes. *J. Appl. Phys.* **1996,** *80,* 2367-2371.

Mastragostino et al. published a cyclic voltammagram of an ITO electrode in 1M $LiClO_4$ propylene carbonate (Figure 1.4.13) which agreed with Cogan et al. in their study on the electrochromism of ITO in a non-aqueous media.[62] They assign the process occurring at 1.5 V vs. Li^+/Li to lithium ion insertion/extraction. In the same study they demonstrated that it was possible to use commercial ITO glass substrates (2000 Å thickness and 20 Ω resistance) in an electrochromic device as an optically passive charge balancing electrode in the presence of $LiClO_4$ dissolved in propylene carbonate. This study, in addition to many others, provide indication that lithium intercalation into ITO would be suitable counter process for our aryl amine based ECD's.[63, 64,65,66,67,68,69]

---

[62] Corradini, A.; Marinangeli, A.M.; Mastragostino, M. ITO as Counter-Electrode in a Polymer based electrochromic Device. *Electrochimica Acta* **1990,** *35,* 1757-1760.

[63] Golden, S. J.; Steele, B. C.H. Thin Film Tin-Doped Indium oxide Counter-Electrode For Electrochromic Applications. *Solid State Ionics* **1987,** *28-30,* 1733-1737

[64] Corradini, A.; Marinangeli, A.M.; Mastragostino, M. ITO as Counter-Electrode in a Polymer based electrochromic Device. *Electrochimica Acta* **1990,** *35,* 1757-1760

[65] Cogan, S. F.; Anderson, E. J.; Plante, T.D., Rauh, D. Electrochemical Investigation of Electrochromism in Transparent Conductive Oxides. *Applied Optics* **1985,** *24,* 2282-2283.

[66] Steele, B. C. H.; Golden, S. J. Variable Transmission Electrochromic Windows Utilizing Tin-Doped Indium Oxide Counterelectrodes. *Appl. Phys. Lett.* **1991,** *59,* 2357-2359.

[67] Benkhelifa, F.; Ashrit, P. V.; Girouard, F. E.; Truong, V-V. Near Room Temperature Deposited Indium Tin Oxide Films as Transparent Conductors and Counterelectrodes in Electrochromic Systems.*Thin Solid Films* **1993,** *232,* 83-86.

[68] Ingram, M. D.; Duffy, J. A.; Monk, P. M. S. Chronoamperometric Response of the Cell ITO $|H_xWO_3|PEO\text{-}H_3PO_4(MeCN)|ITO$. *J. Electroanalytical Chem.* **1995,** *380,* 77-82.

[69] Mastragostino, M.; Zanelli, A.; Casalbore-Micele, G.; Geri, A. An Electrochromic Window Based on Poly(*N*-methyl-10,10-dimethylphenazsiline) and ITO Electrodes. *Syn. Metals* **1995,** *68,* 157-160.

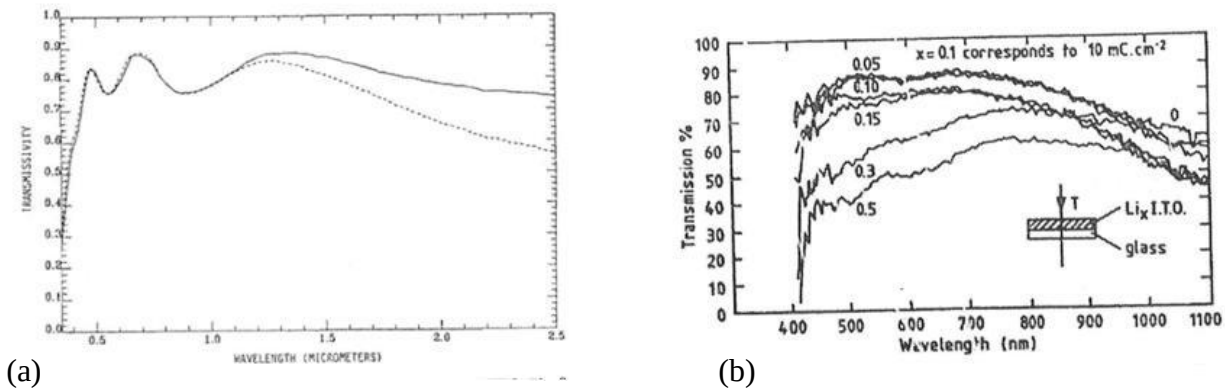

(a) (b)

Figure 1.4.12. (a) vis-NIR transmissivity of ITO glass substrate (340 nm thickness). Two reversible state are shown: --- colored with ~15 mC/cm^2 of Li^+ delivered to the ITO; bleached with ~ 15 mC/cm^2 of Li^+ removed. Figure is from ref 57. (b) vis-NIR % transmission spectrum of ITO glass substrate (340 nm thickness) after varied amounts of lithium insertion. Figure is from ref 58.

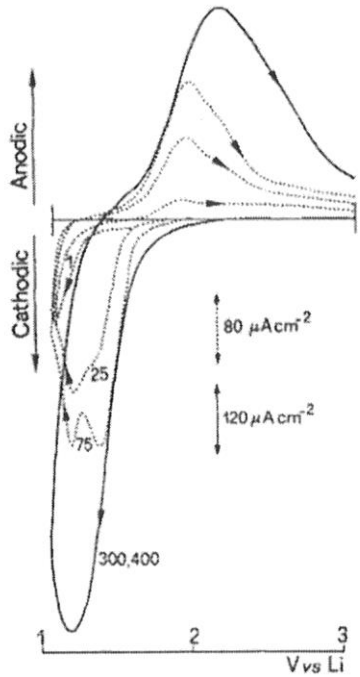

Figure 1.4.13. Cyclic Voltammetry at 50 mV/s of ITO electrode in 1M $LiClO_4$ in propylene carbonate. From ref 60.

1.4.4.2 Electrochromic Profile of TAPD in Singular Device State

When 3 V is applied for 30 s, the **TAPD** ECD transitions through three optical states as depicted in Figure 1.4.14.

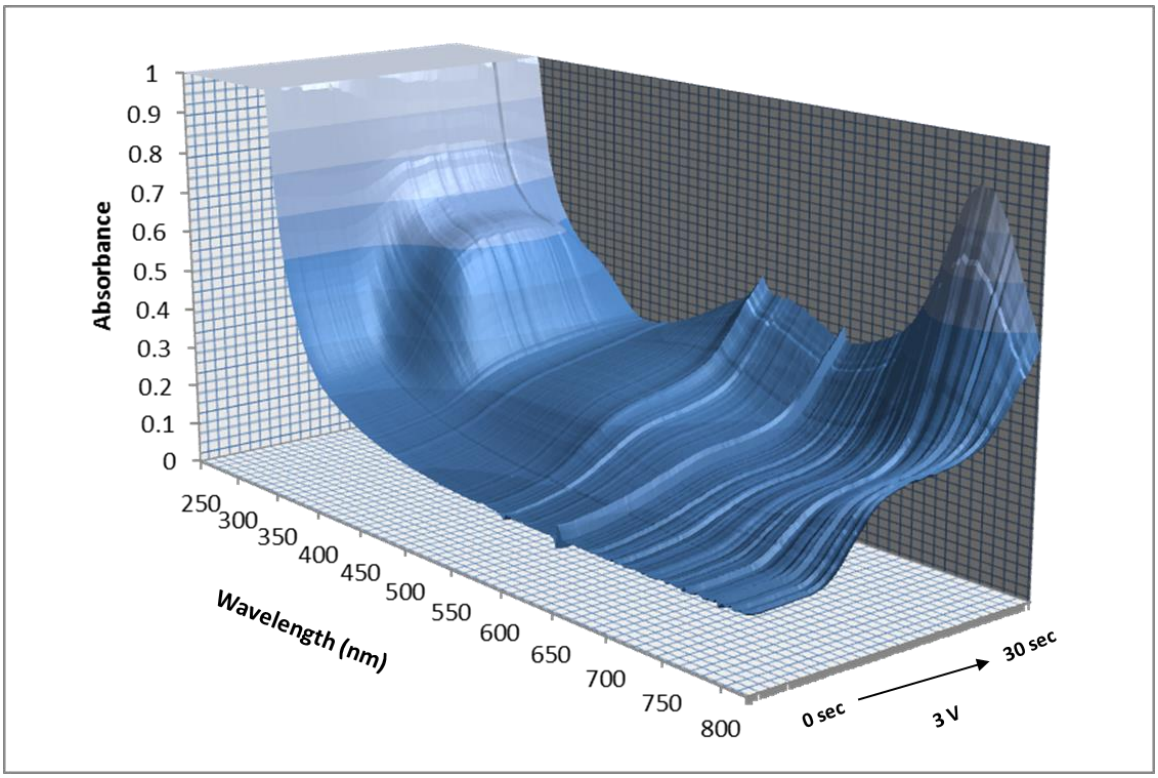

Figure 1.4.14. 3D optical profile of **TAPD** in the device state after the application of 3 V for 30 s.

A comparison of each optical state in the device with the UV-vis profiles of TAPD and its cation salts (prepared in solution by chemical oxidation) reveals that the expected electrochemistry does occur. The λ_{max} values of each colored state in the ECD agree with known values for **TAPD**$^{\cdot+}$ and to **TAPD**$^{++}$(Figures 1.4.3, 1.4.4). Since the ITO coated glass substrate absorbs at wavelengths below 300 nm, only wavelengths in the visible region are comparable. In the first anodic transition, **TAPD** loses an electron to form **TAPD**$^{\cdot+}$. The active area of the device goes from colorless to brownish-red (Figure 1.4.15). The third and final optical state of

the device occurs as **TAPD**$^{\cdot+}$ is oxidized to **TAPD**$^{++}$. A brownish red to blue color change is observed (Figure 1.4.16).

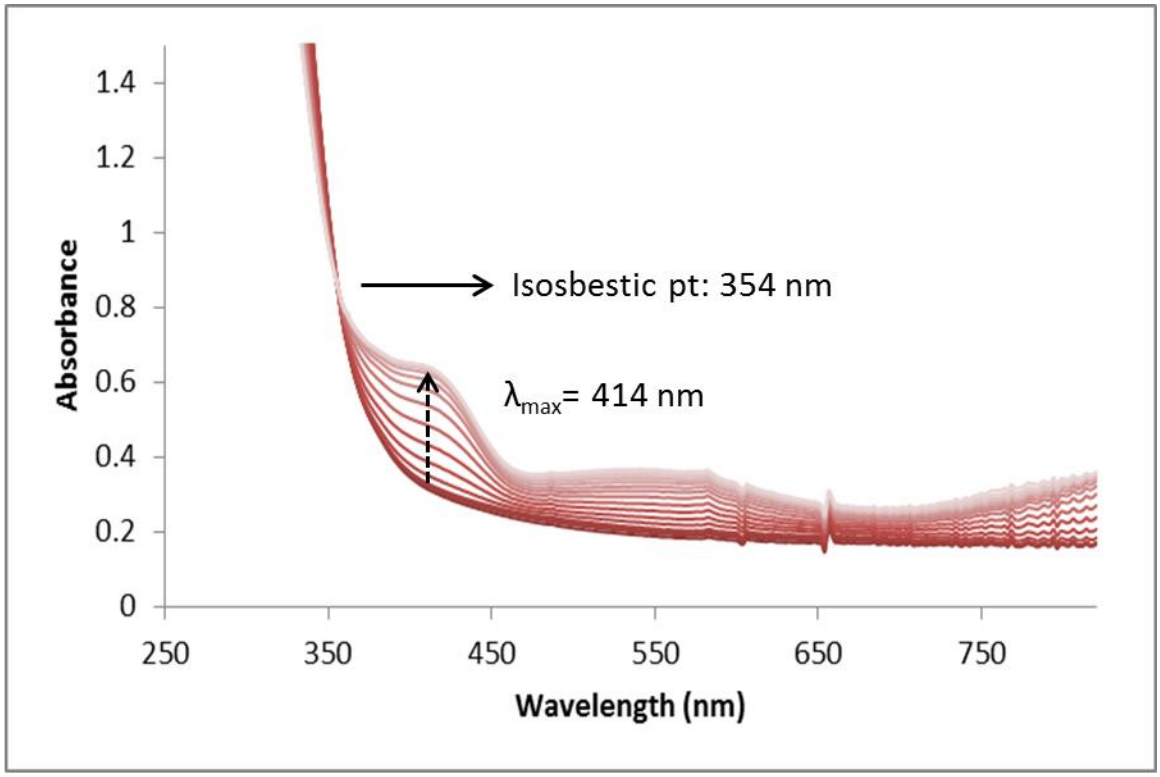

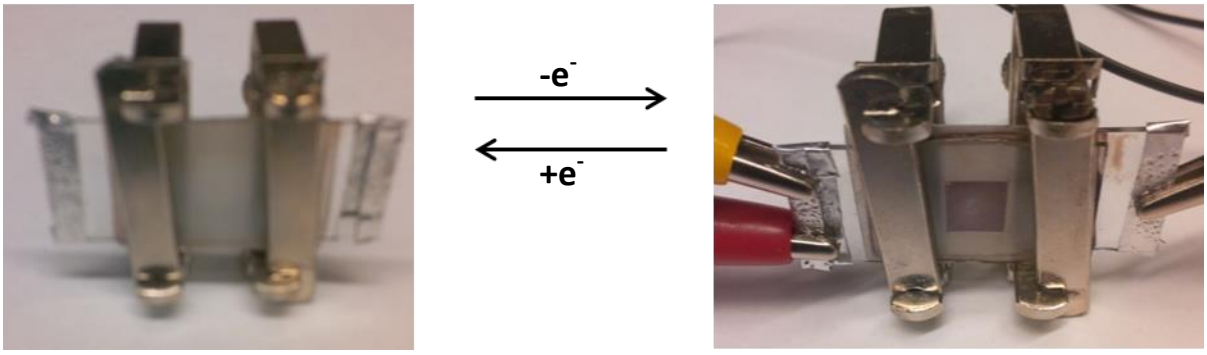

Figure 1.4.15. Time-resolved UV-vis absorption spectra of the first color transition, corresponding to the formation **TAPD**$^{\cdot+}$(brownish-red) from **TAPD** (colorless).Spectra taken every 1 s over 20 s.

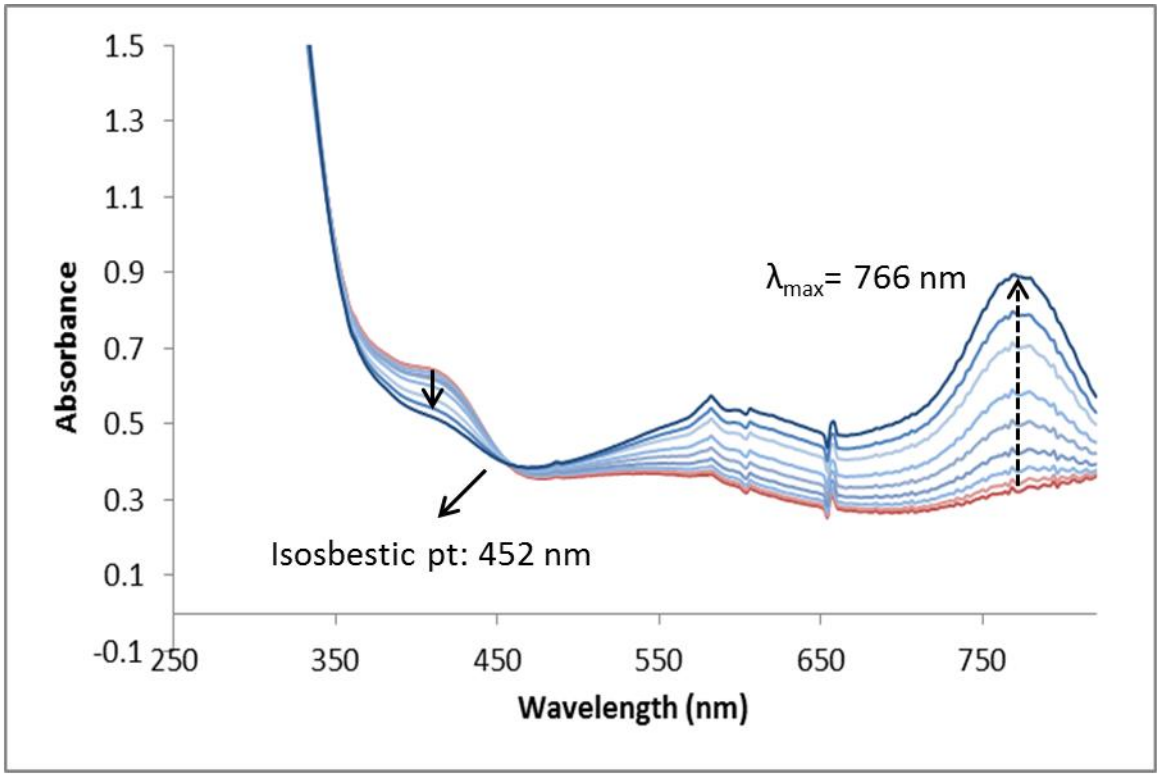

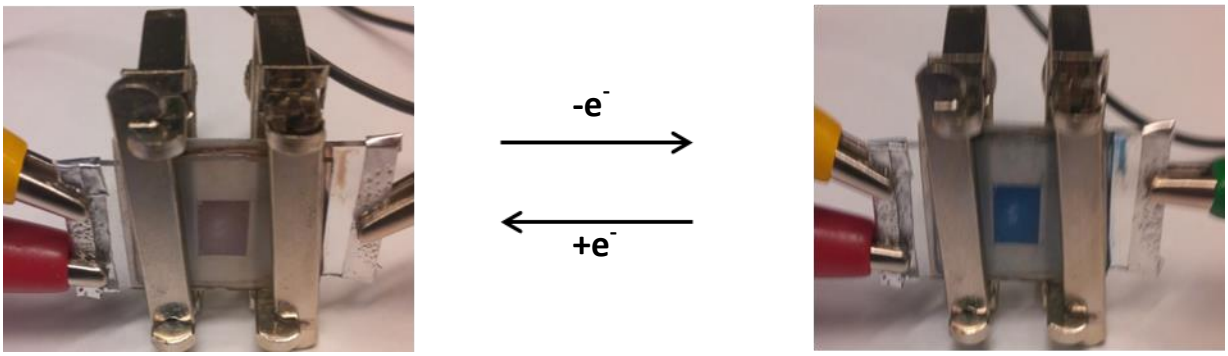

Figure 1.4.16. Time-resolved UV-vis absorption spectra of the second color transition, corresponding to the formation **TAPD**$^{++}$ (blue) from **TAPD**$^{\cdot+}$ (brownish-red). Spectra taken every 1 s over 10 s.

1.4.4.3 A Demonstration of Multi-Electrochromism: Control of Color by Varying Potential

The previous section described the optical states exhibited by the **TAPD** device at a single applied voltage of 3V. This section quantitatively investigates whether those multiple colored states can be turned on and subsequently off as a function of the applied potential. This

quality is a key principle in describing a material as a multi-colored electrochromic molecular dye.

The spectroelectrochemical response of the **TAPD** ECD is demonstrated in Figure 1.4.17. At an applied voltage of 1.0 V until 1.7 V, brownish-red **TAPD**$^{\cdot+}$, is generated and dominates the color of the device. At more positive voltages, 2.0 V to 3.0 V, blue **TAPD**$^{++}$ forms, reaching a maximum intensity at 2.5 V. From this information, we chose three operating voltages for the device, each designed to deliver a different optical state during electrochromic switching. To generate the colorless transmissive state, a voltage of 0.0 V could be applied, for the first color transition, 1.5 V and for the second color transition, 2.5 V is sufficient. Pictures of the multiple colored states in the device are shown in figure 1.4.18.

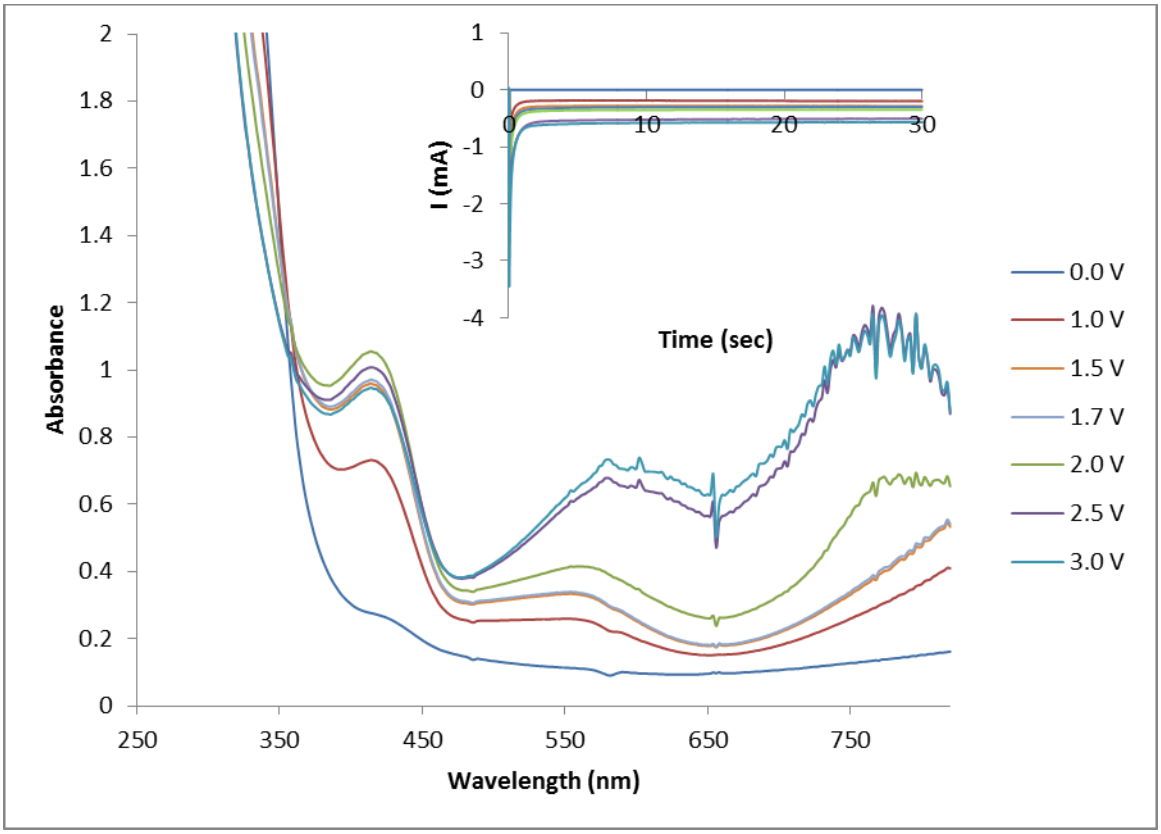

Figure 1.4.17. Spectroelectrochemical response of **TAPD** in ECD. Each voltage is held for 30 s, until steady state current is reached (inset).

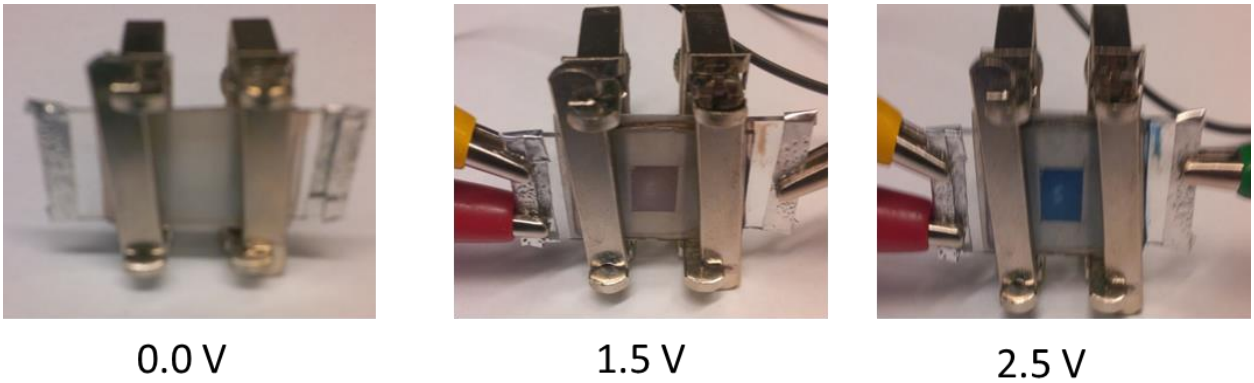

Figure 1.2.18. Pictures of TAPD ECD at chosen operating voltages.

1.4.4.4 Open Circuit Stability: Self Bleaching Feature

Type 1 ECD's generally have low open circuit stability, bleaching when voltage is no longer applied. This self-bleaching feature is a useful attribute in EC applications since no electrical power is needed affect the loss in color. In Figure 1.4.19, the device is turned "on" by applying a potential of 3.0 V to induce a series of color changes (see figures 1.4.15 and 1.4.16). Figure 1.4.20 depicts the optical profile of a **TAPD** ECD in its "blue" or **TAPD**$^{++}$ state under open circuit conditions. Over the course of several minutes, the cell undergoes cathodic transitions from **TAPD**$^{++}$ (blue) to **TAPD**$^{+}$ (reddish-brown) to **TAPD** (colorless). This bleaching occurs as a result of recombination between the oxidized amminium salts and a reduced species (most likely Sn^{II}). It is important to note that isosbestic points (at 354 nm and 452 nm for the first and second transitions, respectively) are maintained through each transition indicating mass conservation and chemical stability. After the device is bleached, it becomes colored again when an anodic potential is applied. This reversibility is further demonstrated and discussed in section 1.4.4.5.

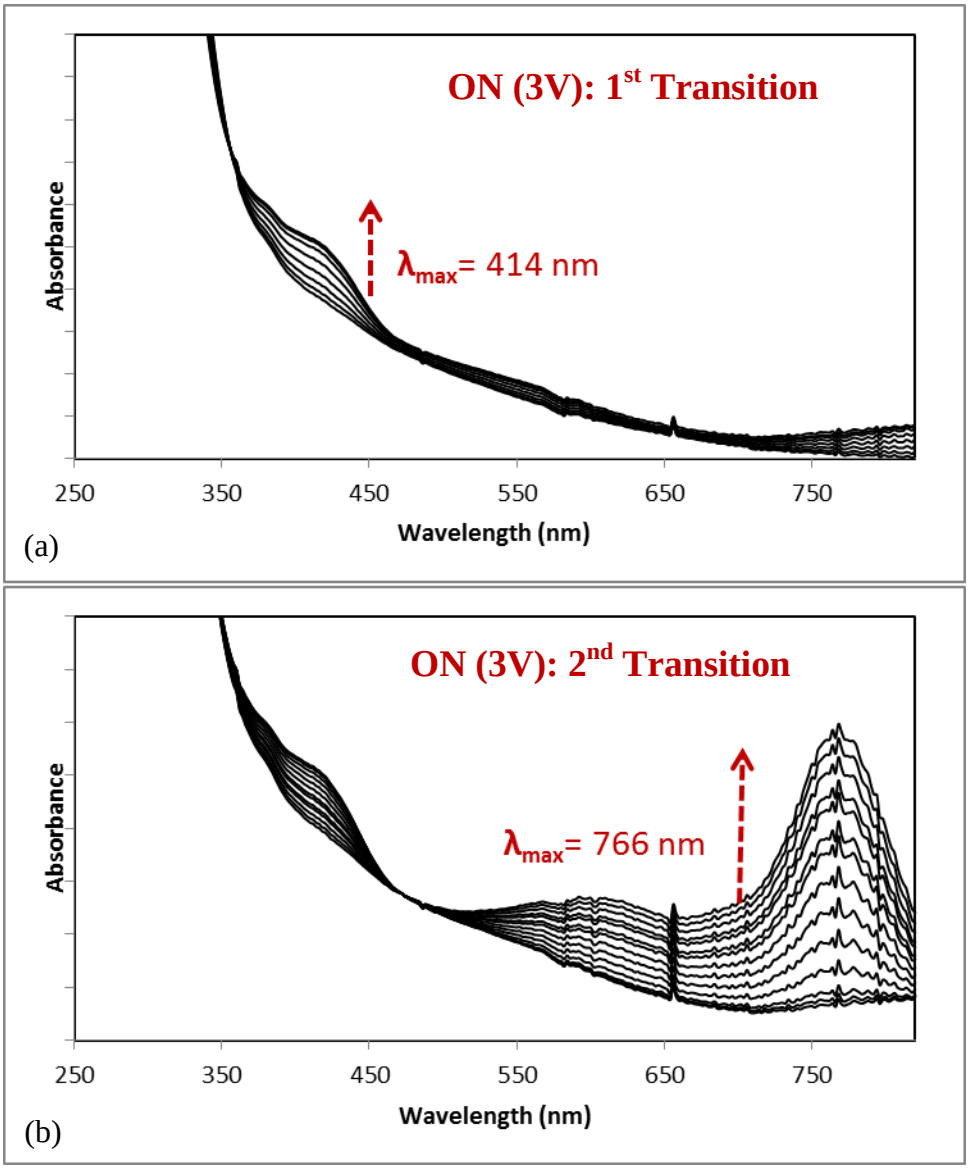

Figure 1.4.19. Time-resolved UV-vis absorption spectra of TAPD in the "On" device state (3.0 V)-(a) first anodic transition, (b) second anodic transition

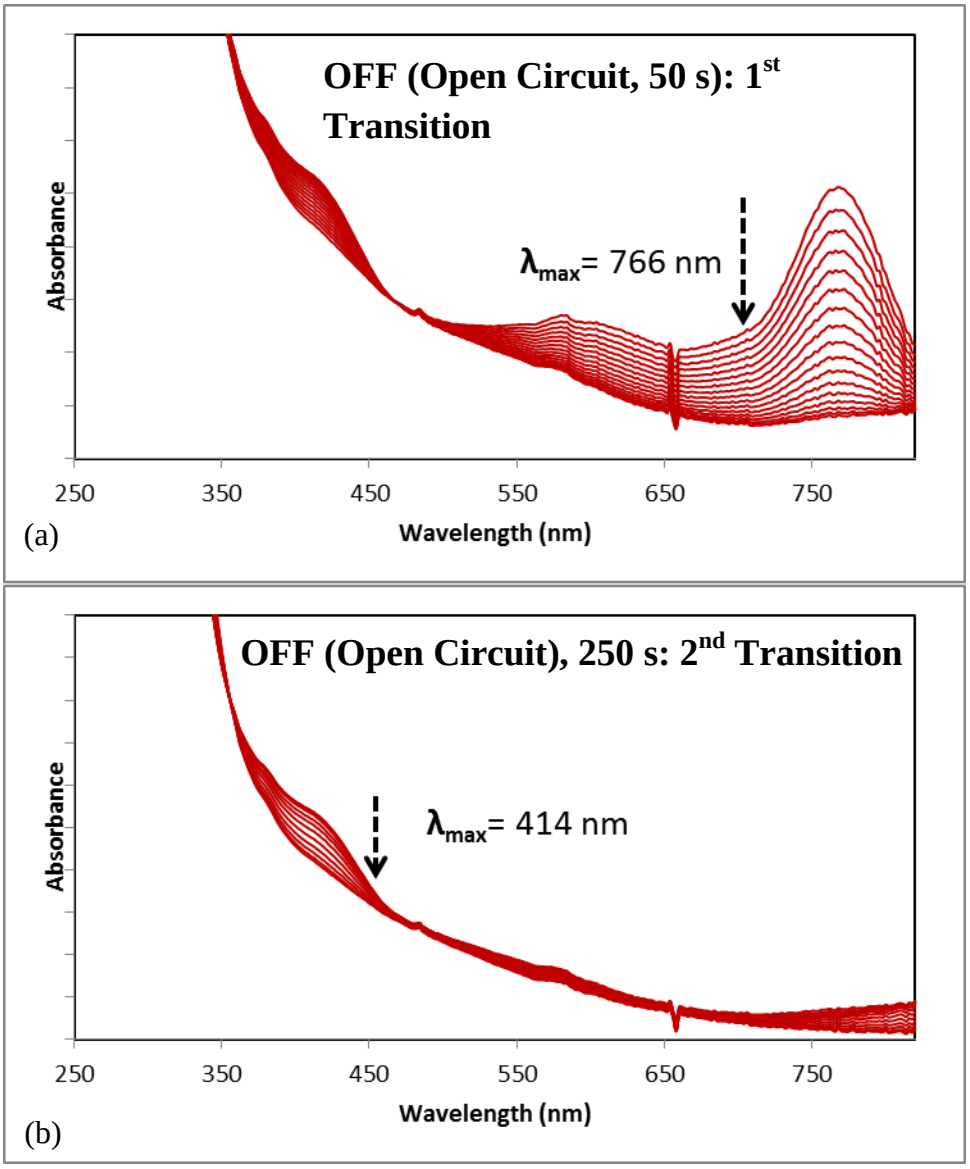

Figure 1.4.20. Time-resolved UV-vis absorption spectra of TAPD in the "Off" device state, (open circuit conditions)- (a) first cathodic transition, (b) second cathodic transition.

The time it takes for the device to bleach (bleaching time) depends on mass transport related factors such as cell gap and solution viscosity.[2, 18] In chapter 2, we explore the effect that the formal charge of an electrochrome has on bleaching and coloration kinetics. In an 88.9 µm device (with MeCN/PMMA/PC/Li^+ gel electrolyte), bleaching from the blue, dicationic state to the completely reduced, neutral colorless state occurs in five minutes. Figure 1.4.21 shows that bleaching of the reddish brown radical monocationic state (λ_{max} = 414 nm) occurs considerably

more slowly than the decoloration of the blue dicationic state (λ_{max} = 766 nm) with bleaching times of 250 s and 50 s, respectively. $TAPD^{\cdot+}$ has a less positive E° value than $TAPD^{++}$ (0.46 V vs 0.92 V) which contributes to the difference in bleaching time.

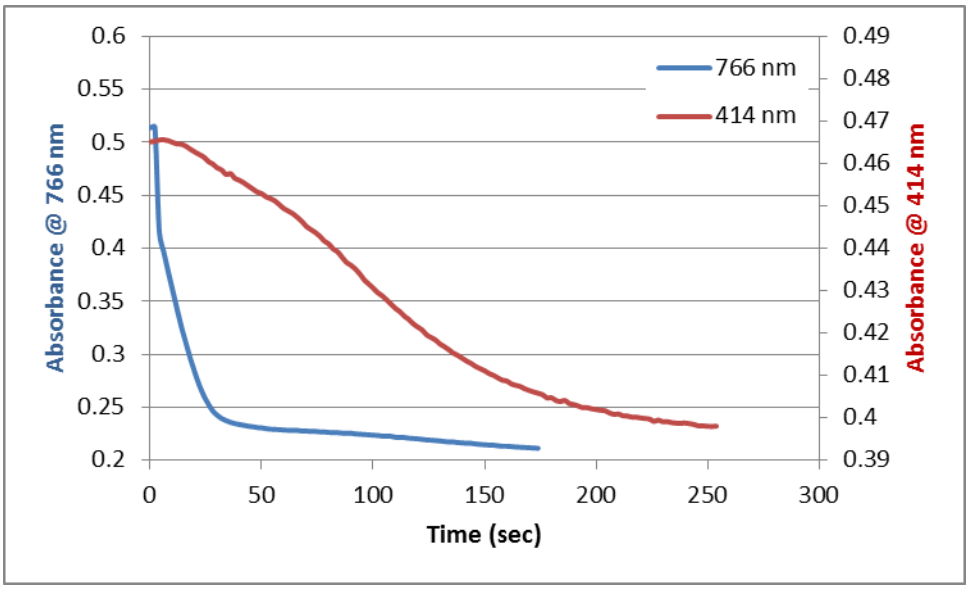

Figure 1.4.21 Bleaching time comparison of the "blue" absorbance band (766 nm) and the reddish brown absorbance band (414 nm).

Self-bleaching occurs as a result of recombination- electron transfer between the reduced and oxidized species in the cell. The amount of time it takes for recombination to occur is controlled by mass transport, namely diffusion.[2] Figure 1.4.22 demonstrates this process. In the "off" state of the device, there is no voltage applied (open circuit conditions) and no color. The fully reduced electrochrome is evenly dispersed in the gel electrolyte between the two ITO electrodes. When an anodic potential is applied, oxidation occurs at the anode, generating positively charged ions in solution. At the cathode, a solid state reduction takes place as ITO (presumably Sn^{IV}) accepts electrons. These electrochemical redox processes are accompanied by the detectable color changes discussed previously. When open circuit conditions are applied, the electron deficient positively charged ions diffuse to the reduced ITO (Sn^{II}) of the cathode and are neutralized, returning the device to its original "off" state.

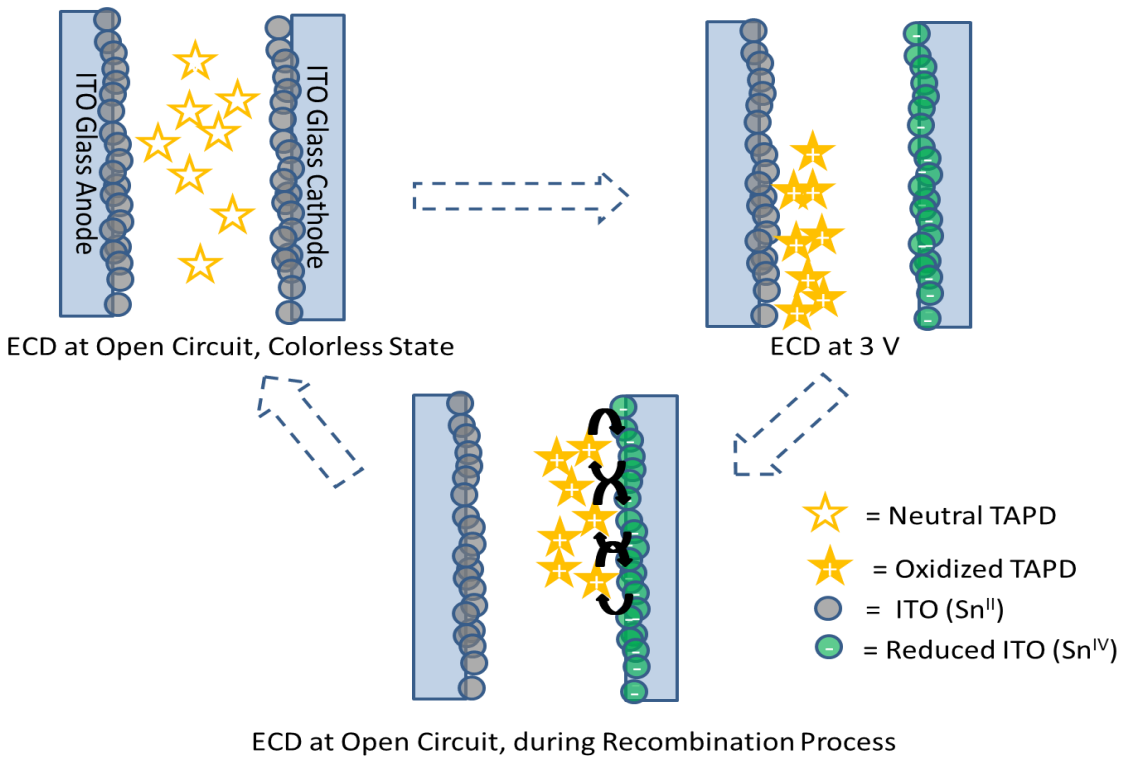

Figure 1.4.22. Schematic representation of recombination process in TAPD based singular ECD.

1.4.4.5 Electrochromic Device Switching in Singular Device State

The most important characteristic of an electrochromic molecular dye is its ability to switch between colored states in the device state. Thus, **TAPD** is electrochromically switched at 766 nm (blue to colorless and vice versa). Over eleven cycles, the optical contrast (ΔT_{766nm}) of the device remains near 62% (figure 1.4.23).

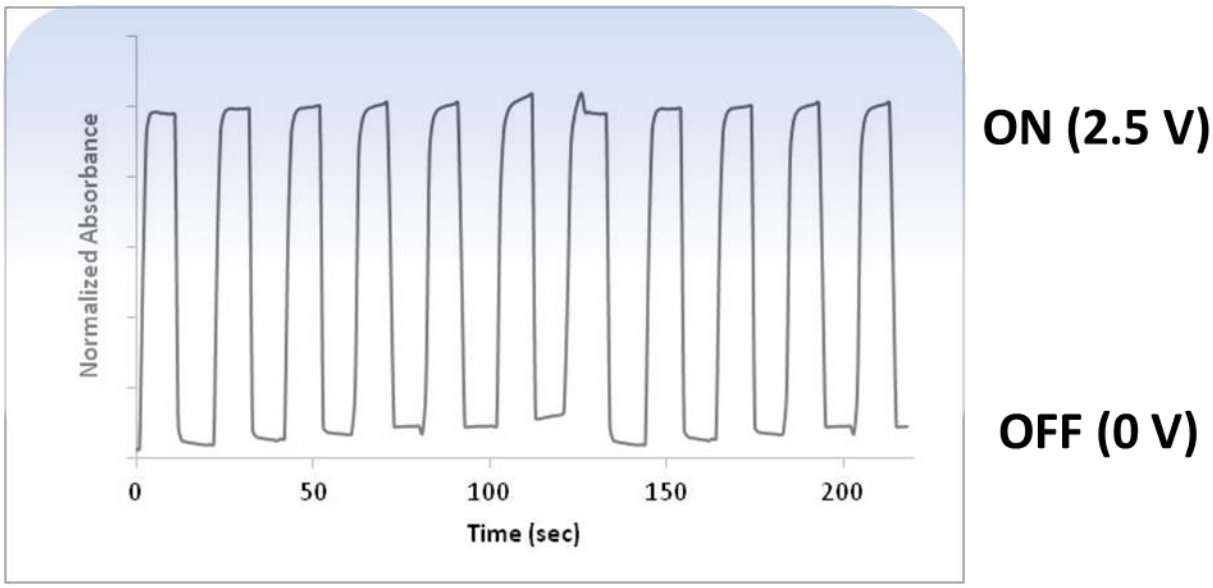

Figure 1.4.23. Electrochromic switching of TAPD at 766 nm (10 s at 2.5 V, 10 s at 0.0 V).

The most ideal way to demonstrate the multielectrochromism of a molecular dye is to apply it to singular-type ECD. In a singular type configuration, there is only one active electrochrome contributing color in the device. The counter material is optically passive or minimally coloring. ITO is the most practical material to use in this fashion however its use directly decreases the cycle life of the ECD. The use of ITO reduction (~-1.7 V vs. SCE) as the counter/cathodic process with the oxidation of **TAPD** (0.46 V and 0.92 vs. SCE) as the working/anodic process causes high operating voltages to induce coloration in the device (> 1.5 V). This, in turn, decreases the stability of the counter electrode. In order to improve the cycle life of the **TAPD** based ECD, a more suitable counter electrochrome would have to be incorporated into the device. Heptyl viologen (**HV**) is a common cathodically coloring electrochrome that has been proven compatible with phenylenediamine based electrochromes.[18-20] Compared to ITO, **HV** undergoes electrochemical reductions at significantly less cathodic

voltages (-0.95 V and -0.44 vs SCE). In the dual-type device, this should decrease the operating voltage and hinder irreversible degradation of the ITO electrode surface.

1.4.5 Electrochromic Device Switching in Complementary Dual Device State

We incorporate TAPD into a dual electrochromic system with heptyl viologen, **HV**, as a robust counter electrochromic material. **HV(BF$_4$)$_2$** is used to prepare an ECD similar to Ho et al. using **TAPD** in place of **TMPD**.[18] In theory, **HV(BF$_4$)$_2$** undergoes two reversible 1 e$^-$ reductions, shown in scheme 1.4.3. A cyclic voltammogram (figure 1.4.24) shows one cathodic wave at -0.448 V for the reduction of the colorless **HV(BF$_4$)$_2$** to form the blue **HV$^{\cdot+}$(BF$_4$)$_2$**. For the CV scan, voltages are kept above -0.6 V to avoid forming **HV^0**. Reaction of **HV^0** with the **HV(BF$_4$)$_2$** in the bulk solution leads to an irreversible dimerization (equation 1.4.2).[70]

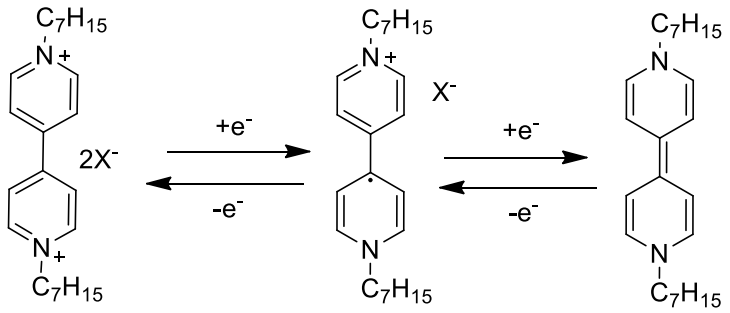

Scheme 1.4.3. Redox scheme for heptyl viologen (**HV**).

---

[70] Compton, R.G.; Monk, P.M.S.; Rosseinsky, D.R.; Waller, A.M. Electron Paramagnetic Resonance Spectroscopy of Electrodeposited Species from Solutions of 1,1′-bis-(*p*-cyanophenyl)-4,4′-bipyridilium (cyanophenyl paraquat, CPQ). *J. Chem. Soc. Faraday Trans.* 1990, *86*, 2583.

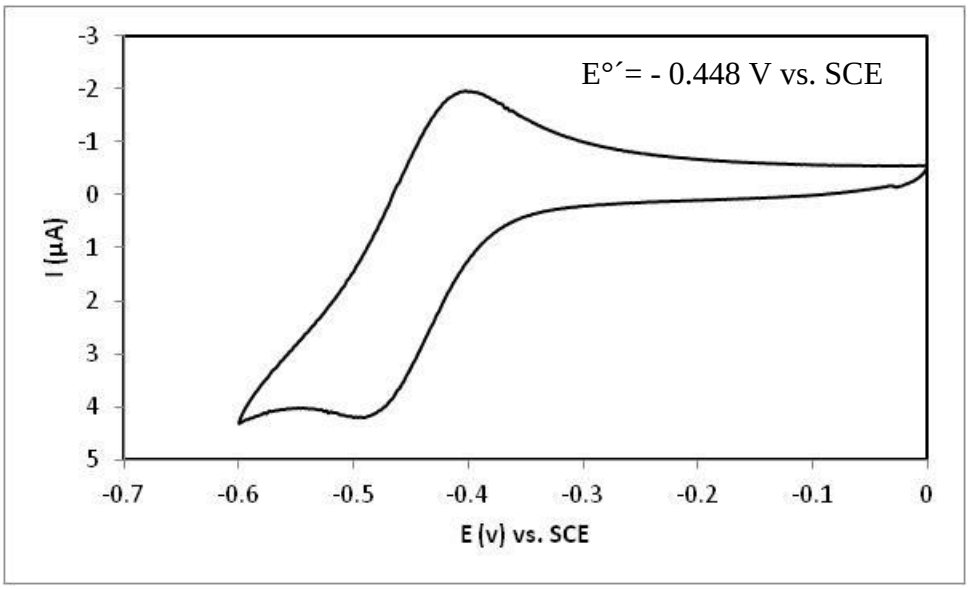

Figure 1.4.24. Cyclic voltammogram of 1.0 mM **$HV(BF_4)_2$** at Pt disc electrode in propylene carbonate (0.1 M Bu_4NBF_4) at 200 mVs^{-1} scan rate.

$$HV^{2+} + HV^{0} \longrightarrow (HV^{\cdot +})_2$$

Eq. 1.4.2. Dimerization of **$HV^{\cdot +}$**

$HV(BF_4)_2$ is used to prepare an ECD similar to that of Ho, et al. using **TAPD** in place of TMPD.[18] Figure 1.4.25 shows a CV of the **TAPD/ $HV(BF_4)_2$** ECD as potential is scanned from -0.5 V to 2.5 V. There are four redox processes observed, 2-1 e^- oxidations for **TAPD** and 2-1e^- reductions for **$HV(BF_4)_2$**. There is 0.4 V difference between the first redox processes for **TAPD** and **$HV(BF_4)_2$** (0.42 V and 0.00 V, respectively) . This difference represents the minimum amount of voltage required to turn-on the ECD. Figure 1.4.26 shows that at an applied voltage of 0.4 V the device begins to change colors. While not entirely noticeable to the eye, it is noted by a small change in absorbance in the visible region of the spectrum.

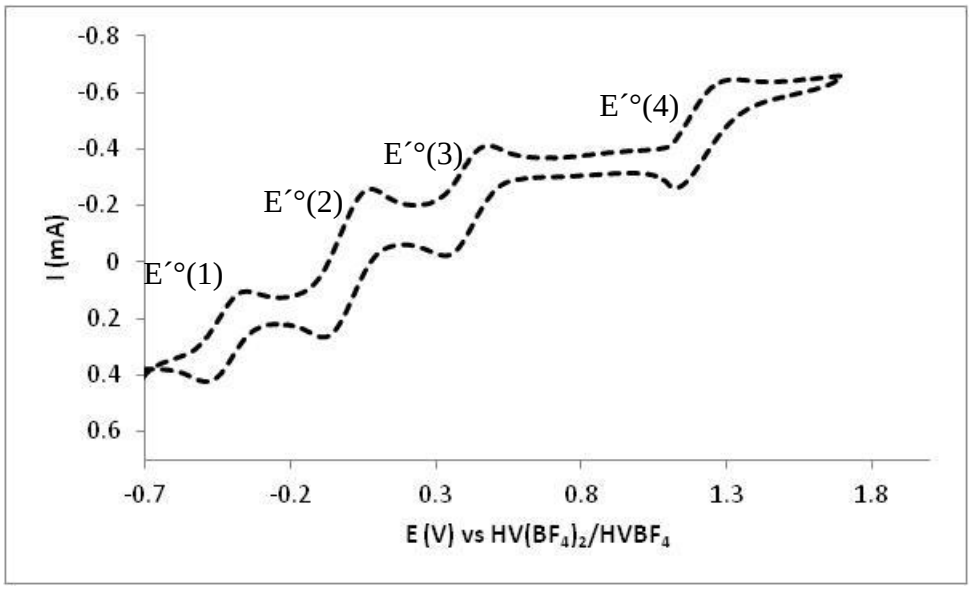

Figure 1.4.25. Cyclic voltammogram of **TAPD/HV(BF$_4$)$_2$** ECD at 100 mVs^{-1}.

	E° (V)	E_{pa} (V)	E_{pc} (V)	E_{pp} (V)
1	-0.440	-0.371	-0.509	0.138
2	0.000	0.076	-0.077	0.153
3	0.417	0.493	0.340	0.153
4	1.216	1.306	1.126	0.180

Table 1.4.1. Summary of redox couple data for the **TAPD/HV(BF$_4$)$_2$** ECD.

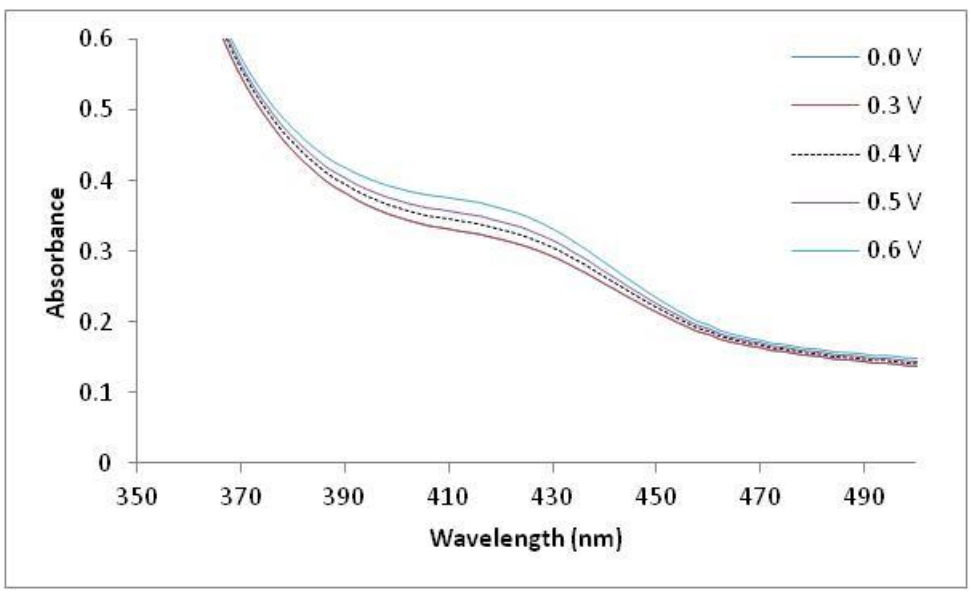

Figure 1.4.26. Spectroelectrochemical response of **TAPD/HV(BF$_4$)$_2$** dual-type ECD at low potentials (0.0-0.6 V). Each potential was held for 30 s.

The spectroelectrochemical response of the dual ECD is depicted in Figure 1.4.27 and 1.4.28. There are primarily two colored states, brownish-red and blue, similarly to the **TAPD** singular ECD. This indicates that **TAPD** electrochromism dominates the device and is in fact the primary electrochrome, in contrast to previous studies where *p*-phenylenediamine based electrochromes (TMPD) are labeled secondary to the cathodically coloring viologen species.

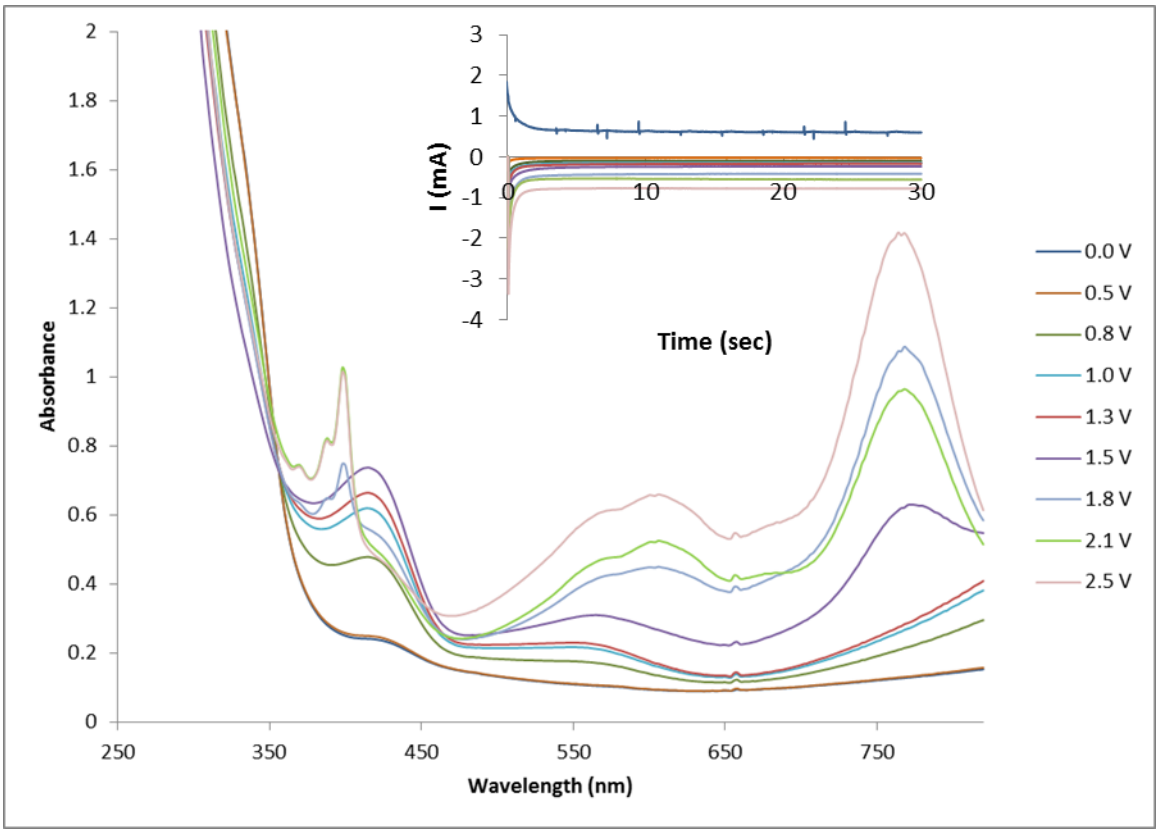

Figure 1.4.27. TAPD/HV(BF$_4$)$_2$ dual-type ECD at various applied potentials, 0.0 V-2.5 V. Each potential was held 30 s, until steady state current reached (see inset).

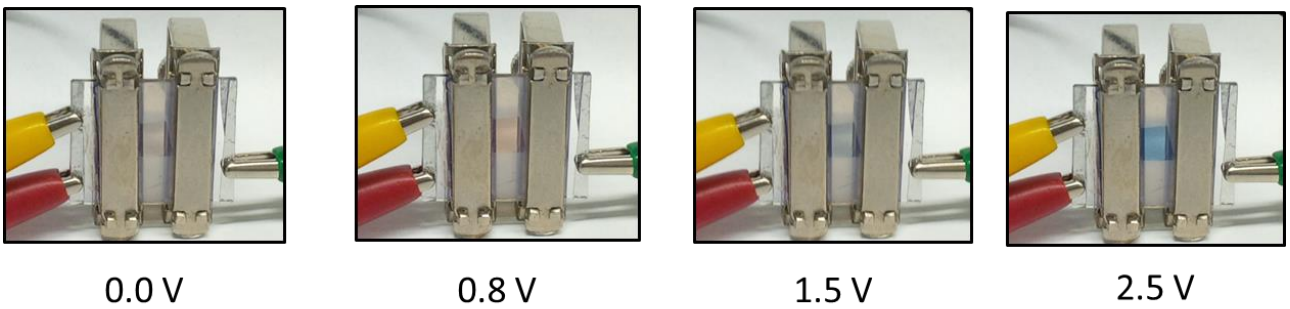

Figure 1.4.28. TAPD/HV(BF$_4$)$_2$ dual-type ECD at various applied voltages.

Our configuration leads to a higher optical contrast ($\Delta\%T_{766}$ = 99.7%)[71] due to the enhanced optical properties of TAPD cation salts (ε_{414} = 10100 $M^{-1}cm^{-1}$, ε_{766} = 72500 $M^{-1}cm^{-1}$) compared to TMPD cation salts (ε_{615} = 9210 $M^{-1}cm^{-1}$). Figure 1.4.29 shows >40 electrochromic cycles (8 s switches). Coloration times for the **TAPD/HV(BF_4)$_2$** ECD were comparable to the TMPD/HV(BF_4)$_2$ system at 2.0 s however, the bleaching time (0.0 V applied) was much faster in the **TAPD/HV(BF_4)$_2$** system (1.0 s vs. 8.0 s in the TMPD/HV(BF_4)$_2$ ECD). This is due in part to the smaller cell gap of the device (89.9 µm vs 140 µm in the TMPD/HV(BF_4)$_2$ ECD) Table 1.4.2 summarizes the comparison of spectroelectrochemical characteristics.[72,73,74]

Anodic Material	Cathodic Material	Electrochrome Concentration (M)	Cell Gap (µm)	Electrolyte	Operating Voltage	Δ%T (%)	τ_c (s)	τ_b (s)	Cycle Life	ref.
TMPD	HV(ClO_4)$_2$	0.05 M	190.0	MeCN	0.6 V	84	N/A	N/A	N/A	34
TMPD	HV(BF_4)$_2$	0.05 M	140.0	TBABF_4/PMMA/PC	0.8 V	75.5	2.5	8	10^2	32,33
TAPD	HV(BF_4)$_2$	0.01 M	89.9	LiClO_4/PMMA/PC/MeCN	0.8 V	64.9(adj: 99.7)	< 2.0 s	< 1.0 s	10^3	This Work

Table 1.4.2. Comparison of results obtained in this work with selected data taken from literature.[69]

[71] The optical contrast value of 99.7% in the **TAPD/HV** ECD refers to an ECD with a concentration of 0.05 M and a cell gap of 140 µm.

[72] Selby, T. D.; Kim, K.-Y.; Blackstock, S. C. Patterned Redox Arrays of Polyarylamines I. Synthesis and Electrochemistry of a *p*-Phenylenediamine and Arylamino-Appended *p*-Phenylenediamine Arrays. *Chem. Mater*. **2002**, *14*, 1685.

[73] Kim, K.-Y.; Hassenzahl, J. D.; Selby, T. D.; Szulczewski, G. J.; Blackstock, S. C. Patterned Redox Arrays of Polyarylamines II. Growth of Thin Films and Their Electrochemical Behavior. *Chem. Mater*. **2004**, *14*, 1691.

[74] Li, J. C.; Kim, K.-Y.; Blackstock, S. C.; Szulczewski, G. J. Patterned Redox Arrays of Polyarylamines III. Effect of Molecular Structure and Oxidation Potential on Film Morphology and Hole-Injection in Single-Layer Organic Diodes. *Chem. Mater*. **2004**, *16*, 4711.

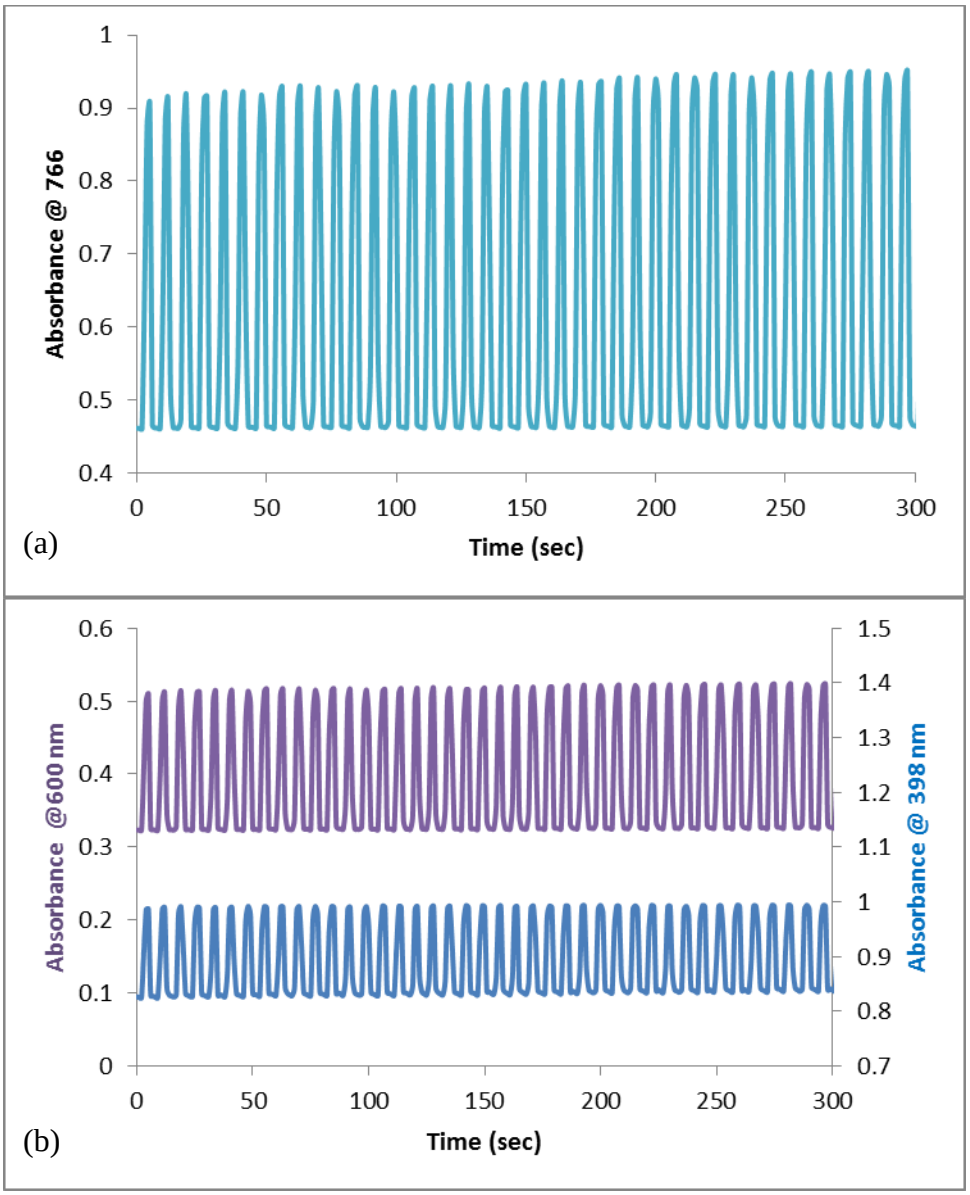

Figure 1.4.29. Electrochromic switching of **TAPD/HV(BF_4)$_2$** dual-type ECD (On= 0.8 V for 4 s, Off= 0.0 V for 4 s) at 766 nm (a), 414 nm (b), and 600 nm (b).

There was a noticeable effect of operating voltage on cycle life. It was possible to achieve over 1000 cycles at an operating voltage of 0.8 V with negligible change in optical contrast (Figure 1.4.30b only shows 85-8s cycles). This is an order of magnitude higher than the TMPD/HV(BF_4)$_2$ configuration. At an operating voltage of 2.5 V, while significantly more colored, the **TAPD/HV(BF_4)$_2$** ECD was only able to undergo 16 cycles before experiencing a degradation in optical contrast of over 60%. This lack of toleration of higher operating voltages

is due to the electrochemical instability of ITO and could be avoided by replacing the OTE material with a more electrochemically robust material. Figure 1.4.30 depicts the cycle life dependence on operating voltage.

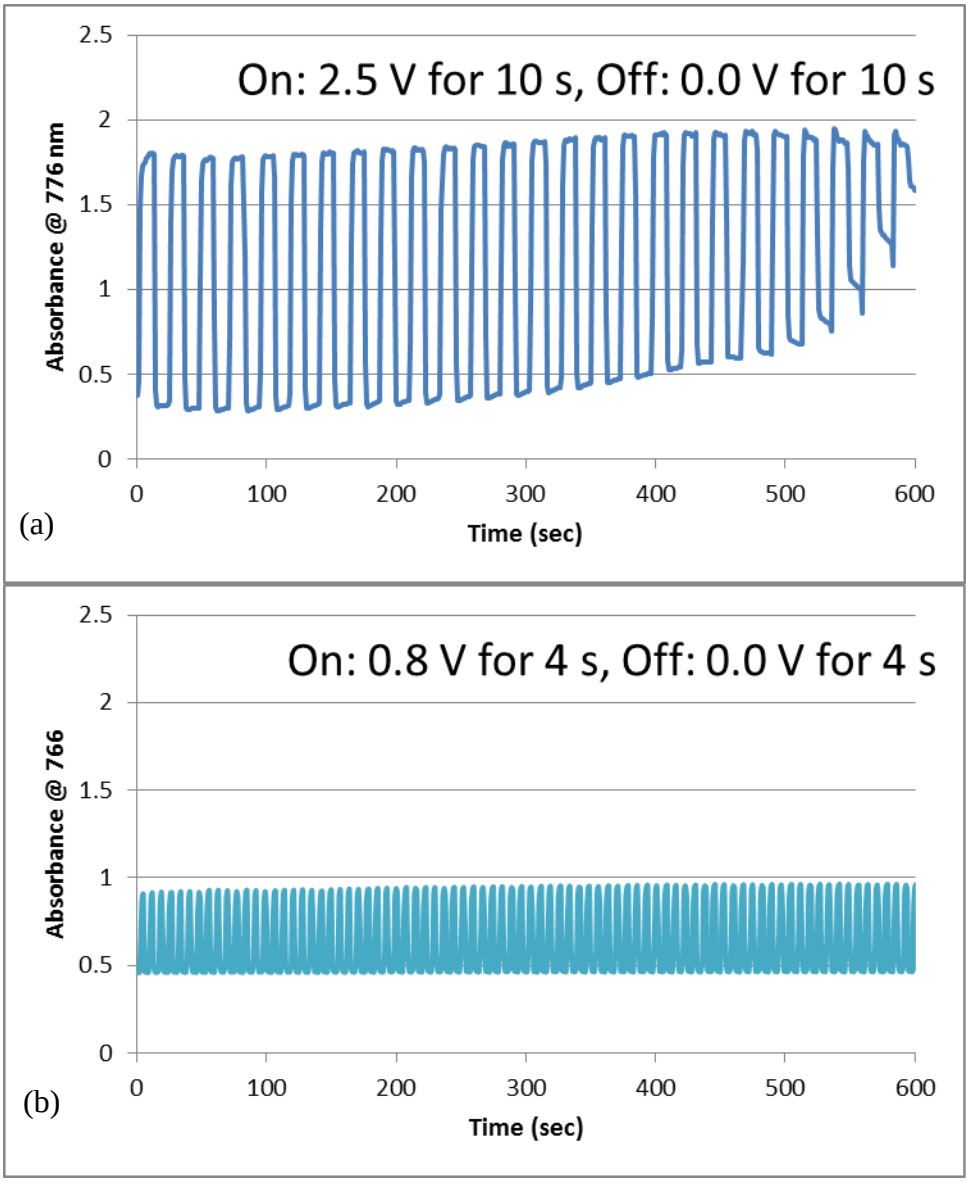

Figure 1.4.30. Electrochromic cycling of **TAPD/HV(BF$_4$)$_2$** dual-type ECD using operating voltages of 2.5 V (a) and 0.8 V (b).

The electroactive material, **TAPD**, is a multi-colored electrochromic molecular dye, owing its multiple hues to the air-stable amminium cationic salts that are formed upon electrochemical oxidation. A singular-type ECD effectively exploits the multiple colors

exhibited by **TAPD** at specific applied voltages. **TAPD** can also be employed as a primary electrochrome in a dual-type solution state configuration with heptyl viologen as the cathodically coloring color-reinforcing material. **TAPD**- based devices exhibit improved electrochromic switching characteristics (i. e. optical contrast, bleaching time, cycle life) compared to previously studied *p*-phenylenediamine based electrochromic dyes and could be highly useful in applications such as electrochromic fabrics. Future work involves further developing arylamino-based electrochromes that possess more intricate electronic structures, allowing more color combinations to be electrochemically switched.

1.5 Experimental

Experimental

General Methods and Materials. *N, N, N´, N´*-tetra-1,4-anisyl-1,4-phenylenediamine, **TAPD**, was synthesized by Lester Gray.[75] 1,1´- diheptyl-4,4´-bipyridimium dibromide was purchased from TCI America and used without further purification (purity confirmed by NMR). Propylene carbonate (PC) and polymethylmethacrylate (PMMA) were purchased from Alfa Aesar. Dichloromethane was obtained from VWR and distilled over CaH_2 in accordance with a known purification procedure.[76] HPLC grade Acetonitrile (MeCN) was purchased from EMD Millipore Chemicals. Lithium perchlorate ($LiClO_4$) was purchased from Aldrich. *N*-Tetrabutylammonium tetrafluoroborate ($TBABF_4$), a supporting electrolyte, was purchased from TCI America or OakWood Chemicals and was purified by recrystallization from 30 % ethanol three times then dried in a vacuum oven (100 °C, 0.1 Torr) for 30 h.[56] Inorganic oxidant, ceric ammonium nitrate (CAN), was purchased from Fisher. All materials were used without further purification unless otherwise noted.

ITO glass (ITO thickness: 120-160 nm, sheet resistance: 5-15 W/sq, nominal transmittance: >85%, glass thickness: 1.1 mm) was purchased from Delta Technologies (CB-50IN-1111) and subjected to the following cleaning procedure: The ITO side was determined using multimeter resistance measurement. The slide was rinsed and soaked in ACS grade acetone (Aldrich Chemicals) for 5.0 min. It was then sonicated (Fisher Scientific FS-10) for 10 min in a

---

[75] Gray, L.T. The Application of Arylamines as Redox Auxiliaries, Polar Crystals and Organic Semiconductors. Ph.D Dissertation, The University of Alabama, Tuscaloosa, AL, 2012.
[76] Perrin, D. D. and Armarego, W. L. F., Purification of Laboratory Chemicals, Pergamon Press: Oxford, 1988.

dilute aqueous soap solution. After sonication, the slide was rinsed thoroughly with distilled water, acetone, and dichloromethane. The surface was then dried using stream of N_2 gas.

Electrochemistry. (Figures 1.4.1, 1.4.24) Cyclic voltammetry (CV) and chronoamperometry were performed on a PAR 273 electrochemical potentiotstat (EG&G Instruments) A four-necked CV cell (10 mL) equipped with a stir bar, Pt disc (1.6 mm diameter) working electrode, a Pt wire counter electrode, and a saturated calomel electrode (SCE) reference was used for routine (solution state) CV measurements. $TBABF_4$ (0.1 M) was used as supporting electrolyte for electrochemical experiments unless otherwise noted. A capacitor (0.1 µF), connected between the reference electrode and counter electrode, was used to reduce background noise.

In each case, TBABF4 (0.823 g, 2.50 mmol) was dissolved in freshly distilled methylene chloride to 25.0 mL in a volumetric flask to give a 0.100 M solution. An amount (8.0 mL) of this solution was placed in a four-neck electrochemical cell with a magnetic stir bar. A blank CV scan (0.0 to 1.2 V vs SCE, 50 mV/s) was measured to ensure that no trace impurities existed in the solution as prepared. An amount of **TAPD** (4.3 mg, 8.0 x 10-3 mmol) or **$HV(BF_4)_2$** (4.2 mg, 8.0 x 10-6 mol) which would give a 1.0 mM solution was added to and thoroughly dissolved in the electrolyte solution. The potential was scanned from 0.0 to 1.2 V vs SCE at a rate of 100 mV/s and -0.7 to 0 V at 200 mV/s for **TAPD** and **$HV(BF_4)_2$**.

Chemical Oxidation. (Figures 1.4.2, 1.4.3, 1.4.4) A solution of **TAPD,** 1.03×10^{-5} M , was prepared by dissolving **TAPD** (1.5 mg, 0.00281 mmol) in 10 mL of MeCN. A small aliquot of the solution (366 µL) was diluted to 10 mL using a volumetric flask. The diluted solution (1.03×10^{-5}) subjected to redox titration with 1 and 2 molar equivalents of CAN to afford

TAPD$^{\cdot+}$and **TAPD**$^{2+}$ as nitrate (NO_3^-) salts, respectively. For UV-vis spectroscopy, an HP8452A Diode Array Spectrophotometer equipped with a 1 cm path length quartz cell (Starna) was used.

Preparation of Gel Electrolyte.[77] The gel electrolyte is composed of Acetonitrile (MeCN), Propylene Carbonate (PC), Polymethylmethacrylate (PMMA), and Lithium Perchlorate ($LiClO_4$) in a weight ratio of 70:20:7:3 of each component, respectively. PMMA (.547 g) was dissolved in 7 mL of MeCN. The mixture was stirred and heated until homogeneous. PC (1.31 mL, 1.564 g) and $LiClO_4$ (.235g, 2.21 mmol) were then added and the mixture stirred for 15 min at room temperature.

Construction of Singular ECD. (Figures 1.4.14, 1.4.15, 1.4.16, 1.4.17, 1.4.19, 1.4.20, 1.4.21, 1.4.23) TAPD (1.33 mg ,2.50x10^{-6} mol) was dissolved in 0.25 mL of gel electrolyte. The gel electrolyte solution was applied to the ITO glass anode (equipped with spacer), the ITO glass cathode was then added to complete a sandwich-type device. For 88.9 μm spacing, Polyethylene Plastic Sheeting (Husky Brand) was used. The ITO sandwich was held together with metal clamps for the duration of the experiment. Aluminum foil tape (Shurtape AF-100) was used for efficient contact between ITO and metal spring clips. See figure 1.2.9 for a photograph of ECD.

Synthesis of $HV(BF_4)_2$.[78] 1,1´- diheptyl-4,4´-bipyridimium tetrafluoroborate, **$HV(BF_4)_2$**, was prepared from 1,1´- diheptyl-4,4´-bipyridimium dibromide by a salt exchange reaction: A 5 mL of a saturated aqueous solution of the dibromide salt was added to 5 mL of saturated aqueous

---

[77] Beaupre´, S.; Dumas, J.; Leclerc, M. Toward the Development of New Textile/Plastic Electrochromic Cells Using Triphenylamine-Based Copolymers. *Chem. Mater.* **2006**, *18*, 4011-4018.

[78] Ho, K. C.; Fang, Y-W.; Hsu, Y-C; Chen, L-C. The Influences of Operating Voltage and Cell Gap on the Performance of a Solution-Phase Electrochromic Device Containing HV and TMPD. *Solid State Ionics* **2003,** *165*, 279-287

lithium tetrafluoroborate solution. The white precipitate was filtered and recrystallized from warm ethanol.

Construction of Dual ECD. (Figures 1.4.25, 1.4.26, 1.4.27, 1.4.29, 1.4.30) TAPD (2.66 mg ,5.00x10^{-6} mol) and **$HV(BF_4)_2$** (2.64 mg, 5.00x10^{-6} mol) were dissolved in 0.50 mL of gel electrolyte. The gel electrolyte solution was applied to the ITO glass anode (equipped with spacer), the ITO glass cathode was then added to complete sandwich-type device. For 88.9 μm spacing, Polyethylene Plastic Sheeting (Husky Brand) was used. The ITO sandwich was held together with metal clamps for the duration of the experiment. Aluminum foil tape (Shurtape AF-100) was used for efficient contact between ITO and metal spring clips (figure 1.2.9).

Spectroelectrochemistry (and electrochromic switching). Spectroelectrochemical data were recorded using a PAR 273 electrochemical potentiostat (EG&G Instruments) and HP8452A Diode Array Spectrophotometer operating concurrently (appendix 1 or figure 3). The clamped ECD was placed in front of the spectrophotometer beam in order to perform optical measurements. For electrochemical measurements, ITO glass was used as working and counter electrode material. Voltages were referenced to the counter electrode, ITO reduction and **$HV^{++}(BF_4)_2$** reduction for the singular and dual ECD, respectively. A photograph of the spectroelectrochemical set-up can be found in chapter 1 (figure 1.2.10). Cyclic voltammetry of the **TAPD**/**HV** dual ECD was performed at a scan rate of 100 mVs^{-1}.

Chapter 2

The Synthesis and Study of Anionic Arylamines as New Radical Zwitterions and Electrochromic Molecular Switches

2.1 Introduction

2.1.1 Motivation #1: Investigating the Effect of Formal Molecular Charge on Electrochromic Switching Kinetics

Since an electrochromic device (ECD) is fundamentally an electrochemical cell, switching kinetics are governed by three rates:[79]

1. The rate of electron transport through the electrode material
2. The rate of electron movement through the heterogeneous bulk solution-electrode interface
3. The rate at which the electrochrome travels through the bulk solution to reach the electrode

[79] Monk, P.M.S.; Mortimer, R. J.; Rosseinsky, D. R. *Electrochromism and Electrochromic Devices;* Cambridge: UK, 2007

Of the three, rate #3 is the limiting process thus, electrochromic switching kinetics are a function of mass transport. Mathematically, mass transport is described by the Nernst-Planck equation (Equation 2.1).[80]

$$J_i = \underbrace{\frac{z_i F}{RT} c_i \left(\frac{\partial \emptyset(x)}{\partial x}\right)}_{\textbf{Migration}} + \underbrace{c_i \overline{v_i}\,(x)}_{\textbf{Convection}} - \underbrace{D_i \left(\frac{\partial c_i(x)}{\partial x}\right)}_{\textbf{Diffusion}}$$

Equation 2.1. Nernst-Plank equation

The equation combines three mechanisms of mass transport: migration, convection, and diffusion. The modes interconnect in an additive fashion. The first term refers to migration, movement resulting from the ohmic conduction of current. The second term of the equation is convection, the physical movement of the solution. The final term is for diffusion, movement as a result of concentration gradients in solution. J_i is the flux, the amount of ions, *i*, reaching the solution-electrode interface per unit time. In electrochromic devices, convection is neglected as there is only a negligible amount of physical movement in the solution. Thus, only diffusion and migration are considered effective modes of transport in electrochromic devices. Variables effecting diffusion include the diffusion coefficient for the species, *i*, as well as the change in concentration per unit distance, $\frac{\partial c_i(x)}{\partial x}$. In the migration portion of the equation, variables include the strength of the electric field, $\emptyset(x)$ along the *x*-axis, the concentration of the species, c_i, the temperature of the solution, T, and the valence of the ionic species, z_i. In the case of phenylenediamine-based molecular dyes, like **TAPD** or **TMPD**, coloration kinetics are a result of only diffusion. Because they are neutral, the valence, z_i, is 0 making the contribution of migration to the solution mass transport kinetics also 0.

[80] Bard, A. J.; Faulkner, L. R. *Electrochemical Methods;* Wiley: US, 2001.

In Chapter 2, we aim to effect faster coloration and bleaching times by synthetically altering an electrochrome, adding formal charge without changing the redox state of the chromophore. In doing so, we hope to maintain the optical and electrochemical characteristics of the electrochrome while effecting the valence of the molecular species, z_i. The expectation is that by incorporating a formal charge, we increase the contribution that migration makes to the mass transport kinetics, thereby affecting the electrochromic switching dynamics.

Our rationale was inspired in part by the viologen family of electrochromic molecular dyes (Scheme 2.1.1). Inarguably, the most developed class of electrochromic molecular dyes, they commonly exhibit three redox states: dicationic, monocationic, and neutral.[1,81,82] In ECD's they are incorporated in their dicationic form, as quaternized bipyridilium salts since it is the most stable form of the redox system. While it has not been formally studied, the effect that a positive molecular charge has on cathodic electrochromic switching kinetics has been alluded to.[1,83] Thus, using a new anionic phenylenediamine-based anodic electrochrome, PD-sulfonate, we intend to investigate the effect of formal charge on electrochromic switching in a type I solution-state ECD (2.1.1).

---

[81] Monk, P.M.S. *The Viologens: Physicochemical Properties, Synthesis and Applications of the salts of 4,4´-Bipyridine*; Wiley: US, 1998.
[82] Monk, P.M.S.; Mortimer, R. J.; Rosseinsky, D. R. *Electrochromism: Fundamentals and Applications;* VCH: Weihein, 1995.

[83] Byker, H.J. Single-Compartment , Self-Erasing, Solution-Phase Electrochromic Devices, Solutions for Use Therein and Uses Thereof. U.S. Patent 4,902,108,1990.

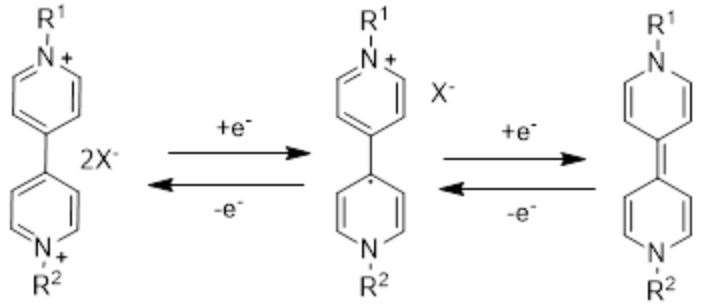

Scheme 2.1.1. Bipyridil redox chemistry.

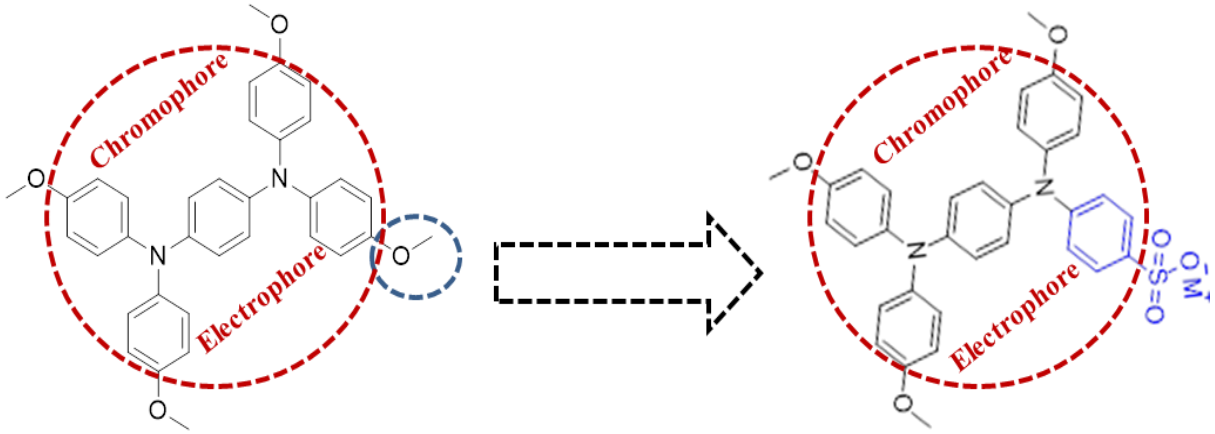

Figure 2.1.1. Pictorial demonstration of rationale behind the design of the anionic PD electrochrome.

2.1.2 Motivation #2: Electrochromic Switching Studies as a Platform for the Isolation of New Stable Radicals

A question rarely asked in electrochromic literature is "What, specifically, is the nature of the species giving rise to the color (s) displayed in a given ECD?" During the course of demonstrating the utility of a system as an electroactive molecular switch, it seems intuitive (at least from a physical organic standpoint) to attempt to isolate and characterize the structure and chemical properties of the colored redox intermediates. Thus, we perform a two-track

investigation. While synthesizing and characterizing new anionic arylamines as electrochromic materials, we take advantage of the intrinsic opportunity to isolate and characterize the new stable radical systems.

2.2 Synthesis and Characterization of Anionic Aryl Amines: A New Class of Radical Based Internal Salts

2.2.1 Synthesis of AA-SO_3^- Na^+ via Indole Sulfonamide Protecting Group

The preparation of the sodium salt, **AA-Sulfonate** (**7**), was accomplished in four steps. Commercially available indole is used to generate the sulfonamide protected aryl bromide (**4**) that is then coupled with dianisyl amine (**2**) to generate the arylamino sulfonamide, **AA-Sulfonamide** (**6**) in moderate yield. The sulfonamide is then hydrolyzed under rigorous basic conditions to yield the sodium arylaminosulfonate salt, (**7**).

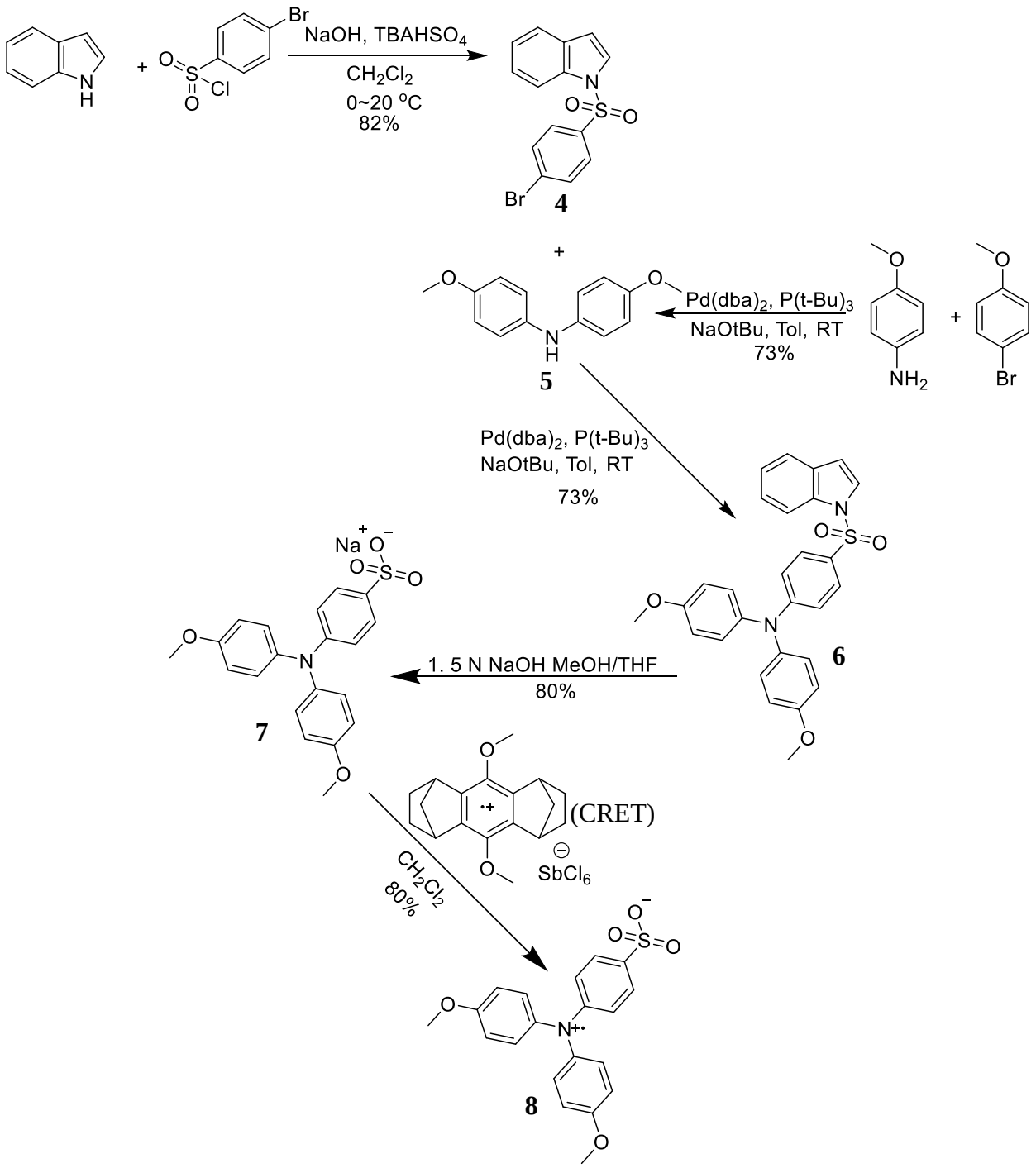

Scheme 2.2.1. Synthesis of **AA-Sulfonate** (**7**) and **AA-Zwitterion** (**8**).

2.2.2 Characterization of New Triarylamine Radical Zwitterion: Electrochemistry, Optical Spectroscopy, and Electron Paramagnetic Resonance (EPR) Studies

The electrochemistry of **AA-Sulfonate** (**7**) is comparable to that of neutral triarylamines, undergoing a 1 e^- reversible anodic redox process at 0.706 V vs SCE (Scheme 2.2.3). This potential is a slightly more cathodic potential than the **AA-Sulfonamide** precursor (**6**) which has an oxidation potential of 0.937 V vs. SCE (Scheme 2.2.2) or dianisylphenylamine (Scheme 2.2.4) which has an oxidation potential of 0.80 V vs. SCE.[84] Table 2.2.1 gives a summary of the electrochemical data for the triarylamines.

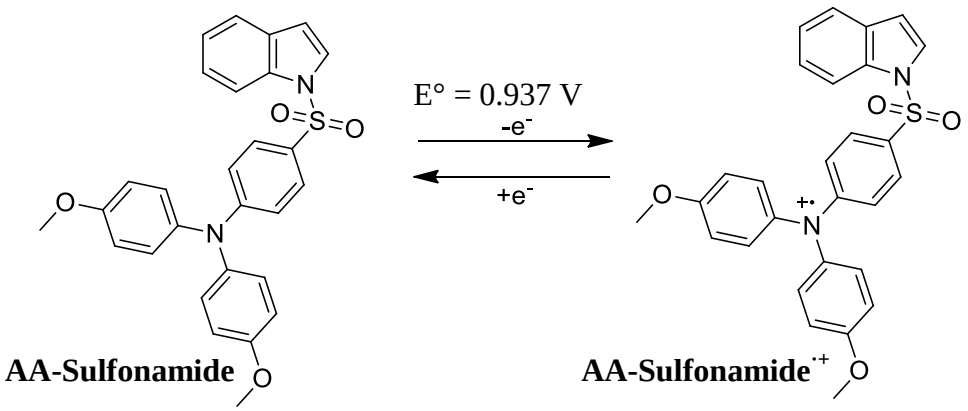

Scheme 2.2.2. Electrochemistry of **AA-Sulfonamide**.

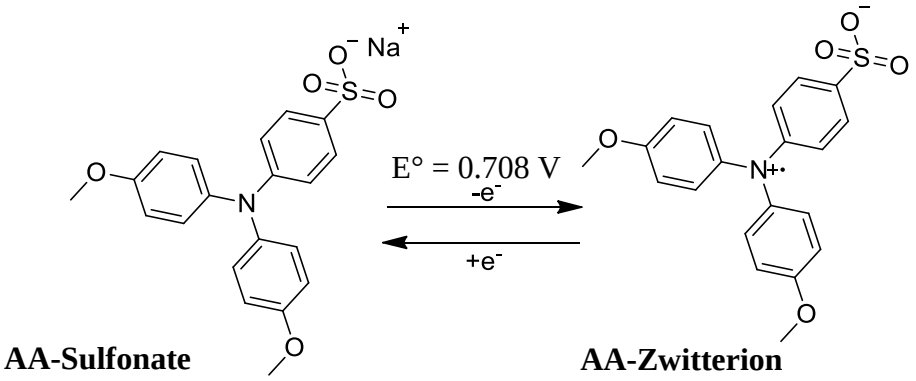

Scheme 2.2.3. Electrochemistry of **AA-Sulfonate**.

---

[84] Kim, K.-Y. Polyarylamino Redox Arrays for Control of Charge Transport and Charge Storage. Ph.D. Dissertation, The University of Alabama, Tuscaloosa, AL, 2003.

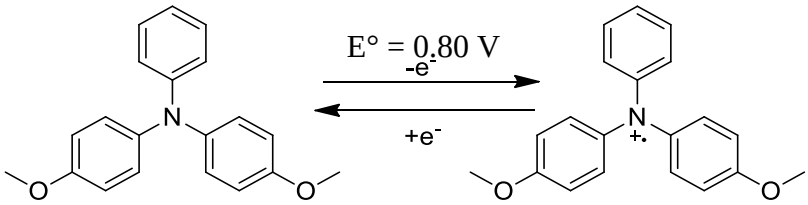

Scheme 2.2.4. Electrochemistry of dianisylphenylamine.

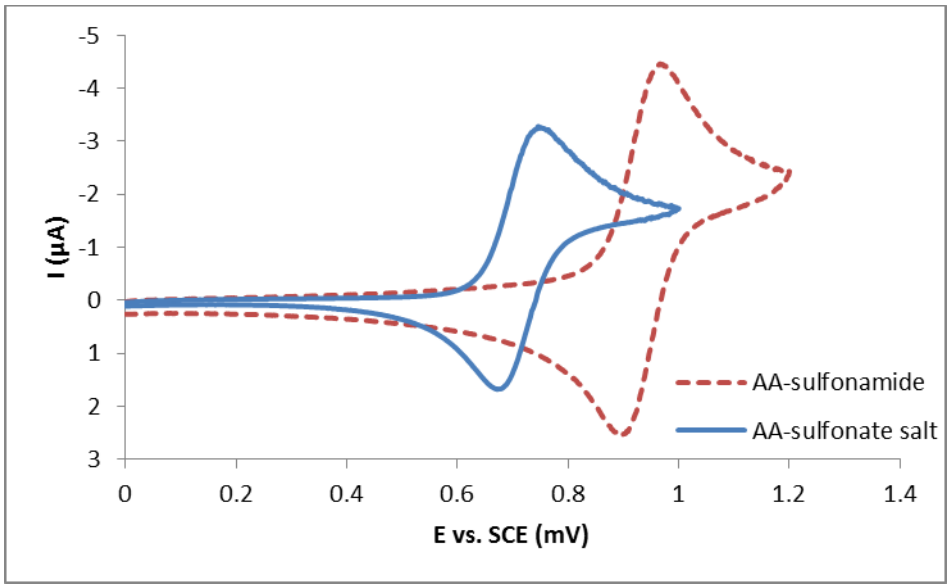

Figure 2.2.1. Cyclic voltammogram of 1.0 mM **AA-Sulfonate** (**4**) (blue line) and 1.0 mM (**3**) (red dashed line) at Pt disc electrode in MeCN (0.1 M Bu_4NBF_4) at 50 mVs^{-1} scan rate.

	E°	E_{pa}	E_{pc}	E_{pp}
AA-Sulfonamide	0.930	0.962	0.898	0.064
AA-Sulfonate	0.708	0.746	0.670	0.076

Table 2.2.1. Summary of electrochemical data for **AA-Sulfonate** and **AA-Sulfonamide**. Potentials are given in volts (V) vs. SCE.

We investigated the optical properties of, **AA-Sulfonamide** (**6**). Upon chemical oxidation with 1 equivalent CRET (Figure 2.2.2), it undergoes a color change from colorless to purple with a major absorbance band at 802 nm (ε_{802} = 13700 $M^{-1}cm^{-1}$). As expected due to its degree of conjugation, the radical cation (Scheme 2.2.2) is chemically stable. Figure 2.2.3 shows that over 15 hours, there is negligible change in the optical absorbance spectrum of the radical cation (**6**$^{\cdot+}$).

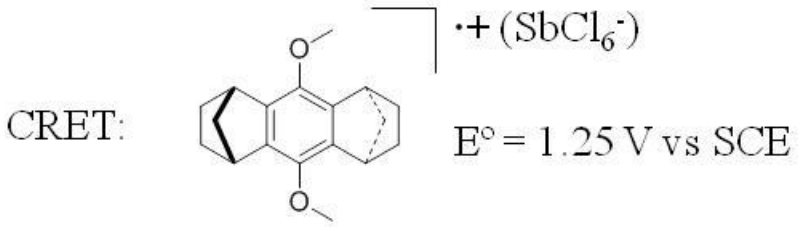

Figure 2.2.2. Structure and oxidation potential of Orange CRET (CRET).[85]

To assess the optical properties and solution state chemical stability of the radical zwitterion (**5**), UV-vis scale (10^{-5} M) chemical oxidation was employed using CRET as an oxidant (figure 2.2.2). As figure 2.2.4 shows, upon losing an electron, **AA-Sulfonate** (**7**) undergoes a noticeable color change from colorless to blue. In the visible region of the electromagnetic spectrum, this blue color is characterized by absorbances at 588 nm and 750 nm with molar absorptivity's of 7820 $M^{-1}cm^{-1}$ and 31200 $M^{-1}cm^{-1}$, respectively. Like the stable radical cation of the sulfonamide precursor (**6**$^{\cdot+}$), The internal salt (**8**) exhibits good chemical stability with no degradation in optical properties over the course of 15 hrs.

[85] Rathore, R.; Kochi, J. K. Isolation of Novel Radical Cations from Hydroquinone Ethers. Conformational Transition of the Methoxy Group upon Electron Transfer. *J. Org. Chem.* **1995,** 60, 4399-4411

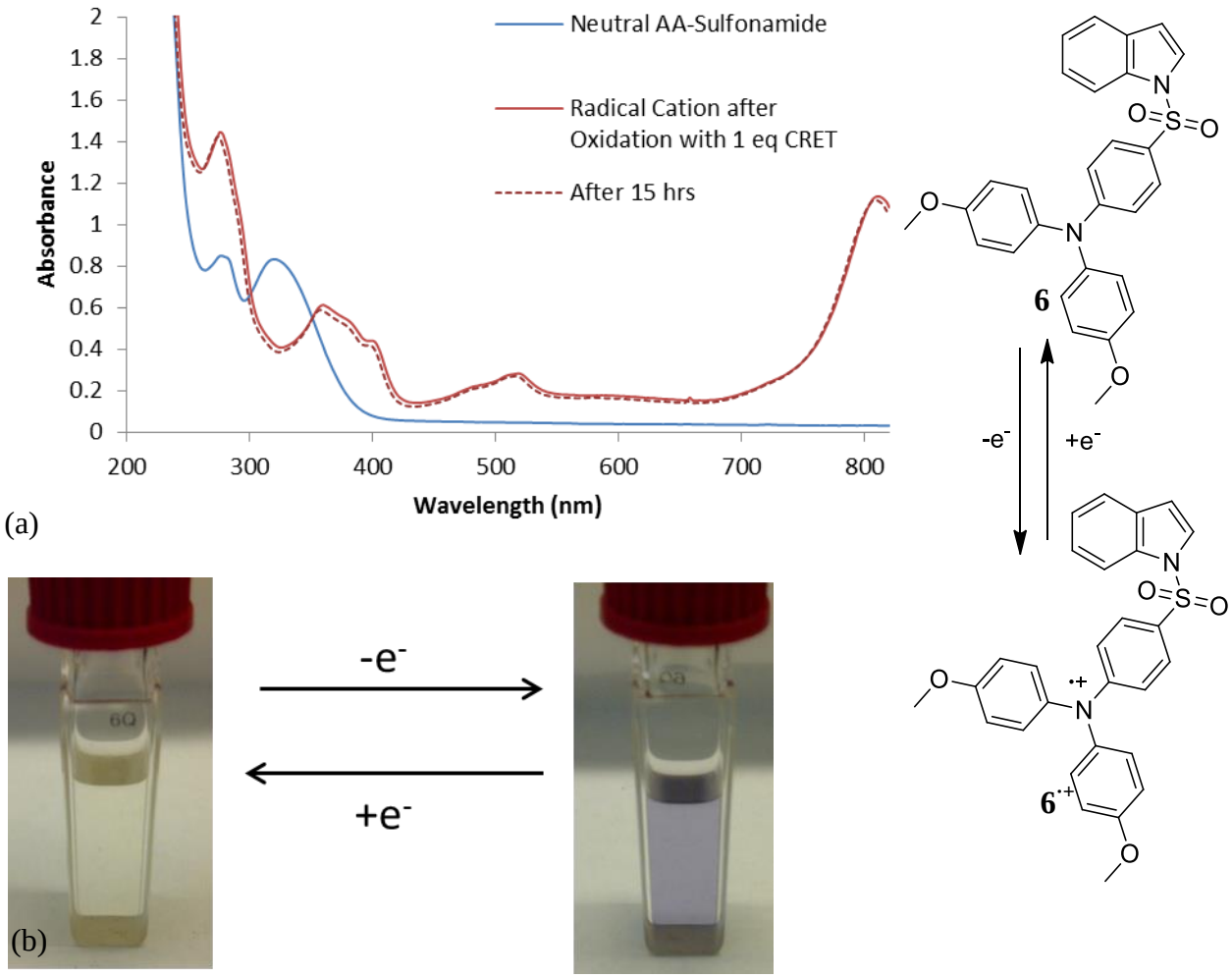

Figure 2.2.3. Chemical stability of 7.84×10^{-5} M **AA-Sulfonamide** radical cation (**6**$^{\cdot+}$). in CH_2Cl_2

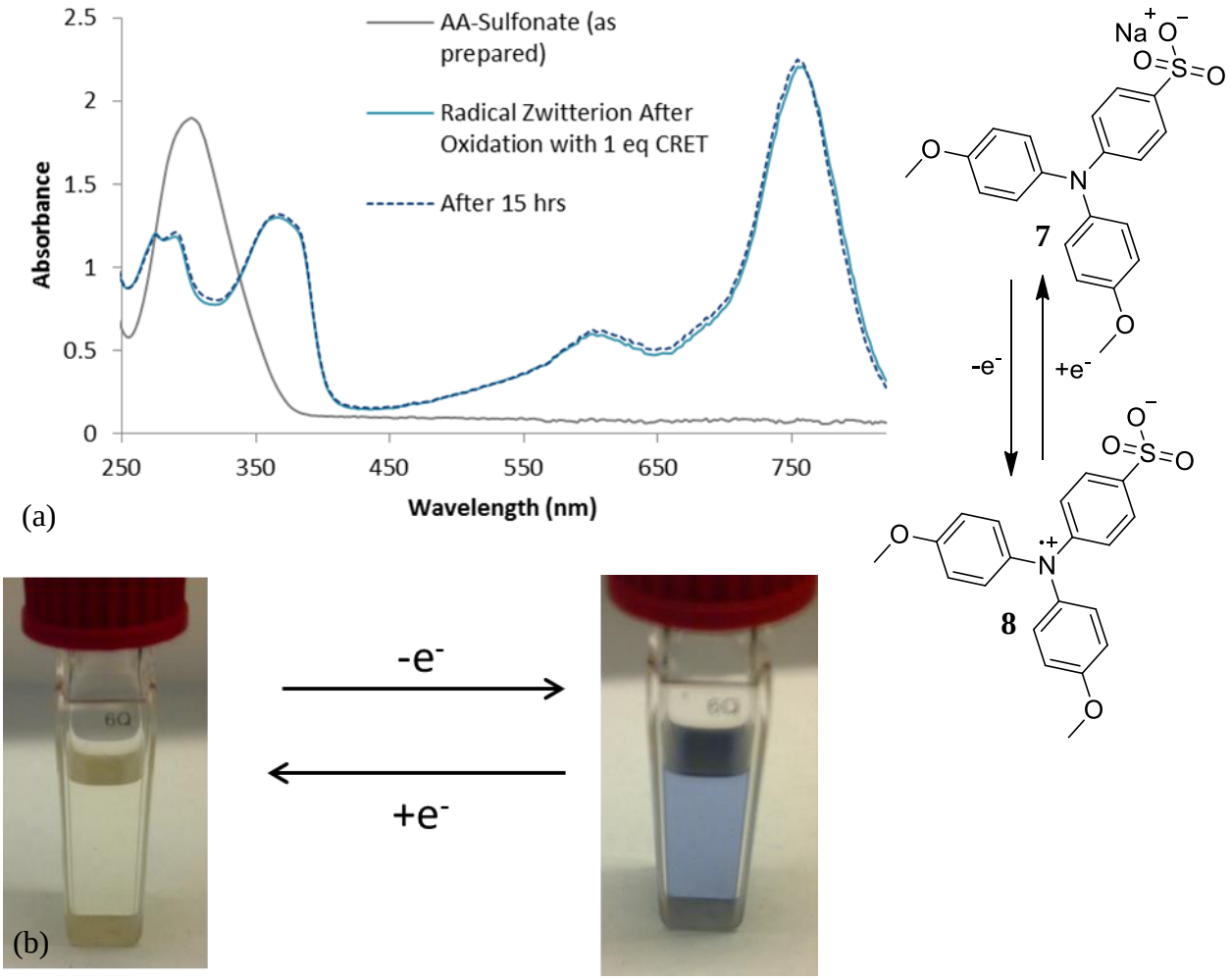

Figure 2.2.4 Chemical stability of 6.87 x10^{-5} M AA-Zwitterion (**8**) in CH_2Cl_2.

For Electron Paramagnetic Resonance (EPR) Spectroscopy, (**5**), was prepared via oxidation with the inorganic oxidant $NOPF_6$. The blue material was isolated as an oxygen stable solid and dissolved in DCM prior to the measurement. The room temperature EPR spectrum is shown in figure 2.2.5 with its a-value.[86] The a-value measures the amount of spin density that the radical electron has on a nucleus. The three line spectrum has an a value of 2.5 G. The result is in agreement with spectrum of triarylamine radical cations where there is a nitrogen centered

[86] EPR measurement taken by Alex Cruce.

radical present. This suggests that although the internal salt, (**7**)**,** has a neutral formal charge state, the nature of the radical in the molecule remains unchanged.

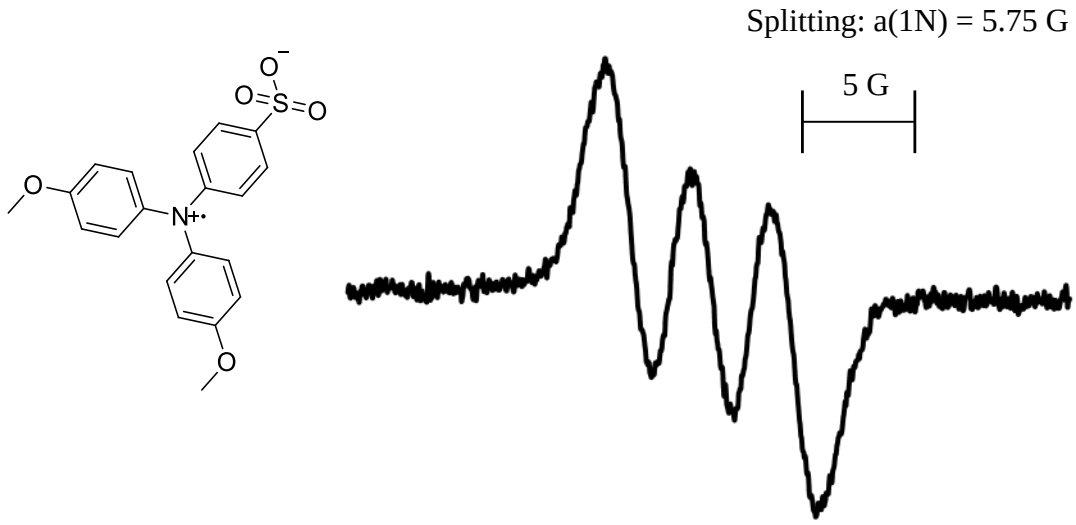

Figure 2.2.5 EPR spectrum of AA-Zwitterion (**8**) in CH_2Cl_2 (0.05 mM) at 22° C.

The preparation and characterization of this new stable arylamino internal salt (**5**) provides evidence that synthesizing a phenylenediamine derivative for electrochromic applications should be facile. The electrochemical and optical properties of an anionic phenylenediamine and its oxidized salts are expected to be similar to neutral phenylenediamines such as **TAPD**, studied in Chapter 1.

2.2.3 Synthesis of PD-SO_3^- Na^+ via Indole Sulfonamide Protecting Group

The preparation of the anionic electrochrome, **PD-Sulfonate** (**11**), shown in Scheme 2.2.2, was affected similarly to AA-sulfonate (**7**).The indole sulfonamide appended aryl bromide (**1**) was coupled with the trianisylphenylenediamine (**9**) via Hartwig Buchwald amination conditions. **PD-Sulfonamide** (**10**) was then hydrolyzed to yield the sodium sulfonate salt (**11**).

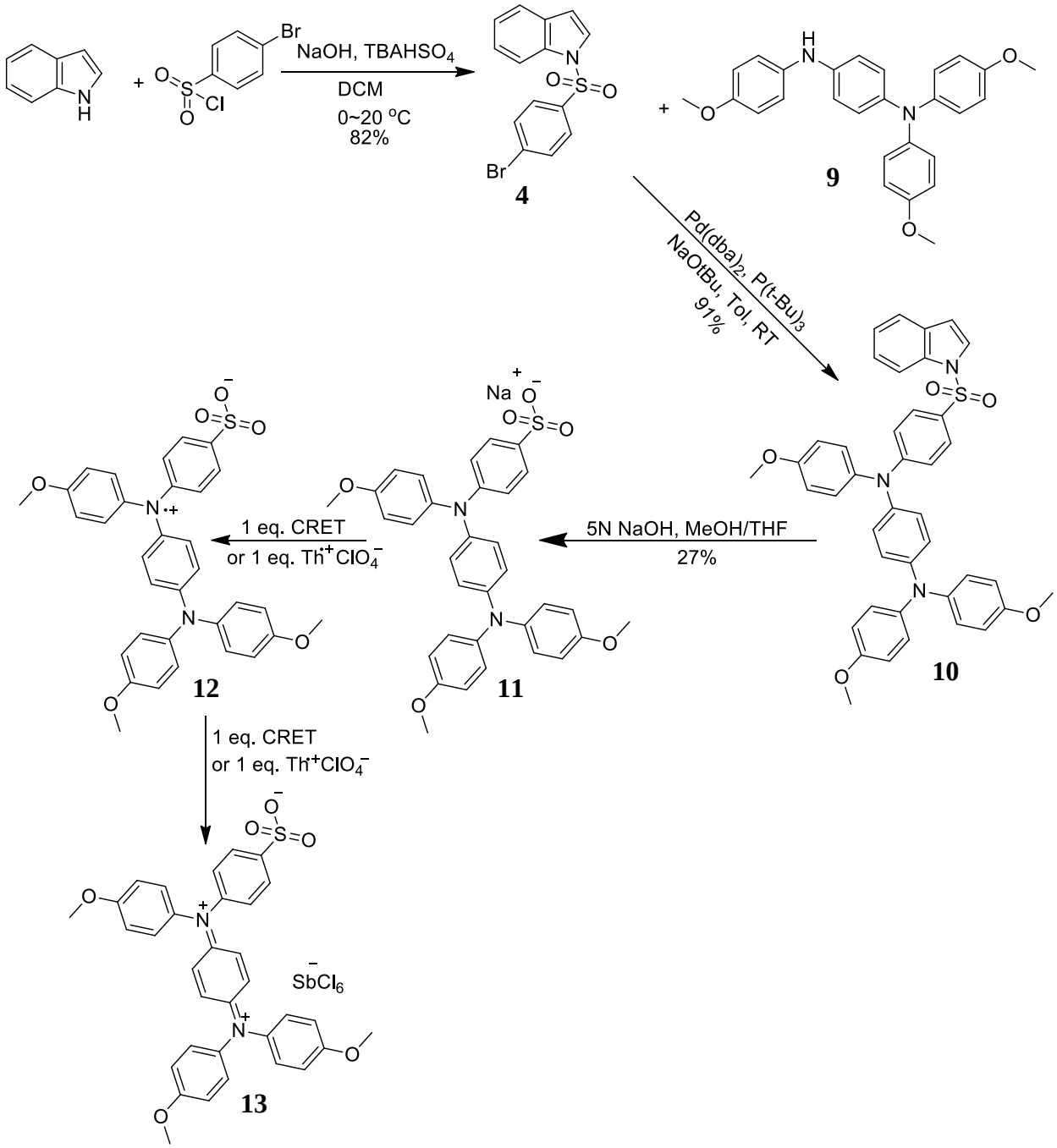

Scheme 2.2.5. Synthesis and chemical oxidation of **PD-Sulfonate (11).**

2.2.4 Characterization of New Phenylenediamine Radical Zwitterion: Electrochemistry, Optical Spectroscopy, and Electron Paramagnetic Resonance (EPR) Studies

Cyclic voltammetry of **PD-Indole** (**10**) and **PD-Sulfonate** (**11**) demonstrate the electrochemical and chemical stability of the systems (Figure 2.2.7 and 2.2.8). The scans closely resemble that of **TAPD** (figure1.2.1). Table 2.2.2 summarizes the electrochemical data for the phenylenediamines.

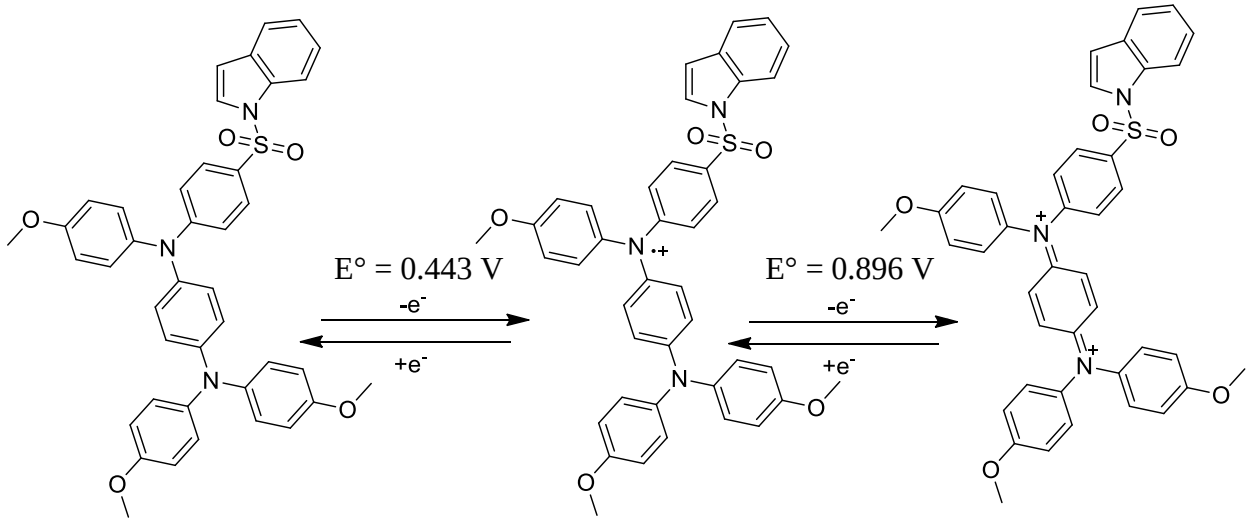

Scheme 2.2.6. Electrochemistry of **PD-Indole**.

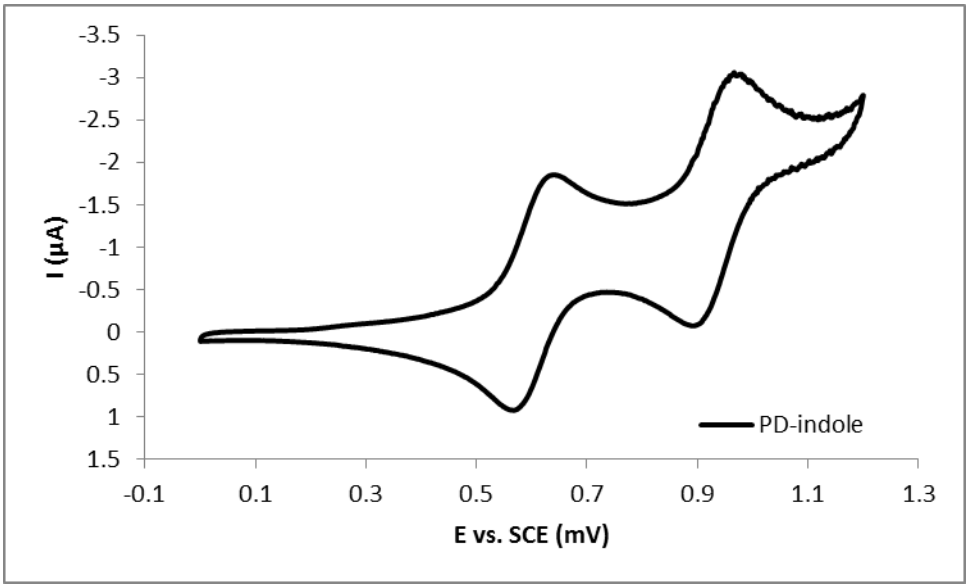

Figure 2.2.7 Cyclic voltammogram of 1.0 mM **PD-Indole** at Pt disc electrode in MeCN (0.1 M Bu_4NBF_4) at 50 mVs^{-1} scan rate.

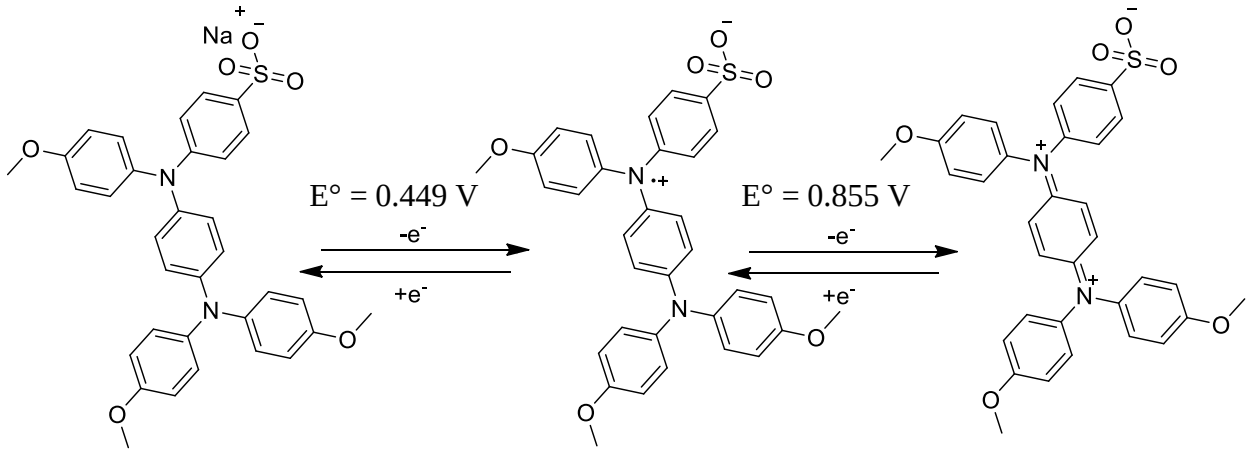

Scheme 2.2.7. Electrochemistry of **PD-Sulfonate**.

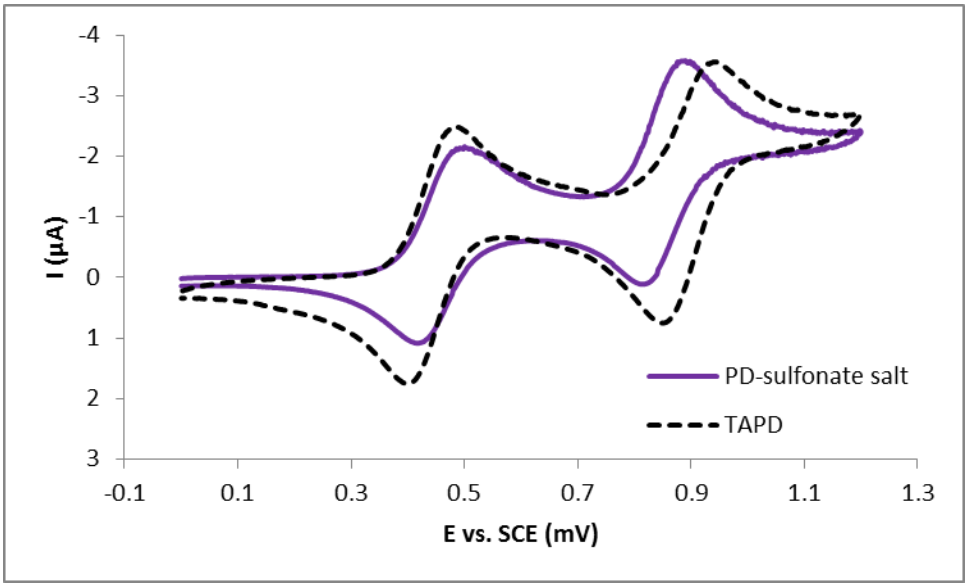

Figure 2.2.8 Cyclic voltammogram of 1.0 mM **PD-Sulfonate** (purple solid) and **TAPD** at Pt disc electrode in MeCN (0.1 M Bu_4NBF_4) at 50 mVs^{-1} scan rate.

	$E_1°$	E_{pa1}	E_{pc1}	E_{pp1}	$E_2°$	E_{pa2}	E_{pc2}	E_{pp2}
TAPD	0.443	0.484	0.402	0.082	0.896	0.938	0.854	0.084
PD-Indole	0.619	0.652	0.586	0.066	0.937	0.976	0.898	0.078
PD-Sulfonate	0.449	0.498	0.400	0.098	0.855	0.816	0.894	0.078

Table 2.2.2 Electrochemical data for **PD-Sulfonate**, **PD-Indole**, and **TAPD**

Before oxidation, **PD-Sulfonate** is colorless, with an absorbance in the UV region of the electromagnetic spectrum at 308 nm (ε= 21300 $M^{-1}cm^{-1}$). The radical internal salt and cation formed by the 1 and 2 electron oxidation of **PD-Sulfonate** bear optical resemblance to **TAPD**$^{\cdot+}$ and **TAPD**$^{++}$. Figure 2.2.10 shows the absorbance spectra of **PD-Sulfonate** during a chemical oxidation of with 1 equivalent of $Th^{\cdot+}ClO_4^-$. **PD-Zwitterion** exhibits an absorbance maximum at 422 nm. This is characterized by a molar absorptivity of 19600 $M^{-1}cm^{-1}$. This absorptivity value is almost twice that of **TAPD**$^{\cdot+}$ (ε_{414} = 10900), indicating that the **PD-Zwitterion** is a more strongly absorbing chromophore.

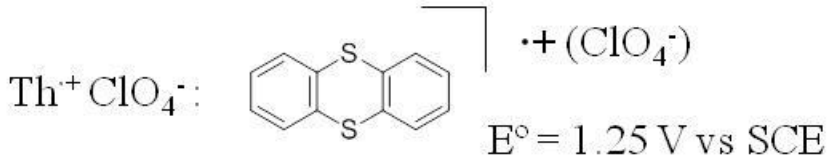

Figure 2.2.9. Structure and oxidation potential of $Th^{\cdot+}ClO_4^{-}$.[87]

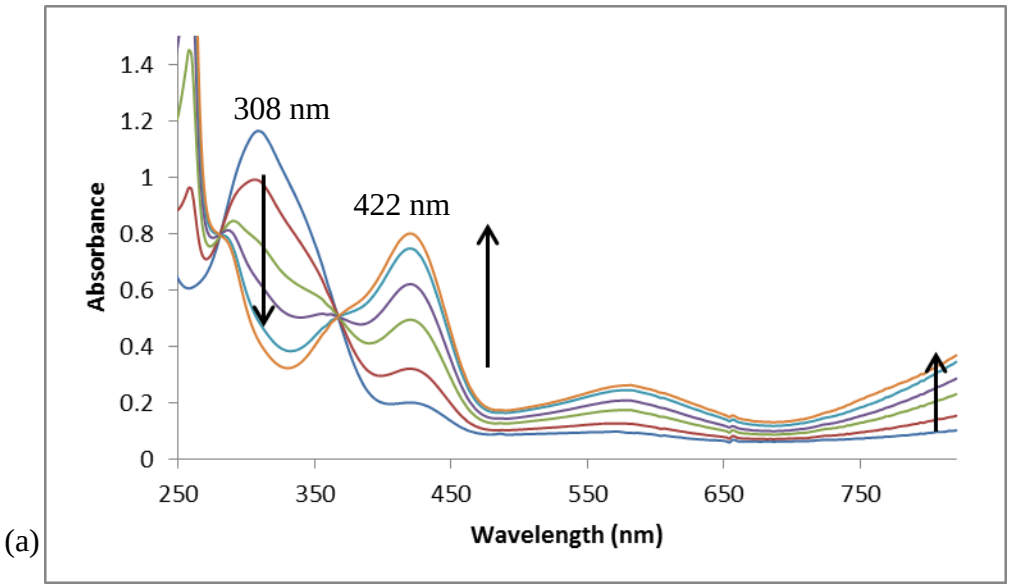

(a)

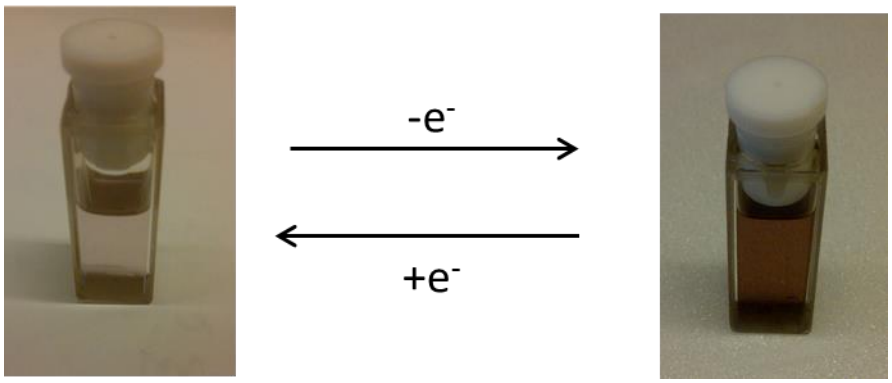

(b)

Figure 2.2.10. (a) UV-vis scale redox titration of **PD-Sulfonate (**5.46×10^{-5} M in CH_2Cl_2) with $Th^{\cdot+}ClO_4^{-}$ (in 20% increments)to yield **PD-Zwitterion**. (b) Photographs of **PD-Sulfonate** and **PD-Zwitterion** solutions.

[87] Murata, Y. Shine, H. J. Ion Radicals. XVIII. Reactions of Thianthrenium Perchlorate and Thianthrenium Trichlorodiiodide. *J. Org. Chem.* **1969,** *34*, 1603.

The chemical stability of **PD-Zwitterion** is shown in Figure 2.2.10. After oxidation of **PD-Sulfonate** with 1 eq. of the organic oxidant, CRET, **PD-Zwitterion** maintains its optical features even after 7 days in ambient conditions (25 °C in air).

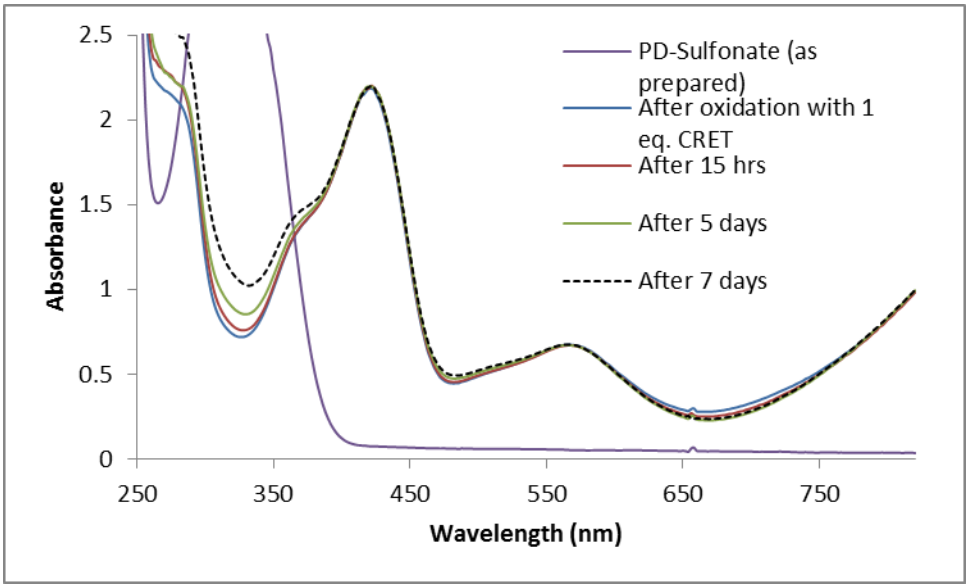

Figure 2.2.11. Time-resolved Optical Spectra of **PD-Zwitterion** after oxidation of **PD-Sulfonate** (1.12×10^{-4} M in CH_2Cl_2) with 1 eq. CRET.

The second anodic transition of **PD-Sulfonate** forms the doubly oxidized, **PD-Cation**. With a maximum absorbance at 780 nm and a molar absorptivity of 33100 $M^{-1}cm^{-1}$, it exhibits a bright blue color. In the transition from the brownish red **PD-Zwitterion** (12) to the blue **PD-Cation** (**13**), the absorbance band at 422 nm bleaches completely while a broad band at 780 nm forms. The isosbestic point at 466 nm suggests a clean transition from one species to another.

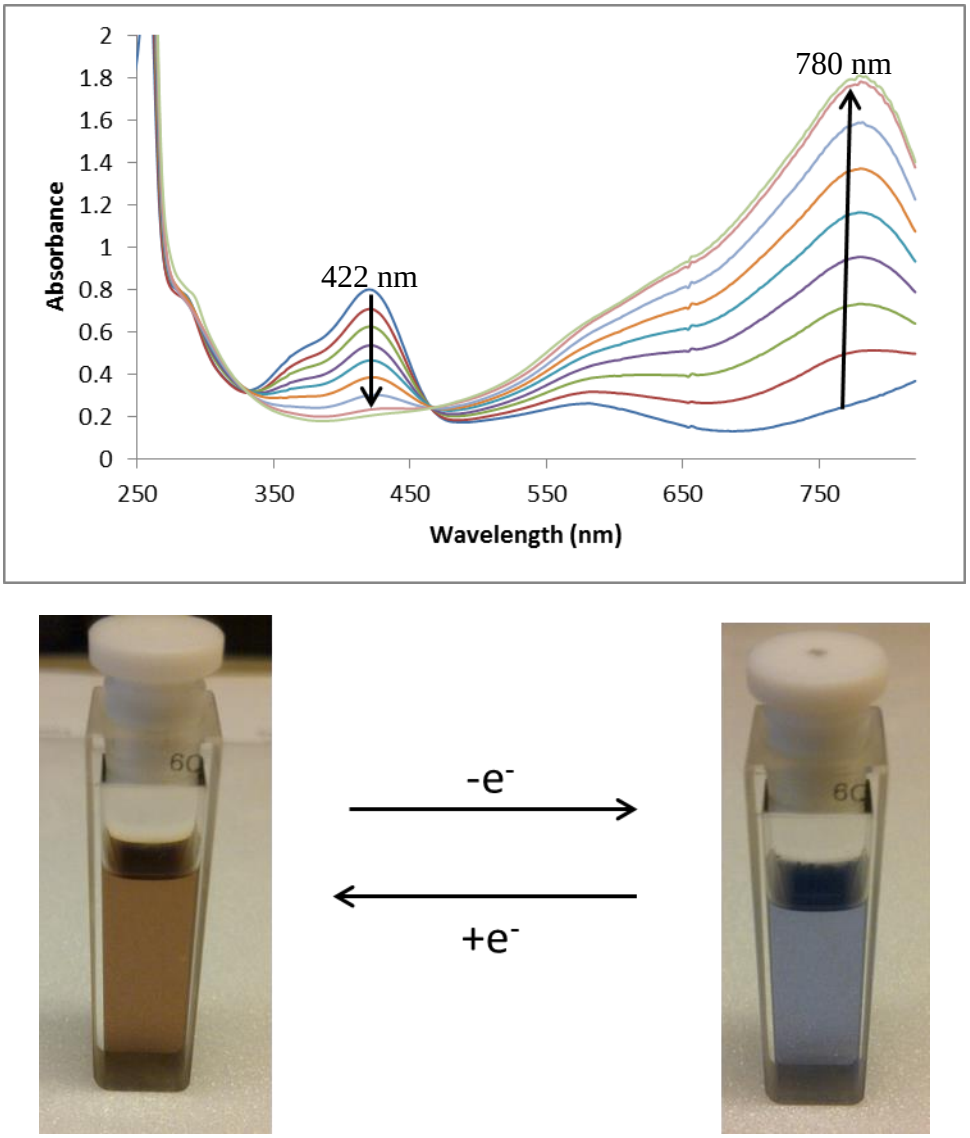

Figure 2.2.12. UV-vis scale titration of **PD-Zwitterion** (5.46×10^{-5} M in CH_2Cl_2) with $Th^{\cdot+}$ ClO_4^- yielding **PD-Cation**.

Previous studies with **TAPD** have shown that the twice-oxidized, dication, is chemically less stable in solution than the once oxidized, monocation. The case of **PD-Sulfonate** is no different. PD-Cation was prepared via chemical oxidation with $Th^{\cdot+}$ ClO_4^-. The chemical stability of **PD-Cation** was monitored via UV-vis absorbance spectroscopy. Within 30 minutes, **PD-Cation** slowly begins to undergo a reductive decay to **PD-Zwitterion**. By 24 hours, there is

optically no sign of **PD-Cation**. More studies are needed to determine the exact nature of this reductive decay.

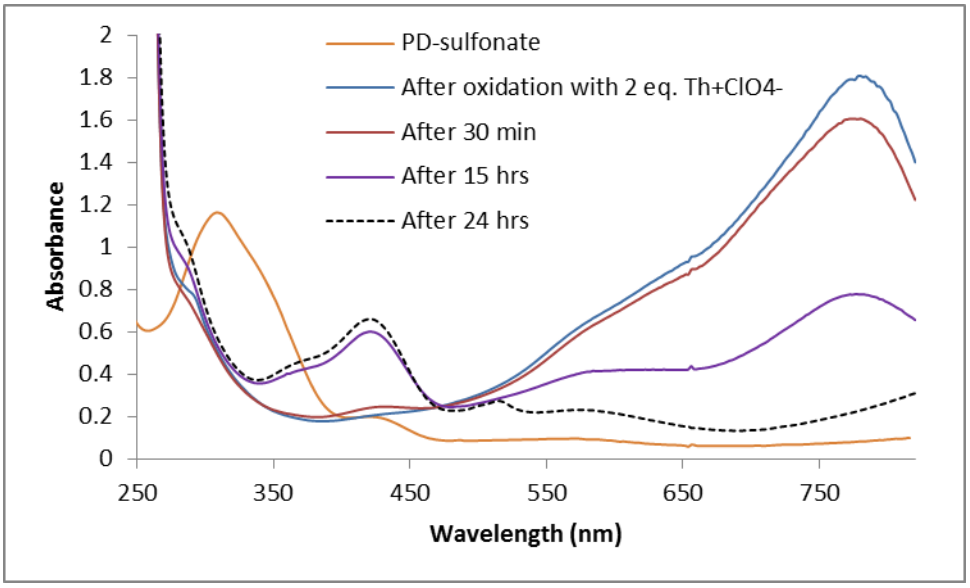

Figure 2.2.13. UV-vis scale titration of **PD-Zwitterion** (5.46×10^{-5} M in CH_2Cl_2) with $Th^{\cdot+}$ ClO_4^- yielding PD^{++}-SO_3^-.

Electron Paramagnetic Resonance (EPR) Spectroscopy is applied to the **PD-Zwitterion** internal salt to study electron distribution of the radical.[88] The five-line spectrum (figure 2.2.12) shows an a(2N) value of 5.75 G. The value is consistent with phenylenediamine-centered radicals, indicating similar spin densities. The five-line spectrum for **TAPD**$^{\cdot+}$ is shown in Figure 2.2.13. In the case of **PD-Zwitterion**, the radical is indeed shared evenly between the two nitrogens.

[88] EPR measurement taken by Alex Cruce.

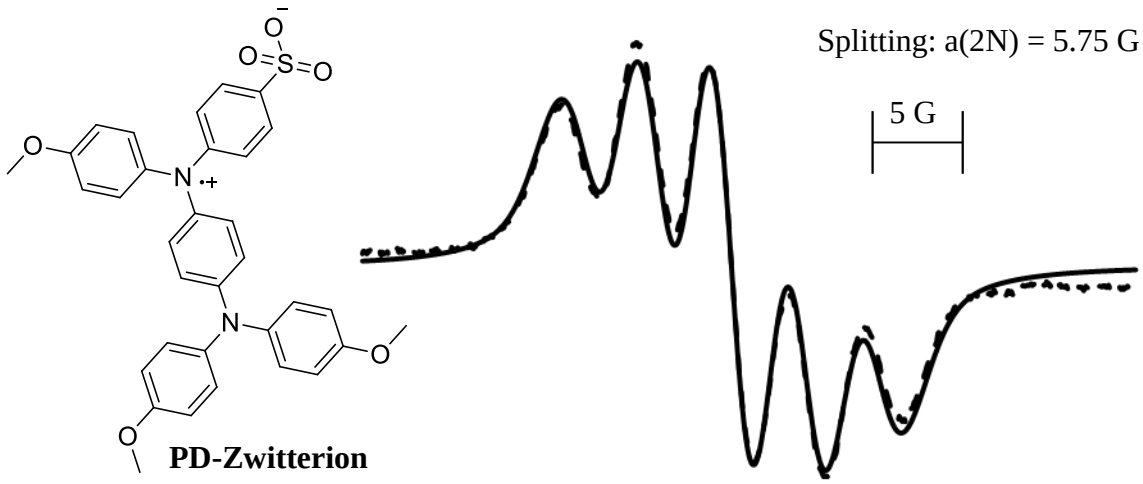

Figure 2.2.14. EPR spectrum of PD-Zwitterion in CH_2Cl_2 (0.05 mM) at 22° C. The dashed line represents the measured spectrum and the straight line is the simulated spectrum.

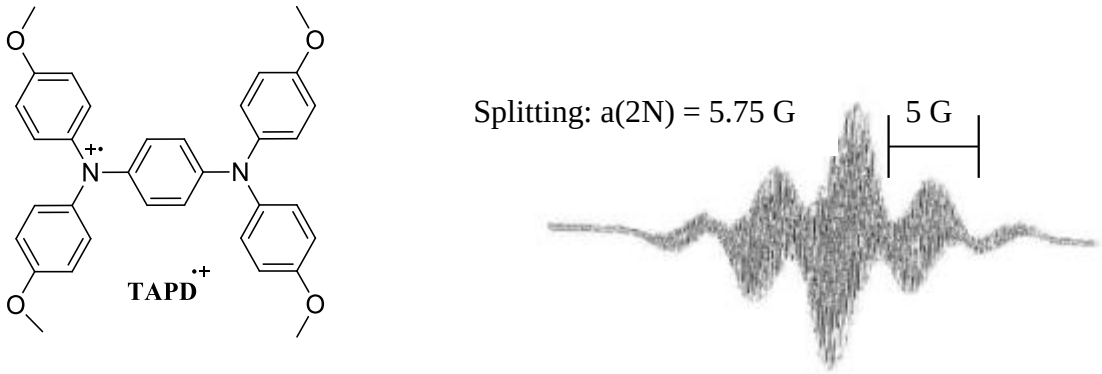

Figure 2.2.15. Electron spin resonance (ESR) spectrum on 0.05 mM **TAPD$^{\cdot+}$ ClO$_4^-$** at 22° C.[89]

[89] Selby, T. D. Polyamino Redox Arrays for Control of Spin Alignment and Charge Transport. Ph.D. Dissertation, The University of Alabama, Tuscaloosa, AL, 2001.

2.3 Electrochromic Switching of PD-SO_3^- Na^+ vs TAPD: The Effect of Molecular Charge on Switching Kinetics in Type I Electrochromic Device State

2.3.1 Spectroelectrochemical Response of PD-Sulfonate in ECD State: Turn-on and Operating Voltages

To investigate the electrochromic switching characteristics, **PD-Sulfonate** was applied to a singular electrochromic device. Figure 2.3.1 shows a general schematic of the sandwich-type device components. As the optically transparent electrode material is ITO and aluminum tape is used as the electrical contact. The ECD apparatus is identical to what was used to characterize **TAPD** in chapter 1 (figures 1.2.9 and 1.2.10). **PD-Sulfonate** is dissolved in the gel electrolyte As stated in Chapter 1, the gel is composed of MeCN, propylene carbonate, polymethylmethacrylate (PMMA), and lithium perchlorate ($LiClO_4$).

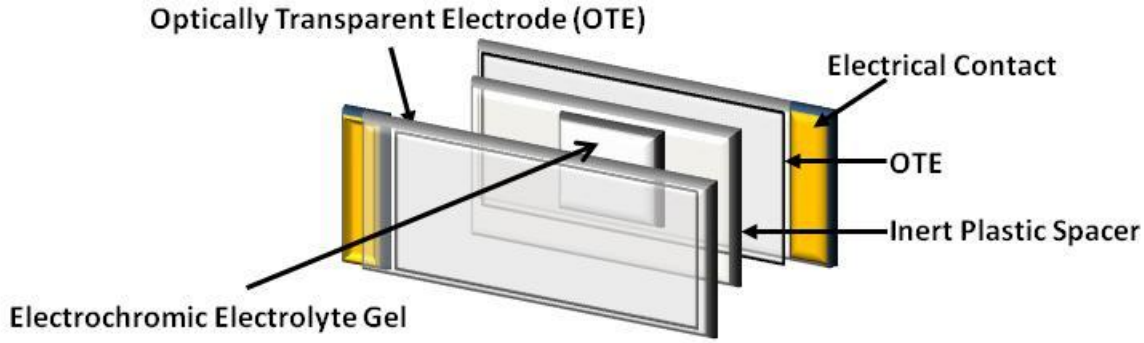

Figure 2.3.1. General Schematic of Type I ECD.

The spectroelectrochemical response of the **PD-Sulfonate** ECD is shown in figure 2.3.2. Between the applied voltages of 0 V and 3 V **PD-Sulfonate** exhibits three distinct optical states, resembling the transitions of **TAPD**. The colors can be described as colorless, reddish-brown, and blue. This is the expected result and provides additional evidence that the appendage of the

anionic sulfonate moiety does not noticeably affect the properties of the phenylenediamine chromophore.

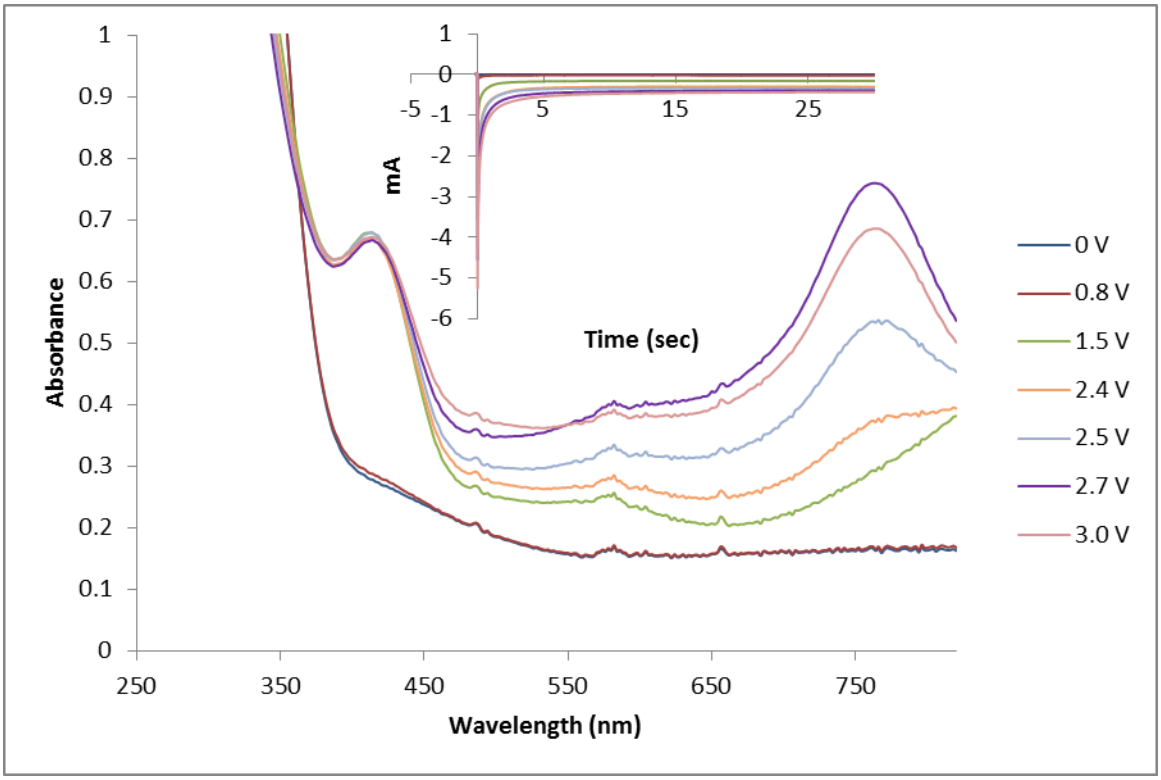

Figure 2.3.2. Spectroelectrochemical response of **PD-Sulfonate** in ECD singular device state.

Turn-on and operating voltages of the ECD are also determined from the spectroelectrochemical response. As figure 2.3.4 shows, at an applied voltage of 0.8 V, an increase in absorbance at 414 nm occurs as **PD-Sulfonate** begins to undergo oxidation to the **PD-Zwitterion** (scheme 2.2.5). The turn-on voltage of **PD-Sulfonate** (0.8 V) is less than that of **TAPD** (1.0 V), although according to CV measurements, the redox potential for the oxidations are equivalent (Figure 2.2.8). A reasonable explanation of this result would be that the appendage of the anionic sulfonate group leads to a higher concentration of **PD-Sulfonate** at the anode of the ECD. The voltage at which **PD-Sulfonate** begins to oxidize to **PD-Cation** is noted

by an increase in absorbance at 780 nm. Figure 2.3.5 is a plot of absorbance at 780 nm at varied voltages from 2 to 3 V (applied until steady state is reached, 30 s). The turn-on voltage for the second anodic transition of **PD-Sulfonate** is 2.4 V. This value is comparable to that of **TAPD**.

The operating voltage of an ECD is a value chosen by the user. In the context of our work, it is the voltage at which coloration reaches a maximum for a given redox state. Like the turn-on voltage of an ECD, it can be determined from the spectroelectrochemical response data. An applied voltage of 1.5 V is sufficient to generate the reddish-brown **PD-Zwitterion** and 2.7 V yields the blue **PD-Cation** (figure 2.3.4, figure 2.3.5). Figure 2.34 and Figure 2.3.5 show the measured absorbance at 422 nm and 780 nm after a voltage (0 V – 3 V) for 30 s, until a steady state is reached.

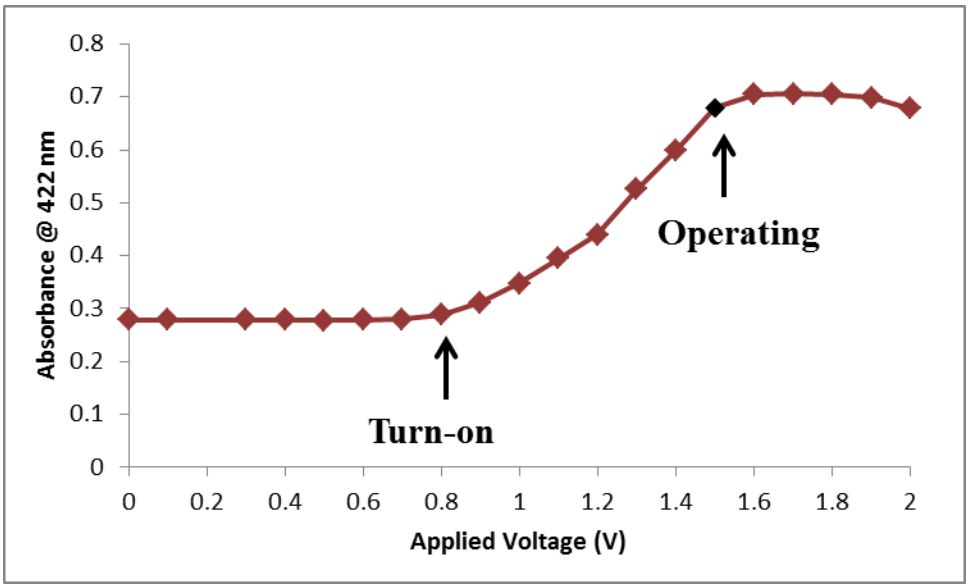

Figure 2.3.4. Absorbance at 422 nm as a result of applied voltages between 0-2 V. The black marker denotes the chosen operating voltage to affect electrochromic switching from colorless to brownish-red.

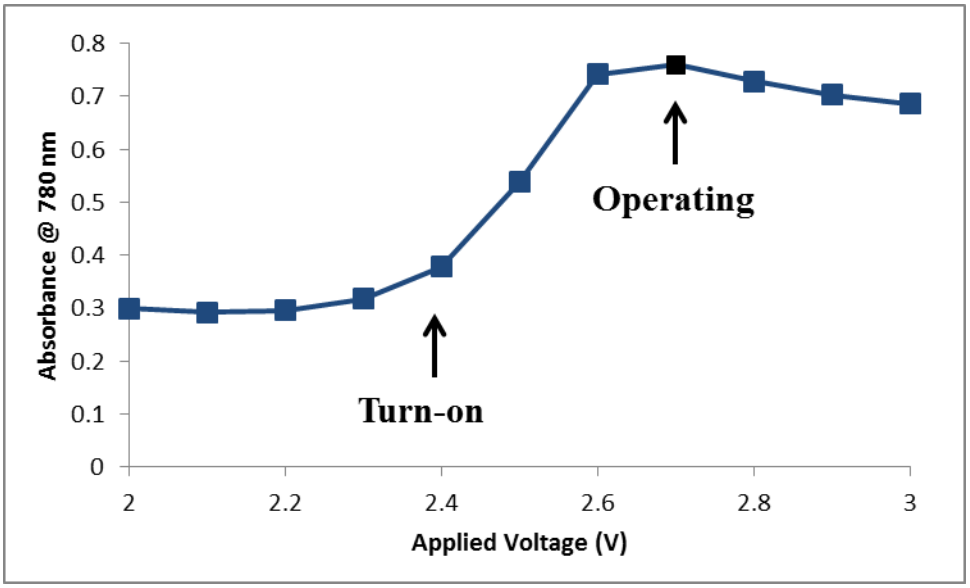

Figure 2.3.5. Absorbance at 780 nm as a result of applied voltages between 0-2 V. The black marker denotes the chosen operating voltage to affect electrochromic switching from colorless to brownish-red.

2.3.2. Electrochemical Coloration/ Open Circuit Bleaching Comparative Study

	$E_1°$	$E_2°$	λ_{max} (-1e$^-$)	$\varepsilon_{\lambda max}$	λ_{max} (-2e$^-$)	$\varepsilon_{\lambda max}$
TAPD	0.46	0.92	414 (reddish brown)	10100	766 (blue)	72500
PD-SO$_3^-$	0.45	0.86	422 (reddish brown)	19600	780 (blue)	33100

Table 2.2.3. Summary of optical and electrochemical data of **TAPD** and **PD-Sulfonate** (**PD-SO$_3^-$**).

To prove the effect that the formal charge has on an electrochrome in a singular solution state ECD, the electrochromic switching of the anionic **PD-Sulfonate** will be compared to the neutral **TAPD**. Since the electrochemical and optical properties of the two molecules are similar (Table 2.2.3), the differences in EC switching can be attributed to the difference in formal charge. Figure 2.3.6 shows the time resolved response of the **TAPD** ECD when 3 V is applied. In 10 s, the device transitions from the colorless **TAPD** to **TAPD**$^{\cdot+}$ as determined from the increase in the absorbance at 414 nm. Within the next 20 s, the final anodic transition of **TAPD** to **TAPD**$^{++}$ occurs. When open circuit conditions are applied, the device self-bleaches returning

to its resting colorless state (Figure 2.3.7). Over 5 min, There is a reversal in optical absorbance activity as the ECD turns form blue to reddish-brown to colorless. Open circuit bleaching in an ECD is a result of the diffusion-controlled recombination between oxidized and reduced species in solution. The redox chemistry of TAPD is shown in Scheme 1.2.2.

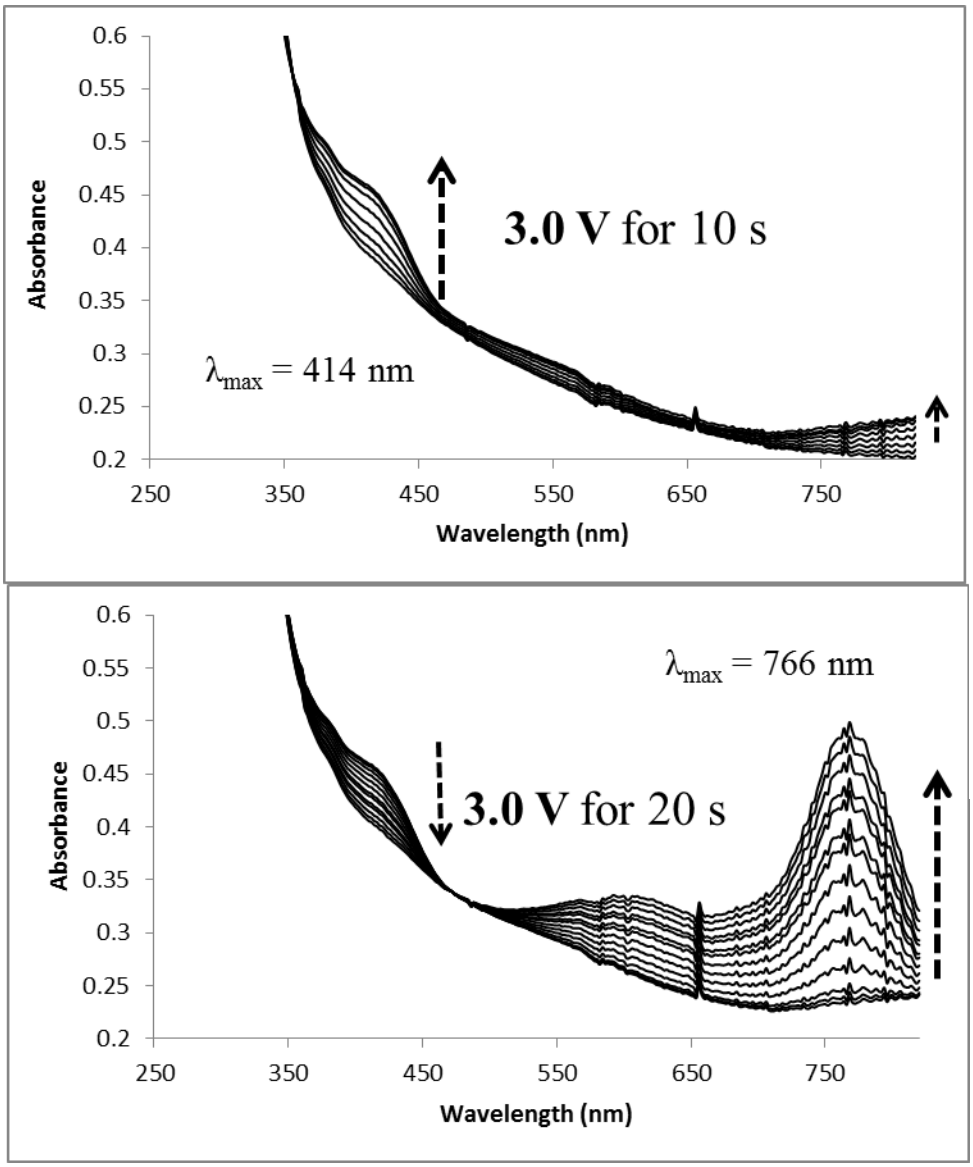

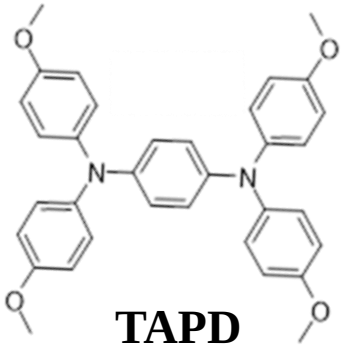

Figure 2.3.6 Electrochemical coloration of **TAPD** (.00754 M in gel electrolyte) in ECD state. Spectrum taken every 1 s.

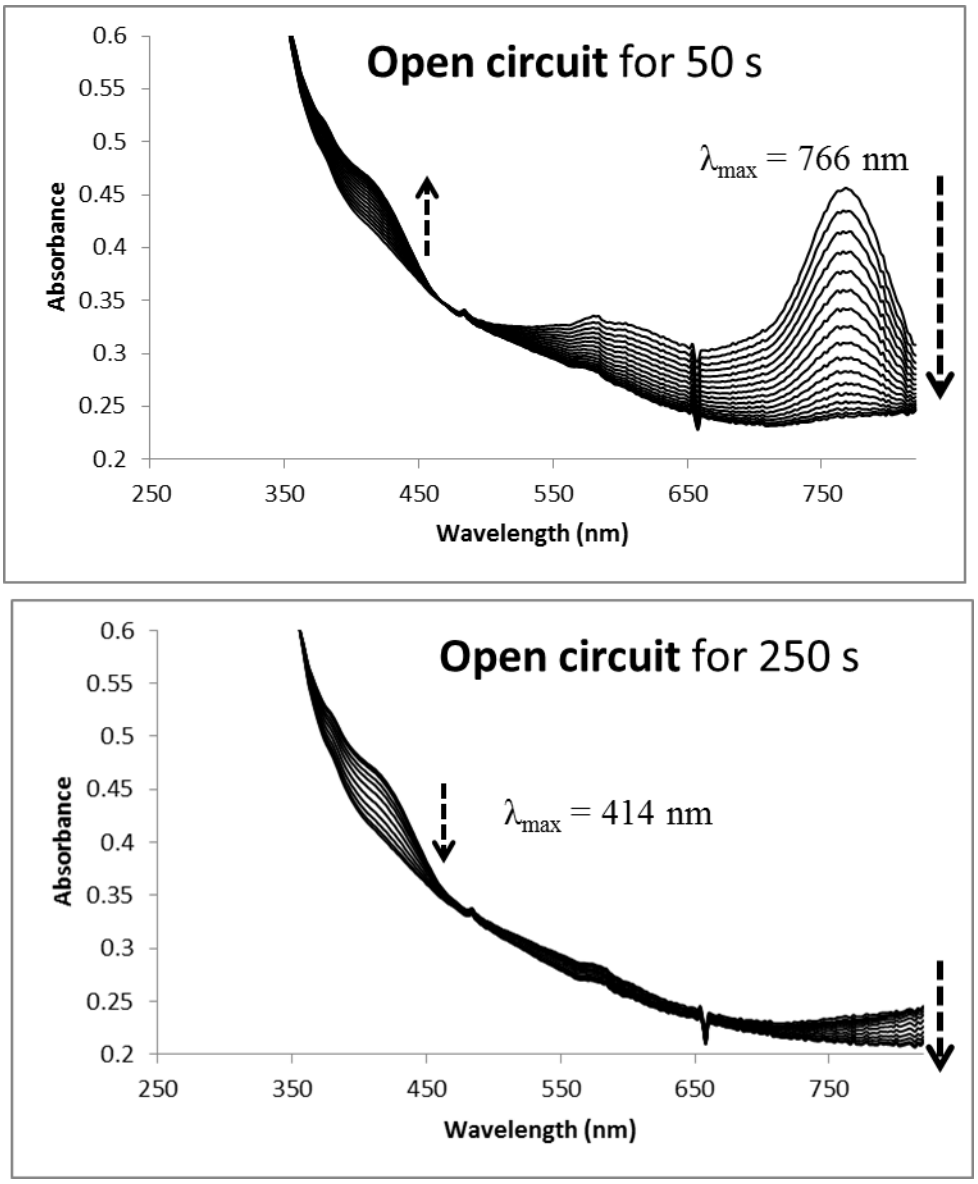

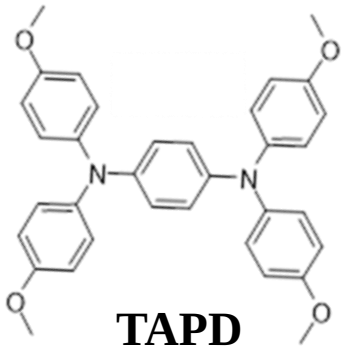

Figure 2.3.7 Open circuit bleaching of **TAPD** (.00754 M in gel electrolyte) in ECD state. Spectrum taken every 2 s.

In the case of **PD-Sulfonate**, full coloration to the blue **PD-cation** state occurs in 3 s when 2.7 V is applied to the singular device (Figure 2.3.8). The negative charge on the electrochrome attracts it to the anode. Surprisingly, under open circuit conditions, complete bleaching occurs in only 20 s (Figure 2.3.9). It isn't obviously clear why **PD-Sulfonate** undergoes open circuit bleaching more quickly than **TAPD**. It is necessary to take a closer look at the chemical species' that are present at the time self bleaching begins.

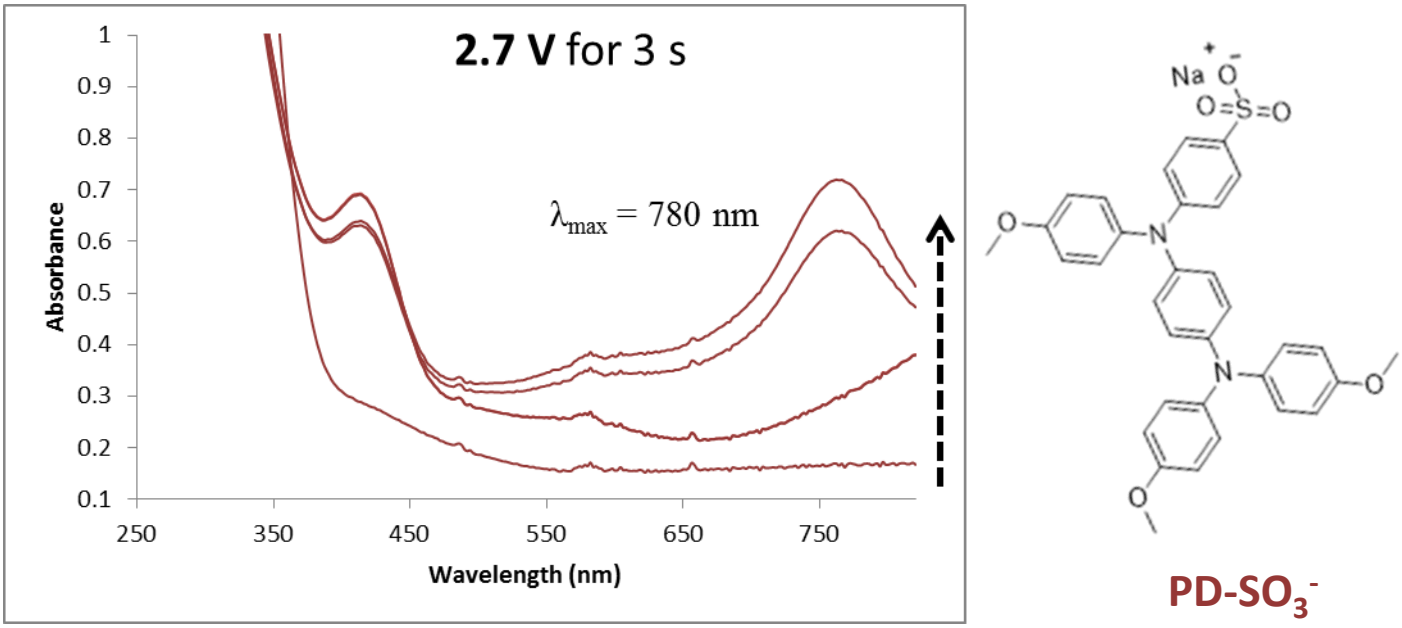

Figure 2.3.8 Electrochemical coloration of **PD-Sulfonate** (.00934 M in gel electrolyte) in ECD state. Spectrum taken every 1 s.

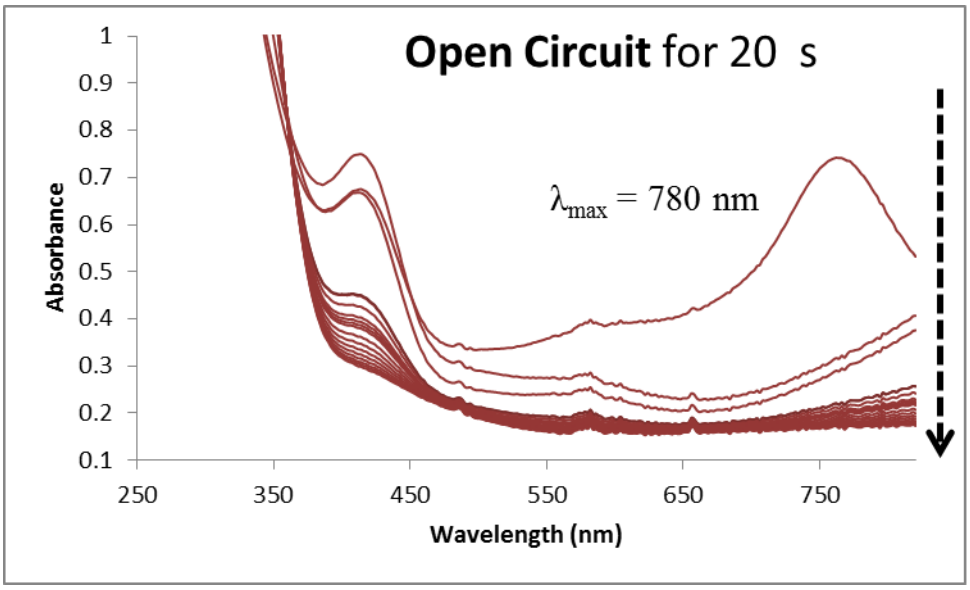

Figure 2.3.9 Open circuit bleaching of **PD-Sulfonate** (.00934 M in gel electrolyte) in ECD state. Spectrum taken every 1 s.

When steady-state coloration is reached after the application of 2.7 V (figure 2.3.8), **PD-Cation** is present as it is generated at the anode. At the cathode, we propose a solid state reduction process involving ITO (see chapter 1 for discussion of the counter electrode process). A notable fact is that only 20% of **PD-Cation** is actually present (as determined using the Beer-

Lambert law equation using 88.9 µm as the cell pathlength and 33100 $M^{-1}cm^{-1}$ as the molar absorption coefficient at 780 nm). The presence of an absorbance band at 422 nm signifies the presence of **PD-Zwitterion**. Beer-Lambert analysis (molar absorption coefficient of 19600 $M^{-1}cm^{-1}$) of this band indicates a 22% presence of **PD-Zwitterion**. This leaves a significant amount of **PD-Sulfonate** in the ECD when it is maximally colored. When the voltage is removed from the system, open circuit conditions are applied. This system initially undergoes a disproportionation reaction occurs between **PD-Sulfonate** and **PD-Cation** to generate **PD-Zwitterion**. The disproportionation, shown in scheme 2.2.6, occurs more quickly than it would in the **TAPD** system since the reactants are oppositely charged. The internal salt then diffuses and recombines with the reduced ITO to generate **PD-Sulfonate** (see figure 1.2.22). It isn't clear why **PD-Zwitterion** undergoes open circuit bleaching faster than **TAPD**$^{\cdot+}$.

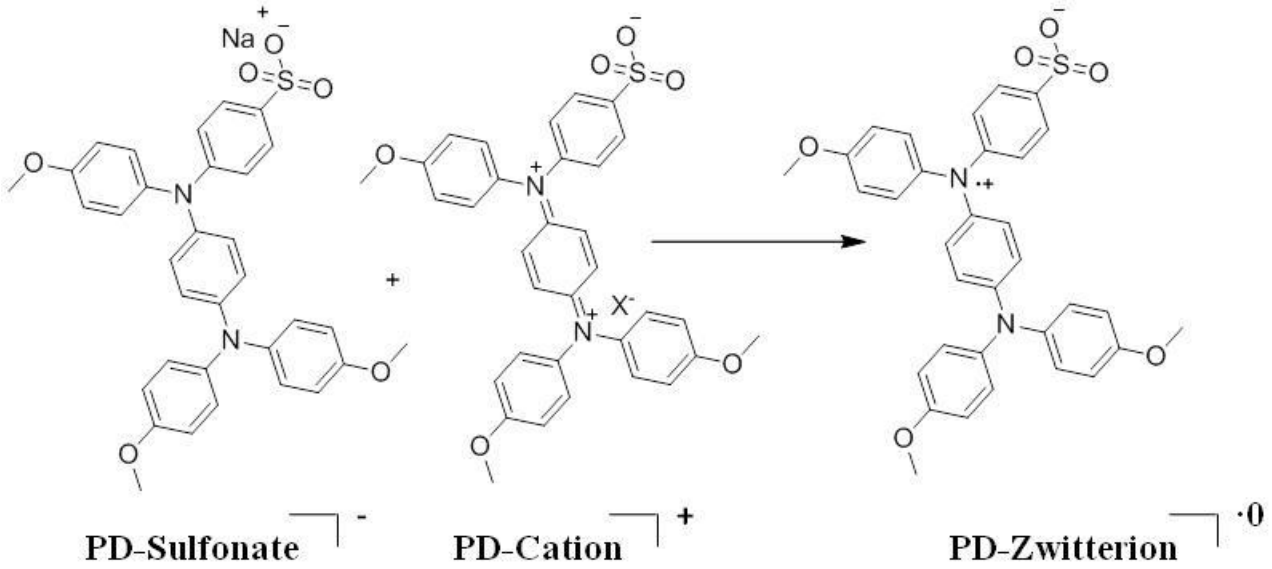

Scheme 2.2.8. Disproportionation reaction of **PD-Sulfonate** and **PD-Cation**.

2.3.2 Multielectrochromic Switching of PD-Sulfonate

PD-Sulfonate reversibly switches to 2 colored states as a result of applied voltage. Figure 2.3.10 shows electrochromic cycling from **PD-Sulfonate** to **PD-Zwitterion** in the device state. In the figure, modulation in absorbance is monitored at 2 visible region wavelengths, 422 nm and 780 nm. In figure 2.3.10, cycling conditions are 1.5 V for 3 s to generate color (reddish brown) and 0.0 V for 3 s to remove color. Only 50 cycles are shown although up to 250 cycles have been measured. Future work includes more in depth testing of the cycle life in the singular ECD state.

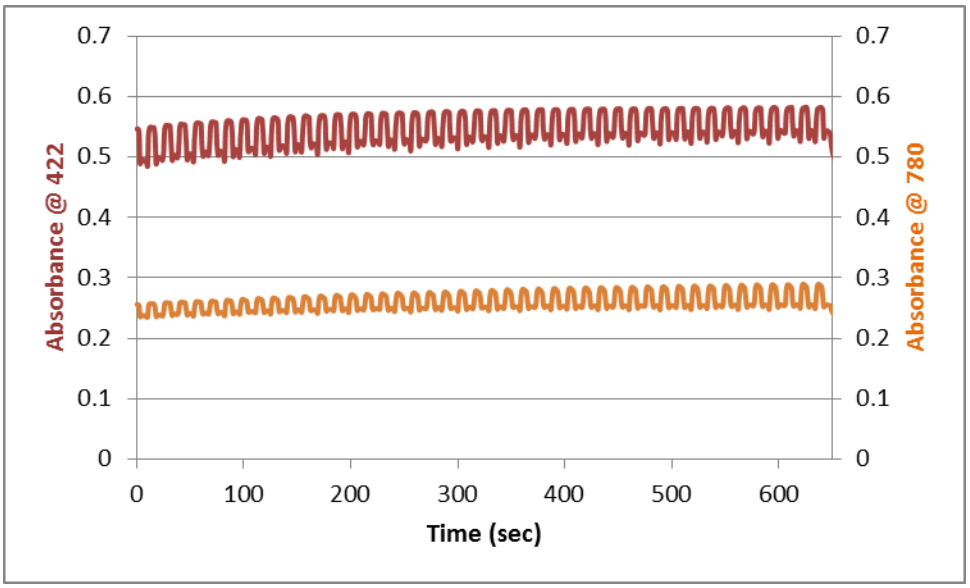

Figure 2.3.10. Electrochromic switching of **PD-Sulfonate** (.0116 M in gel electrolyte) in singular ECD from reddish brown to colorless.

To affect electrochromic switching to blue **PD-Cation** state, 2.7 V was applied for 3 s for coloration followed by 0.0 V for 3 s for bleaching. The electrochromic cycling of **PD-Sulfonate** to generate **PD-Cation** is shown in figure 2.3.11(a). An interesting feature of the cycle data is the inverse modulation of absorbance at 776 nm and 422 nm (figure 2.3.11(b)). When 2.7 V is applied to the ECD, absorbance at 776 nm increases as blue **PD-Cation** is generate while absorbance at 422 nm decreases as **PD-Zwitterion** oxidizes to generate **PD-Cation**. When the

cathodic potential of 0.0 V is applied the reverse occurs indicating reduction of **PD-Cation** to yield **PD-Zwitterion**.

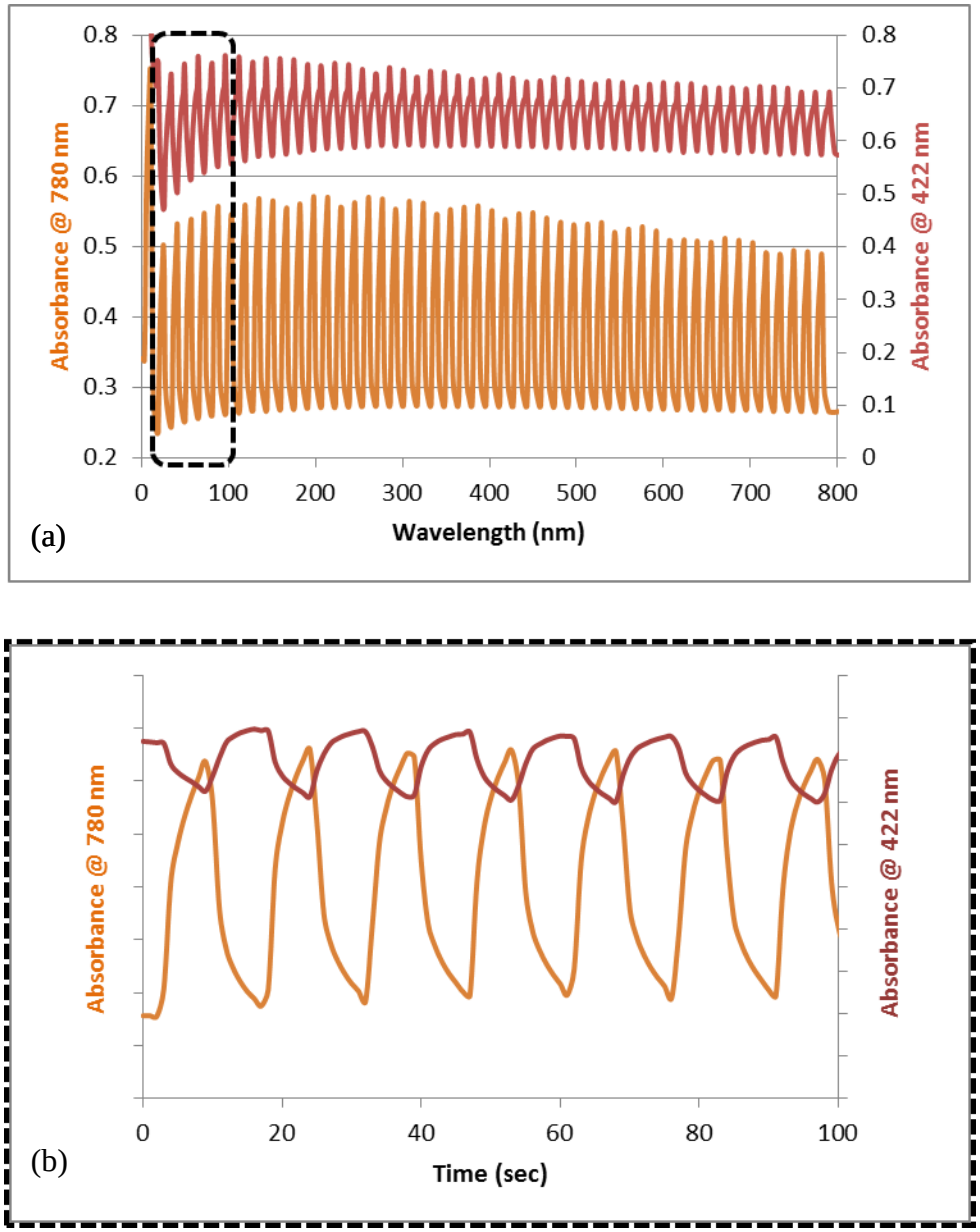

Figure 2.3.11. Electrochromic switching of **PD-Sulfonate** (.0116 M in gel electrolyte) in singular ECD to blue colored state.

2.4 Perspectives on Future Work: Additional Synthetic Adjustments to Electrochrome Charge State

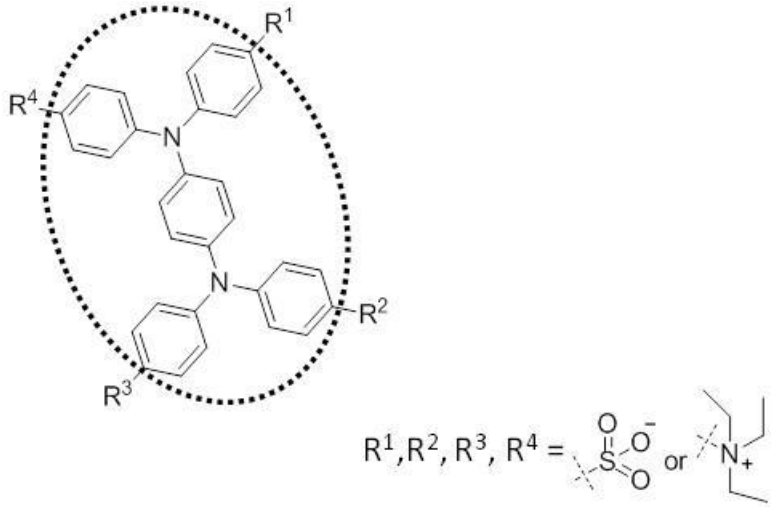

Figure 2.4.1. Generic illustration of potential PD-based cationic/anionic electrochromes.

Additional studies include investigating the effect of more than one anionic appendage (SO_3^-) on the switching kinetics of an anodically coloring electrochrome. Similar studies involving positively charged phenylenediamines are also of interest as future work (Figure 2.4.1).

2.5 Experimental

General Methods and Materials. 1H-NMR spectra were recorded on Bruker AM-500 or AM-360 instruments with chemical shifts reported relative to the deuterated solvent or TMS. All CHN analyses were completed by Atlantic Microlab. EPR spectra were recorded on a Bruker ELEX SYSE-680 spectrometer.[90] ATR IR spectra were obtained on a Bruker ALPHA Spectrometer.

p - Anisidine was purchased from Aldrich and purified via sublimation according to a known procedure.[91] *N, N, N´*-tri-1,4-anisyl-1,4-phenylenediamine (**9**) was provided by Dr. Les Gray and synthesized according to know procedure.[92] *p* – bromoanisole, palladium dibenzylideneacetone ($Pd(dba)_2$), tri *tert*-butylphosphine ($P(t\text{-}Bu)_3$), sodium *tert*-butoxide (NaO*t*-Bu), *p*-bromobenzenesulfonylchloride anhydrous toluene, and anhydrous tetrahydrofuran (THF) were purchased from Aldrich and used without further purification. Basic alumina III was prepared by adding 6 wt% distilled H_2O to basic alumina I (purchased from Aldrich). Tetrabutylammonium hydrogensulfate ($TBAHSO_4$) and indole was purchased from Alfa Aesar and used without further purification. Sodium Hydroxide (NaOH) was purchased from Fisher in pellet form and crushed using a ceramic mortar and pestle to form powder. Methanol (MeOH) was purchased from VWR and used without further purification. Dichloromethane was obtained from VWR, was pre-dried by stirring over sulfuric acid (H_2SO_4), washed, neutralized, and finally distilled

[90] All EPR spectra taken by Alex Cruce.
[91] Perrin, D. D. and Armarego, W. L. F., Purification of Laboratory Chemicals, Pergamon Press: Oxford, 1988.
[92] Gray, L.T. The Application of Arylamines as Redox Auxiliaries, Polar Crystals and Organic Semiconductors. Ph.D Dissertation, The University of Alabama, Tuscaloosa, AL, 2012.

from Calcium Hydride (CaH_2) under nitrogen atmosphere according to standard literature procedures.[7]

General methods and materials for spectroelectrochemistry and electrochromic switching can be found in chapter 1 experimental.

Electrochemistry (Figures 2.2.1, **2.2.7**, **2.2.8).** See chapter 1 experimental. Cyclic voltammetry of **AA-Sulfonate**, **AA-Sulfonamide**, **PD-Indole**, and **PD-Sulfonate** was performed at a scan rate of 50 mVs^{-1}.

Chemical Oxidation.

AA-Sulfonamide (Figure 2.2.3)- A solution of **AA-Sulfonamide**, $7.84x10^{-5}$ M, was prepared by dissolving **AA-Sulfonamide** (1.52 mg, 0.00314 mmol) in 1.0 mL of dry CH_2Cl_2 (0.00314 M). An aliquot of the solution (250 μL) was diluted to 10 mL. The diluted solution was subjected to redox titration with 1 molar equivalent of CRET to afford **AA- Sulfonamide**$^{\cdot+}$. For UV-vis spectroscopy, an HP8452A Diode Array Spectrophotometer equipped with a 1 cm path length quartz cell (Starna) was used.

AA-Sulfonate (Figure 2.2.4)- A solution of **AA-Sulfonate**, $6.87x10^{-5}$ M, was prepared by dissolving **AA-Sulfonate** (1.11 mg,0.00272 mol) in 1.0 mL of dry CH_2Cl_2 (0.00272 M). An aliquot of the solution (250 μL) was diluted to 10 mL. The diluted solution was subjected to redox titration with 1 molar equivalent of CRET to afford **AA-Zwitterion**. For UV-vis spectroscopy, an HP8452A Diode Array Spectrophotometer equipped with a 1 cm path length quartz cell (Starna) was used.

PD-Sulfonate (Figure 2.2.10, **2.2.12**, **2.2.13)-** A solution of **PD-Sulfonate**, 5.46×10^{-5} M, was prepared by dissolving **PD-Sulfonate** (1.32 mg, 0.00218 mmol) in 1 mL dry CH_2Cl_2 (.00218 M). An aliquot of the solution (250 μL) was diluted to 10 mL. The diluted solution was subjected to redox titration with 1 and 2 molar equivalents of CRET to afford **PD-Zwitterion** and **PD-Cation**, respectively. For UV-vis spectroscopy, an HP8452A Diode Array Spectrophotometer equipped with a 1 cm path length quartz cell (Starna) was used.

PD-Sulfonate (Figure 2.2.11)- A solution of **PD-Sulfonate**, 1.12×10^{-4} M in dry CH_2Cl_2, was subjected to redox titration with 1 equivalent of CRET to afford **PD-Zwitterion**. For UV-vis spectroscopy, an HP8452A Diode Array Spectrophotometer equipped with a 1 cm path length quartz cell (Starna) was used.

Preparation of Electrochromic Gel Electrolyte - See chapter 1 experimental

Construction of PD-Sulfonate ECD. (Figures 2.3.2, 2.3.4, 2.3.5, 2.3.6, 2.3.7, 2.3.8, 2.3.9, 2.3.10, 2.3.11) PD-Sulfonate (3.02 mg ,0.005 mmol) was dissolved in 0.50 mL of gel electrolyte. The gel electrolyte solution was applied to ITO glass anode (equipped with spacer), the ITO glass cathode was then added to complete a sandwich-type device. For 88.9 μm spacing, Polyethylene Plastic Sheeting (Husky Brand) was used. The ITO sandwich was held together with metal clamps for the duration of the experiment. Aluminum foil tape (Shurtape AF-100) was used for efficient contact between ITO and metal spring clips. See figure 1.2.9 or figure 2.3.1 for a picture of ECD.

Spectroelectrochemistry and electrochromic switching. See chapter 1 experimental

Preparation of Dianisylamine (5)

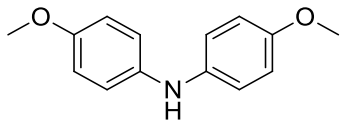

5

p-anisidine (2.00 g, 16.2 mmol) and *p*-bromoanisole (3.04 g, 16.2 mmol) were added into a flame dried round bottom flask. The mixture was transported into a nitrogen purged dry box where the 50 ml of toluene, $Pd(dba)_2$ (46.6 mg, .081 mmol) .5 % mole, $P(t\text{-Bu})_3$ (16.7 mg, .081 mmol), NaO*t*-Bu (1.87 g, 19.5 mmol) were added. The mixture was capped with a rubber septum and removed from the dry box. The reaction mixture stirred under nitrogen for eight hours at room temperature. The reaction was monitored via TLC (ethyl acetate:hexanes 1:3) until both starting materials were no longer present and the product became visible. After the disappearance of the starting materials, the mixture was filtered through basic alumina III and washed with ethyl acetate. The crude product was concentrated in vacuo and recrystallized from EtOH to yield 2.71 g of AA 9 as a pink solid.

Yield: 73% MW = 229.28 $gmol^{-1}$ mp = 98-100 °C

1H NMR (360 MHz, CDCl3 , 25 °C):

δ 6.93 (d, J 8.90, 4H), 6.81 (d, J 8.86, 4H), 5.26 (s, 1H), 3.76 (s, 6H).

Preparation of 1-(4-Bromophenylsulfonyl)-1*H*-indole (4)[93]

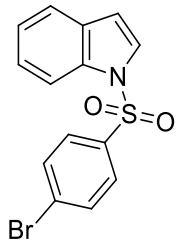

4

To a solution of $TBAHSO_4$ (72.5 mg, .214 mmol) in 20 mL of anhydrous methylene chloride was added finely powdered NaOH (.512 g, 12.8 mmol) at 0°C under nitrogen atmosphere. After stirring for 10 min, indole (.500 g, 4.27 mmol) was dissolved in the heterogeneous solution. After stirring 5 min, a solution of *p*-bromobenzenesulfonyl chloride (1.20 mg, 4.69 mmol) dissolved in 12 mL dichloromethane was added drop wise to the reaction mixture over 10 min. The reaction mixture was then allowed to warm to 25°C and stir for 3 hrs under slow nitrogen gas purge. The reaction was monitored via TLC (ethyl acetate:hexanes 1:5) until the limiting reagent was no longer present and the product became visible. The pale yellow mixture was filtered and the white residue was washed thoroughly with dichloromethane. The filtrate was concentrated under vacuum at 50 °C. The white solid was recrystallized from 50% EtOH/ distilled H_2O to yield colorless crystals (1.18 g, 4.27 mmol).

Yield: 82% MW = 336.20 $gmol^{-1}$ mp = 72-74 °C

1H NMR (360 MHz, CDCl3 , 25 °C):

δ 7.96 (d, 1H, *J*= 8.28 Hz), 7.73 (d, 2H, *J*= 8.64 Hz), 7.56 (d, 2H, *J*= 9 Hz),7.53 (1H, *J*= 3.6 Hz), 7.33 (t, 1H, *J*= 7.2 Hz), 7.246 (t, 1H, *J*= 7.2 Hz), 6.68 (d, 1H, *J*= 3.6 Hz)

[93] Kwak, K. W.; Lee, I.-S.; Ramalingan, C. Novel Furanylarylene Arylsulfonylindolesulfonamides: Synthesis and Their Antibacterial Evaluation *Chem. Pharm. Bull.* **2009,** *57,* 591-591.

Preparation of **4-((1*H*-indol-1-yl)-*N*,*N*-bis(4-methoxyphenyl)aniline (AA-Sulfonamide, 6)**

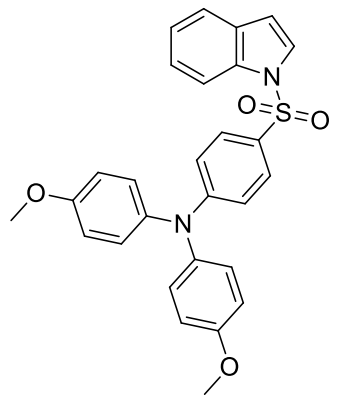

6

In a drybox (purged with N_2), **5** (.454 g, 1.98 mmol) and **4** (.667 g, 1.98 mmol) were dissolved in 10 mL anhydrous toluene in 25 mL RB flask equipped with magnetic stir bar. Once the solution was homogeneous, 59.4 µL of 1.0 M tri-*tert*-butylphosphine in toluene (.0594 mmol) was added. This was followed by the addition of $Pd(dba)_2$ (34.2 mg, .0594 mmol) then sodium *tert*-butoxide (.285 g, 2.97 mmol). The reaction mixture was capped with a rubber septum, brought out of the drybox and stirred at room temperature for 90 min under slow N_2 purge. The reaction was monitored via TLC (ethyl acetate:hexanes 1:5) until the starting materials were no longer present and the product became visible. The reddish brown mixture was then taken up in 20 mL EtOAc and filtered through 7 mm basic alumina, activity III. The solvent was evaporated under vacuum at 50 °C. The residue was then recrystallized from 40% THF in hexanes to yield pure solid (.699 g, 1.44 mmol).

Yield: 73% MW = 484.57 $gmol^{-1}$ mp = 119-121 °C

1H NMR (360 MHz, CDCl3 , 25 °C):

δ 7.96 (d, 1H, *J* = 6.1 Hz), 7.57 (d, 2H, *J* = 6.8 Hz), 7.53 (m, 2H), 7.28 (t, 1H, *J* = 5.4 Hz), 7.21 (t, 1H, *J* = 5.4 Hz), 7.03 (d, 4H, *J* = 6.1 Hz), 6.83 (d, 4H, *J* = 6.1 Hz), 6.67 (d, 2H, *J* = 6.8 Hz), 6.62 (d, 1H, *J* = 2.5 Hz), 3.78 (s, 6H)

^{13}C NMR (125 MHz, $CDCl_3$, 25 °C):

δ 158.0, 153.9, 151.1, 139.0, 135.5, 131.4, 129.1, 128.9, 127.2, 125.0, 123.7, 122.0, 117.0, 116.0, 114.5, 109.1, 56.8

ESI HRMS *m/z* calcd for $C_{28}H_{24}N_2O_4S$ $[M-H]^+$ 484.1457, found 484.1439.

Preparation of **Sodium 4-(bis(4-methoxyphenyl)amino)benzenesulfonate (AA-Sulfonate, 7)**

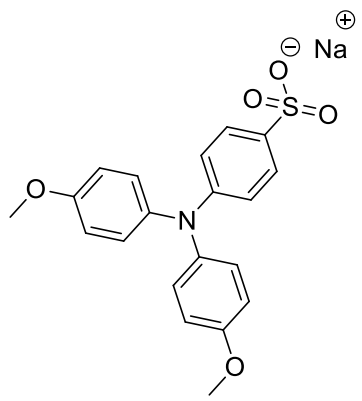

7

In 50 mL thick walled Shlenk flask equipped with a stir bar, **AA-Sulfonamide** (.200 g, .413 mmol) was dissolved in 20 mL THF/MeOH (1:1). NaOH (1.5 N, .991 mL, 4.95 mmol) was then added and the reaction mixture was heated to 135 °C (in oil bath) for 16 hrs. The reaction mixture was allowed to cool to room temperature and concentrated to a brownish residue and taken up in 10 mL of anhydrous ether. The original reaction vessel was rinsed with 20 mL distilled water into a separatory funnel with the ether solution and extracted 3 times with 10 mL ether. The aqueous layer was allowed to sit at room temperature until crystals formed and filtered via vacuum filtration (.123 g)

Yield: 73% MW = 407.42 $gmol^{-1}$ mp = 47-49 °C

1H NMR (360 MHz, DMSO-*d*6, 25 °C):

δ 7.37 (d, 2H, *J* = 6.1 Hz), 6.99 (d, 4H, *J* = 6.5 Hz), 6.89 (d, 4H, *J*=6.5), 6.66 (d, 2H, *J* = 6.1 Hz), 3.73 (s, 6H)

^{13}C NMR (125 MHz, DMSO-*d*6, 25 °C):

δ 154.6, 147.4, 139.6, 139.3, 125.8, 117.4, 114.3

IR (neat, cm^{-1}):

2965 (w), 2836 (w), 1590 (s), 1508 (s) 1234 (s), 1167 (s), 1029 (s), 827 (s), 641.5 (s), 525.3 (s)

ESI MS *m/z* calcd for $C_{20}H_{18}NO_5S^-$ $[M-H]^-$ 384.43, found 384.1.

Preparation of **N^1-(4-((1*H*-indol-1-yl)sulfonyl)phenyl)-N^1,N^4,N^4-tris(4-methoxyphenyl)benzene-1,4-diamine (PD-Sulfonamide, 10)**

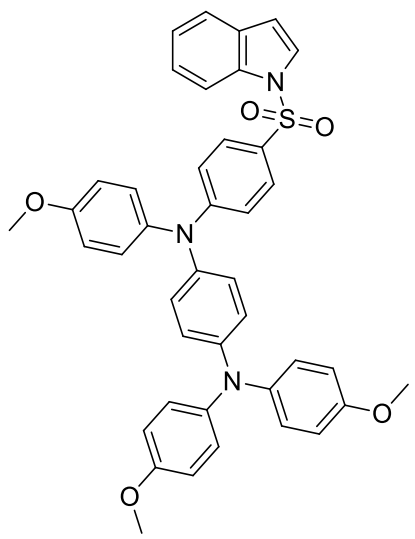

10

In a drybox (purged with N_2), **9** (.500 g, 1.17 mmol) and **4** (.394 g, 1.17 mmol) were dissolved in 10 mL anhydrous toluene in 25 mL RB flask equipped with magnetic stir bar. Once the solution was homogeneous, 58.5 µL of 1.0 M tri-*tert*-butylphosphine in toluene (.0585 mmol) was added. This was followed by the addition of $Pd_2(dba)_3$ (33.6 mg, .0585 mmol) then sodium *tert*-butoxide (.169 g, 1.76 mmol). The reaction mixture was capped with rubber septum, brought out of the drybox and stirred at room temperature for 3 hrs under slow N_2 . The reaction was monitored via TLC (ethyl acetate:hexanes 1:5) until the starting materials were no longer present and the product became visible. The reddish brown mixture was then taken up in 20 mL EtOAc and filtered through 7 mm basic alumina, activity III. The solvent was removed en vacuo. The crude residue was then recrystallized from 40% THF/hexanes to yield pure solid (.668 g).

Yield: 91% MW = 681.80 mp 119-122 °C

1H NMR (360 MHz, CDCl3 , 25 °C):

δ 7.96 (d, 1H, *J* = 6.1 Hz), 7.57 (d, 2H, *J* = 9.0 Hz), 7.52 (m, 2H), 7.27 (t, 1H, *J* = 7.2 Hz), 7.19 (t, 1H, *J* = 7.56 Hz), 7.03 (m, 6H), 6.82 (m, 10H), 6.69 (d, 2H, *J* = 9.0 Hz), 6.61 (d, 1H, *J* = 3.6 Hz), 3.78 (m, 9H)

^{13}C NMR (125 MHz, $CDCl_3$, 25 °C):

δ 158.5, 156.9, 154.4, 147.8, 141.0, 138.6, 137.7, 135.2, 131.5, 130.0, 129.9, 129.3, 128.1, 128.0, 125.6, 124.3, 122.7, 121.3, 116.7, 116.3, 115.9, 114.4, 109.9, 80.6, 57.1, 57.0

ESI HRMS *m/z* calcd for $C_{41}H_{35}N_3O_5S$ $[M-H]^+$ 681.2297, found 681.2321.

Preparation of **sodium 4-((4-(bis(4-methoxyphenyl)amino)phenyl)(4-methoxyphenyl)amino)benzenesulfonate (PD-Sulfonate, 11)**

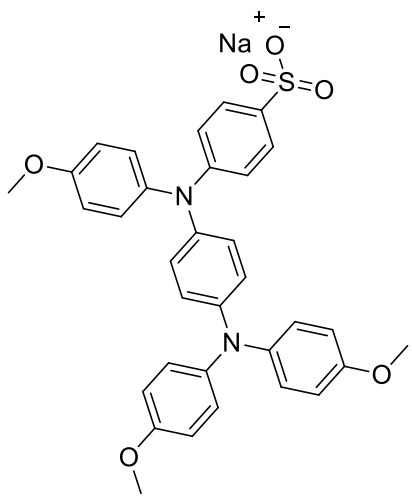

11

In a 10 mL thick walled Shlenk flask equipped with stir bar, **N^1-(4-((1*H*-indol-1-yl)sulfonyl)phenyl)-N^1,N^4,N^4-tris(4-methoxyphenyl)benzene-1,4-diamine** (50.0 mg, .0733 mmol) was dissolved in 2.8 mL THF/MeOH (1:1). NaOH (.176 mL, 0.880 mmol) was then added and the reaction mixture was heated to 135 °C (in oil bath) for 16 hrs. The reaction mixture was allowed to cool to room temperature and

concentrated to a brownish residue and taken up in 3 mL of anhydrous ether. The original reaction vessel was rinsed with 5 mL distilled water into a separatory funnel with the ether solution and extracted 3 times with 3 mL ether. The aqueous layer was allowed to sit at room temperature until crystals formed and filtered via vacuum filtration (12.0 mg)

Yield: 27% MW = 604.65 $gmol^{-1}$ mp 190-192 °C

1H NMR (360 MHz, DMSO-*d*6, 25 °C):

δ 7.44 (d, 2H, *J* = 8.6 Hz), 7.05 (m, 6H), 6.94 (m, 8H), 6.80 (d, 2H, *J* = 6.84 Hz), 6.77 (d, 2H, *J* = 6.84), 3.79 (s, 3H), 3.77 (s, 6H)

^{13}C NMR (125 MHz, DMSO-*d*6, 25 °C):

δ 156.9, 156.4, 149.3, 145.2, 141.6, 141.3, 141.0, 128.1, 127.9, 127.2, 126.7, 122.7, 120.0, 116.3, 116.2, 57.0

IR (neat, cm^{-1}):

3034 (w), 2830 (w), 1590 (m), 1495 (s), 1240 (s), 1029 (s), 824 (s), 523 (m)

ESI MS *m/z* calcd for $C_{33}H_{29}N_2O_6S^-$ $[M-H]^-$ 581.2, found 581.3.

Chapter 3

Development of Photoelectrochromic Switching Devices based on Redox Auxiliary Catalysis

3.1 Introduction

The term photoelectrochromism has several meanings in literature. In *Electrochromism and Electrochromic Devices*, it refers to systems that possess a photosensitive electrochromic property.[94,95] One such system is the metal oxide, Li-W-O. When sputtered onto an ITO electrode and incorporated into an ECD configuration, the film exhibits electrochromic switching characteristics specifically when irradiated with UV-light at 365 nm. These types of systems are considered "photo-activated." More recently the definition has expanded to describe electrochromic systems that are powered by a photovoltaic source.[96,97,98] Also termed a "self-powered ECD," the device is a hybrid device containing a photovoltaic electrical system coupled to an electrochromic electrode. In contrast to photo-activated photoelectrochromic

---

[94] Monk, P.M.S.; Mortimer, R. J.; Rosseinsky, D. R. *Electrochromism and Electrochromic Devices;* Cambridge: UK, 2007.
[95] De Paoli, M.-A.; Noguiera, A. F.; Machado, D. A.; Longa, C. All-Polymeric Electrochromic and Photoelectrochemical Devices: New Advances. *Electrochim. Acta*, **2001,** *46,* 4243-4249.
[96] Malara, F.; Cannavale, A.; Carallo, S.; Gigle, G. Smart Windows for Building Integration: a New Architecture for Photovoltachromic Devices. *ACS Applied Materials & Interfaces.* **2014,** Ahead of print.
[97] Leftherotis, G.; Syrrokostas, G.; Yianoulis, P. Photocoloration Efficiency and Stability of Photoelectrochromic Devices. *Solid State Ionics* **2013,** *231,* 30-36.
[98] Jiao, Z.; Song, J.; Sun, X. W.; Liu, X. W.; et al. A Fast-Switching Light-Writable and Electric-Erasable Negative Photoelectrochromic Cell Based on Prussian Blue Films. *Solar Energy Materials & Solar Cells.* **2012,** *98,* 154-160.

devices, these are photo-driven. In both types of photoelectrochromism, a system exhibits electrochromism only during irradiation. A third description of photoelectrochromism refers to a system that chromogenically responds to alternating electrochemical and photochemical stimulus. Thus, the system is both electrochromic and photochromic. There are few examples of such materials. Yoneyama, et al. developed a photoelectrochromic system based on polyaniline/TiO_2/ITO thin films.[99,100] When irradiated in a neutral aqueous solution (with 20% methanol), the blue film turns yellow as polyaniline is photoreduced by TiO_2. When an anodic potential is applied (0.5 V vs SCE), the film returns to its blue state. Chidichimo, et al. used the organic dye, methylene blue as a photoelectrochrome.[101,102,103] Like polyaniline, methylene blue undergoes a photoreduction when irradiated (with red light) in the presence of an electron donor (triethylamine) which bleaches the molecule. The blue color returns when 0.4 V DC is applied as methylene blue is oxidized. We present the first photoelectrochromic system based on a reversible chemical reaction. Unlike previously studied photoelectrochromic systems, there is no change in oxidation state between the colored and bleached chemical species'. The photoelectrochromic switch is between two optically distinct isomers in contrast to redox states.

We have developed new molecular switches that function by a novel mechanism that we have termed redox-auxiliary (RA) catalysis.[104] In redox-auxiliary catalysis, the activation barrier

---

[99] Yoneyama, H.; Takahashi, N.; Kuwabata, S. Formation of a Light Image in a Polyaniline Film Containing Titanium (IV) Oxide Particles. *J. Chem. Soc.,Chem. Commun.* **1992,** 716-717.
[100] Yoneyama, H. Writing with Light on Polyaniline Films. *Adv. Mater.* **1993,** *5,* 394-396.
[101] De Filpo, G.; Nicoletta, F.P.; Chidichimo, G. Flexible Nano-Photo-Electrochromic Film. *Chem. Mater.* **2006,** *18,* 4662-4666.
[102] Macchione, M.; DeFilpo, G.; Nicoletta, F.; Chindichimo, G. Improvement of Response Times in Photoelectrochromic Organic Film. *Chem. Mater.* **2004,** *16.* 1400-1401.
[103] Macchione, M.; DeFilpo, G.; Nicoletta, F.; Chindichimo, G. Laser-Writable Electrically Eraseable Photoelectrochromic Organic Film. *Adv. Mater.* **2003,** *15,* 327-329
[104] Gray, L.T. The Application of Arylamines as Redox Auxiliaries, Polar Crystals and Organic Semiconductors. Ph.D Dissertation, The University of Alabama, Tuscaloosa, AL, 2012.

of a chemical transformation is lowered by the electronic influence of a synthetically appended stable redox center (figure 3.1.1). When the RA loses an electron, a reaction is triggered at the reactive function causing a color change. The process is intrinsically catalytic when the reversibility of the RA redox chemistry allows it ($RA^{\cdot+}$) to be reduced by its neutral form (RA).

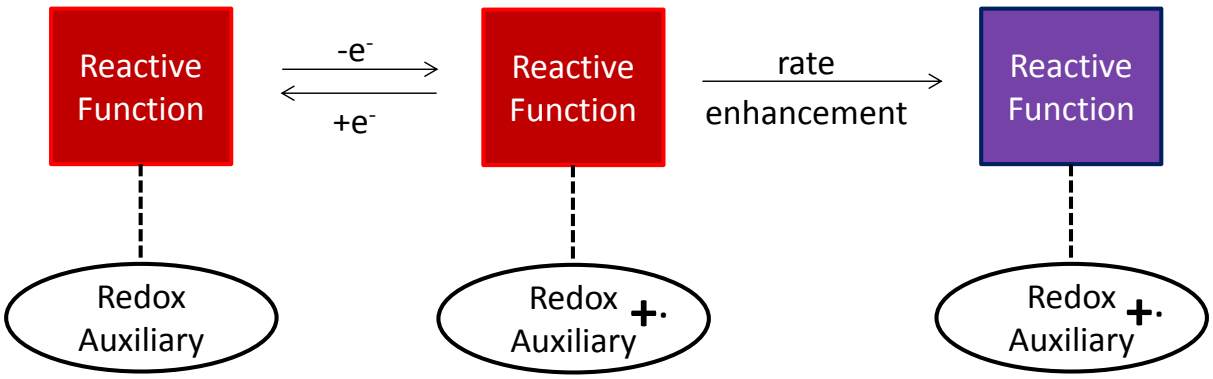

Figure 3.1.1. Figurative representation of the redox auxiliary effect. Taken from reference 82.

A majority of the work presented uses the 2+2 photoisomerization of norbornadiene (N) to yield quadricyclane (Q) as the reactive function (scheme 3.1.1). It is a good candidate in that the process is the thermally reversible. Synthetically altering the N/Q parent system to incorporate a redox auxiliary allows for the electrochemical cycloreversion of Q to N (scheme 3.1.2).

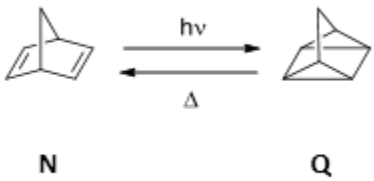

Scheme 3.1.1. Photoconversion of N to Q and the thermal back conversion.

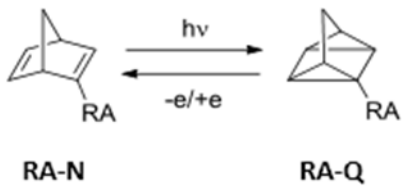

Scheme 3.1.2. Photoconversion of the RA appended N to Q and the electrochemical back conversion.

The redox auxiliary appendage is defined as an attached redox group that acts as a stable radical carrier. We chose the triarylamine (AA) group for this function due to its reversible redox chemistry and oxygen stable radical cations. Scheme 3.1.3 is the redox auxiliary catalytic cycle for the N/Q system. The RA-N photoconverts to RA-Q, a voltage is applied to generate $RA^{\cdot+}$-Q which then quickly isomerizes to $RA^{\cdot+}$-N. In a catalytic fashion, the electron hole is transferred to a new molecule of RA-Q, starting the cycle again.

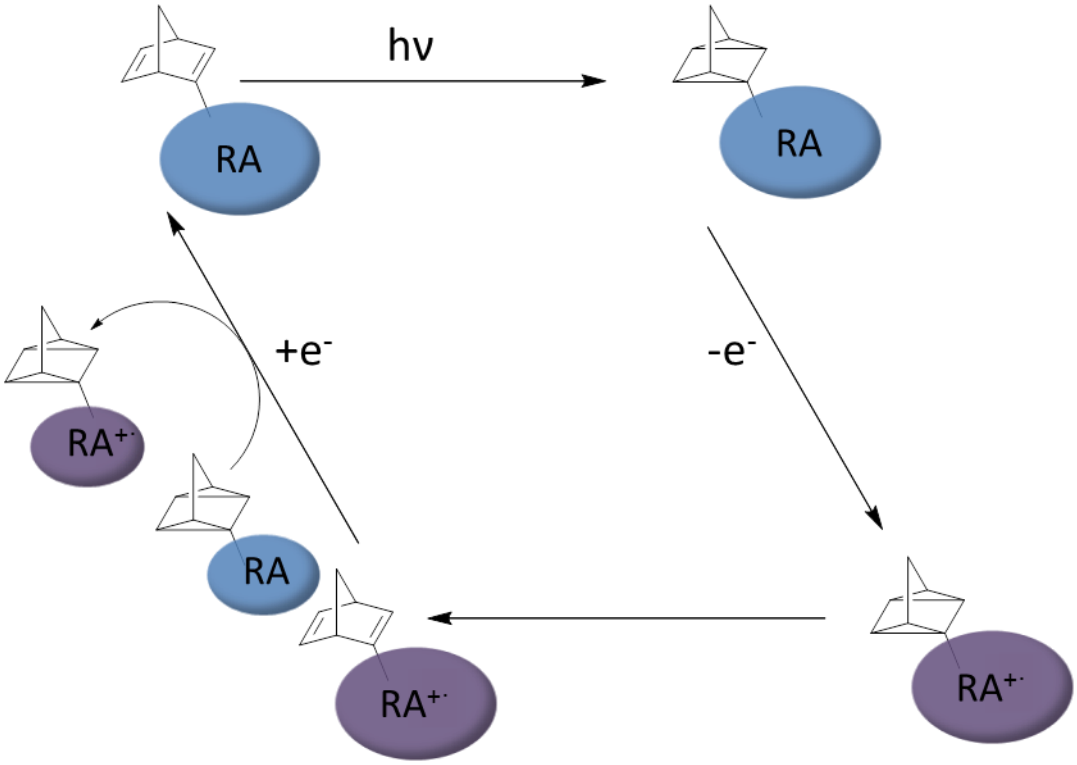

Scheme 3.1.3. Redox auxiliary mediated chain reaction mechanism using the norbornadiene/quadricyclane (N/Q) photoisomerization as the reactive function.

AA-N-Ts is shown in scheme 3.1.4. Les Gray synthesized and investigated the material as a photoelectrochromic redox auxiliary system. The key results of his studies were:

1. **AA-N-Ts** is a yellow amorphous sold that bleaches upon irradiation with UV/vis light (Φ_{405} = 0.60).
2. **AA-Q-Ts** is thermally stable with a half-life ($t_{½}$) of 237 hours at 20 °C in benzene.
3. **AA-N/Q-Ts** system exhibits reversible electrochemistry
4. In bulk solution, **AA-Q-Ts** quantitatively converts to **AA-N-Ts** in the presence of a catalytic amount of the chemical oxidant, CRET.

Aspects of the system not thoroughly demonstrated are the electrochemical conversion of **AA-Q-Ts** to **AA-N-Ts** and subsequent photoelectrochromic cycling in the device state.

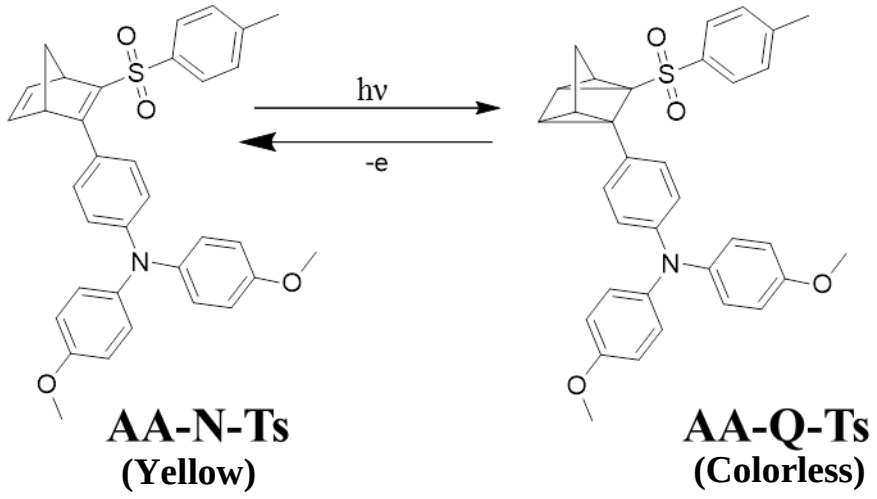

Scheme 3.1.4. Photoelectrochemical cycling between **AA-N.-Ts** and **AA-Q-Ts**.

3.2 Results and Discussion: Photoelectrochromic Cycling of Redox-Auxiliary Appended Photosystems

3.2.1 $(Tol)_3TBABF_4$ as a Gel Electrolyte for Photoelectrochromic Cycling

For effective photoelectrochromic cycling to take place, a suitable media-in which both optimal photochemistry and electrochemistry could occur- would need to be developed. Les Gray's work demonstrated that while **AA-N-Ts** has a relatively high quantum yield (Φ_{405}) of 0.60 (in benzene), the photochemistry is highly dependent on the solvent environment. In aromatic solvents, such as toluene or benzene, **AA-N-Ts** quantitatively converts to **AA-Q-Ts** in 5 s under arc lamp irradiation.[105] In order to ensure that only the application of electrochemical energy, as opposed to thermal energy, leads to the back conversion of **AA-Q-Ts** to **AA-N-Ts**, the chosen photoelectrochromic media would have to exhibit **AA-Q-Ts** thermal stability. In benzene at 25 ºC, **AA-Q-Ts** has a half-life ($t_{1/2}$) of 237 hours indicating that in terms of both photochemistry and AA-Q-Ts thermal stability, aromatic solvent systems are ideal.

In polar aprotic solvents (tetrahydrofuran, acetone), **AA-N-Ts** photoreacts more slowly and conversion to **AA-Q-Ts** is not quantitative as detectable amount of **AA-N-Ts** are present. In acetonitrile, irradiation of **AA-N-Ts** leads to a photostationary state and further irradiation actually causes an increase in the concentration of **AA-N-Ts**. These results suggest that standard solvent systems used in organic electrochemistry (tetrahydrofuran, acetone, acetonitrile, propylene carbonate etc.) won't be applicable for the photoelectrochromic cycling of **AA-N-Ts**.

The ideal photoelectrochromic medium would have to account for **AA-N-Ts'** photosensitivity while also being able to effectively pass a current. For device studies, qualities like viscosity and chemical stability are also important.

---

[105] Gray, L.T. The Application of Arylamines as Redox Auxiliaries, Polar Crystals and Organic Semiconductors. Ph.D Dissertation, The University of Alabama, Tuscaloosa, AL, 2012.

We came across an aromatic electrolytic system developed in 1985 by C. J. Picket. It not only possessed aromaticity, a wide anodic electrochemical range, and high viscosity (η = 1.5±0.1 CP, 28 °C), it could be prepared easily from readily available (and cheap) materials.[106] When the common electrolyte, $TBABF_4$, is mixed with toluene, the salt dissolves and the transparent solution partitions into two clear layers (Figure 3.2.1). The top layer is toluene only while the syrupy bottom layer is a 3:1 toluene:$TBABF_4$ mixture (also denoted as $(tol)_3TBABF_4$ or 1.4 M $TBABF_4$ in toluene). Table 3.2.1 summarizes the physical properties of $(tol)_3TBABF_4$ or 1.4 M $TBABF_4$ in toluene.[2] The electrochemical window of $(tol)_3TBABF_4$ is shown in figure 3.2.2. The potential range is from ~-2.8 V to 1.2 V (vs ferrocene redox couple) or -2.3 V to 1.7 V (vs SCE). For purely arylamine electrochromic applications, an anodic potential limit of 1.7 V is too small (see chapters 1 and 2). We expect the switching from **AA-Q-Ts** to **AA-N-Ts** to be a reaction catalyzed by the formation of a miniscule amount of **AA-N/Q-Ts**$^{\cdot+}$ (scheme 3.1.1) thus requiring only a small applied voltage (<1.5 V vs SCE).

[106] Picket, C. J. "A simple Hydrocarbon Electrolyte: Completing the Electron-transfer Series $[Fe_4S_4(SPh)_4]^{1-/2-/3-/4-}$," *J. Chem. Soc.* **1985**, 323-326.

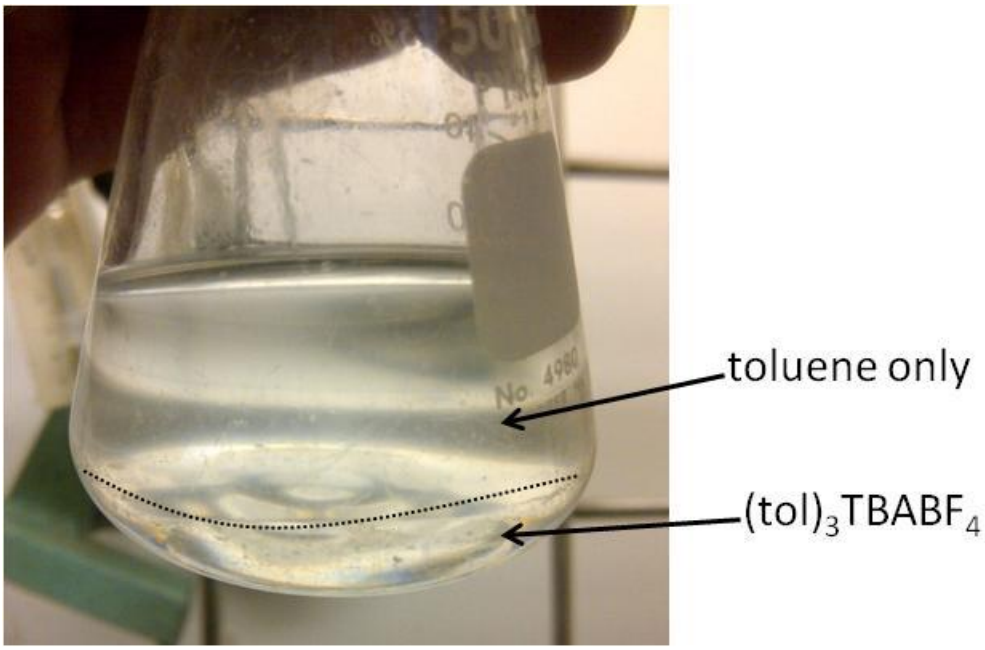

Figure 3.2.1. Photograph of $(tol)_3TBABF_4$ /toluene heterogeneous mixture.

	MP (°C)	Density (g/mL)	Viscosity (CP)	Specific Conductance $10^{-3}\Omega^{-1}cm^{-1}$	Electrochemical Window (V)
$(tol)_3TBABF_4$	22	0.98	1.5±0.1	1.2±0.1	4

Table 3.2.1. Physical properties of $(tol)_3TBABF_4$.

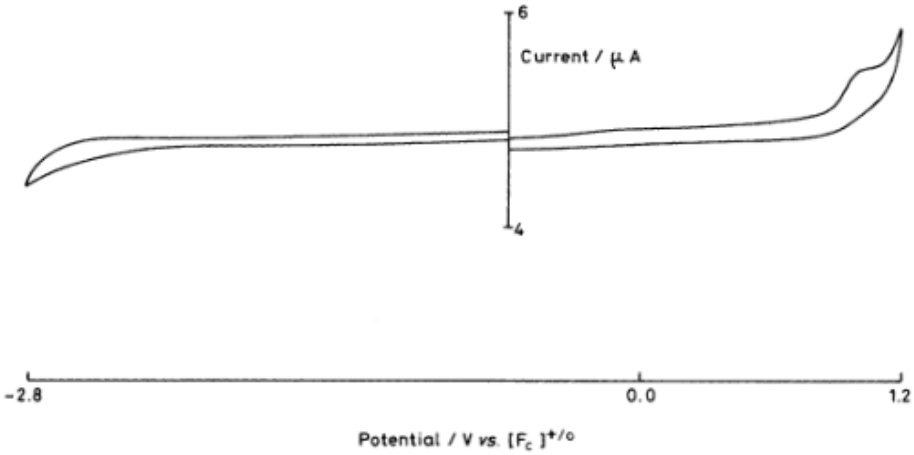

Figure 3.2.2. Cyclic voltammogram of $(tol)_3TBABF_4$ with scan rate of 100 mV/s at Pt disc electrode (area: 0.034 cm^2). Taken from reference 2.

3.2.2 Irradiation of AA-N-Ts and Chemical Stability of AA-Q-Ts in $(tol)_3TBABF_4$ Bulk Solution State

In figure 3.2.3, a concentrated solution of **AA-N-Ts** (0.97 mM) in $(tol)_3TBABF_4$ was irradiated using an arc lamp. Within 1 minute, **AA-N-Ts** underwent complete photoreaction to yield **AA-Q-Ts** as determined from the bleaching of the absorbance band at 388 nm (19100 $M^{-1}cm^{-1}$). This modulation in the visible region of the electromagnetic spectrum is accompanied by a color change from yellow to colorless (figure 3.2.4). **AA-N-Ts** has the unique characteristic of being a negative photochromic system. It is also worth noting that **AA-Q-Ts** was chemically stable after 15 min in $(tol)_3TBABF_4$. This result shows that thermal conversion of **AA-Q-Ts** to **AA-N-Ts** won't be a contributing factor within the time-scale of a photoelectrochromic switch (< 2 min).

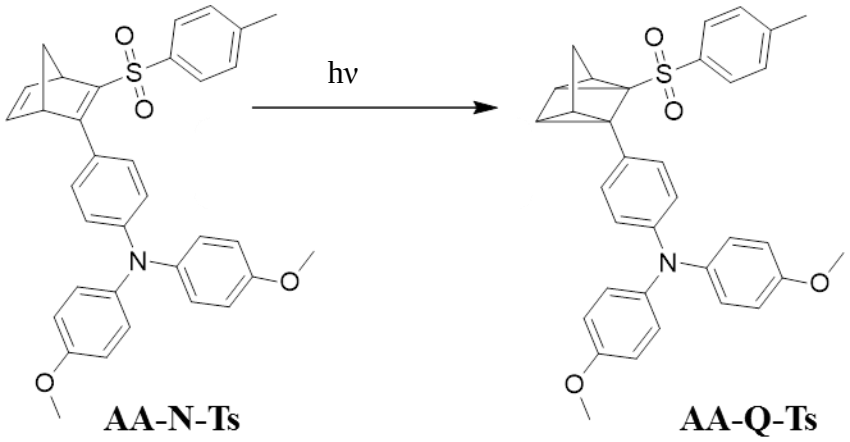

Scheme 3.2.1. Photochemical conversion of **AA-N-Ts** to **AA-Q-Ts** .

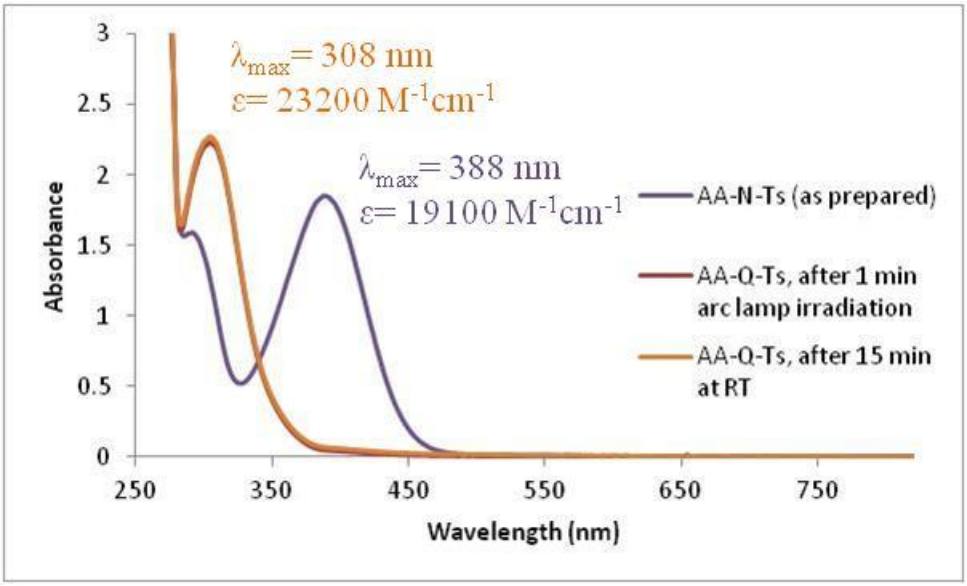

Figure 3.2.3. Irradiation of 0.97 mM AA-N-Ts in $(tol)_3TBABF_4$ using an arc lamp equipped with 385 nm filter, yielding AA-Q-Ts.

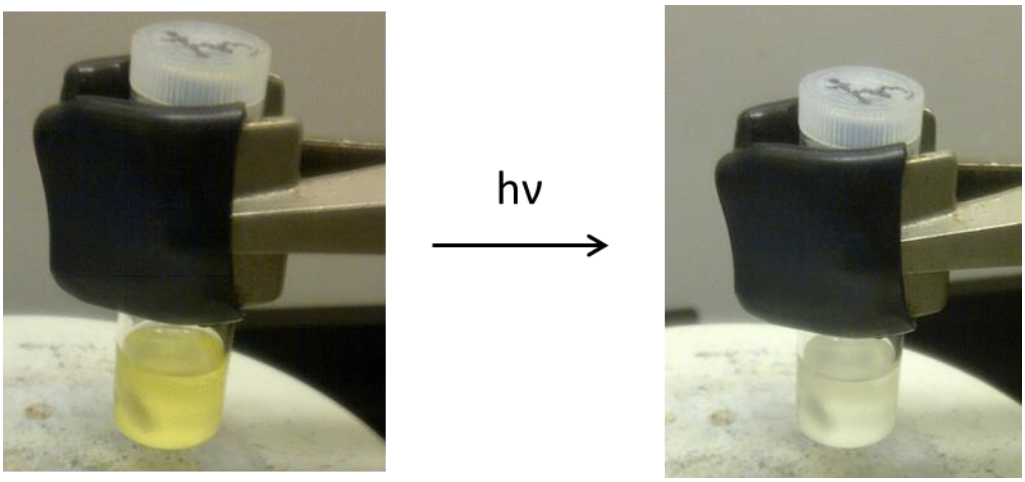

Figure 3.2.4. Photograph showing the negative photochromism of **AA-N-Ts**/**AA-Q-Ts** system.

3.2.3 Electrochemistry of AA-N-Ts in $(Tol)_3TBABF_4$ Bulk Solution State

To demonstrate that **AA-N-Ts** was capable of undergoing a reversible 1 e^- electrochemical oxidation at a Pt disc electrode, **AA-N-Ts** (1.0 mM) was subjected to a cyclic voltammetry scan. Figure 3.2.5 shows the scan between 0 V and 1.3 V vs SCE. At 0.891 V, **AA-N-Ts** is oxidized to

AA-N-Ts$^{\cdot+}$. This redox potential corresponds favorably to previous measurements (0.859 V in CH_2Cl_2 vs SCE).

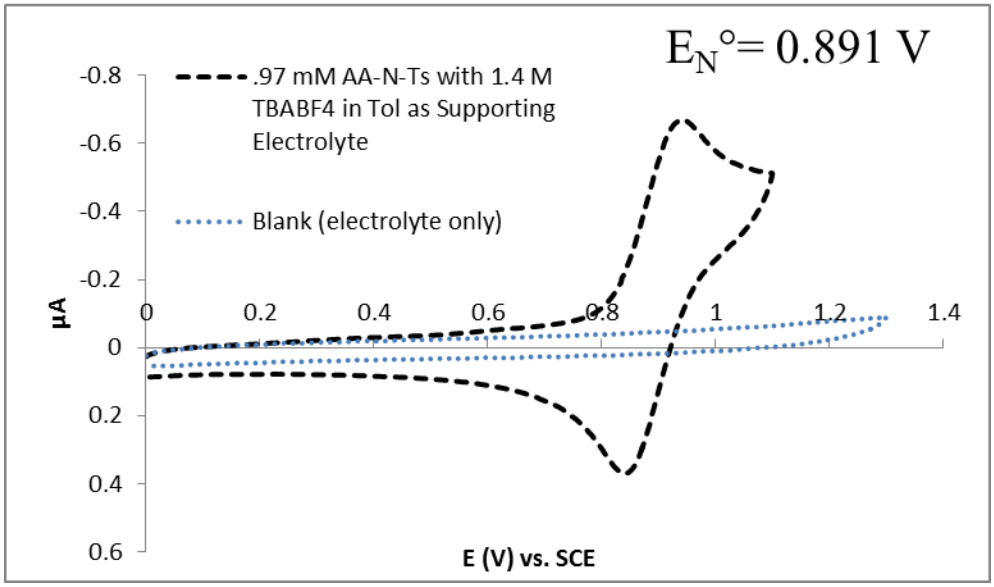

Figure 3.2.5. Cyclic Voltammetry (CV)of 0.97 mM **AA-N-Ts** (**N**) in $(tol)_3TBABF_4$ Bulk Solution State. Scan Rate: 50 mV/s

Figure 3.2.6 shows an overlay of cyclic voltammograms. The red scan is that of **AA-N-Ts** while the green scan was taken after photoconversion to **AA-Q-Ts**. The fact that the two scans overlap shows that both **AA-N-Ts** and **AA-Q-Ts** have equivalent oxidation potentials. To further prove that the green CV scan is in fact that of **AA-Q-Ts** and not **AA-N-Ts**, optical spectra were taken after several CV's to demonstrate that there was little conversion back to **AA-N-Ts** and that the solution was predominately **AA-Q-Ts** (Figure 3.2.7).

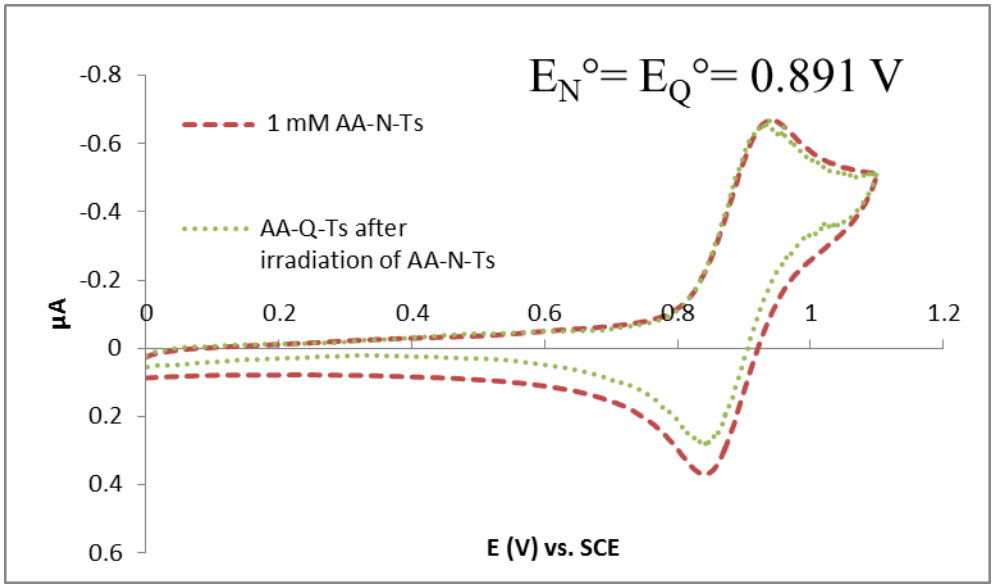

Figure 3.2.6. Cyclic Voltammograms of 1.0 mM **AA-N-Ts (N)** (red dash) and 1.0 mM **AA-Q-Ts (Q)** (green dot). Scan Rate: 50 mV/s

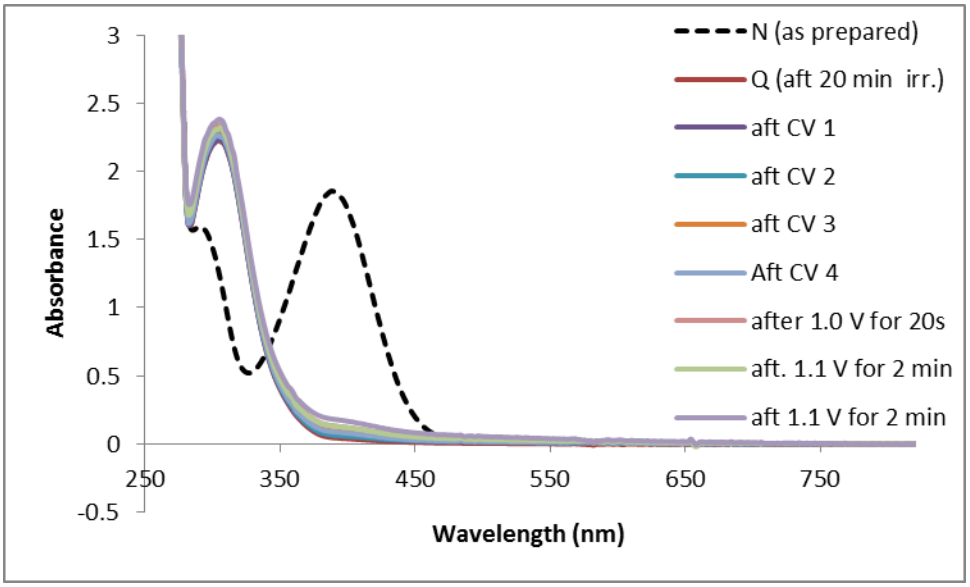

Figure 3.2.7. Electrochemical response of **AA-Q-Ts** (0.97 mM in $(Tol)_3TBABF_4$) at Pt disc electrode.

3.2.4 Oxidative Catalysis of AA-Q-Ts to AA-N-Ts via Chemical Oxidation in $(Tol)_3TBABF_4$

The result shown in figure 3.2.7 was discouraging, prompting the question of whether **AA-Q-Ts** can undergo an oxidative reversion to generate **AA-N-Ts**. More importantly, would the reversion be catalytic? To answer these questions, a solution of AA-N-Ts in $(tol)_3TBABF_4$ was irradiated

to yield **AA-Q-Ts**. The colorless solution was then subjected to catalytic amount of the organic oxidant, CRET. Figure 3.2.8 shows the result of the experiment as an overlay of optical absorbance spectra. Upon addition of 1 mol % CRET and 10 minutes of stirring, **AA-Q-Ts** converts quantitatively back to **AA-N-Ts**. The conversion is also clean as noted by the isosbestic point at 348 nm.

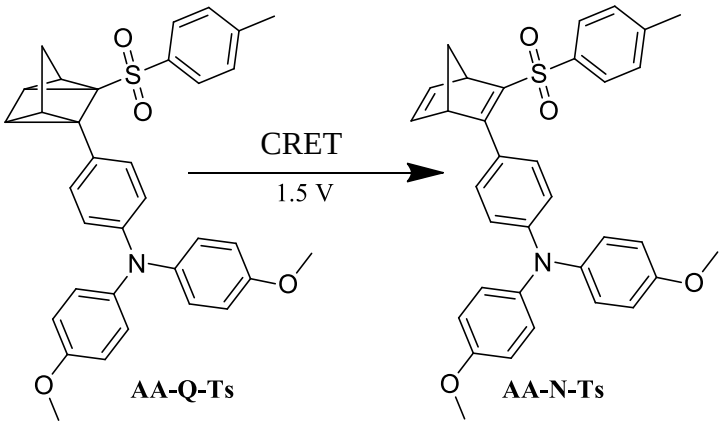

Scheme 3.2.2. Oxidative back conversion of **AA-Q-Ts** to **AA-N-Ts** with CRET .

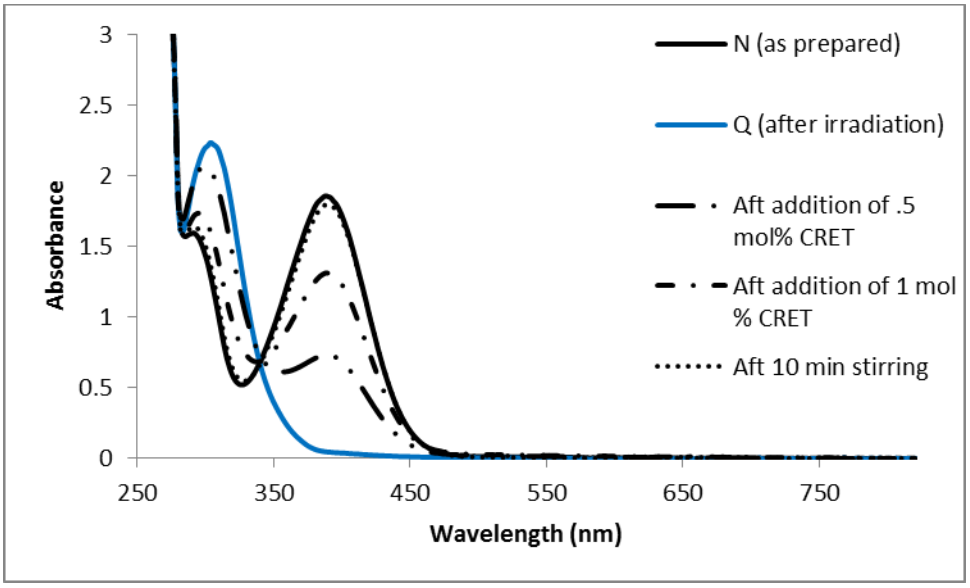

Figure 3.2.8. Catalytic conversion of **AA-Q-Ts** (1.0 mM) to **AA-N-Ts** after addition of 1 mol% CRET

3.2.5 Photoelectrochromic Switching of AA-N-Ts in Device State

After demonstrating the facile photochemistry, stable electrochemistry, and catalytic back conversion of the **AA-N-Ts/AA-Q-Ts** system, the photoelectrochromic system is applied an ITO sandwich type device set-up (figure 3.2.9). In the photoelectrochromic device (PECD) yellow/clear color switching is expected to occur readily as a result of two stimuli: (1) irradiation and (2) applied voltage (figure 3.2.10).

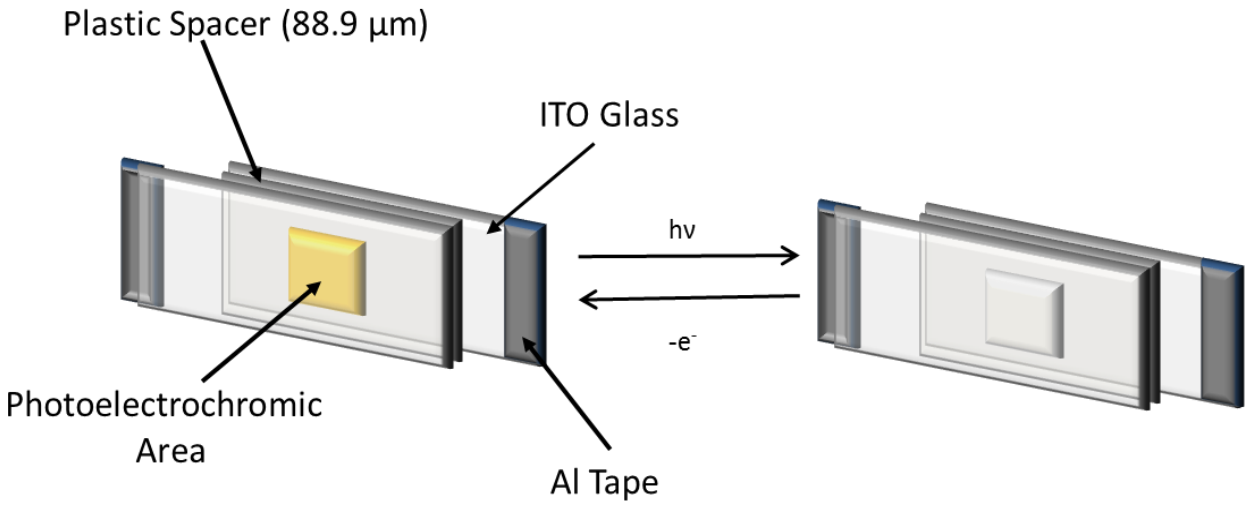

Figure 3.2.9. Generic representation of photoelectrochromic device with labeled components.

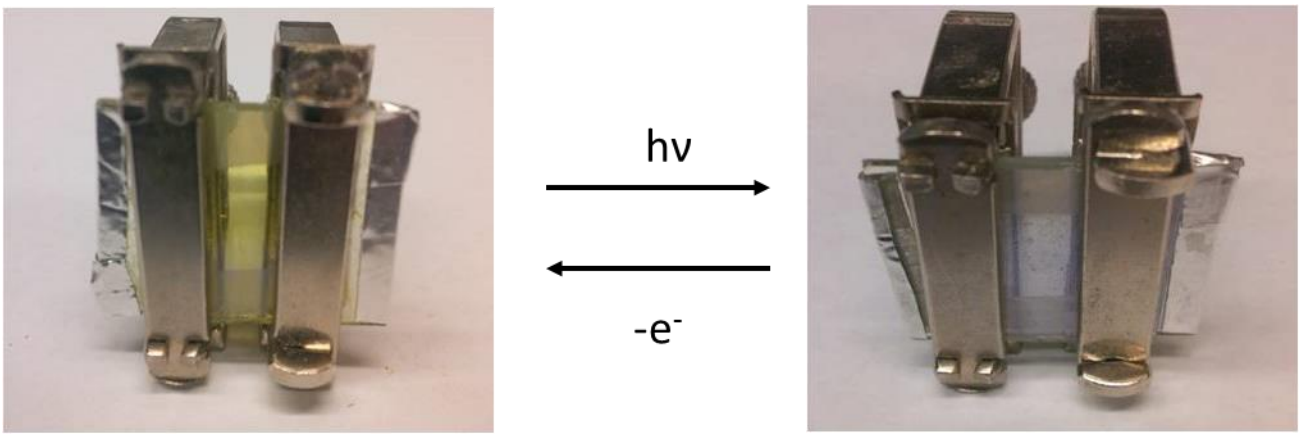

Figure 3.2.10. Picture of **AA-N-Ts**/**AA-Q-Ts** negative photochromism in the device state.

Figure 3.2.11 shows a photograph of the PECD switching apparatus. A 380 nm LED flashlight is clamped to the UV-vis Spectrophotometer and used for irradiation. The PECD stands in front of both the spectrophotometer beam and the beam of the LED light. Because the

380 nm LED light is positioned at an angle, it does not interfere with the spectrophotometer's beam and both can operate simultaneously. Electrical leads are attached to the anode and cathode of the PECD. As with the singular ECDs presented in Chapters 1 and 2, the reference and cathode are coupled with the counter electrochemical process being that of ITO reduction (Section1.2.4.1).

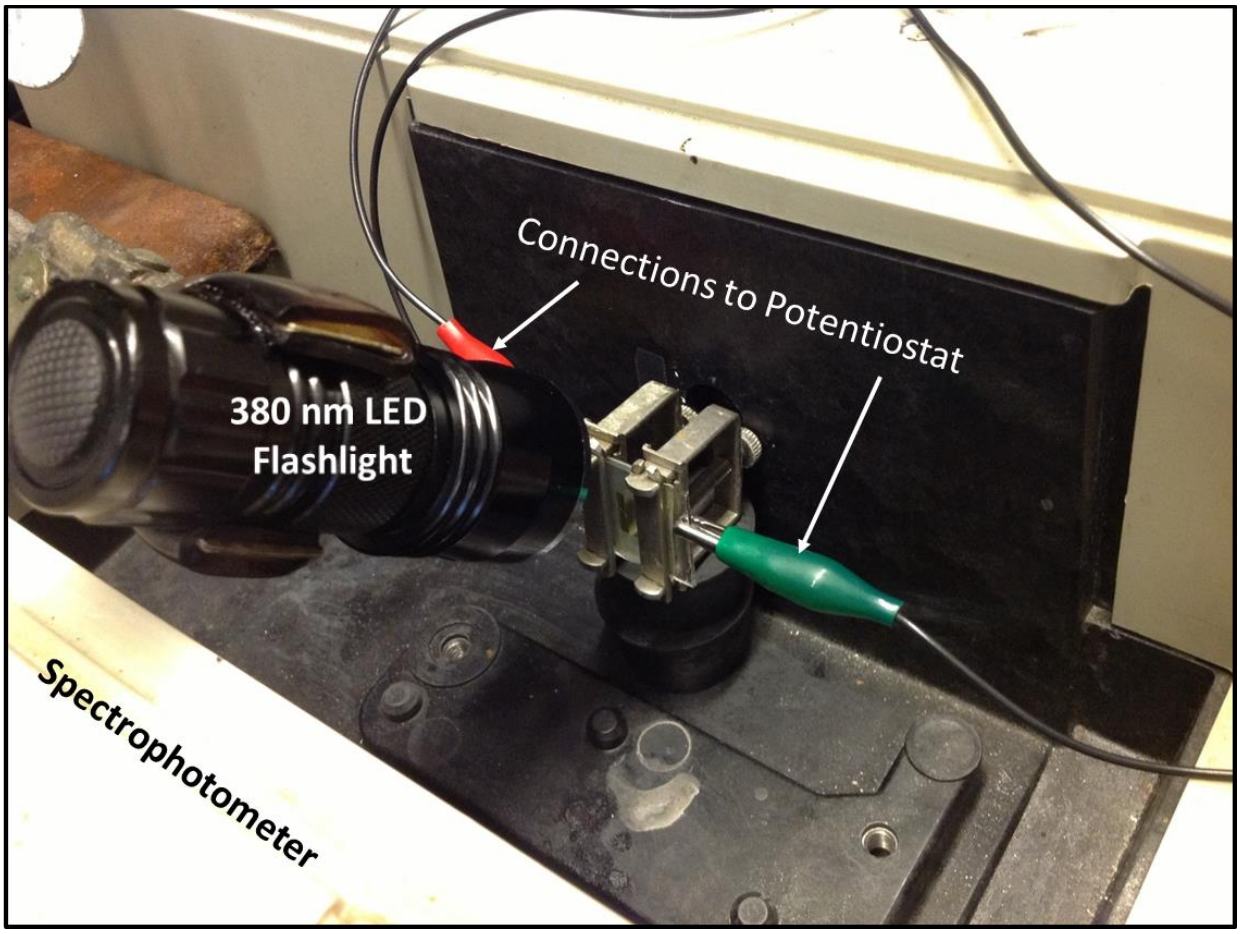

Figure 3.2.11. Photograph of PECD apparatus equipped with 380 nm LED flashlight.

Using an arc lamp (equipped with 385 nm filter), **AA-N-Ts** is converted to **AA-Q-Ts** in the PECD within 90 s of irradiation (scheme 3.2.1 / figure 3.2.12). Interestingly, when a 380 nm LED flashlight is used instead, irradiation to **AA-Q-Ts** occurs within 15 s (figure 3.2.13) even though the concentration of **AA-N-Ts** is considerably higher (.01 M vs .00765 M). The 380 nm

LED directly irradiates the π-π^* band (λ_{max} = 388 nm) of AA-N-Ts, making the photoreaction more facile.

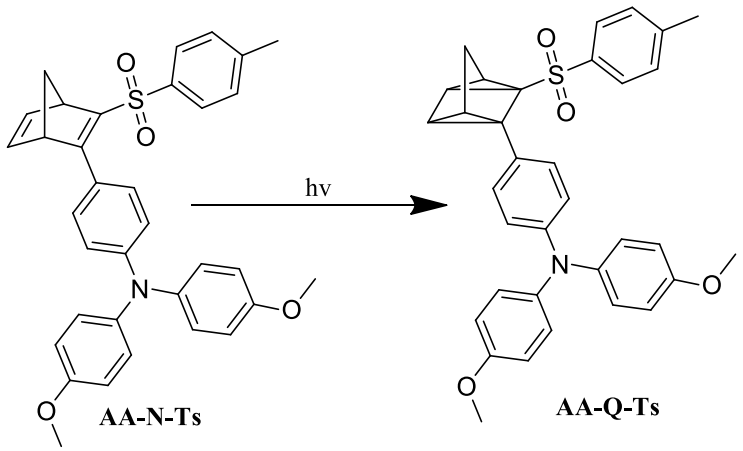

Scheme 3.2.3. Photoconversion of **AA-N-Ts** to **AA-Q-Ts** with arc lamp irradiation.

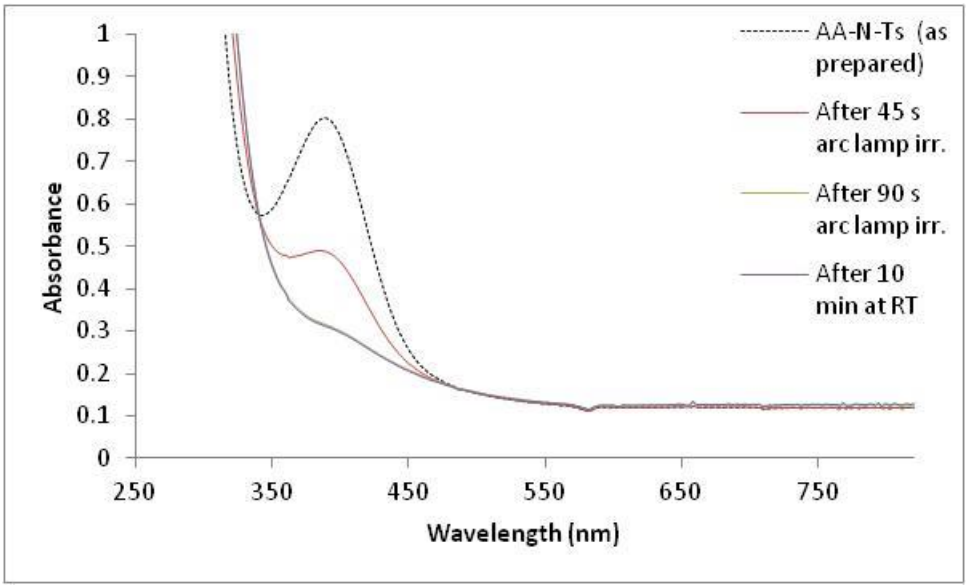

Figure 3.2.12. Irradiation of .00765 M **AA-N-Ts** to **AA-Q-Ts** with arc lamp in PECD state.

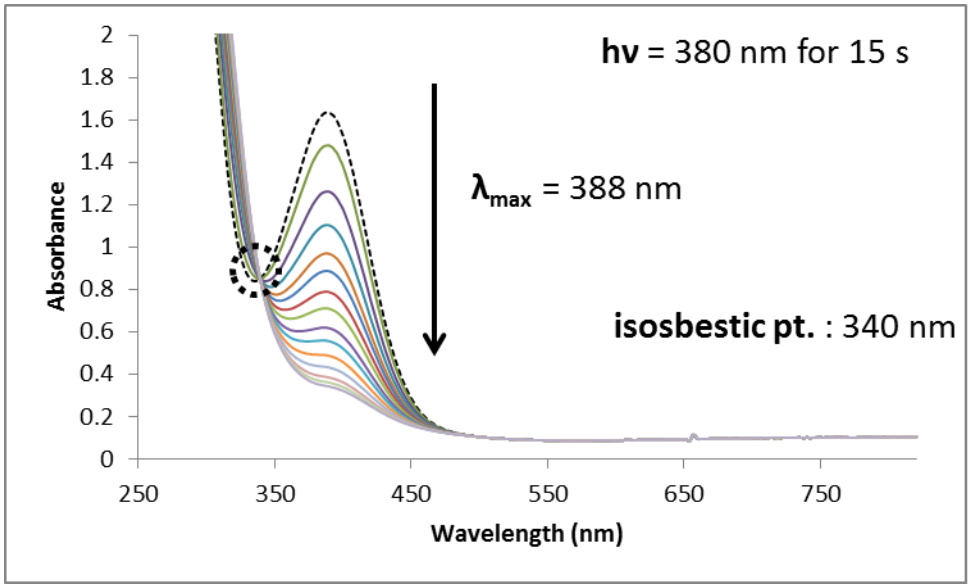

Figure 3.2.13. Irradiation of .01 M **AA-N-Ts** to **AA-Q-Ts** with 380 nm LED in PECD state. A spectrum is taken every 1 s.

To effect the electrochemical back conversion of **AA-Q-Ts** to **AA-N-Ts**, a voltage of 1.5 V of was applied to the PECD for 25s. **AA-Q-Ts** converts quantitatively and cleanly to **AA-N-Ts** with an isosbestic point at 340 nm within 25 s (scheme 3.2.2 / figure 3.2.14). The presence of an isosbestic point is an important feature of the results as it ensures clean conversion between only the two species. Presence of **AA-N/Q-Ts**$^{\cdot+}$ in a significant amount would also be detectable in the optical spectrum as a characteristic intense long wavelength absorbance band. These facts suggest a catalytic electrochemical mechanism behind the transformation of **AA-N-Ts** to **AA-Q-Ts**.

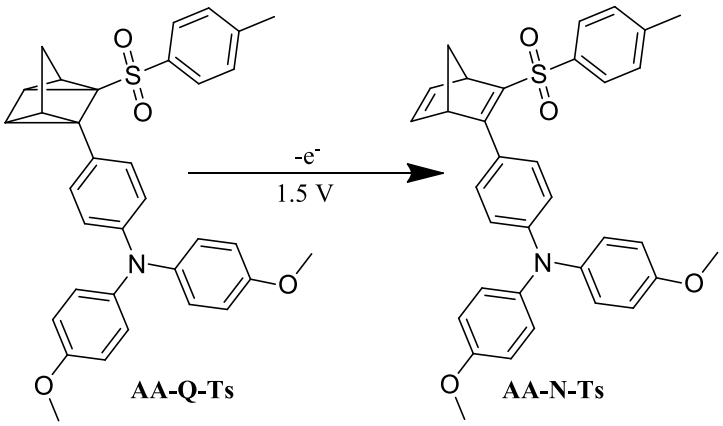

Scheme 3.2.4. Electrochemical back conversion of **AA-Q-Ts** to **AA-N-Ts** with 1.5 V.

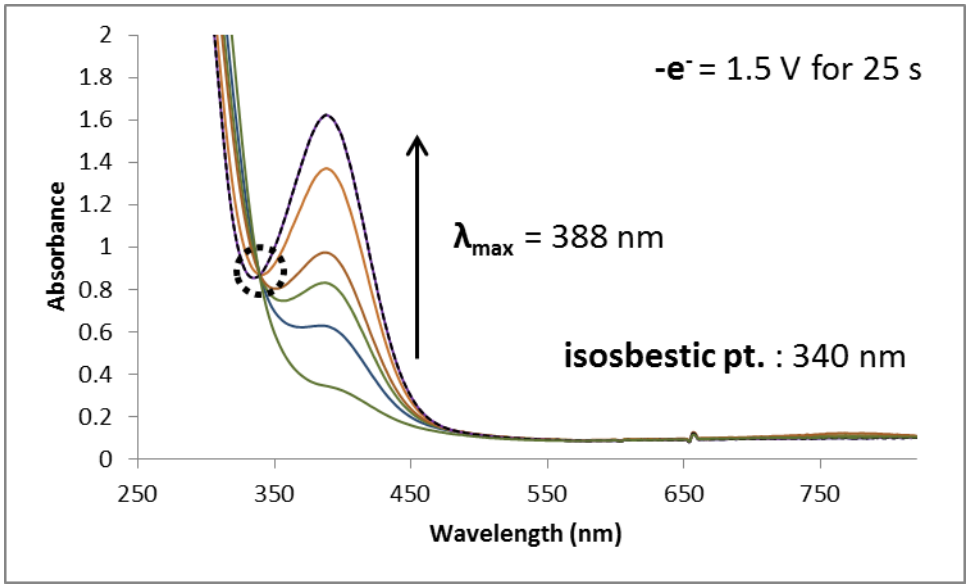

Figure 3.2.14. Electrochemical back conversion of **AA-Q-Ts** to **AA-N-Ts** in PECD state. A spectrum taken every 5 s.

3.2.5.1: Turn-On Voltage of AA-N-Ts PECD

The turn-on potential of the PECD is an important parameter that tells the user the specific voltage at which **AA-Q-Ts** begins to convert to AA-N-Ts. Figure 3.2.15 shows the absorbance at 388 nm (λ_{max}) as voltages from 0.0 V to 2.0 V are applied. At the application of 1.4 V, absorbance at 388 nm begins to increase indicating the formation of **AA-N-Ts**. The turn-on voltage of 1.4 V also indicates the voltage at which **AA-N/Q-Ts**$^{\cdot+}$ begins to form. This value

for the turn-on voltage is expected since only a small amount (< 1 mol %) of **AA-N/Q-Ts**$^{\cdot+}$ is actually needed to convert **AA-Q-Ts** to **AA-N-Ts**.

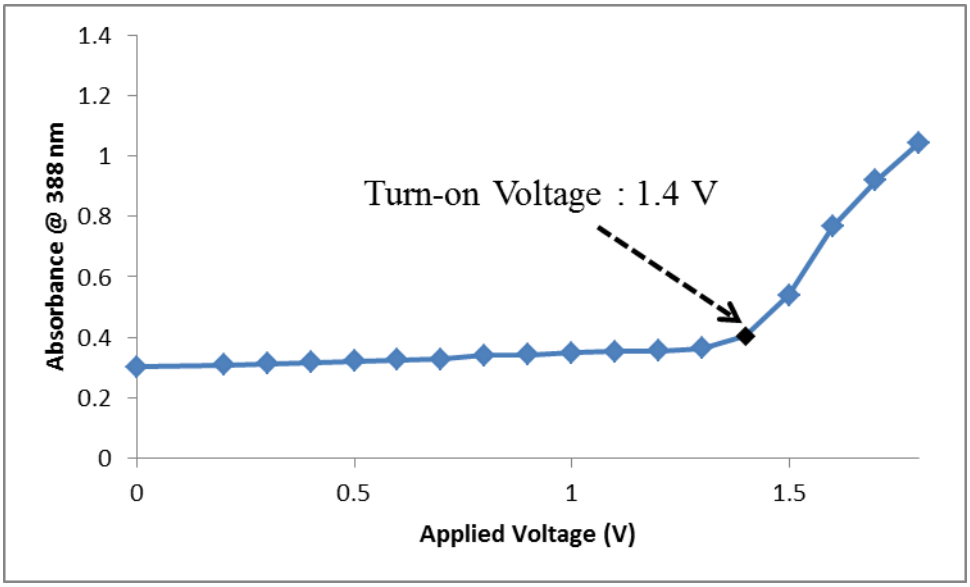

Figure 3.2.15. Absorbance vs applied voltage data for .00934 M **AA-N-Ts** in PECD. Each potential is applied for 30 s.

3.2.5.2 Photoelectrochromic Cycling of AA-N-Ts in PECD

To demonstrate the reversibility of the **AA-N-Ts/AA-Q-Ts** photoelectrochromic switching, several (~15) cycles are shown if figure 3.2.16. The details of the cycling are (spectra taken every 30 s):

OFF: 2 min irradiation with 380 nm LED

Q Hold: 1 min no irradiation, no applied voltage

ON: 1.5 V for 20 s

N Hold: 1 min no irradiation, no applied voltage

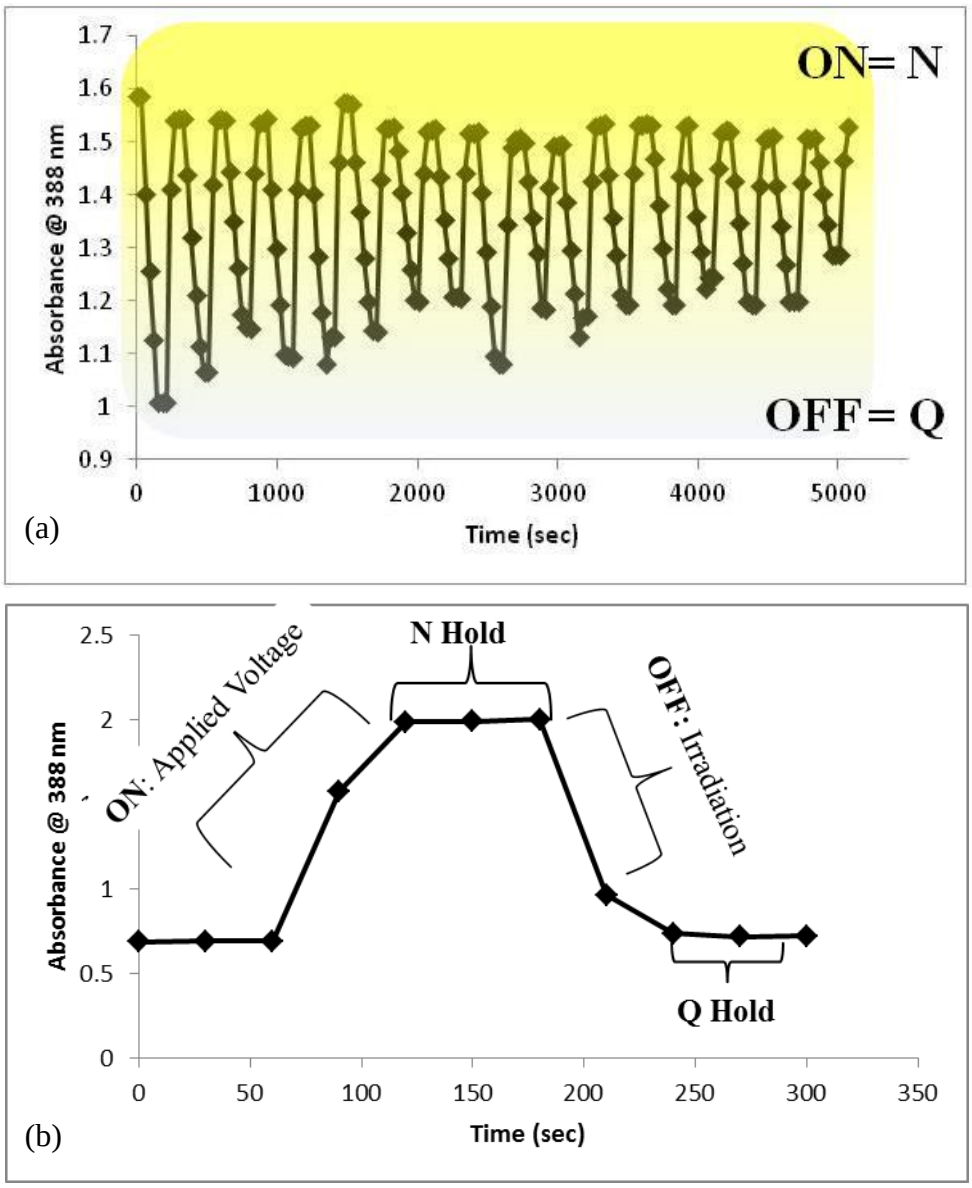

Figure 3.2.16. Photoelectrochromic cycling of 0.00798 M **AA-N-Ts** in PECD. (a) A single cycle with labeled segments.

To demonstrate sample integrity throughout the cycles, optical absorbance spectra are overlaid from cycles 2, 5, 8, 11, 14, and 17 and an isosbestic point is shown at 339 nm (Figure 3.2.17).

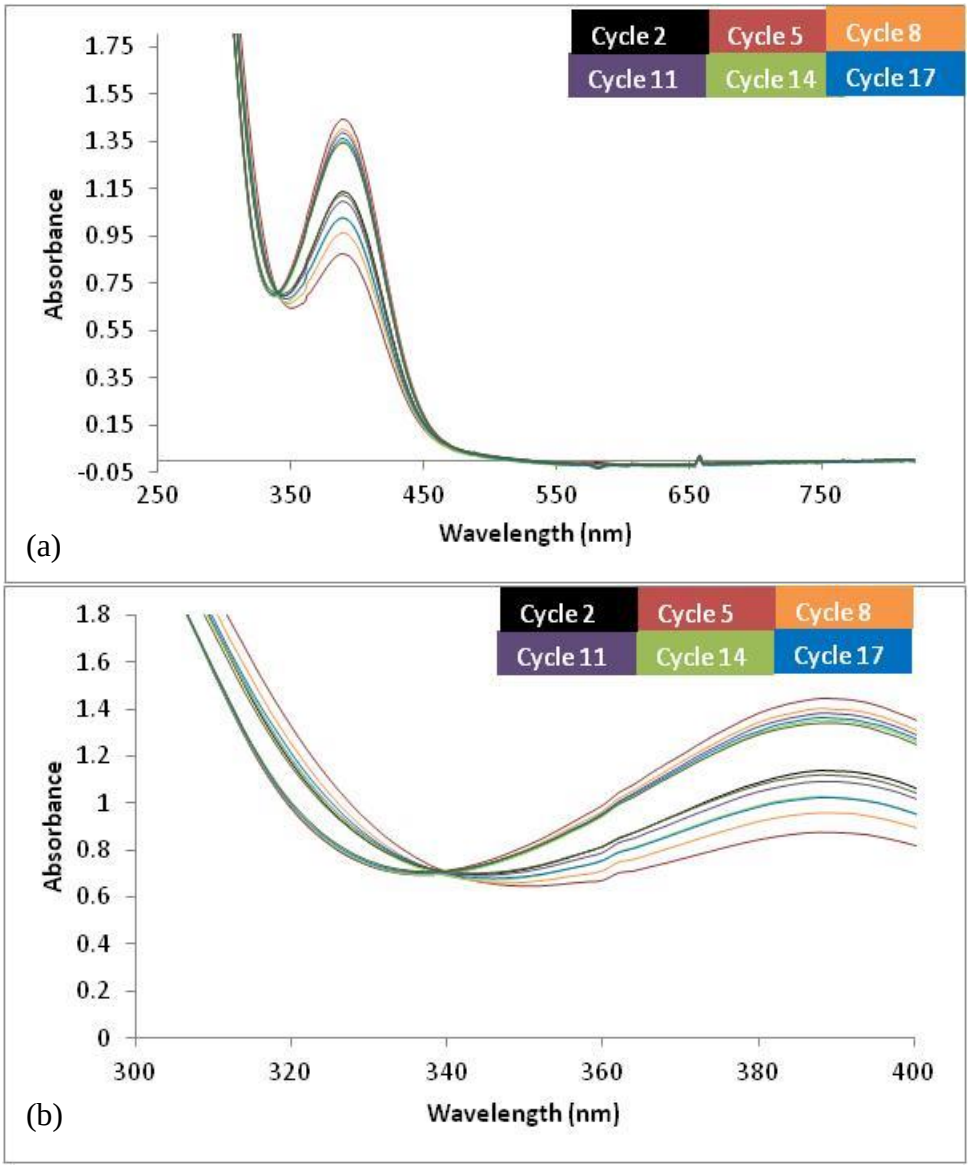

Figure 3.2.17. Overlay (a) and blow-up (b) of optical spectra from cycles 2, 5, 8, 11, 14, and 17 of figure 3.2.16.

A noticeable feature of the cycling data in figure 3.2.16 is that the photosensitivity of **AA-N-Ts** decreases as cycling progresses. By cycle 16 (ΔA_{388} = 0.220), the irradiation of **AA-N-Ts** lead to 60% less photoconversion than in cycle 1 (ΔA_{388} = 0.547). The accumulation of **AA-N-Ts**$^{\cdot+}$ as potential is regularly applied to the PECD is the reason for this effect. Eventually, the

radical cation is reduced via recombination with the reduced material in the cell. To prove that the inability of **AA-N-Ts** to photoisomerize as it cycled is due to an increase in radical cation concentration, several experiments were carried out.

The first set of experiments was a cell gap study (figure 3.2.18). Three **AA-N-Ts** PECD's of differing cell gaps were subjected to identical cycling conditions. Concentrations were also adjusted so that there was roughly the same amount of material being switched in each device. The expectation would be that in the PECD with the smaller cell gap, the decrease in **AA-N-Ts** photosensitivity would be less pronounced since the cathode is closer. The assumption is that recombination which is controlled by mass transport would be more favorable if the reduced material (assumed to be reduced ITO), is closer in proximity to the anode. The results, shown in figure 3.2.18, are precisely the opposite. At a cell gap of 25.2 µm, the smallest gap in the study, the degradation of **AA-N-Ts** photochemistry was much more pronounced than in the 50.4 µm or 88.9 µm studies. Because the concentration of **AA-N-Ts** was increased to accommodate the decrease in cell gap, this may have caused even more **AA-N-Ts**$^{\cdot+}$ to be formed at the anode, making the feature even more dramatic.

The system was cycled as follows (spectra taken every 30 s):

OFF: 1 min irradiation with 380 nm LED

Q Hold: 1 min no irradiation, no applied voltage

ON: 1.6 V for 20 s

N Hold: 1 min no irradiation, no applied voltage

There is also a noticeable difference in **AA-Q-Ts** thermal stability between the three studies, with the 25.2 µm cycles exhibiting some **AA-Q-Ts** thermal conversion to **AA-N-Ts**

during the 1 minute Q hold (figure 3.2.18). This result is also consistent with the presence of **AA-N-Ts**$^{\cdot+}$

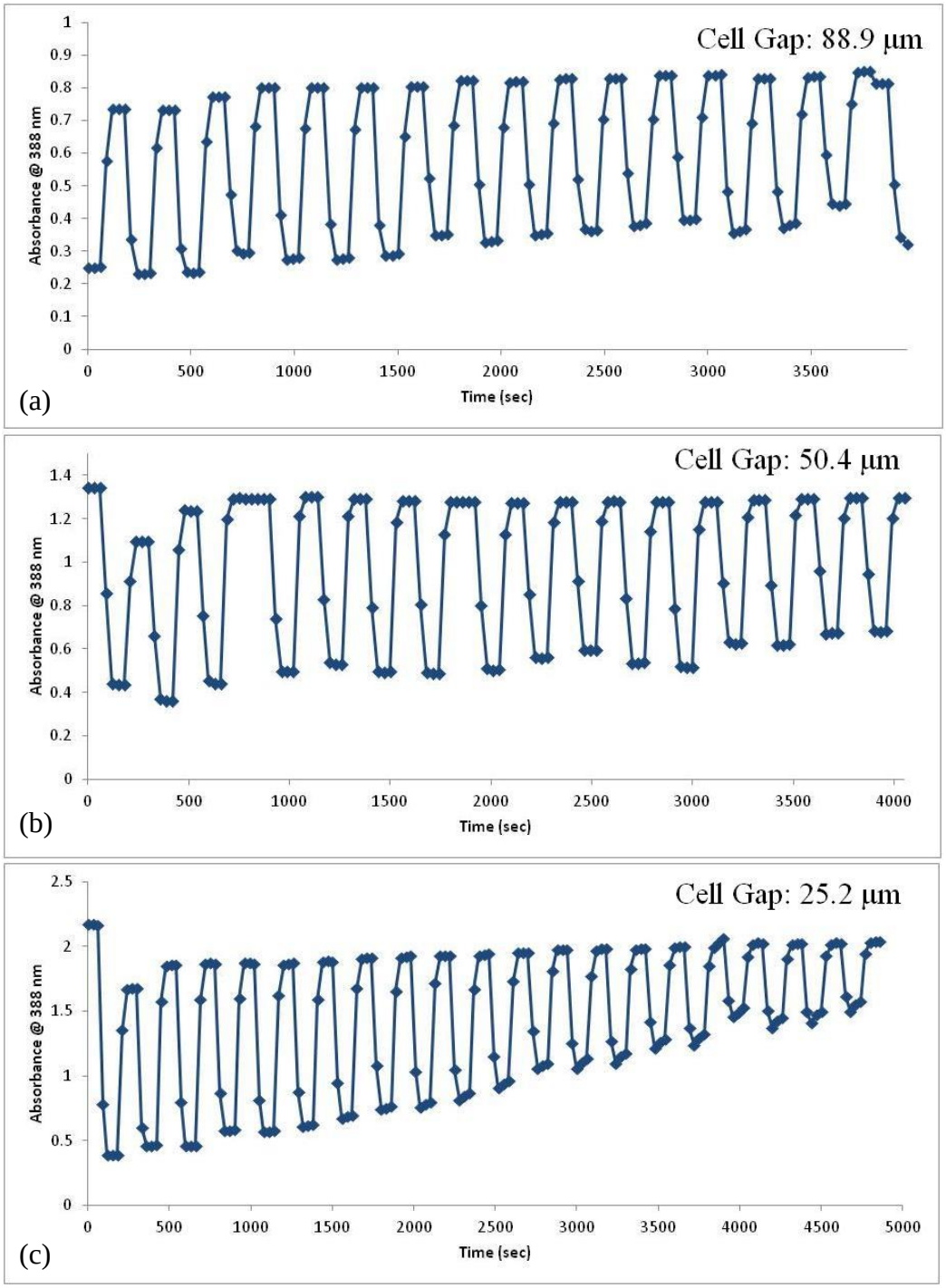

Figure 3.2.18. Photoelectrochromic cycling of **AA-N-Ts** PECD's with various cell gaps.

The **AA-N-Ts** PECD was subjected to an extended N Hold time in between a set of cycles. The expectation is that during the extended N hold time, the radical cation reduces back to the neutral **AA-N-Ts** thereby restoring photosensitivity and **AA-Q-Ts** thermal stability. By the 10 th photoelectrochromic cycle, 1 min of irradiation leads to an optical contrast (Δ%T) of 14.9%. This is just over half of the optical contrast from irradiation during cycle 1 (~26 %). After a 1 hour hold time, optical contrast is restored to 25.7% a when the PECD is irradiated for 1 min. This result is further proof that an accumulation of redox auxiliary (RA) radical cation can lead to the photochemical instability of PECD's based on RA catalysis.

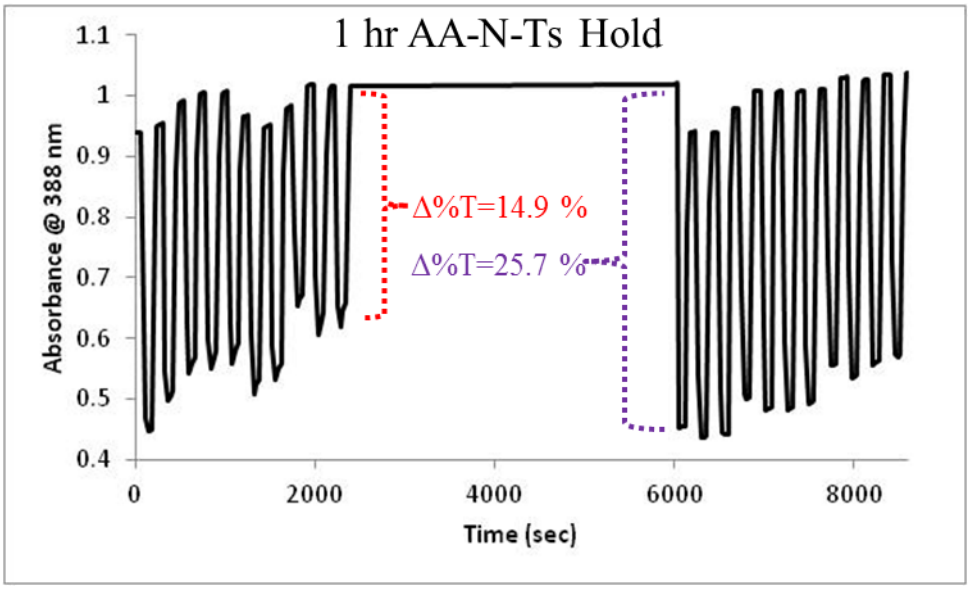

Figure 3.2.19. Photoelectrochromic cycling of 0.00750 M **AA-N-Ts** PECD with an extended **AA-N-Ts** hold time.

3.2.6. Photoelectrochromic Cycling of AA-N-Ts in PECD: Evidence of Redox Auxilliary Catalysis

To demonstrate redox auxiliary catalysis is indeed the mechanism behind the electrochemical back conversion of **AA-Q-Ts** to **AA-N-Ts**, a PECD was irradiated (figure 3.2.20) for 30 s (figure 3.2.21), subjected to an applied voltage for a short period of time (5 s), and then monitored under open circuit conditions. The PECD continues changing colors that is,

generating **AA-N-Ts** even during the absence applied potential indicating a catalytic process (figure 3.2.21 and figure 3.2.22).

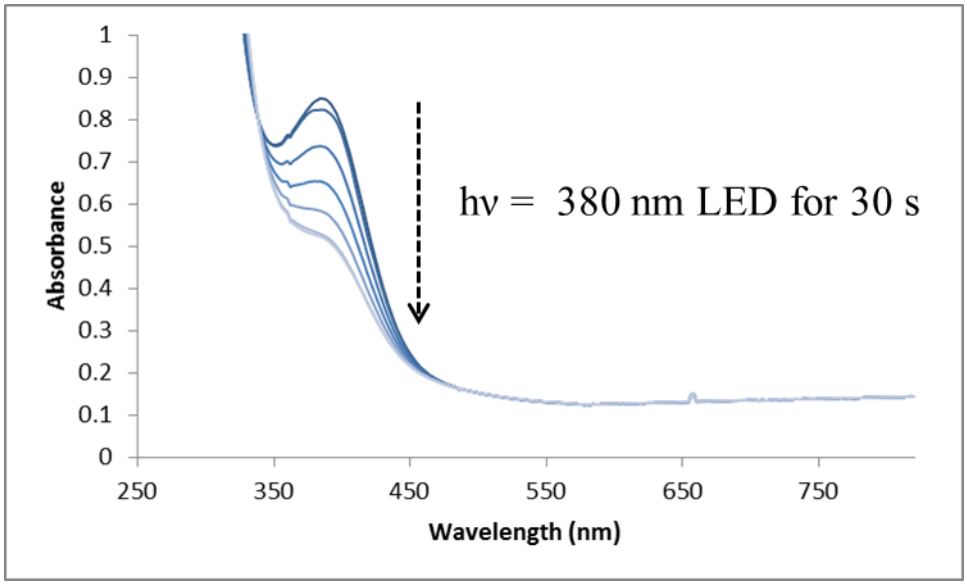

Figure 3.2.20. Time resolved optical spectra of **AA-N-Ts** PECD irradiation. Spectra taken every 5 s.

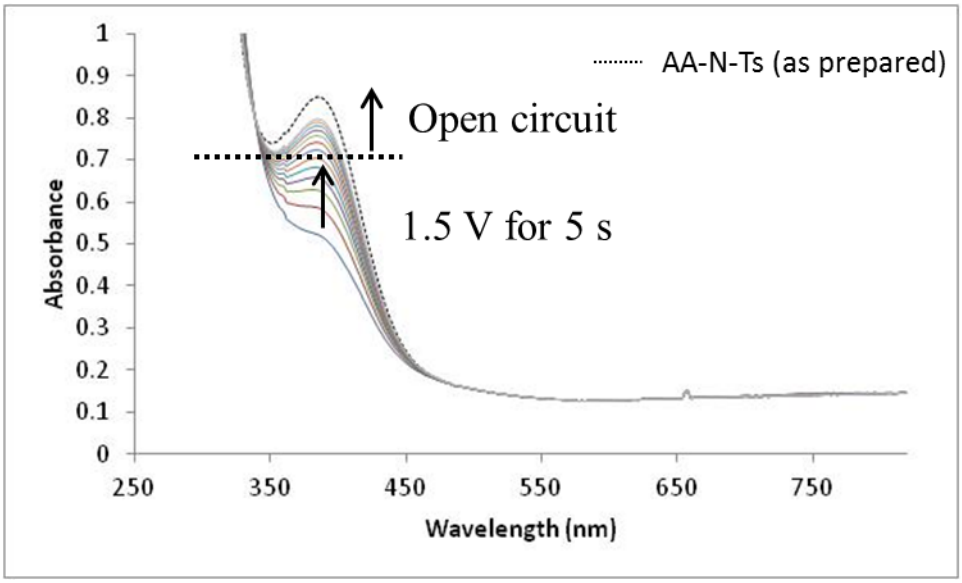

Figure 3.2.21. Time resolved optical spectra of **AA-Q-Ts** PECD as 1.5 V is applied for 5 s. Spectra taken every 1 s.

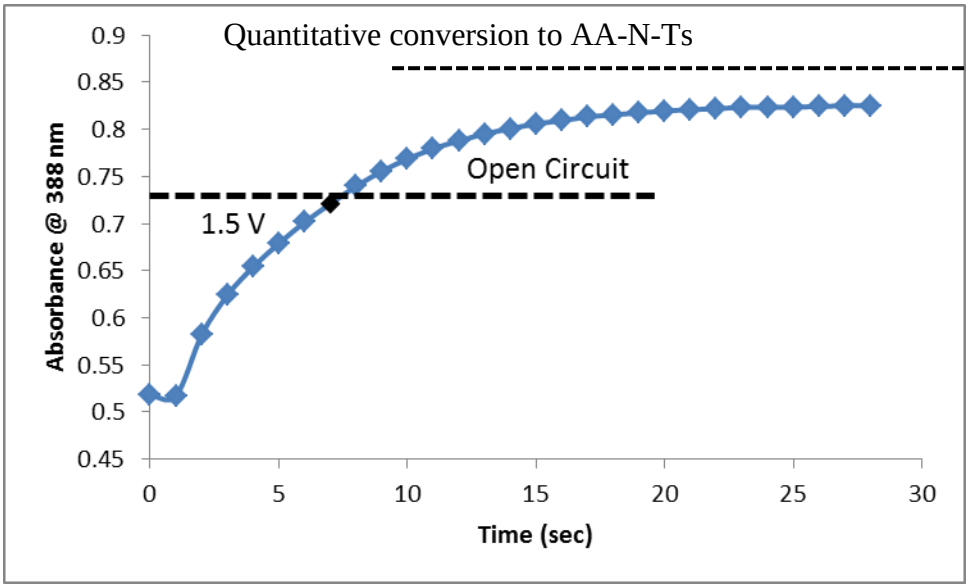

Figure 3.2.22. Absorbance vs time profile of **AA-Q-Ts** PECD as 1.5 V is applied for 5 s.

The process of calculating the percentage of **AA-N-Ts**$^{\cdot+}$ (**N**$^{\cdot+}$) electrochemically generated is demonstrated in figure 3.2.23.

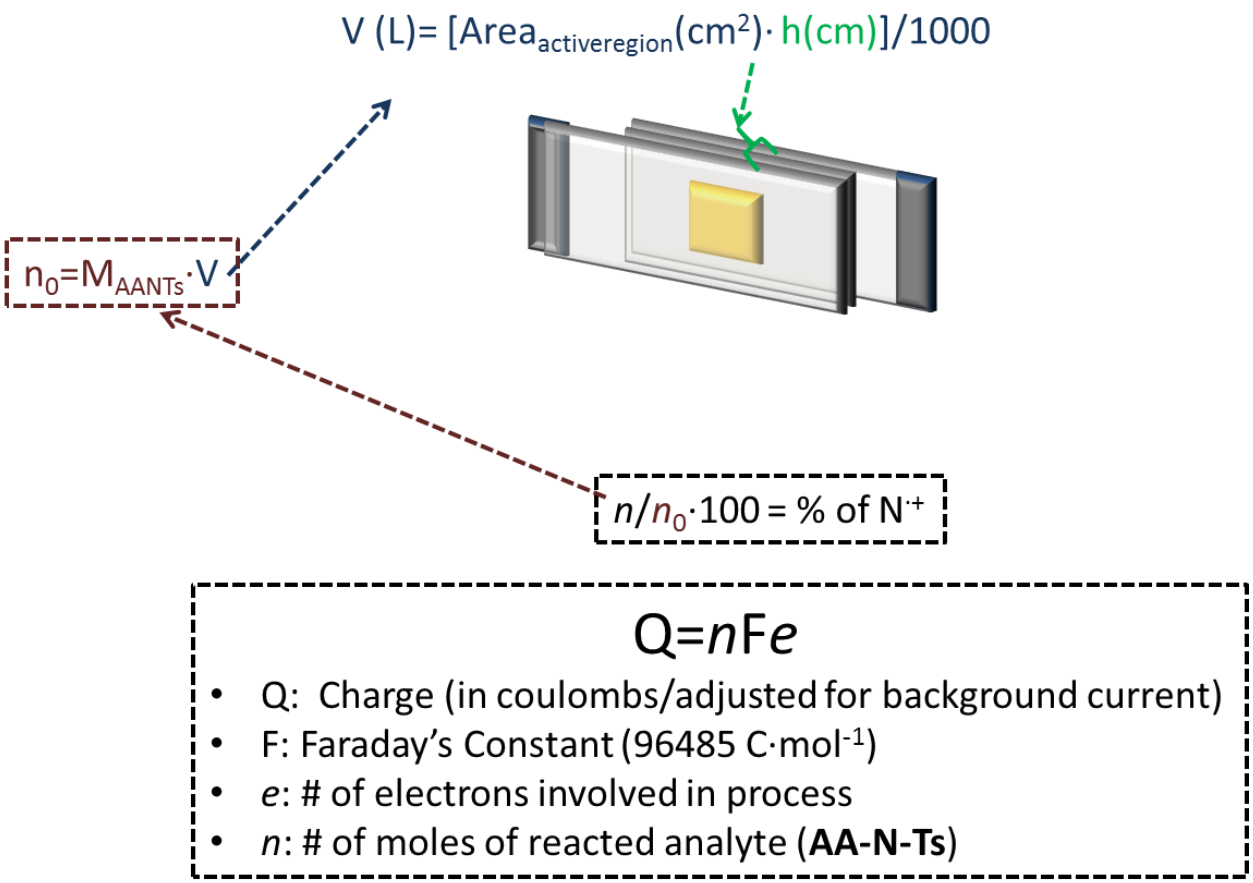

Figure 3.2.23. Calculation process for % of $\mathbf{N^{\cdot+}}$ generated at electrode.

At the turn-on voltage, 1.4 V, the amount of non-faradaic current being passed is significant compared to the amount of current actually attributable to the oxidation of **AA-N-Ts**. In figure 3.2.24, the background current at 1.4 V is calculated by extrapolation using current values directly measured at applied voltages where there is no faradaic activity.

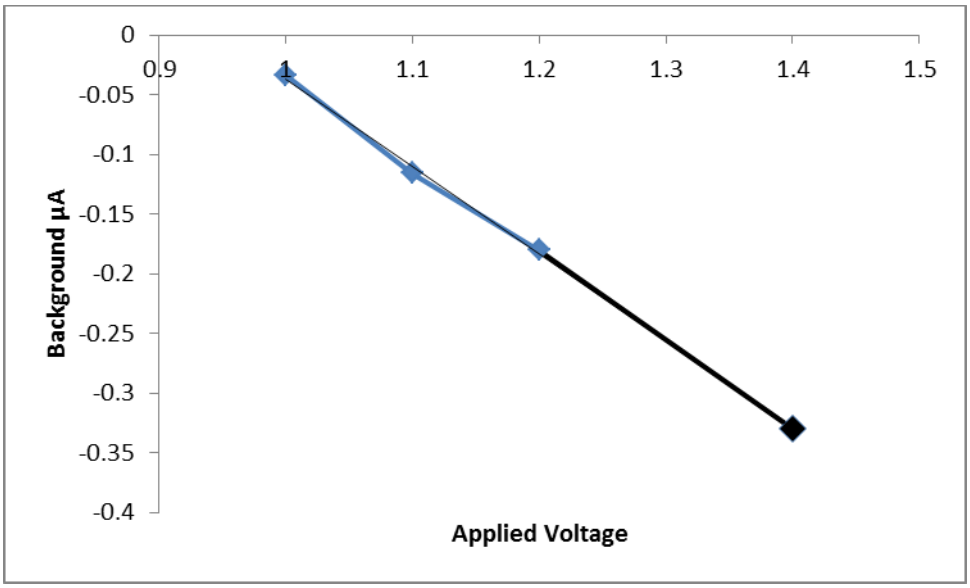

Figure 3.2.24. Background current of **AA-N-Ts** (0.00728 M) PECD at 1.4 V.

The values used to calculate %$N^{\cdot+}$ are listed in figure 3.2.25. At an applied voltage of 1.4 V for 30 s, only 1% of AA-N-Ts is electrochemically oxidized leading to complete conversion of **AA-Q-Ts** to **AA-N-Ts** with a catalytic turnover number of 100.

Background current (I_B) for 1.4 V at 30 s : -0.3295 µA
Measured current ($I-I_B$) : -1.40 µA (Q=-42.0 µC)
M: .00728 M **AA-N-Ts**
Area: 0.9 cm^2
h: 88.9 µm
n : $4x10^{-10}$ mol
n_0 : $4x10^{-8}$ mol
% of $N^{+\cdot}$: 1%
Turnover # : 100

Figure 3.2.25. Actual values used to calculate %$N^{\cdot+}$.

3.2.7. Expanding the Scope: Photoelectrochromic Cycling of RA-Appended Azobenzene Derivatives

To demonstrate the general utility of $(tol)_3TBABF_4$ as an electrolytic medium for photoelectrochromic systems, the photoelectrochromic switching of an RA-appended azobenzene mechanical switch is presented (Scheme 3.2.3). Like **AA-N-Ts**, **AA-NN-Ph** has been synthesized and characterized as a photoelectrochemical switch that catalytically converts from *cis* to *trans* via the redox auxiliary catalysis mechanism.[107]

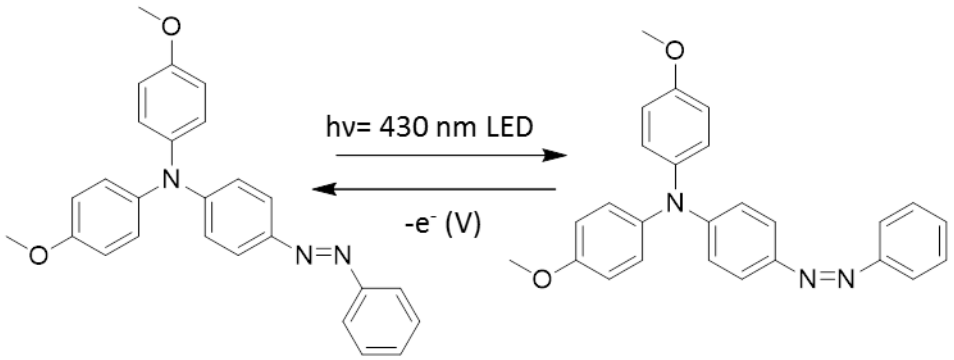

Scheme 3.2.4. Photoelectrochemical cis/trans isomerism of **AA-NN-Ph**.

When the ***trans*-AA-NN-Ph** PECD (figure 3.2.26) is irradiated with 430 nm LED light, it converts to a *cis*:*trans* photostationary state (~80:20 as determined by NMR) composed of mostly ***cis*-AA-NN-Ph**. At a concentration of .00733 M, the process occurs within 30 s (figure 3.2.27). The *cis* form has a half-life ($t_{½}$) of 3 hrs in benzene and exhibits thermal stability in the device state (figure 3.2.27).

[107] **AA-NN-Ph** synthesized by Carl St. Louis

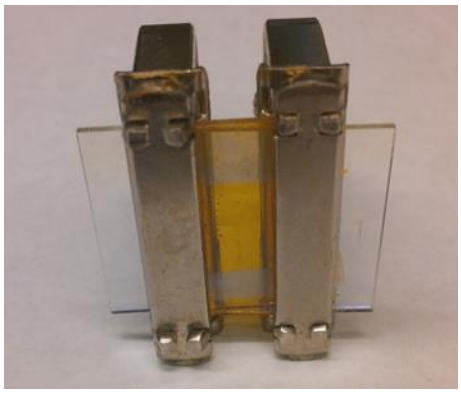

Figure 3.2.26. Photograph of ***trans*** **AA-NN-Ph** PECD.

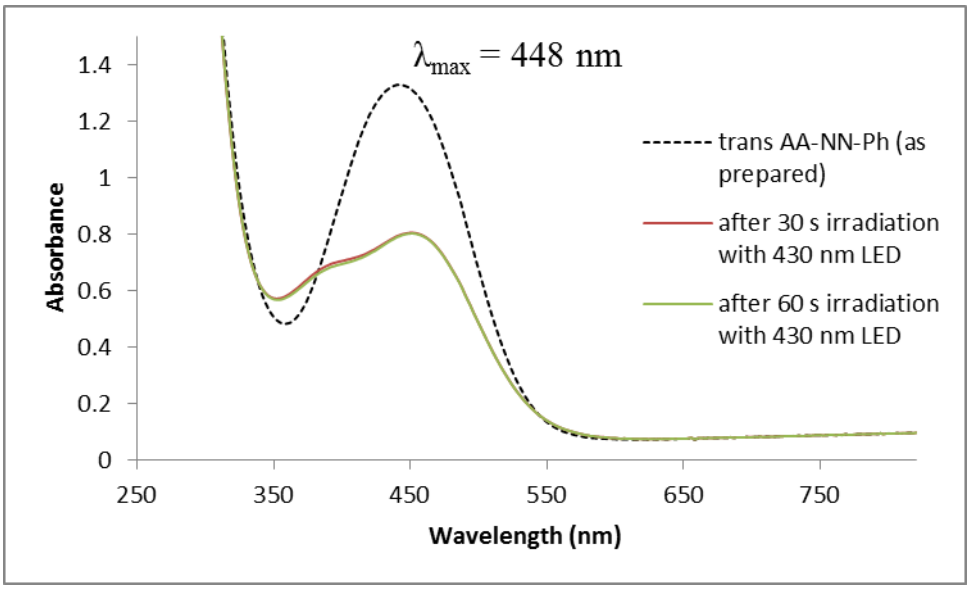

Figure 3.2.27. Irradiation of 0.00733 M ***trans*** **AA-NN-Ph** PECD to yield ***cis*** **AA-NN-Ph** in photostationary state (PSS).

The application of 1.5 V results in the back conversion from ***cis*** **AA-NN-Ph** to ***trans*** **AA-NN-Ph** with an isosbestic point 380 nm (figure 3.2.28).

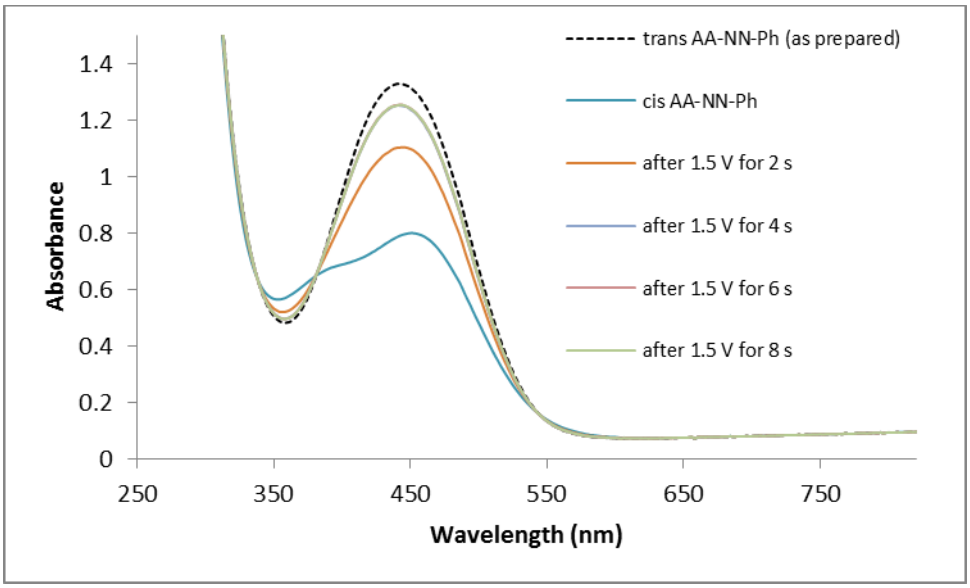

Figure 3.2.28. Electrochemical back conversion of ***cis* - AA-NN-Ph** to ***trans* - AA-NN-Ph**.

In figure 3.2.29, 100-2 s manual photoelectrochromic cycles are shown in the **AA-NN-Ph** PECD. The cycling conditions are 1 s irradiation with 430 nm LED flashlight followed by 1.5 V applied for 1 s. An overlay of optical spectra shows the retention of two isosbestic points (380 nm and 340 nm) throughout the 100 switches (figure 3.2.30).

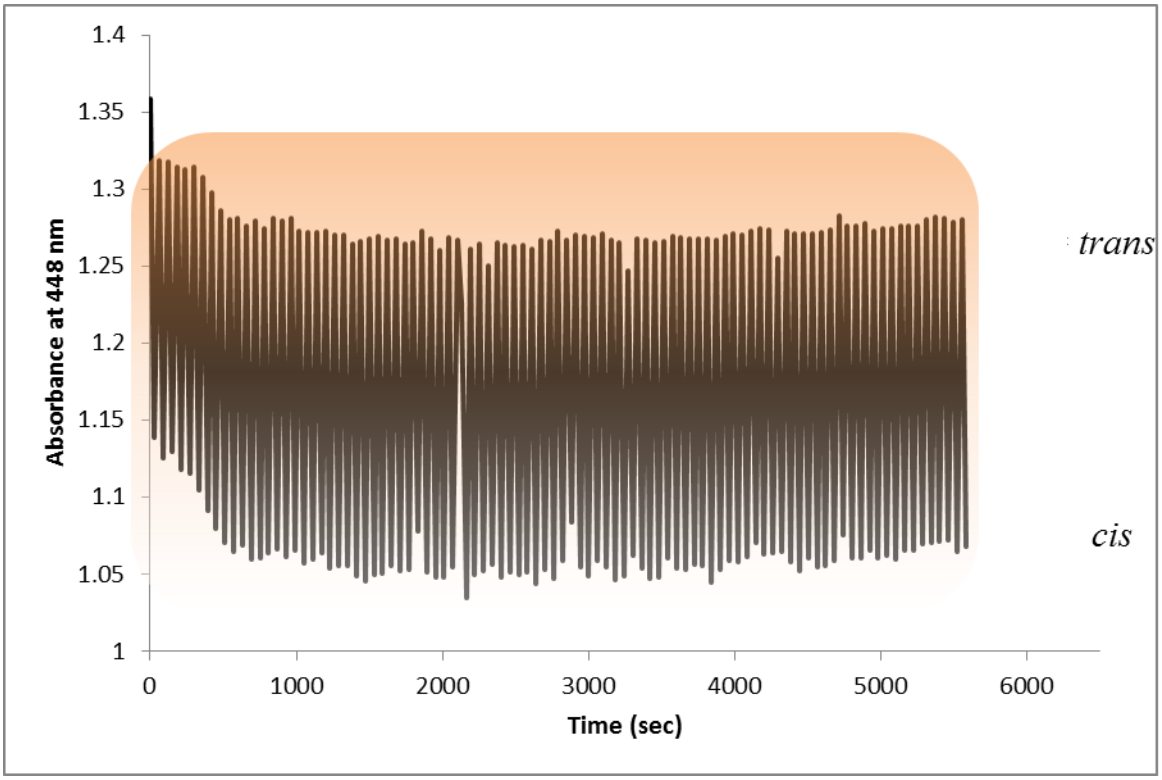

Figure 3.2.29. 100 photoelectrochromic switching cycles in .00830 M **AA-NN-Ph** in PECD.

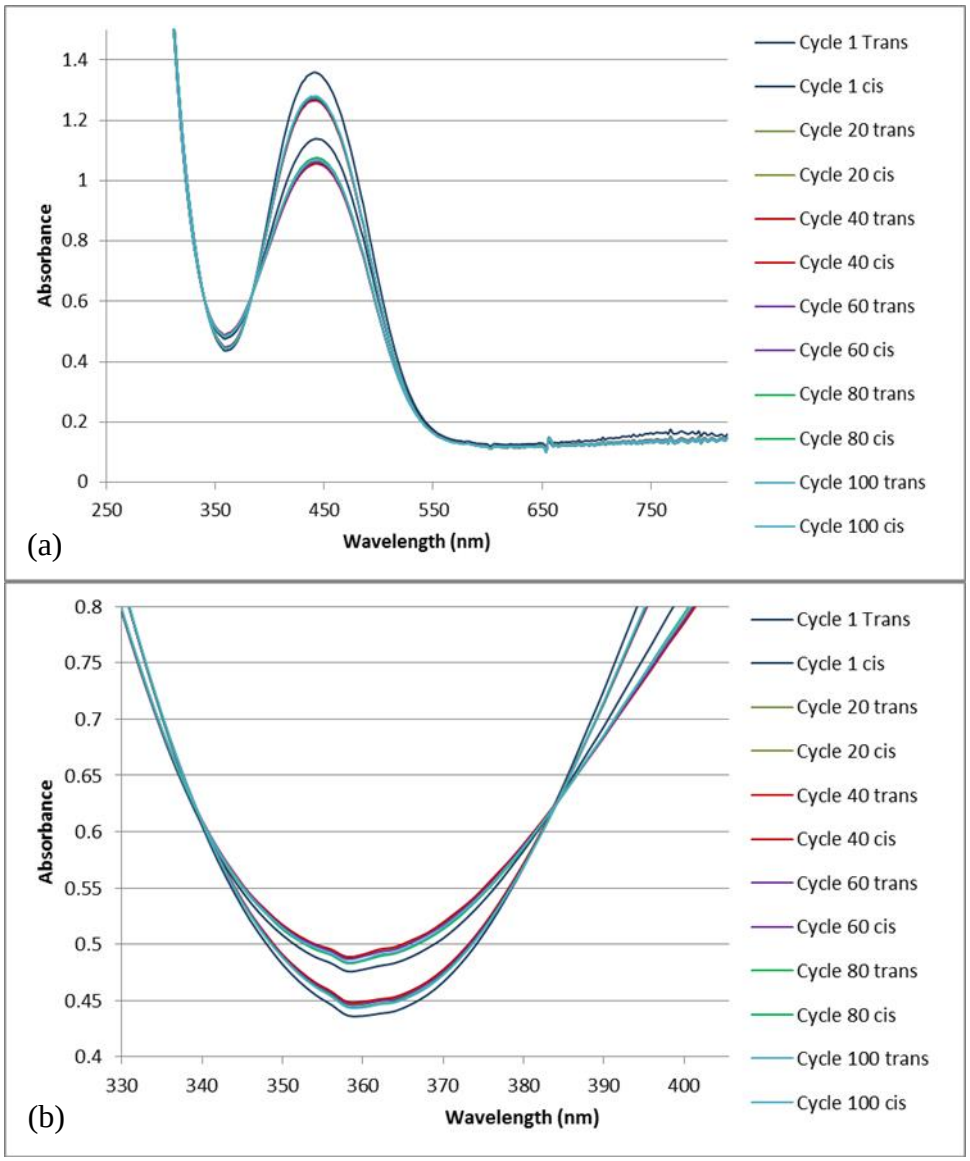

Figure 3.2.30. (a) Optical absorbance spectra of ***cis*** and ***trans*** - **AA-NN-Ph** every 20 cycles during the 100 cycles shown in figure 3.2.29. (b) Close-up of isobestic points.

3.2.8. Towards Totally Automated Photoelectrochemical Switching : 1000 Cycles and Counting

Using an electrical power supply with a timer, it is possible to fully automate photoelectrochromic switching. The automated switching apparatus is pictured in figure 3.2.31. Using this set-up we were able to obtain over 1300 cycles in an **AA-NN-An** based PECD (figure 3.2.32 and figure 3.2.33). As the instruments move in and out of phase with one another, the cycles exhibit unusual shapes that regularly repeat themselves. The pattern that a set of switches

take depends on the cycle details and is a result of the four pieces of equipment (spectrophotometer, potentiostat, timer, lamp) moving in and out of sync.

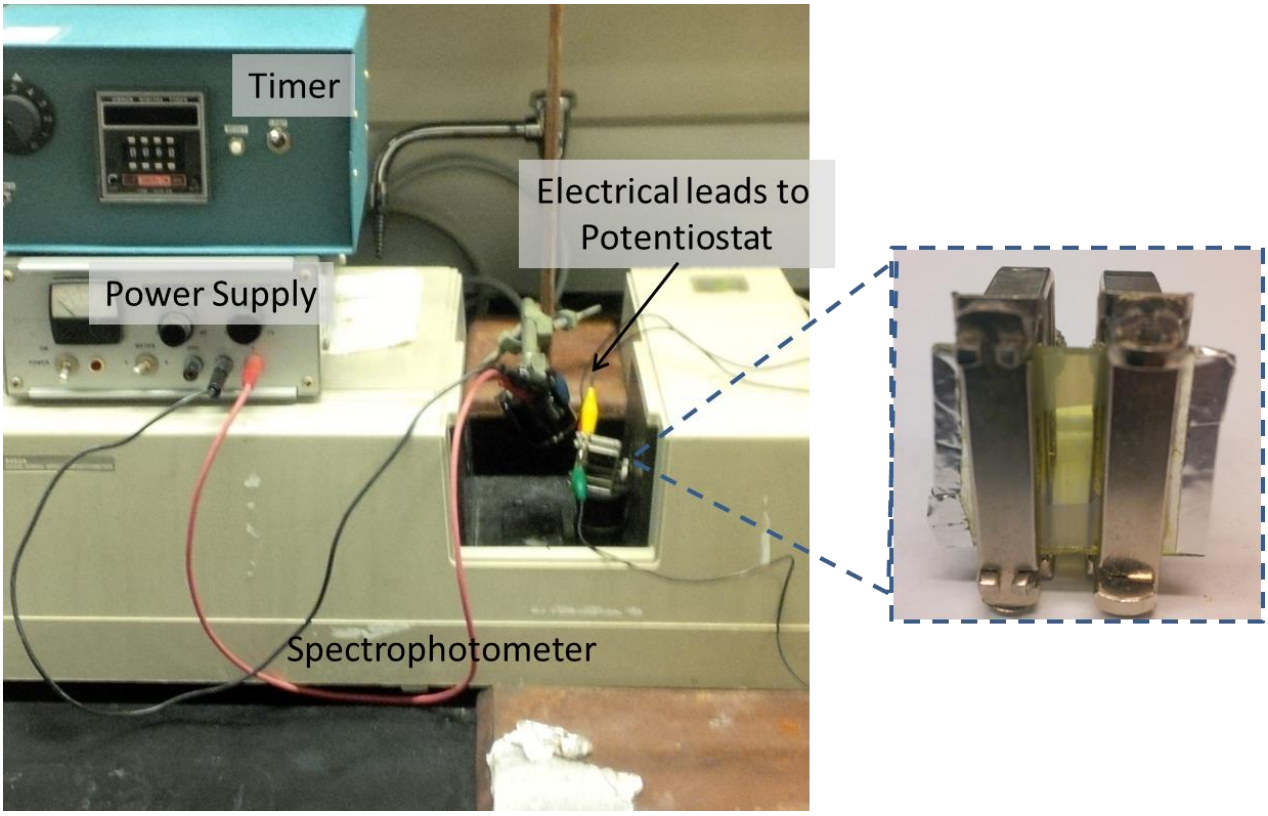

Figure 3.2.31. Photograph of automated photoelectrochromic cycling set-up.

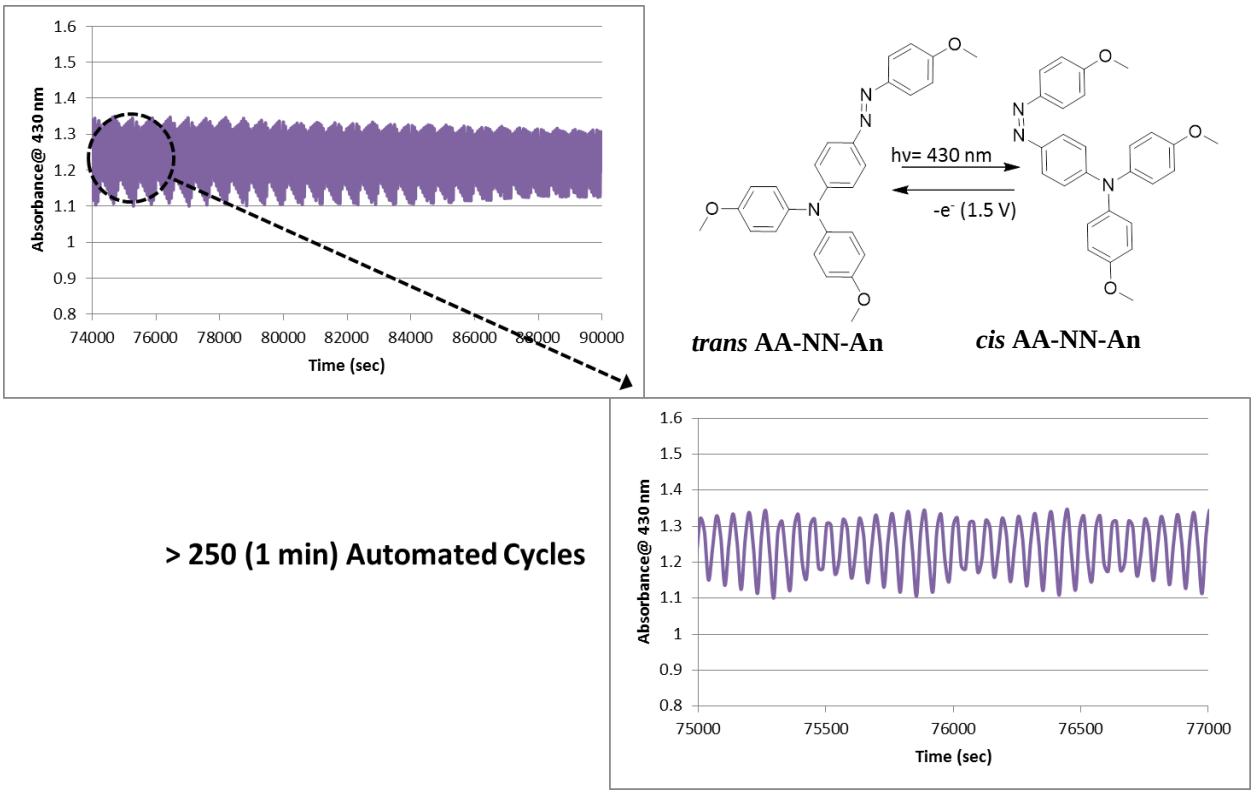

Figure 3.2.32. Automated photoelectrochromic cycling (> 250) of **AA-NN-An**.

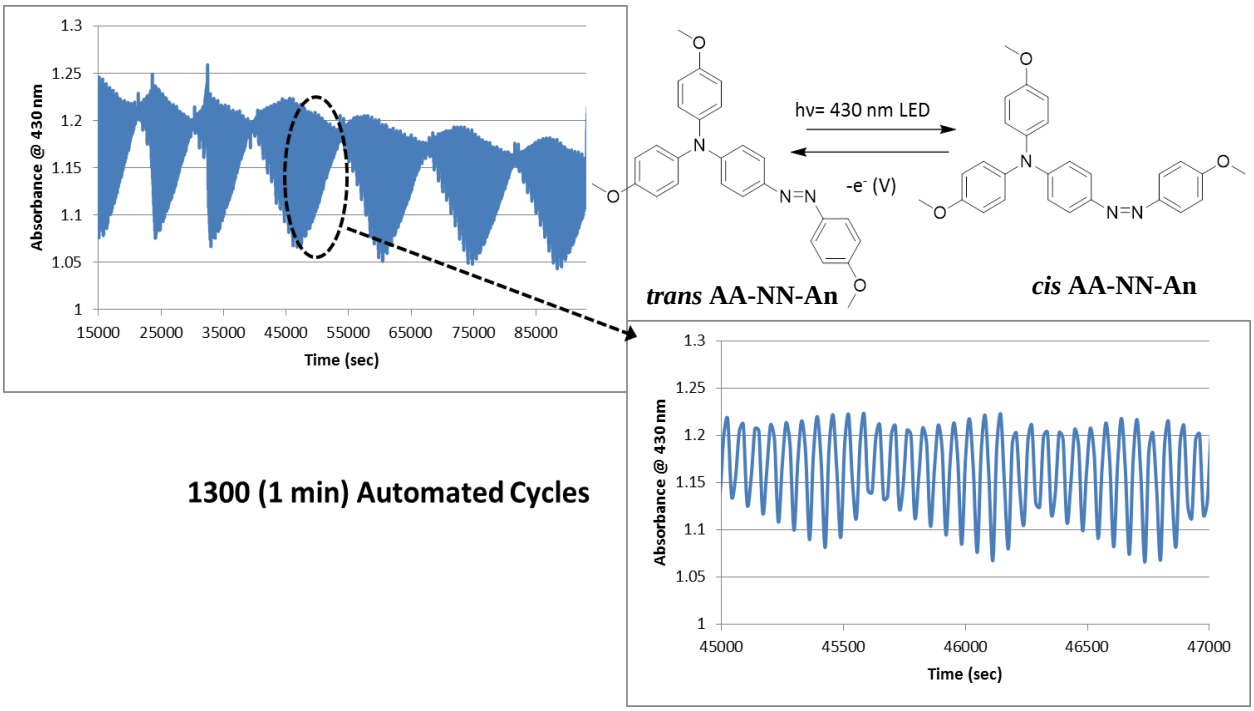

Figure 3.2.33. Automated photoelectrochromic cycling (> 1300) of **AA-NN-An**.

3.2.9 Shelf-Life of $(Tol)_3TBABF_4$ – based PECD

The stability of the AA-N-Ts PECD with respect to time was investigated over 3 months. The device was subjected to five cycles each month. The switches at 388 nm are shown in figure 3.2.34. An overlay of optical spectra from each set of switches show an isosbestic point at 345 nm indicating conservation of sample integrity. Details of the cycling are:

ON (conversion of **AA-Q-Ts** to **AA-N-Ts**): Electrochemical stimulus in the form of 1.5 V for 2 minutes resulting in an increase in absorbance at 388 nm.

OFF (conversion of **AA-N-Ts** to **AA-Q-Ts**): Photochemical stimulus in the form of irradiation with an 380 nm LED light source for 2 minutes resulting in a decrease in absorbance at 388 nm.

By the 4th month, leakage of the electrolytic media rendered the device no longer switchable. The shelf-life of the PECD is limited not by the chemical stability of the photoelectrochrome in the $(Tol)_3$ ($(Bu_4N)BF_4$) but by the device configuration. Incorporation of a chemical sealant like epoxy resin is expected to increase shelf-life so that the limiting factor is the chemical stability of the photoelectrochrome.

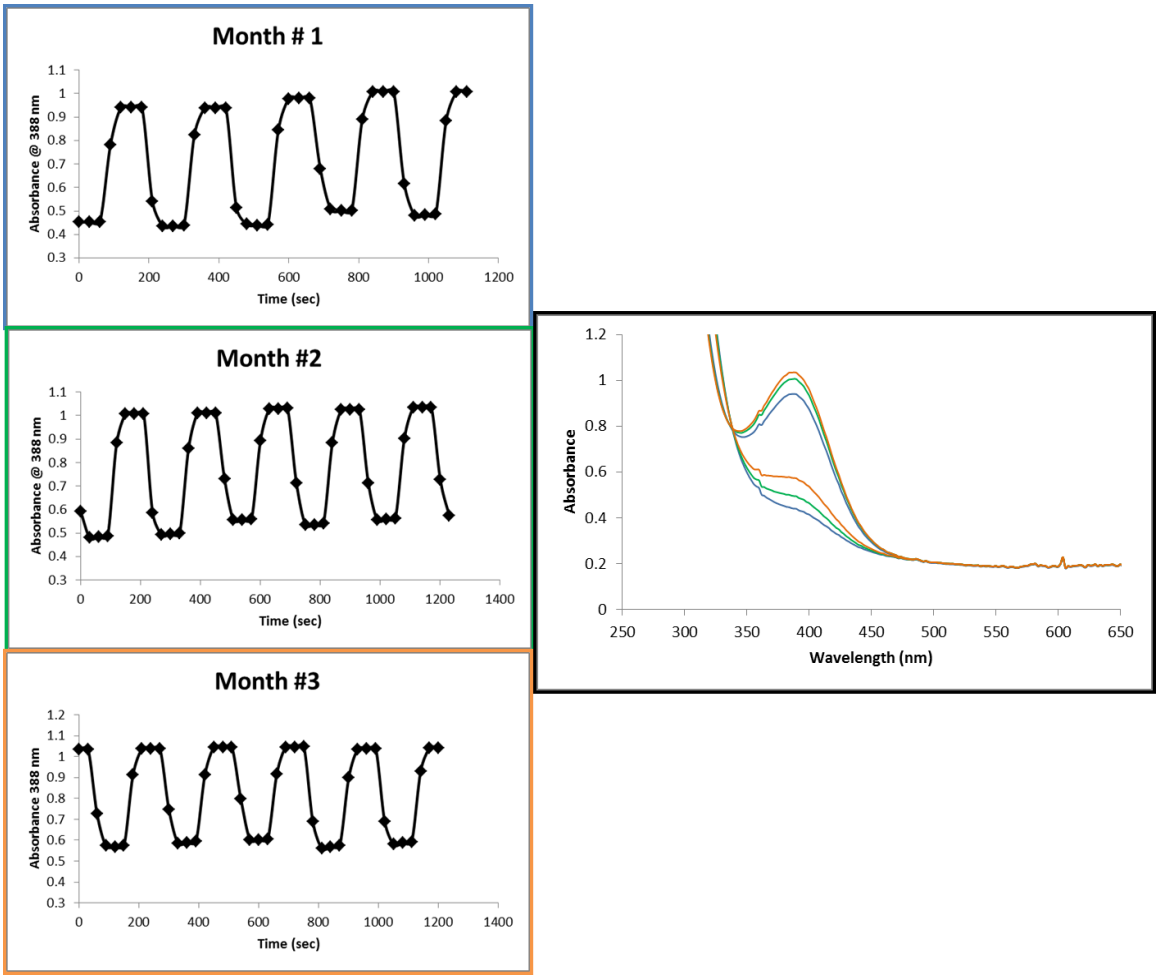

Figure 3.2.34 Shelf life study of 0.00728 M **AA-N-Ts** PECD.

3.3 Experimental

Experimental

General Methods and Materials. ITO coated glass was purchased from Delta Technologies (part no. CB-50IN-1111) and cleaned according to procedure detailed in chapter 1. Tetrabutylammonium tetrafluoroborate ($TBABF_4$) was purchased from Oakwood Chemicals, recrystallized 3 times from 50% ethanol and dried in an evacuated oven (100 °C, 0.1 Torr) for 30 hours.[108] Anhydrous toluene was purchased from Aldrich and used without further purification. **AA-N-Ts**, **AA-NN-Ph**, and **AA-NN-An** was synthesized by colleagues using a published procedures. [109,110]

Electrochemistry. (Figures 3.2.5, 3.2.6) Cyclic voltammetry (CV) and chronoamperometry were performed on a PAR 273 electrochemical potentiotstat (EG&G Instruments) A four-necked CV cell (10 mL) equipped with a stir bar, Pt disc (1.6 mm diameter) working electrode, a Pt wire counter electrode, and a saturated calomel electrode (SCE) reference was used for routine (solution state) CV measurements. $TBABF_4$ (0.1 M) was used as supporting electrolyte for electrochemical experiments unless otherwise noted. A capacitor (0.1 µF), connected between the reference electrode and counter electrode, was used to reduce background noise.

To prepare cyclic voltammetry solutions of 1.0 mM, **AA-N-Ts** (4.32 mg, 0.008 mmol) was added to 8 mL of tol_3TBABF_4 gel (1.4 $TBABF_4$ in toluene). The potential was scanned from 0.0 to 1.1 V vs SCE at a rate of 50 mVs^{-1}. A blank CV scan (0.0 to 1.3 V vs SCE, 50 mV/s) was measured to ensure that no trace impurities existed in the solution as prepared.

---

[108] Perrin, D. D. and Armarego, W. L. F., Purification of Laboratory Chemicals, Pergamon Press: Oxford, 1988.
[109] Gray, L.T. The Application of Arylamines as Redox Auxiliaries, Polar Crystals and Organic Semiconductors. Ph.D, University of Alabama, Tuscaloosa, AL, August 2012.
[110] Carl St. Louis

For cyclic voltammetry of **AA-Q-Ts**, a 1.0 mM solution of **AA-N-Ts** in four-necked CV cell was irradiated with a 500 W Hg-Xe arc lamp behind an Oriel cut-off filter (380 nm) and a water-filled quartz cylinder (to absorb IR) until the yellow solution was completely bleached-indicating quantitative conversion of **AA-N-Ts** to **AA-Q-Ts**. The potential was scanned from 0.0 to 1.1 V vs SCE at a rate of 50 mVs^{-1}. A blank CV scan (0.0 to 1.3 V vs SCE, 50 mVs^{-1}) was measured to ensure that no trace impurities existed in the solution as prepared.

Preparation of $(tol)_3TBABF_4$ gel.[111] In a 50 mL oven dried glass jar equipped with stir bar, 5.33 g of $TBABF_4$ was dissolved in 15 mL of anhydrous toluene at room temperature. After 5 min or when $TBABF_4$ dissolved, stopped stirring the colorless solution to allow phases to settle. The bottom phase was Tol_3TBABF_4 gel (10 mL, 1.62 M) and the top phase was toluene (5 mL) as determined by ^1H NMR Spectroscopy. The jar was then capped and stored in cabinet under ambient conditions.

Arc lamp photoconversion of 0.97 mM AA-N-Ts with irradiation >380 nm in $(tol)_3TBABF_4$ gel. (Figure 3.2.3)

To prepare a 0.97 mM solution, **AA-N-Ts** (1.57 mg, 0.00291 mmol) was dissolved in 3.0 mL of $(tol)_3TBABF_4$. The sample was then irradiated with the 500 W Hg-Xe arc lamp behind an Oriel cut-off filter (380 nm) and a water-filled quartz cylinder (to absorb IR). An HP8452A Diode Array Spectrophotometer equipped with a 1 mm path length quartz cell (Starna) was used to record UV-vis spectra.

---

[111] Picket, C. J. "A simple Hydrocarbon Electrolyte: Completing the Electron-transfer Series $[Fe_4S_4(SPh)_4]^{1-/2-/3-/4-}$," *J. Chem. Soc.* **1985,** 323-326.

Electrochemical response of AA-Q-Ts at Pt disc electrode. (Figure 3.2.7)

A 0.97 mM solution of **AA-N-Ts** was prepared by dissolving **AA-N-Ts** (4.19 mg, 0.00776 mmol) in 8.0 mL of $(tol)_3TBABF_4$. The yellow sample was placed in a 4-necked CV cell then irradiated with the 500 W Hg-Xe arc lamp behind an Oriel cut-off filter (380 nm) and a water-filled quartz cylinder (to absorb IR) for 20 min while stirring to yield the colorless **AA-Q-Ts**. To record UV-vis spectra, a 400 μL aliquot of the solution was added to a 1 mm quartz cuvette (Starna 1-G-1) using a glass syringe. An HP8452A Diode Array Spectrophotometer was used to record UV-vis spectra. For cyclic voltammetry conditions, see previously outlined procedure.

Catalytic conversion of AA-Q-Ts (1.0 mM in tol_3TBABF_4) to AA-N-Ts after addition of 1 mol% CRET. (Figure 3.2.8)

To prepare a 1.0 mM solution, **AA-N-Ts** (1.62 mg, 0.00300 mmol) was dissolved in 3.0 mL of $(tol)_3TBABF_4$ and placed in a 1 cm quartz cuvette equipped with stirbar. The yellow solution was then irradiated with a 500 W Hg-Xe arc lamp behind an Oriel cut-off filter (380 nm) and a water-filled quartz cylinder (to absorb IR) until bleached to generate **AA-Q-Ts**. A 0.3 mM stock solution of CRET was made by dissolving CRET (1.80 mg, 0.00300 mmol) in 10 mL of dry CH_2Cl_2 in a 10 mL volumetric flask. Using a 500 μL glass syringe, 100 μL of the CRET solution was added to the quartz cuvette containing **AA-Q-Ts**. An HP8452A Diode Array Spectrophotometer equipped was used to record UV-vis spectra.

Irradiation of 0.00765 M AA-N-Ts to AA-Q-Ts with arc lamp in PECD state. (Figure 3.2.12)

A 0.00765 M solution of **AA-N-Ts** was prepared by dissolving **AA-N-Ts** (4.13 mg, 0.00765 mmol) in 1 mL of tol_3TBABF_4. The solution was applied to the PECD using the procedure outlined above. The PECD was then irradiated with a 500 W Hg-Xe arc lamp behind an Oriel cut-off filter (380 nm) and a water-filled quartz cylinder (to absorb IR) for 90 s. UV-Vis spectra were recorded on an HP8452A Diode Array Spectrophotometer.

Spectroelectrochemistry. UV-Vis spectra were recorded on an HP8452A Diode Array Spectrophotometer. Electrochemistry was performed on a PAR 273 electrochemical potentiotstat (EG&G Instruments). For irradiation, LED flashlights were used with appropriate eyewear (HQRP-US) unless otherwise noted. For irradiation of **AA-N-Ts**, a 380 nm LED flashlight was used. For both **AA-NN-Ph** and **AA-NN-An** studies, a 430 nm LED flashlight was used. Spectroelectrochemistry data were recorded using both the spectrophotometer and potentiostat in tandem. The working electrode and counter electrode was ITO. The system was referenced to the counter electrode.

Preparation of AA-N-Ts photoelectrochromic device. (Figures 3.2.13, 3.2.14)

AA-N-Ts solutions (0.0100 M) were prepared by dissolving **AA-N-Ts** (2.70 mg, 0.00500 mmol) in 0.5 mL of the tol_3TBABF_4 gel. The gel solution was applied to a ITO glass anode (equipped with spacer), the ITO glass cathode was then added to complete yellow sandwich-type device. Polyethylene Plastic Sheeting (Husky Brand) was used as spacer in the PECD. The thickness of the spacer was 88.9 µm unless otherwise noted. Before applying spacer to clean ITO glass substrate, a square (area: 0.9 cm^2) was cut out of the plastic sheet. The ITO sandwich was

held together with two closed jaw compressor clamps for the duration of the experiments. The spectroelectrochemistry data was recorded using both the spectrophotometer and potentiostat in tandem. The working electrode and counter electrode was ITO. The system was referenced to the counter electrode. For a photograph of PECD, see figure 3.2.10. For a photograph of apparatus, see figure 3.2.11. The PECD was irradiated using an LED flashlight (380 nm).

Preparation of AA-N-Ts photoelectrochromic device. (Figure 3.2.15)

An **AA-N-Ts** solution (0.00934 M) was prepared by dissolving **AA-N-Ts** (2.52 mg, 0.00467 mmol) in 0.5 mL of the tol_3TBABF_4 gel. The gel solution was applied to a ITO glass anode (equipped with spacer), the ITO glass cathode was then added to complete yellow sandwich-type device. Polyethylene Plastic Sheeting (Husky Brand) was used as spacer in the PECD. The thickness of the spacer was 88.9 µm unless otherwise noted. Before applying spacer to clean ITO glass substrate, a square (area: 0.9 cm^2) was cut out of the plastic sheet. The ITO sandwich was held together with two closed jaw compressor clamps for the duration of the experiments. The spectroelectrochemistry data was recorded using both the spectrophotometer and potentiostat in tandem. The working electrode and counter electrode was ITO. The system was referenced to the counter electrode. For a photograph of PECD, see figure 3.2.10. For a photograph of apparatus, see figure 3.2.11. A range anodic potentials (0.0 V to 2.0 V) were applied in 0.1 V increments for 30 s. After each voltage application, the system is allowed to come to equillibrium under open circuit conditions for 30 s.

Preparation of AA-N-Ts photoelectrochromic device. (Figure 3.2.16, 3.2.17, 3.2.19, 3.2.20, 3.2.21, 3.2.22)

An **AA-N-Ts** solution (0.00798 M) was prepared by dissolving **AA-N-Ts** (2.15 mg, 0.00399 mmol) in 0.5 mL of the tol_3TBABF_4 gel. The gel solution was applied to an ITO glass anode (equipped with spacer), the ITO glass cathode was then added to complete yellow sandwich-type device. Polyethylene Plastic Sheeting (Husky Brand) was used as spacer in the PECD. The thickness of the spacer was 88.9 µm unless otherwise noted. Before applying spacer to clean ITO glass substrate, a square (area: 0.9 cm^2) was cut out of the plastic sheet. The ITO sandwich was held together with two closed jaw compressor clamps for the duration of the experiments. The spectroelectrochemistry data was recorded using both the spectrophotometer and potentiostat in tandem. The working electrode and counter electrode was ITO. The system was referenced to the counter electrode. For a photograph of PECD, see figure 3.2.10. For a photograph of apparatus, see figure 3.2.11.The photoelectrochromic cycling conditions were:

OFF: 2 min irradiation with 380 nm LED

Q Hold: 1 min no irradiation, no applied voltage

ON: 1.5 V for 20 s

N Hold: 1 min no irradiation, no applied voltage

Photoelectrochromic cycling of AA-N-Ts PECD's with various cell gaps. (Figure 3.2.18)

For 88.9 µm cell gap, an **AA-N-Ts** solution (0.00728 M) was prepared by dissolving **AA-N-Ts** (1.96 mg, 0.00364 mmol) in 0.5 mL of the tol_3TBABF_4 gel. For 50.4 µm cell gap, an **AA-N-Ts** solution (0.0178 M) was prepared by dissolving **AA-N-Ts** (4.79 g, 0.00890 mmol) in 0.5 mL of the tol_3TBABF_4 gel. For 25.2 µm cell gap, an **AA-N-Ts** solution (0.0291 M) was prepared by

dissolving **AA-N-Ts** (7.83 mg, 0.00595 mmol) in 0.5 mL of the tol_3TBABF_4 gel. The gel solutions were applied to devices according to previously outlined procedures.

The systems were cycled as follows (spectra taken every 30 s):

OFF: 1 min irradiation with 380 nm LED flashlight

Q Hold: 1 min no irradiation, no applied voltage

ON: 1.6 V for 20 s

N Hold: 1 min no irradiation, no applied voltage

Preparation of *trans* - AA-NN-Ph photoelectrochromic device. (Figures 3.2.27, 3.2.28)

***trans* - AA-NN-Ph** solutions (0.00733 M) were prepared by dissolving ***trans* - AA-NN-Ph** (1.50 mg, 0.00367 mmol) in 0.5 mL of tol_3TBABF_4. The gel solution was applied to a ITO glass anode (equipped with spacer), the ITO glass cathode was then added to complete orange sandwich-type device. Polyethylene Plastic Sheeting (Husky Brand) was used as spacer in the PECD. The thickness of the spacer was 88.9 µm unless otherwise noted. Before applying spacer to clean ITO glass substrate, a square (area: 0.9 cm^2) was cut out of the plastic sheet. The ITO sandwich was held together with two closed jaw compressor clamps for the duration of the experiments. The spectroelectrochemistry data was recorded using both the spectrophotometer and potentiostat in tandem. The working electrode and counter electrode was ITO. The system was referenced to the counter electrode. For a photograph of PECD, see figure 3.2.26. For a photograph of apparatus, see 3.2.11. The PECD was irradiated using an LED flashlight (430 nm).

Preparation of *trans* - AA-NN-Ph photoelectrochromic device. (Figure 3.2.29, 3.3.30)

A ***trans* - AA-NN-Ph** solution (0.00830 M) was prepared by dissolving ***trans* - AA-NN-Ph** (1.70 mg, 0.00416 mmol) in 0.5 mL of tol_3TBABF_4. The gel solution was applied to a ITO glass anode (equipped with spacer), the ITO glass cathode was then added to complete orange sandwich-type device. Polyethylene Plastic Sheeting (Husky Brand) was used as spacer in the PECD. The thickness of the spacer was 88.9 µm unless otherwise noted. Before applying spacer to clean ITO glass substrate, a square (area: 0.9 cm^2) was cut out of the plastic sheet. The ITO sandwich was held together with two closed jaw compressor clamps for the duration of the experiments. The spectroelectrochemistry data was recorded using both the spectrophotometer and potentiostat in tandem. The working electrode and counter electrode was ITO. The system was referenced to the counter electrode. The PECD was subjected to 100 photoelectrochromic cycles (1 s - irradiation/ 1 s - 1.5 V applied).

Automated photoelectrochromic cycling of AA-NN-An PECD. (figure 3.2.33)

***trans* - AA-NN-An** solutions (0.00733 M) were prepared by dissolving ***trans* - AA-NN-Ph** (1.61 mg, 0.00367 mmol) in 0.5 mL of tol_3TBABF_4. The gel solution was applied to a ITO glass anode (equipped with spacer), the ITO glass cathode was then added to complete orange sandwich-type device. Polyethylene Plastic Sheeting (Husky Brand) was used as spacer in the PECD. The thickness of the spacer was 88.9 µm unless otherwise noted. Before applying spacer to clean ITO glass substrate, a square (area: 0.9 cm^2) was cut out of the plastic sheet. The ITO sandwich was held together with two closed jaw compressor clamps for the duration of the experiments. The spectroelectrochemistry data was measured using the spectrophotometer, potentiostat, and 430 nm LED light in tandem. The working electrode and counter electrode was

ITO. The system was referenced to the counter electrode. For a photograph of PECD, see figure 3.2.26. For a photograph of the automated photoelectrochromic cycling apparatus, see figure 3.2.31.

Shelf life study of AA-N-Ts PECD. (figure 3.2.34)

An **AA-N-Ts** solution (0.00728 M) was prepared by dissolving **AA-N-Ts** (1.96 mg, 0.00364 mmol) in 0.5 mL of the tol_3TBABF_4 gel. The solution was used to construct a PECD according to previously outline procedure. Every 30 days, the PECD was subjected the following cycling conditions (over a 3 month period):

OFF: 1 min irradiation with 380 nm LED flashlight

Q Hold: 1 min no irradiation, no applied voltage

ON: 1.6 V for 20 s

N Hold: 1 min no irradiation, no applied voltage

Appendix A

NMR spectra

LIST OF NMR SPECTRA FOR SELECTED COMPOUNDS

Figure A1. ^{1}H-NMR Spectrum (360 MHz) of **5** in $CDCl_3$ 141

Figure A2. ^{1}H-NMR Spectrum (360 MHz) of **4** in $CDCl_3$ 143

Figure A3. ^{1}H-NMR Spectrum (360 MHz) of **6** in $CDCl_3$ 143

Figure A4. ^{13}C-NMR Spectrum (125 MHz) of **4** in a$CDCl_3$..... 144

Figure A5. ^{1}H-NMR Spectrum (500 MHz) of **7** in DMSO-*d*6 145

Figure A6. ^{13}C-NMR Spectrum (125 MHz) of **7** in DMSO-*d*6 146

Figure A7. ^{1}H-NMR Spectrum (360 MHz) of **10** in $CDCl_3$ 147

Figure A8. ^{13}C-NMR Spectrum (125 MHz) of **10** in a$CDCl_3$ 148

Figure A9. ^{1}H-NMR Spectrum (500 MHz) of **7** in DMSO-*d*6..... 149

Figure A10. ^{13}C-NMR Spectrum (125 MHz) of **7** in DMSO-*d*6 150

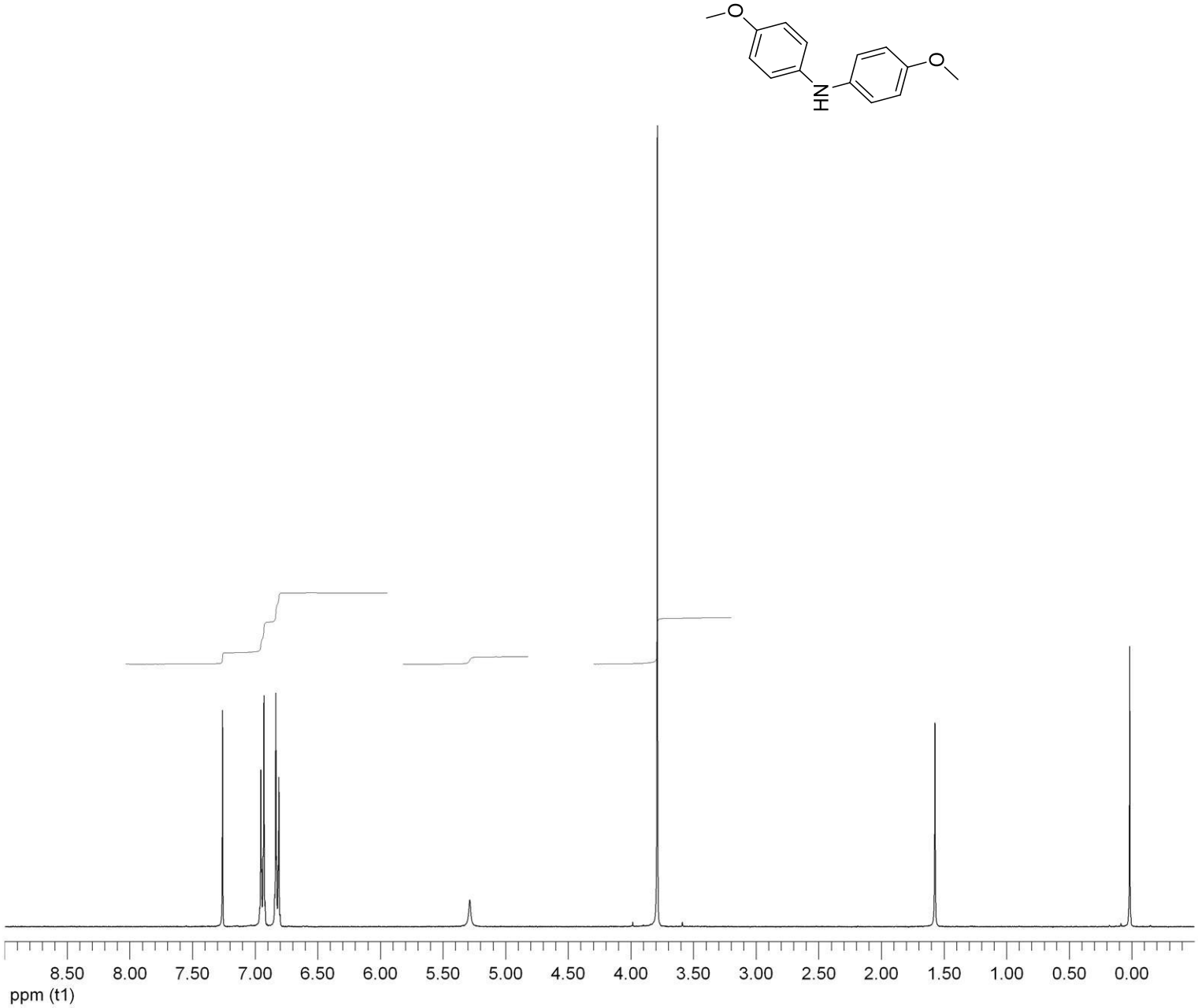

Figure A1. ^{1}H-NMR Spectrum (360 MHz) of **5**.

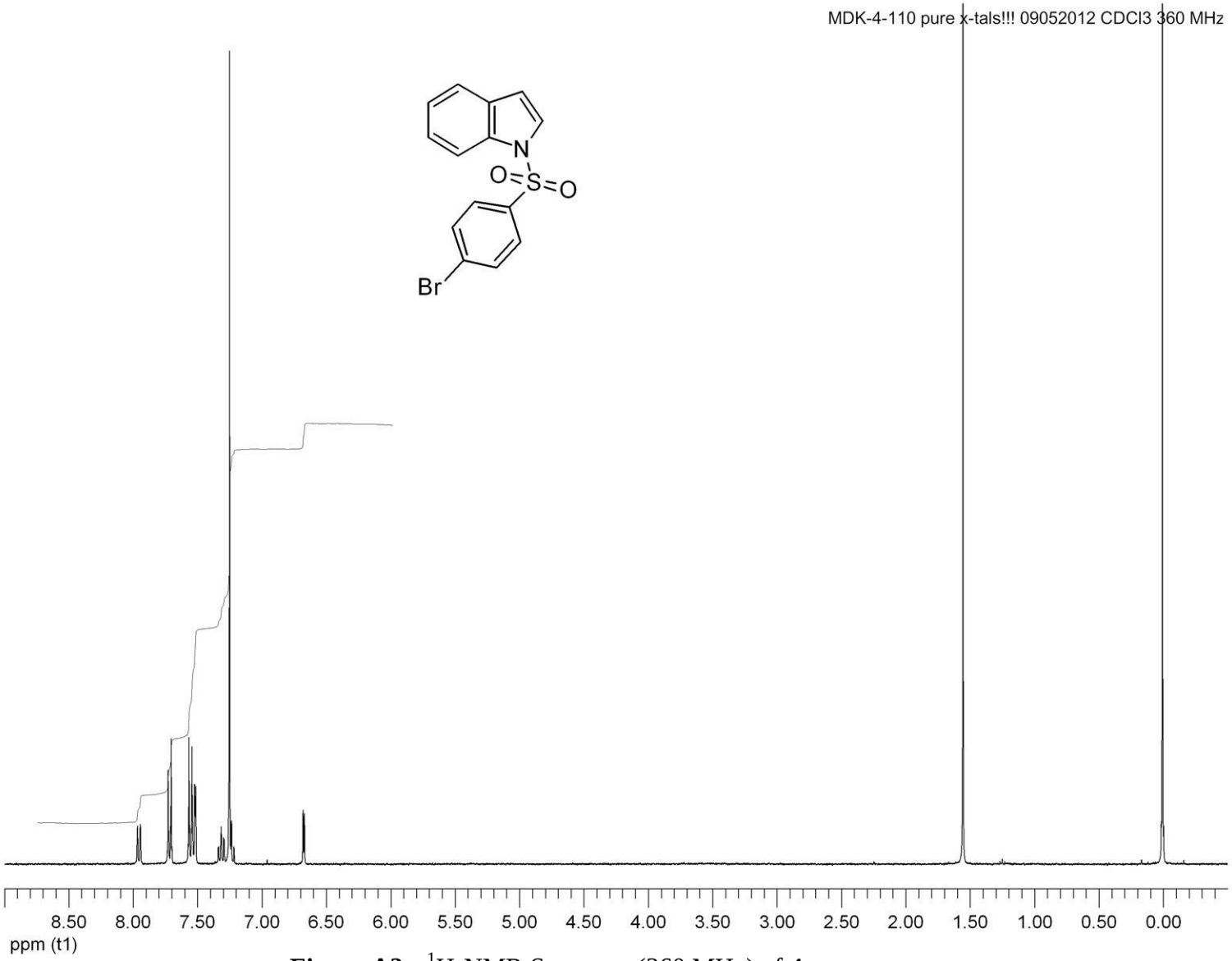

Figure A2. . ^{1}H-NMR Spectrum (360 MHz) of **4**

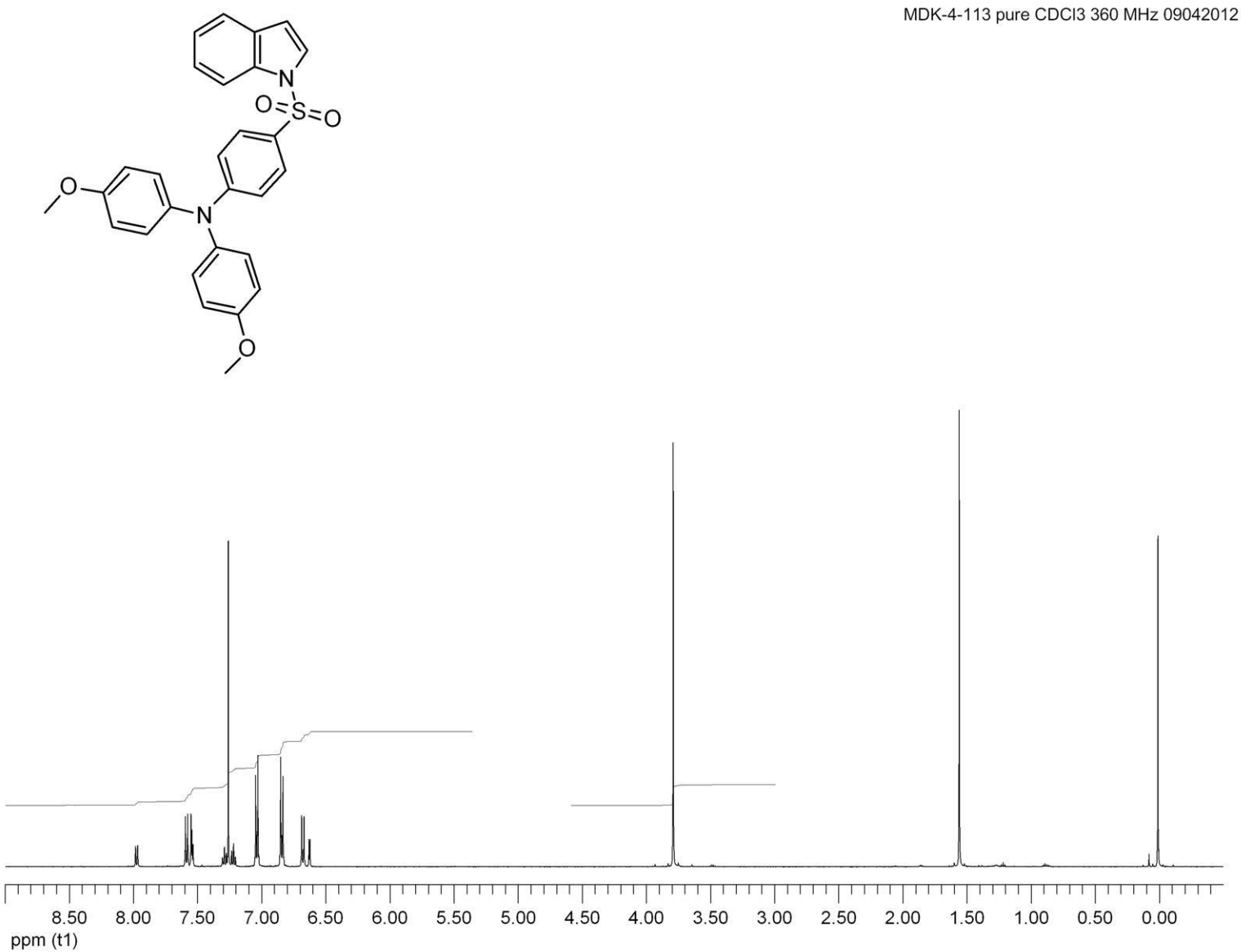

Figure A3. . ^{1}H-NMR Spectrum (360 MHz) of **6**.

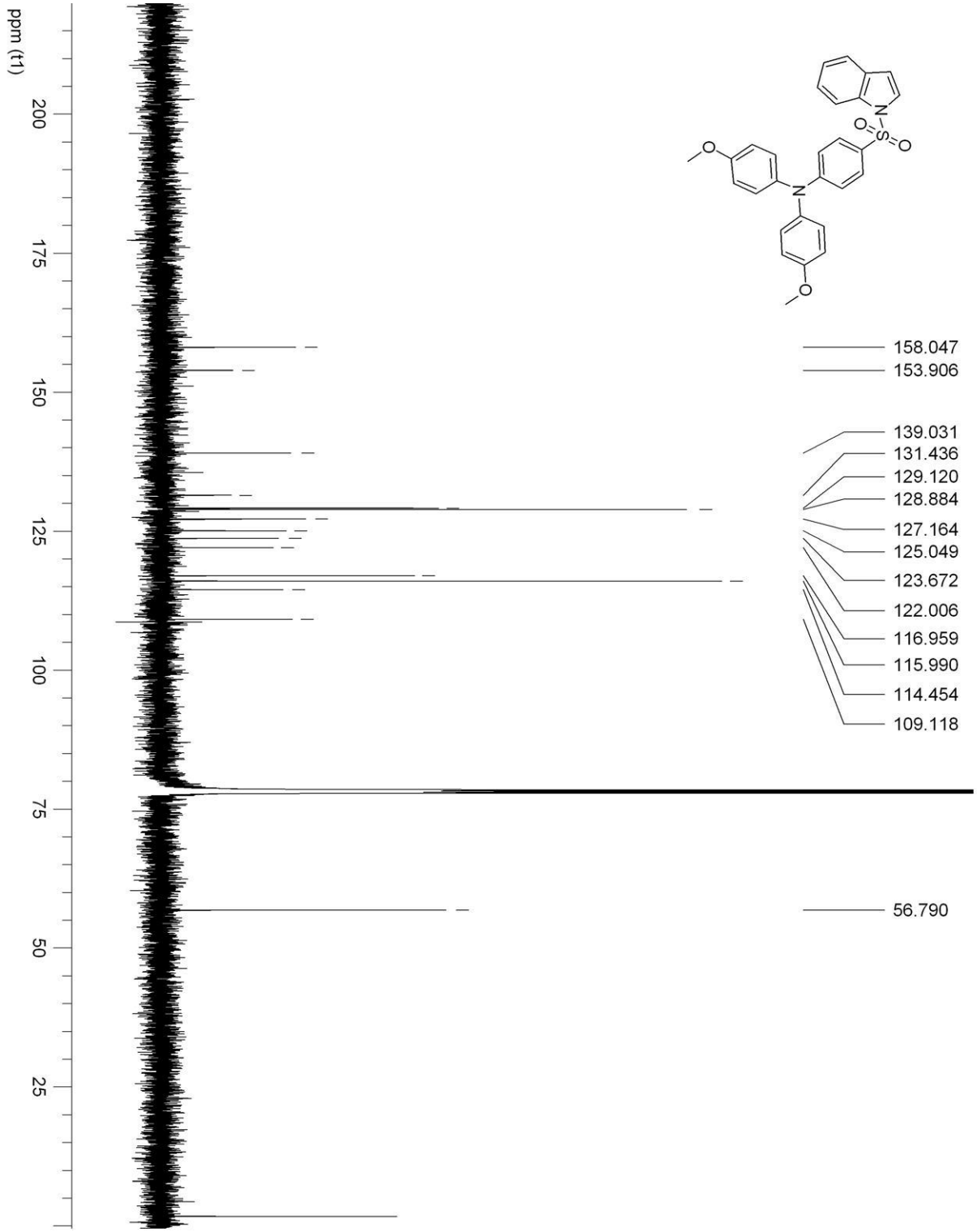

Figure A4. ^{13}C-NMR Spectrum (125 MHz) of **6**.

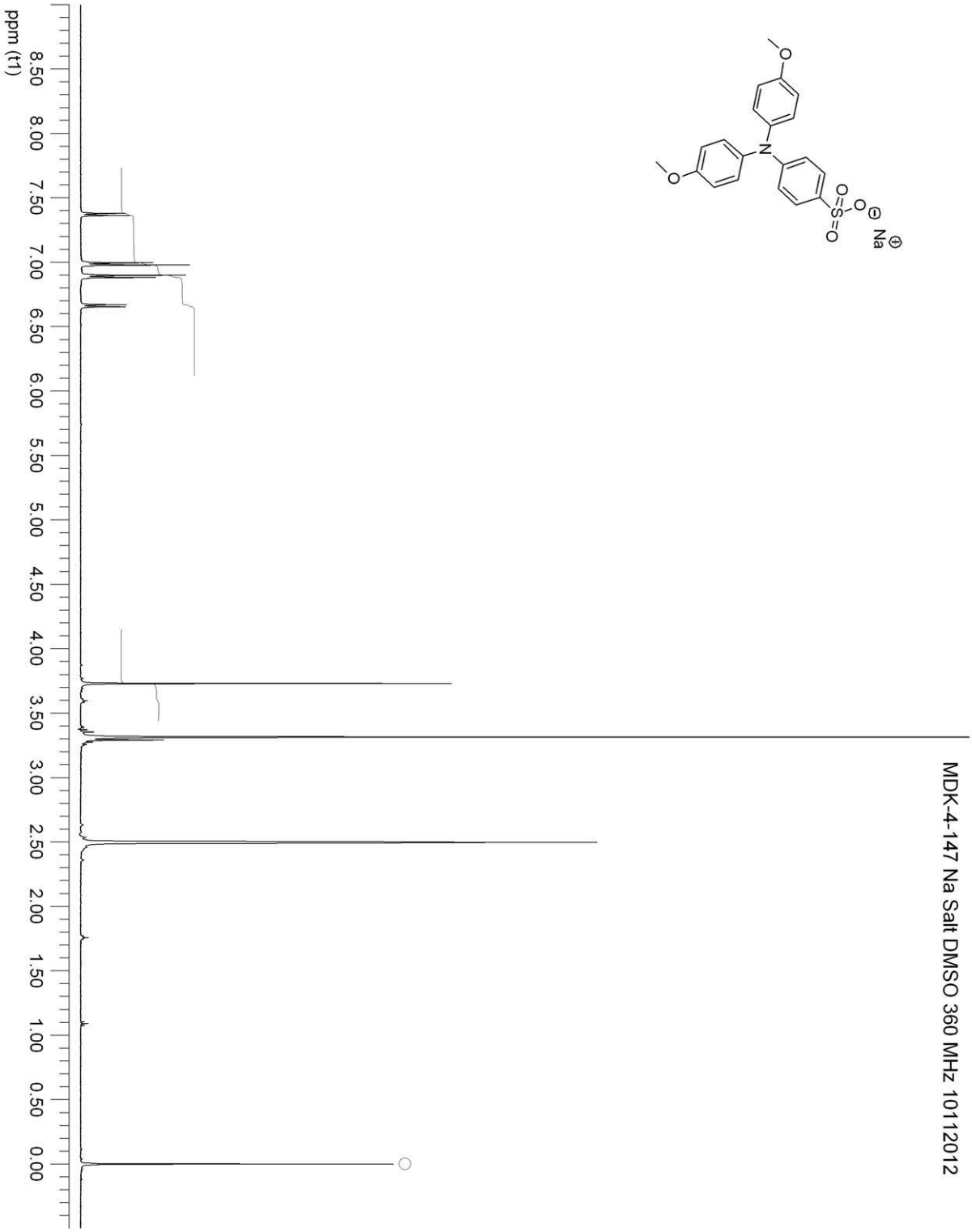

Figure A5. . ^{1}H-NMR Spectrum (360 MHz) of **7**.

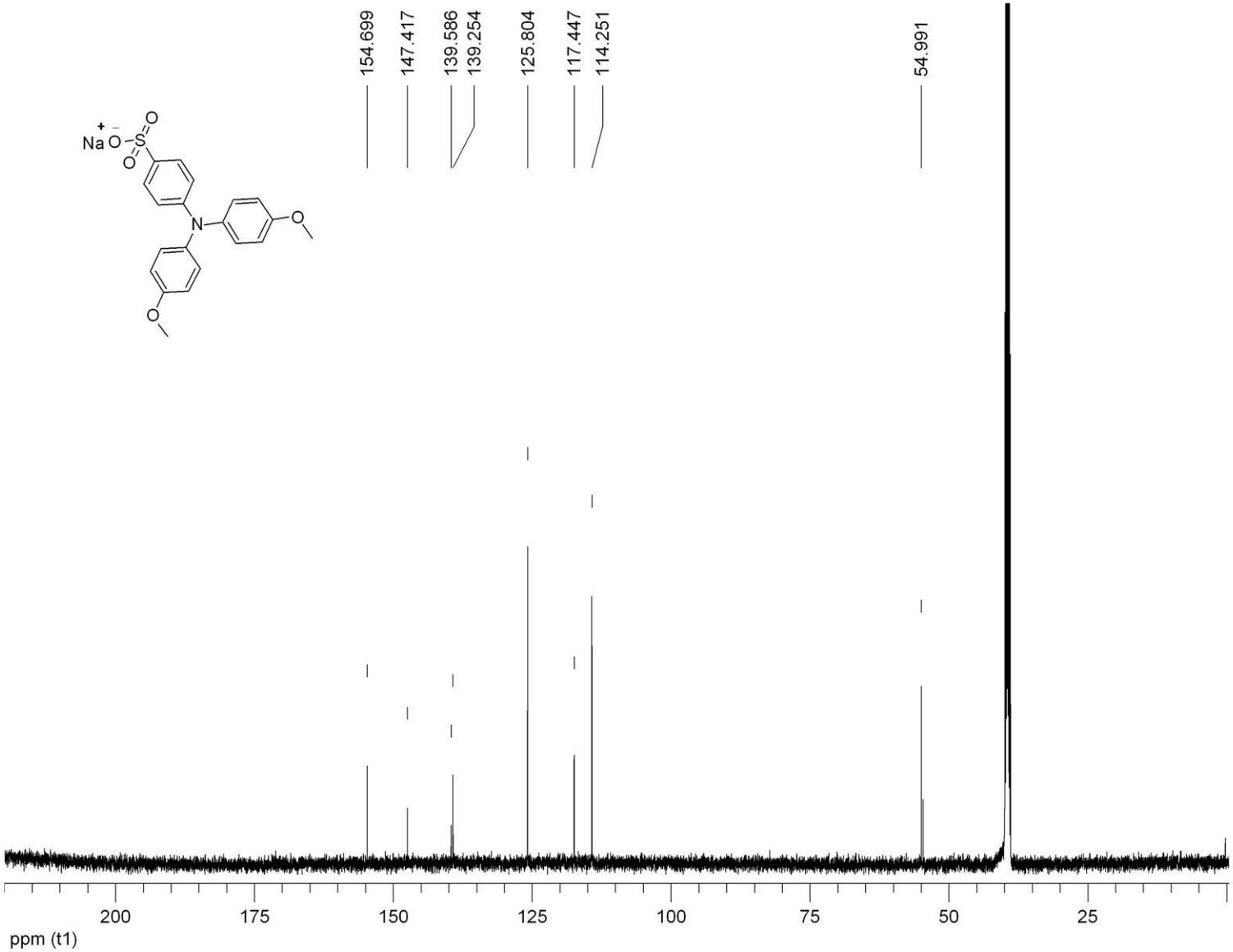

Figure A6. . ^{13}C-NMR Spectrum (125 MHz) of **7**.

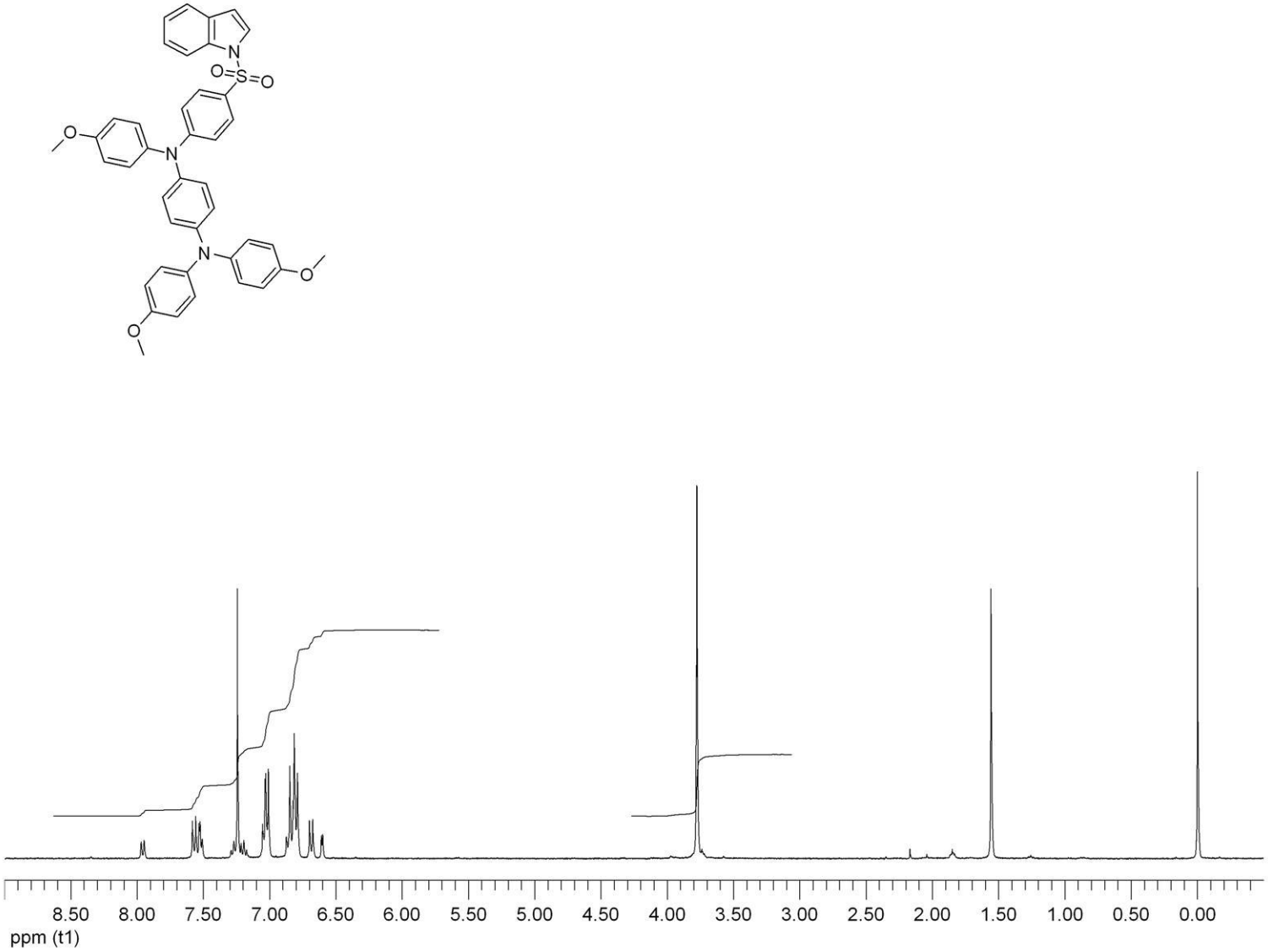

Figure A7. . ^{1}H-NMR Spectrum (360 MHz) of **10**

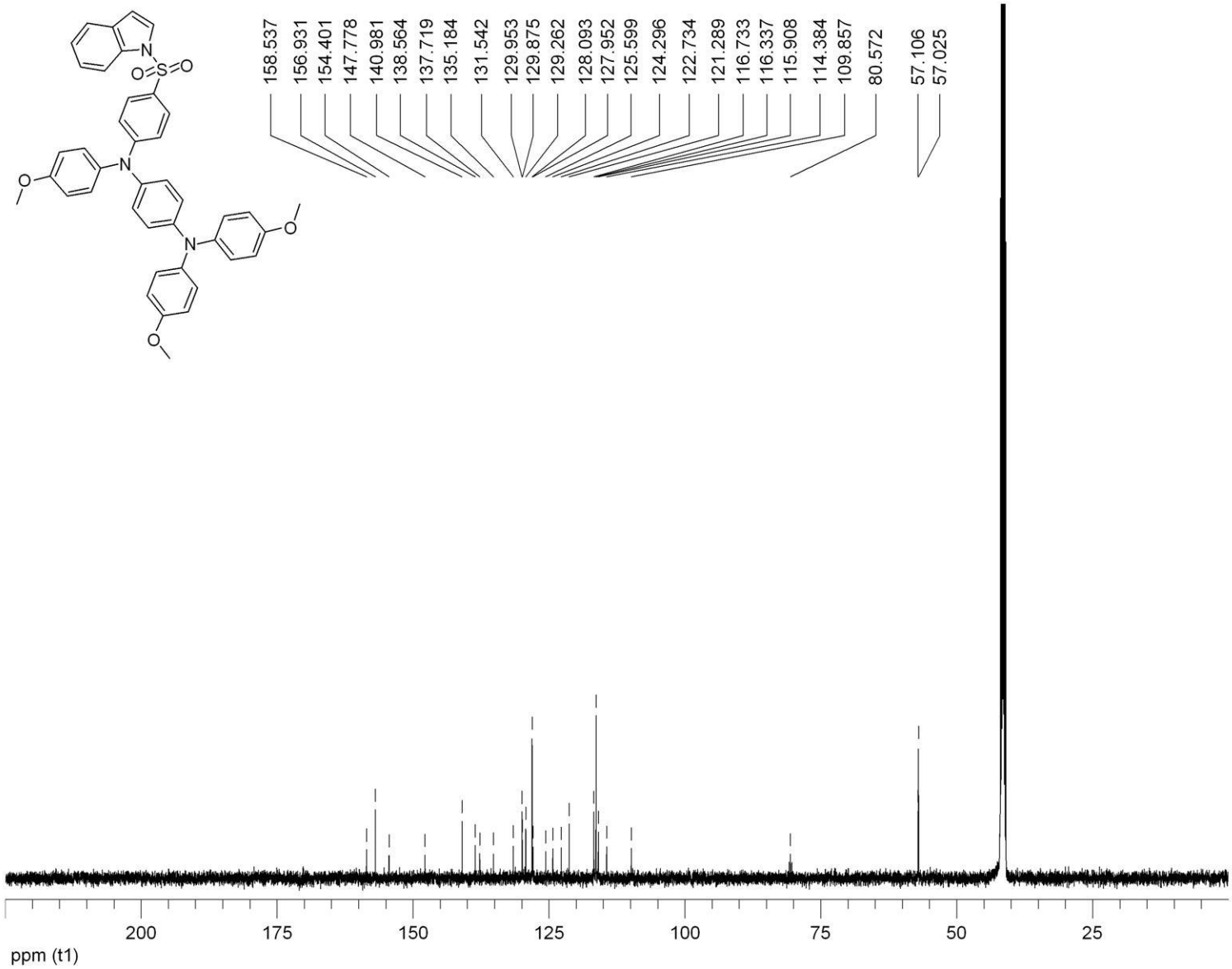

Figure A8. . ^{13}C-NMR Spectrum (125 MHz) of **10**.

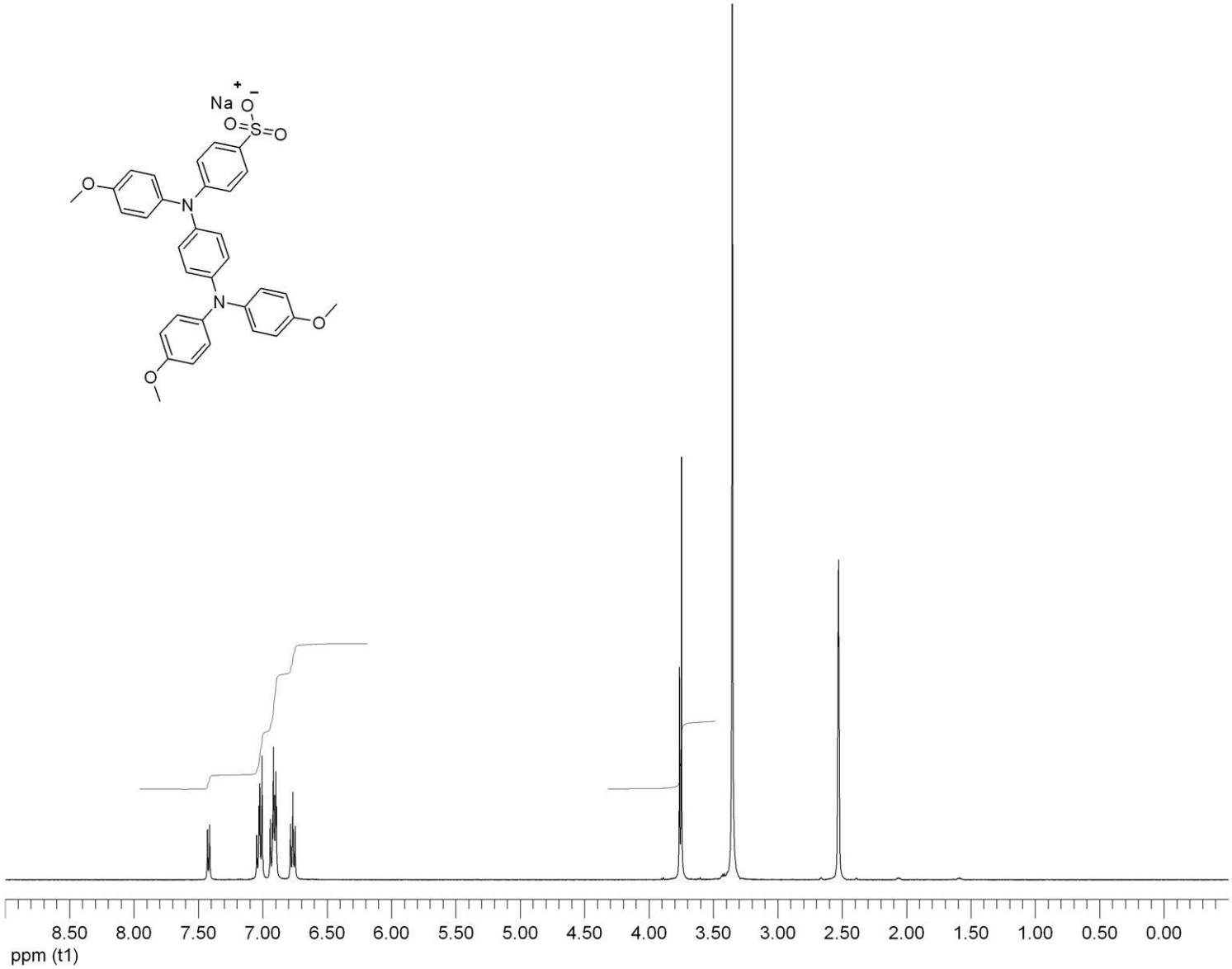

Figure A9. . ^{1}H-NMR Spectrum (360 MHz) of **11**.

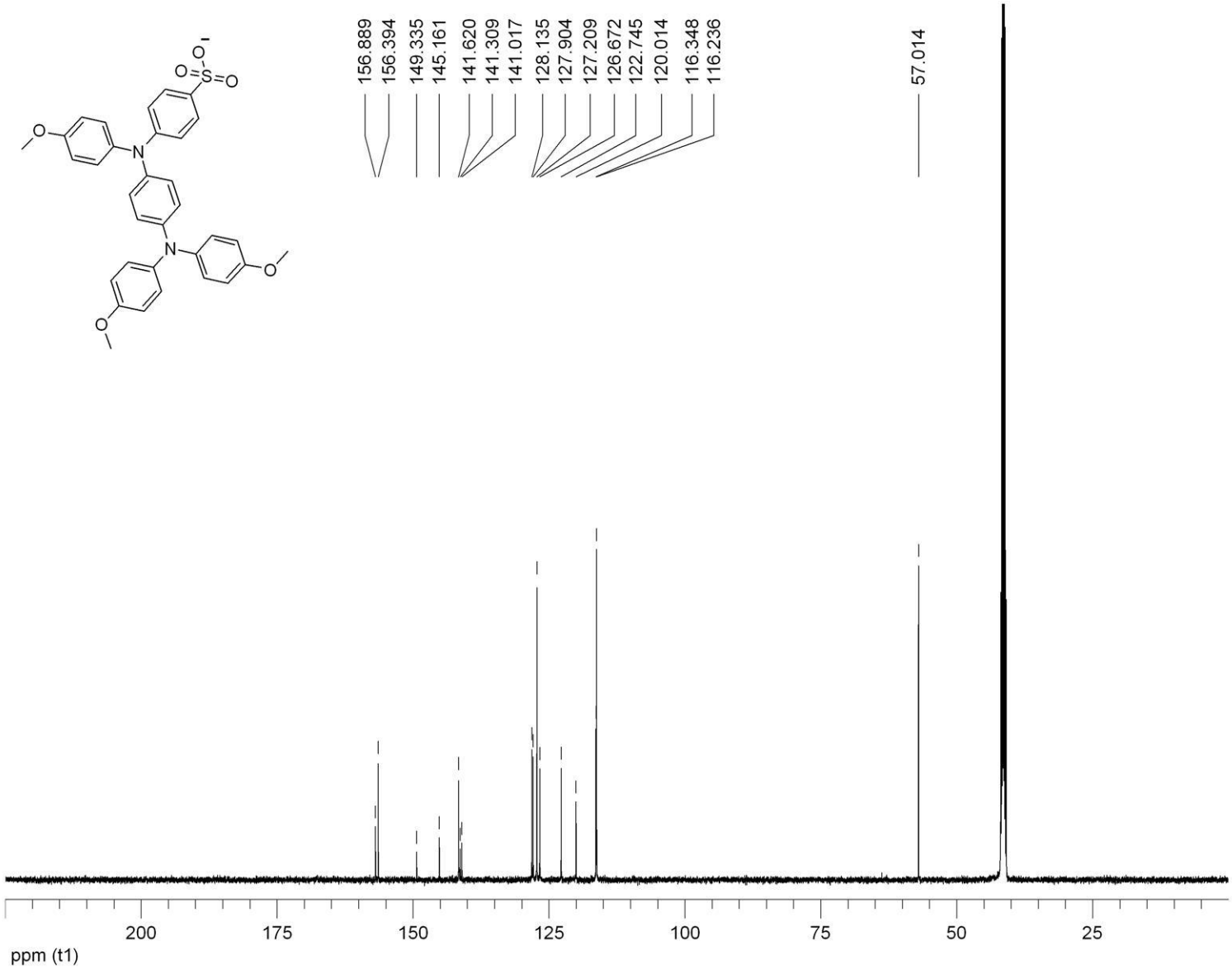

Figure A10. . ^{13}C-NMR Spectrum (125 MHz) of **11**.